Combining carbon monoxide-releasing molecules with anti-VEGF therapy for triple-negative breast cancer therapy

By
Malamati Kourti

Cardiff-China Medical Research Collaborative
School of Medicine
& School of Pharmacy and Pharmaceutical Sciences
Cardiff University

August 2018

A dissertation submitted to Cardiff University in candidature for the degree of *Doctor of Philosophy*

Declaration

This work has not been submitted in substance for any other degree or award at this or any other university or place of learning, nor is being submitted concurrently in candidature for any degree or other award.

Signed …….…… (candidate) Date ……

STATEMENT 1

This thesis is being submitted in partial fulfilment of the requirements for the degree of Doctor of Philosophy.

Signed …….…… (candidate) Date ……

STATEMENT 2

This thesis is the result of my own independent work/investigation, except where otherwise stated, and the thesis has not been edited by a third party beyond what is permitted by Cardiff University's Policy on the Use of Third party Editors by Research Degree Students. Other sources are acknowledged by explicit references. The views expressed are my own.

Signed …….…… (candidate) Date ……

STATEMENT 3

I hereby give consent for my thesis, if accepted, to be available online in the University's Open Access repository and for inter-library loan, and for the title and summary to be made available to outside organisations.

Signed …….…… (candidate) Date ……

STATEMENT 4: PREVIOUSLY APPROVED BAR ON ACCESS

I hereby give consent for my thesis, if accepted, to be available online in the University's Open Access repository and for inter-library loans after the expiry of a bar on access previously approved by the Academic Standards & Quality Committee.

Signed …….…… (candidate) Date ……

Acknowledgements

First, I would like to express my sincere gratitude to all my supervisors for their great support provided during these three years. In particular, I would like to thank Dr. Jun Cai for the positive attitude, patient guidance, encouragement and advice he has provided me with during all these years. I would also like to thank Prof. Andrew Westwell for his great support as a supervisor, his useful advice and supportive attitude. Thank you both for being there for me through good and bad, and for keeping up with my craziness and negativity.

I want to thank Prof. Andrea Brancale for always being available and incredibly friendly. Thank you Prof. Angela Casini for allowing me to work in your lab and special thanks to your team, Dr. Samuel Meier-Menches and Dr. Riccardo Bonsignore for the fruitful collaboration, advice and guidance during my time in the School of Chemistry. Furthermore, I would like to express my gratitude to all members of CCMRC for always being helpful and for every piece of advice they shared with me. Sincere thanks to the Life Sciences Research Network Wales and Cardiff University for their financial support and the opportunity to attend scientific conferences.

Finally, I would like to express my warmest appreciation to my amazing family and my other half for always being there for me, for believing in me more than anyone else and for being the best role model I could possibly have. I am sorry that I was such a pain for three years, but I could never be here if not for you!

Summary

Triple-negative breast cancer (TNBC) is defined by the lack of expression of the oestrogen and progesterone receptors and the overexpression of HER-2. Recently, carbon monoxide (CO) was found to behave as an important endogenous signalling molecule and interestingly, to suppress vascular endothelial growth factor receptor-2 (VEGFR2) and protein kinase B (AKT) phosphorylation. Given that anti-angiogenic drugs exist as one of the few available therapies against TNBC, CO-releasing molecules (CORMs) could be used as part of a combination therapy, in order to reduce cancer-driven angiogenesis. Therefore, the aim of this project was to study any potential anti-angiogenic properties of four commercially available CORMs and after the selection and structural modification of one of them, new analogues would be synthesized and evaluated *in vitro*. The four commercially available CORMs were screened for cytotoxicity against TNBC, epithelial and endothelial cells and found to be moderately toxic. They were also shown to reduce the glycolytic metabolism of TNBC cells, decrease VEGF excretion from both TNBC cell lines tested and downregulate the expression of the cytoprotective enzyme haem oxygenase-1 (HO-1). They were finally reported to moderately inhibit the activation of VEGFR2 and other downstream proteins upon stimulation with VEGF and reduce the tube formation ability of endothelial cells. These results were crucial for the selection of one lead compound, which was subjected to structural modifications and 15 new analogues were produced. The new molecules showed a more favourable cytotoxicity profile, with two of them being selectively toxic against TNBC. All the 15 analogues retained the ability to reduce VEGF excretion from TNBC cells and two of them were chosen for further studies. These two complexes downregulated the expression of HO-1 at similar levels and reduced the phosphorylation of some VEGFR2 downstream proteins more than the parent compound. Finally, both CORMs decreased the tube formation activity of endothelial cells. In summary, two of the commercially available and two of the newly synthesized CORMs showed promising anti-angiogenic properties and should be pursued further, in order to identify a mechanism of action for these organometallic complexes.

Publications

Kourti M, Jiang W, Cai J. Aspects of carbon monoxide (CO) in form of CO-releasing molecules (CORMs) used in cancer treatment: more light on the way. *Oxid Med Cell Longev.* **2017**. doi: 10.1155/2017/9326454

Ziedan NI, Hamdy R, Cavaliere A, Kourti M, Prencipe F, Brancale A, Jones AT, Westwell AD. Virtual screening, SAR and discovery of 5-(indole-3-yl)-2-[(2-nitrophenyl)amino] [1,3,4]-oxadiazole as a novel Bcl-2 inhibitor. *Chem Biol Drug Des.* **2017**, 90(1), p. 147-155. doi: 10.1111/cbdd.12936

Theodosis-Nobelos P, Kourti M, Gavalas A, Rekka EA. Amides of non-steroidal anti-inflammatory drugs with thiomorpholine can yield hypolipidemic agents with improved anti-inflammatory activity. *Bioorg Med Chem Lett.* **2016**, 26(3), p. 910-3. doi: 10.1016/j.bmcl.2015.12.063

Theodosis-Nobelos P, Kourti M, Tziona P, Kourounakis PN, Rekka EA. Esters of some non-steroidal anti-inflammatory drugs with cinnamyl alcohol are potent lipoxygenase inhibitors with enhanced anti-inflammatory activity. *Bioorg Med Chem Lett.* **2015**, 25(22), p. 5028-31. doi: 10.1016/j.bmcl.2015.10.036

Abstracts and Conference presentations

Oral presentations

Kourti Malamati. Carbon-monoxide releasing molecules as novel agents for the anti-VEGF therapy of triple-negative breast cancer. **2018**, *Life Sciences Research Network Wales 5th Annual Drug Discovery Congress, Cardiff Bay, UK*

Kourti Malamati. Combining CO-releasing molecules with anti-VEGF therapy for triple-negative breast cancer therapy. **2017**, *4th China-United Kingdom Cancer Conference, Beijing, China*

Kourti Malamati. Combining CO-releasing molecules with anti-VEGF therapy for triple-negative breast cancer therapy. **2017**, *Division of Cancer and Genetics seminar series, School of Medicine of Cardiff University, Cardiff, UK*

Kourti Malamati. Structurally improved antioxidant Trolox derivatives with pleiotropic activity. **2013**, *16th Pan-Hellenic Pharmaceutical Conference, Book of abstracts, p. 15, Athens, Greece*

Poster presentations

Kourti M., Westwell A., Brancale A., Cai J. Carbon-monoxide releasing molecules as potent anti-angiogenic agents against triple-negative breast cancer. **2018**, *EFMC XXVth International Symposium on Medicinal Chemistry, Ljubljana, Slovenia*

Kourti M., Westwell A., Brancale A., Cai J. Combining CO-releasing molecules with anti-VEGF therapy for triple-negative breast cancer therapy. **2018**, *Life Sciences Research Network Wales Inaugural Sêr Cymru Postgraduate Conference, Bangor, UK*

Kourti M., Westwell A., Brancale A., Cai J. Carbon-monoxide releasing molecules as novel synergistic agents for anti-VEGF therapy of triple-negative breast cancer. **2017**, *Life Sciences Research Network Wales Inaugural Sêr Cymru Postgraduate Conference, Cardiff, UK*

Kourti M., Westwell A., Brancale A., Cai J. Carbon monoxide-releasing molecules as an alternative approach towards the therapy of triple-negative breast cancer. **2017**,

EFMC 17th Hellenic Symposium on Medicinal Chemistry: Designing Targeted and Safer Drugs, Thessaloniki, Greece

Kourti M., Westwell A., Brancale A., Cai J. Carbon-monoxide releasing molecules as novel agents for the anti-VEGF therapy of triple-negative breast cancer. **2016**, *Life Sciences Research Network Wales 3rd Annual Drug Discovery Congress, Cardiff Bay, UK*

Kourti M., Westwell A., Brancale A., Cai J. Carbon-monoxide releasing molecules as novel synergistic agents for anti-VEGF therapy of triple-negative breast cancer. **2016**, *EFMC XXIVth International Symposium on Medicinal Chemistry, Manchester, UK*

Kourti M., Westwell A., Brancale A., Cai J. Carbon-monoxide releasing molecules as novel synergistic agents for anti-VEGF therapy of triple- negative breast cancer. **2016**, *Life Sciences Research Network Wales Inaugural Sêr Cymru Postgraduate Conference, Swansea, UK*

Kourti M., Karagkiozidou V., Papagiouvannis G., Rekka E.A. Design, synthesis and biological evaluation of antidyslipidemic morpholines with antioxidant activity. **2015**, *IXth Joint Meeting in Medicinal Chemistry, Athens, Greece*

Papagiouvannis G., Theodosis-Nobelos P., Tsiakitzis K., Kourti M., Kourounakis P.N., Rekka E.A., Design, synthesis and study of GABA amides and N-acyl-2-pyrrolidones with antioxidant acids. **2015**, *IXth Joint Meeting in Medicinal Chemistry, Athens, Greece*

Kourti M, Vellios A, Rekka E, Kourounakis P. Design of multi-targeting morpholines against hyperlipidemias. *Chem. Med. Chem. **2014**, p. 250, P020, EFMC XXIIIrd International Symposium on Medicinal Chemistry, Lisbon, Portugal*

Tziona P, Theodosis-Nobelos P, Kourti M, Gavalas A, Rekka EA, Kourounakis PN. New potent anti-inflammatory agents through combination of non-steroidal anti-inflammatory drugs with bioactive alcohols. **2014**, *6th International Conference on Oxidative Stress in Skin Medicine and Biology, Book of abstracts, p. 66, Andros, Greece*

Contents

Chapter 1. Introduction 1

1.1 Breast cancer 2

1.1.1 General characteristics of cancer 2

1.1.2 Breast cancer 4

1.1.3 Therapeutic interventions 8

1.2 Triple-negative breast cancer 9

1.2.1 General characteristics 9

1.2.2 Current therapeutic options 12

1.3 Angiogenesis 20

1.3.1 Neovascularization process 21

1.3.2 Angiogenic activators – Growth factors 23

1.3.2.1 Vascular endothelial growth factor 24

1.3.3 Anti-angiogenic agents 29

1.3.3.1 Anti-VEGF-A antibody (Bevacizumab) 32

1.3.4 Reactive oxygen species in angiogenesis 34

1.4 Carbon monoxide 35

1.4.1 General characteristics and toxicity 35

1.4.2 Endogenous production and physiological functions – Haem oxygenases 37

1.4.3 Therapeutic applications 42

1.5 Carbon monoxide-releasing molecules 43

1.5.1 General characteristics 43

1.5.2 Mechanisms of CO release 45

1.5.3 First and second generation CORMs 47

1.5.4 Overview of the family of photo-CORMs 50

1.5.5 Carbon monoxide and CORMs as anti-cancer agents 51

1.5.6 CO and CORMs in relation to reactive oxygen species production 53

1.5.7 Designing new CORM analogues 54

1.6 Hypothesis, purpose and aims of the study 60

Chapter 2. Materials and Methods 62

2.1 Materials 63

2.1.1 Standard reagents and solutions 63
2.1.2 Equipment for chemical synthesis and identification 70
2.1.3 Cell lines 71
2.1.4 Antibodies 71
2.2 Methods 72
2.2.1 Cell culture 72
2.2.1.1 Trypsinization and counting of cells 73
2.2.1.2 Cell storage in liquid nitrogen 73
2.2.1.3 Recovery of cells from liquid nitrogen 74
2.2.2 Cytotoxicity assays 74
2.2.2.1 MTT assay 74
2.2.2.2 IncuCyte™ Cytotoxicity assay 75
2.2.2.3 IncuCyte™ Caspase-3/7 assay (Apoptosis assay) 75
2.2.3 Cell biomass quantification 76
2.2.3.1 Crystal violet assay 76
2.2.4 Metabolic dysfunction detection with the Seahorse Extracellular XF^{e} Flux Analyser 76
2.2.5 Protein detection 77
2.2.5.1 Sodium dodecyl sulphate – Polyacrylamide gel electrophoresis (SDS-PAGE) and Western blotting 77
2.2.6 Enzyme-linked immunosorbent assay (ELISA) 81
2.2.6.1 ELISA for VEGF quantification 81
2.2.6.2 ELISA for pY1175 (pVEGFR2) quantification 83
2.2.7 Tube formation assay 84
2.2.7.1 Tube formation assay using conditioned media 84
2.2.7.2 Tube formation assay with instant treatments 84
2.2.8 Migration assays 85
2.2.8.1 Traditional Scratch wound healing assay 85
2.2.8.2 IncuCyte™ Scratch wound assay 85
2.2.9 Antibacterial activity assessment – ISO Broth Microdilution method 86
2.2.10 Statistical Analysis 87

Chapter 3. Screening of available CORMs 88
3.1 Cytotoxicity assessment 89
3.1.1 Introduction 89
3.1.2 Materials and Methods 94
3.1.3 Results 96
3.1.4 Discussion 105
3.2 Metabolic dysfunction detection 109
3.2.1 Introduction 109
3.2.2 Materials and Methods 111
3.2.3 Results 112
3.2.4 Discussion 117
3.3 Protein expression quantification 120
3.3.1 Introduction 120
3.3.2 Materials and Methods 124
3.3.3 Results 127
3.3.4 Discussion 142
3.4 Migratory ability assessment 147
3.4.1 Introduction 147
3.4.2 Materials and Methods 147
3.4.3 Results 149
3.4.4 Discussion 153
3.5 Angiogenic potential 155
3.5.1 Introduction 155
3.5.2 Materials and Methods 156
3.5.3 Results 157
3.5.4 Discussion 160
3.6 Lead compound for structural modification and further studies 162
Chapter 4. Design and Synthesis of new compounds 168
4.1 Design of new analogues 169
4.2 Synthesis and Characterisation 175
4.3 Discussion 205

Chapter 5. Screening of new analogues 217
5.1 Cytotoxicity assessment 218
5.1.1 Introduction 218
5.1.2 Materials and Methods 218
5.1.3 Results 219
5.1.4 Discussion 222
5.2 Protein expression quantification 224
5.2.1 Introduction 224
5.2.2 Materials and Methods 224
5.2.3 Results 226
5.2.4 Discussion 234
5.3 Angiogenic potential 236
5.3.1 Introduction 236
5.3.2 Materials and Methods 236
5.3.3 Results 237
5.3.4 Discussion 240
Chapter 6. Final Discussion 243
6.1 First and second generation CORMs as anti-angiogenic agents 244
6.2 Design and synthesis of new analogues 248
6.3 Third generation CORMs as anti-angiogenic agents 248
6.4 Comparison between old and new analogues and selection of the final lead compound 250
6.5 Future work 252
List of References 254
Appendix 279
Antibacterial activity assessment 280
Introduction 280
Materials and Methods 282
Results 282
Discussion 286
Selected NMR spectra 287

List of Figures

Chapter 1

Figure 1.1 Observed and projected mortality rates of breast cancer in the UK ... 5

Figure 1.2 Molecular classification of breast cancer and survival by molecular subtype 6

Figure 1.3 Chemical structures of progesterone and oestrogen 7

Figure 1.4 ER and HER activation mechanisms and downstream signalling pathways 8

Figure 1.5 Potential therapeutic targets for TNBC 13

Figure 1.6 Activation of angiogenesis 21

Figure 1.7 The distinct steps of angiogenesis 23

Figure 1.8 Structure of homodimeric VEGF-A 24

Figure 1.9 Alternative splicing of VEGF-A gene and the isoforms produced 25

Figure 1.10 Main receptors of VEGF family and their ligands 25

Figure 1.11 Structure of VEGFR2 and VEGFR2 in complex with VEGF-C 26

Figure 1.12 Cross talks between VEGFR2 and other signalling pathways in ECs ... 27

Figure 1.13 Bevacizumab 33

Figure 1.14 Therapeutic use of CO 36

Figure 1.15 Endogenous production of CO from the enzymatic degradation of haem 38

Figure 1.16 Structures of Haem oxygenase-1 and -2 39

Figure 1.17 The distinct parts of a CORM 45

Figure 1.18 Potential trigger mechanisms for CO release from CORMs 46

Figure 1.19 Induced CO-release from CORM-functionalized IONPs with the application of magnetic field 47

Figure 1.20 Structures of first and second generation CORMs 49

Figure 1.21 Structures of next generation CORMs 57

Figure 1.22 Example of $[Mn(CO)_3(tpm)]^+$–peptide conjugate 57

Figure 1.23 Photo-CORP-1 58

Figure 1.24 B_{12}-ReCORM-2 58

Chapter 3

Figure 3.1 Tetrazolium bromide dye reduction to purple formazan 91

Figure 3.2 Apoptotic pathways mediated by caspases 92

Figure 3.3 Caspase-dependent cell death 93

Figure 3.4 Cytotoxicity of CORMs 97

Figure 3.5 Cytotoxicity and confluence in MDA-MB-231 after CORM treatments at IncuCyte™ 99

Figure 3.6 Cytotoxicity and confluence in MDA-MB-436 after CORM treatments at IncuCyte™ 100

Figure 3.7 Cytotoxicity and confluence in MCF-10A after CORM treatments at IncuCyte™ 102

Figure 3.8 Caspase 3/7 quantification after CORM treatments in MDA-MB-231 at IncuCyte™ 103

Figure 3.9 Caspase 3/7 quantification after CORM treatments in MDA-MB-436 at IncuCyte™ 104

Figure 3.10 Glycolysis stress test in MDA-MB-231 after CORM treatments 114

Figure 3.11 Glycolysis stress test in MDA-MB-231 after CORM treatments combined with Avastin 116

Figure 3.12 VEGFR2 signalling cascade upon stimulation with VEGF-A 121

Figure 3.13 Summarized version of VEGFR2 signalling cascade upon stimulation with VEGF 122

Figure 3.14 VEGF expression in different cell lines 128

Figure 3.15 VEGF expression after CORM treatments 131

Figure 3.16 HO-1 expression after CORM treatments 133

Figure 3.17 Expression of VEGFR2 pathway proteins in HECV after CORM treatments 135

Figure 3.18 Western blot analysis for the different protocols tested 138

Figure 3.19 Expression of VEGFR2 pathway proteins in HUVEC after CORM pre-treatments and VEGF stimulation 140

Figure 3.20 pY1175 levels 141

Figure 3.21 Migratory ability of HECV after CORM treatments 150

Figure 3.22 Migratory ability of MDA-MB-231 after CORM treatments 152

Figure 3.23 Tube formation ability of HECV after conditioned media or CORM treatments 159

Chapter 4

Figure 4.1 Synthetic scheme of CORM-3 169
Figure 4.2 Schlenk line apparatus 177
Figure 4.3 Synthetic scheme for CORM-3 analogues 177
Figure 4.4 Mechanism of reaction for the synthesis of CORM-3 analogues 205
Figure 4.5 ^{1}H NMR spectra of reference and synthesized CORM-3 in DMSO-d_6 206
Figure 4.6 ^{13}C NMR spectra of purchased and synthesized CORM-3 in THF-d_8 207
Figure 4.7 Crystal structure of by-product from synthesis of CORM-3 209
Figure 4.8 Synthetic pathway of MK1c 211
Figure 4.9 Activation of starting materials 212
Figure 4.10 Mechanism of reaction for the synthesis of MK1 212
Figure 4.11 Mechanism of deprotection of the Boc group under acidic conditions for the synthesis of MK1c 213
Figure 4.12 Synthetic pathway of MK4a 214

Chapter 5

Figure 5.1 Cytotoxicity of novel CORMs 221
Figure 5.2 VEGF expression after novel CORM treatments 228
Figure 5.3 HO-1 expression after novel CORM treatments 230
Figure 5.4 Expression of VEGFR2 pathway proteins in HUVEC after novel CORM pre-treatments and VEGF stimulation 232
Figure 5.5 pY1175 levels for novel CORMs 233
Figure 5.6 Tube formation ability of HECV after conditioned media or novel CORM treatments 239

List of Tables

Chapter 1

Table 1.1 Summary of clinical and molecular characteristics of TNBC 10

Table 1.2 Nomenclature and classification of TNBC 11

Chapter 2

Table 2.1 Cell lines used in this study 71

Table 2.2 Primary antibodies used in this study 72

Table 2.3 Recipe for 10ml of 10% resolving gel 79

Table 2.4 Recipe for 3ml of 5% stacking gel 79

Chapter 4

Table 4.1 Common amino acids as ligands of the new CORMs and their chemical properties 170

Table 4.2 Epa values and antioxidant activity of phenolics 174

Table 4.3 Uncommon amino acids as ligands of the new CORMs and their chemical properties 175

Table 4.4 Lipophilicity data of new CORM-3 analogues 215

Table 4.5 Solubility of new CORMs in different solvents 216

Appendix

Table 1 Anti-bacterial assessment expressed as MIC of each CORM against different bacterial strains 284

Table 2 Anti-bacterial assessment expressed as MIC of each CORM against different bacterial strains 285

List of compounds

CORM-3 178
CORM-Ala 180
CORM-Ser 181
CORM-Phe 182
CORM-Tyr 183
CORM-His 184
CORM-Trp 185
CORM-Asp 186
CORM-Cyclopent 187
CORM-Cyclohex 188
CORM-Nitro-Tyr 189
CORM-Dinitro-Tyr 190
CORM-Nitro-Phe 191
CORM-Am-Phe 192
CORM-Benz-Ser 193
CORM-MK4a 194
MK1 195
MK1a 197
MK1b 199
MK1c 200
MK4 201
MK4a 203
MK5 204

Abbreviations

2-DG: 2-Deoxy-glucose

ACHC: 1-Aminocyclohexane-carboxylic acid

ACPC: 1-Aminocyclopentane-carboxylic acid

ADME(T): Absorption, distribution, metabolism, excretion, (toxicity)

AKT/PKB: Protein kinase B

APS: Ammonium persulfate

AR: Androgen receptor

ATP: Adenosine triphosphate

BC: Breast cancer

bFGF/FGF-2: Fibroblast growth factor 2

BL1, BL2: Basal-like 1, Basal-like 2

BRCA1: Breast cancer 1

BSA: Bovine serum albumin

$CDCl_3$: Deuterated chloroform

cGMP: Cyclic guanosine monophosphate

CO: Carbon monoxide

CORM: Carbon monoxide-releasing molecule

DCC: Dicyclohexylcarbodiimide

DCU: Dicyclohexylurea

DFS: Disease free survival

DMAP: Dimethylaminepyridine

DMEM: Dulbecco's modified Eagles' Medium

DMSO: Dimethyl sulfoxide

DNA: Deoxyribonucleic acid

EC: Endothelial cell

ECAR: Extracellular acidification rate

ECD: 1-Ethyl-3-(3-dimethylamino-propyl)carbodiimide

EDTA: Ethylenediaminetetraacetic acid

EGFR: Epidermal growth factor receptor

ELISA: Enzyme-linked immunosorbent assay

EMT: Epithelial mesenchymal transition

eNOS: Endothelial nitric oxide synthase

ER: Oestrogen receptor

ERK: Extracellular signal-regulated kinase

ESI-MS: Electrospray ionization mass spectrometry

Et_2O: Diethyl ether

EtOAc: Ethyl acetate

FAK: Focal adhesion kinase

FBS: Foetal bovine serum

FDA: Food and drug administration

FGFR: Fibroblast growth factor receptor

GTP: Guanosine triphosphate

H_2S: Hydrogen sulphide

HbCO: Carboxyhaemoglobin

HER(2): Human epidermal growth factor receptor (2)

HGF: Hepatocyte growth factor

HIF-1(a): Hypoxia-inducible factor 1(a)

HO(-1/2): Haem oxygenase (-1/2)

HOBt: Hydroxybenzotriazole

HR: Hormone receptor

HRE: Hormone response element

HRP: Horseradish peroxidase

HSP90: Heat shock protein 90

I/R: Ischaemia/reperfusion

IL: Interleukin

IM: Immunomodulatory

IONPs: Iron oxide nanoparticles

JNK: c-JUN N-terminal kinase

LAR: Luminal androgen receptor

LPS: Lipopolysaccharide

M: Mesenchymal

MAPK: Mitogen-activated protein kinase

Mb: Deoxymyoglobin

MbCO: Carboxymyoglobin

MDM2: Mouse double minute 2 homolog

MEBM: Mammary epithelial basal medium

MEK: Mitogen-activated protein kinase kinase

MeOH: Methanol

MeONa: Sodium methoxide

MIP-1b: Macrophage inflammatory protein 1b

MKK3: Dual specificity mitogen-activated protein kinase kinase 3

MMP: Matrix metalloproteinase

Mn: Manganese

mRNA: Messenger ribonucleic acid

MS: Mass spectrometry

MSL: Mesenchymal stem-like

MSNs: Mesoporous silica nanoparticles

mTOR: Mammalian target of rapamycin

MTT: 3-(4,5-Dimethylthiazol-2-yl)-2,5-diphenyltetrazolium bromide

NaH: Sodium hydride

NCK: Non-catalytic region of tyrosine kinase adaptor protein

NF-κB: nuclear factor kappa-light-chain-enhancer of activated B cells

NMR: Nuclear magnetic resonance

NO: Nitric oxide

NOX: NAPDH oxidases

OS: Overall survival

p38 MAPK: p38 mitogen-activated protein kinases

PARP-1: Poly adenosine diphosphate ribose polymerase-1

PBS: Phosphate buffered saline

pCR: Complete pathological response

PDGF: Platelet-derived growth factor

PDPK1: 3-Phosphoinositide-dependent kinase 1

PE: Petroleum ether

PGE2: Prostaglandin E2

PI3K: Phosphoinositide 3-kinase

PK: Pharmacokinetic

PKC: Protein kinase C

PLC-γ: Phophoinositide phospholipase C-γ

PLGF/PGF: Placental growth factor

PR: Progesterone receptor

PTEN: Phosphatase and tensin homolog

RNA: Ribonucleic acid

ROS: Reactive oxygen species

RTK: Receptor tyrosine kinase

Ru: Ruthenium

SCK: Shc-related adaptor protein

SD: Standard deviation

SDS: Sodium dodecyl sulphate

SDS-PAGE: Sodium dodecyl sulphate-polyacrylamide gel electrophoresis

SEM: Standard error of the mean

sGC: Soluble guanylyl cyclase

Src: Proto-oncogene tyrosine protein kinase Src/ Sarcoma oncogene

TBS: Tris buffered saline

TCA: Tricarboxylic acid

TGF: Transforming growth factor

THF: Tetrahydrofuran

TKI: Tyrosine kinase inhibitor

TLC: Thin layer chromatography

TMB: 3,3’,5,5’-Tetramethylbenzidine

TNBC: Triple-negative breast cancer

TNFα: Tumour necrosis factor-α

tPSA: Topological polar surface area

VEGF: Vascular endothelial growth factor

VEGFR: Vascular endothelial growth factor receptor

β-NAD: β-Nicotinamide adenine dinucleotide

Chapter I

General Introduction

1.1 Breast cancer

1.1.1 General characteristics of cancer

Cancer is a family of diseases that involves abnormalities in cell growth, with the potential to invade or spread to other parts of the body. The malignant progression from normal cells to cancer cells is a complex cascade with many steps, where the rate of cell division is disrupted and dysregulated (Sharma et al. 2010). Rapidly dividing and growing tumour cells progressively accrue mutations that help them deviate even more from normal behaviour. There are six hallmarks of cancer, which are required features for a cell to be able to form a malignant tumour and be characterized as cancerous. These hallmarks include:

- Sustaining proliferative signalling
- Evading growth suppressors
- Resisting cell death
- Enabling replicative immortality
- Promoting angiogenesis
- Activating invasion and metastasis

Four novel hallmarks have also been described during the last decade. The first is reprogramming of energy metabolism, referring to the ability of cancer cells to reprogram their glucose metabolism, even in oxygen abundance, favouring glycolysis for their energy production. The second emerging hallmark is genome instability and mutation, indicating the abundant genome maintenance and repair defects found in many tumours, combined with the destabilization of gene copy number and nucleotide sequence. Genome instability is an enabling characteristic associated with the acquisition of the other hallmarks, since these defects have been proven advantageous by accelerating the rate of favourable genotype accumulation. The third hallmark is tumour-promoting inflammation that supplies necessary molecules to the tumour microenvironment, mainly growth factors, survival factors, pro-angiogenic factors and inductive signals for EMT. The final hallmark is evading immune suppression. Immunogenic cells such as cancer cells can evade the immune response by disabling eliminating components of the immune system, expressing

immunosuppressive molecules and recruiting immunosuppressive inflammatory cells (Hanahan and Weinberg 2011).

The causes of cancer progression are various, but around 40% of them are preventable by changing lifestyle factors. A small percentage of 10% are due to hereditary genetics. Common factors that contribute to cancer initiation according to the US National Cancer Institute (www.cancer.gov) include age, smoking, alcohol consumption, unhealthy diet and obesity, infections, radiation (both ionizing and non-ionizing), cancer-causing substances, chronic inflammation, hormones, immunosuppression (linked also to stress) and sunlight (Anand et al. 2008).

Carcinogenesis is a process divided into three defined stages: initiation, promotion and progression. During initiation irreversible changes alter the genotype of the target stem cell leading to immortality. The main process responsible is the interaction of the carcinogen or its active metabolites with nucleic acids leading to mutations in oncogenes and tumour suppressor genes. During the second stage of promotion, an immortalized cell acquires the phenotype and abilities of a malignant cell and can provoke tumour progression. The carcinogen interferes also with the microenvironment of the target stem cell in order to promote the immortalized cell. The stage of promotion requires prolonged exposure to the carcinogen and may be reversible, otherwise it leads to tumour progression. Therefore, carcinogenesis could be described as a cascade phenomenon, resulting in the serial activation of multiple oncogenes and/or the inactivation of tumour suppressor genes. As expected, age decisively contributes to carcinogenesis, as the accumulation of several mutations through the years facilitates both the initiation and promotion of cancer, so aging is characterized as a major risk factor (Anisimov 2007).

Management of the different types of cancer involves a combination of treatment techniques such as radiation therapy (radiotherapy), surgery, chemotherapy – sometimes in the form of targeted therapy –, immunotherapy and palliative care (Maughan et al. 2010; Kaufmann et al. 2013).

Most cancer patient deaths occur due to metastasis of their primary tumour to vital organs. Metastasis is defined as the spread of cancer to other parts of the body

discontinuous from the primary lesion. It is mostly encountered during the late stages of tumour progression and it can occur via the bloodstream or the lymphatic system. The metastatic cascade includes local invasion of the primary tumour cells, intravasation into the bloodstream or lymph, migration to the target site, extravasation and invasion into the target tissue, and establishment of a proliferating secondary tumour assisted by induced angiogenesis. Different subtypes of cancer have a propensity towards particular organs, but overall the most common sites for metastases to occur are the lungs, liver, brain and bones (Keller 2002).

1.1.2 Breast cancer

Cancer deriving from the mammary gland (breast cancer, BC) is the most common cancer type in women and the second most common cancer type worldwide. With almost two million newly diagnosed cases every year, it remains the most frequent cause of cancer-related death in women globally, whereas the new cases of invasive breast cancer in the UK exceed 55,000 per year (Cancer Research UK). The increasing occurrence, the complexity and the heavy economic impact of the required treatment to the overall health system expenditure make breast cancer one of the most urgent health problems in our society (Wehland et al. 2012; Kalimutho et al. 2015).

However, from the early 1990's onwards, the mortality rate has decreased by more than 30% in the western world and especially in the UK, breast cancer survival has doubled in the last 40 years (**Figure 1.1**). This was a result of several measures implemented either concerning the prevention or the management of early breast cancer, as well as the introduction of adjuvant and neoadjuvant therapies and targeted treatments for oestrogen receptor positive breast tumours (Jemal et al. 2010; Kaufmann et al. 2013).

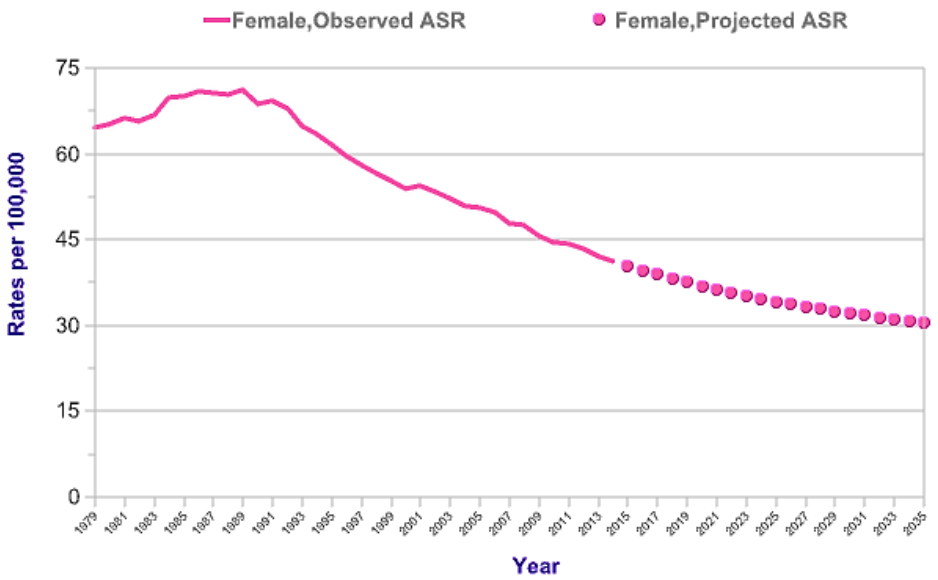

Figure 1.1: Observed and projected mortality rates of breast cancer in the UK from 1979 to 2035. *Source: Cancer Research UK. Access date 1/2/2018.*

The most common histological type of breast cancer is breast adenocarcinoma, which requires a long evolution period from normal to invasive carcinoma. The first stage of malignant transformation of the normal epithelium is characterized by excessive proliferation, known as hyperplasia. At the later stage of carcinoma in situ, cells progress to have a fully malignant phenotype, except for the ability to invade surrounding tissues through the basal membrane. Finally, carcinoma cells acquire invading activity and spread to surrounding areas through the basal membrane (Allred et al. 2001; Adeyinka et al. 2002).

Since breast cancer is a complex and highly heterogeneous disease regarding tumour morphology and gene expression, it is logical to expect that the response to the administered treatment would also vary among patients. Recent classification attempts revealed a diverse profile for breast cancer, thus the molecular subtypes established include; Basal-like (including triple negative breast cancer), Luminal A, Luminal B, HER2-amplified, Normal breast-like, and Claudin-low tumours (**Figure 1.2 A**). However, for prognostic and everyday clinical classification purposes the expression of only three surrogate key proteins (–biological markers) is assessed; the oestrogen receptor (ER), the progesterone receptor (PR) and the human epidermal growth factor receptor 2 (HER2). According to their expression, breast tumours can be categorized in the clinic as hormone receptor (HR)-positive/ HER2-negative, HR-

positive/ HER2-positive, HR-negative/ HER2-negative and HR-negative/ HER2-positive, following immunohistochemical analysis. These subtypes differ greatly in incidence, survival rates and overall response to treatment (Yamamoto and Iwase 2010; Wehland et al. 2012; Jansson et al. 2014; Kalimutho et al. 2015). Regardless of molecular subtype, advanced age, severe comorbidity, advanced stage at diagnosis, lobular carcinoma and urban residence were correlated with higher mortality rates. As for each subtype, HR-positive/ HER2-negative had the longest survival, followed by HR-positive/ HER2-positive, whereas the HR-negative/HER2-negative had the poorest observed survival (Fallahpour et al. 2017) (**Figure 1.2 B**).

A.

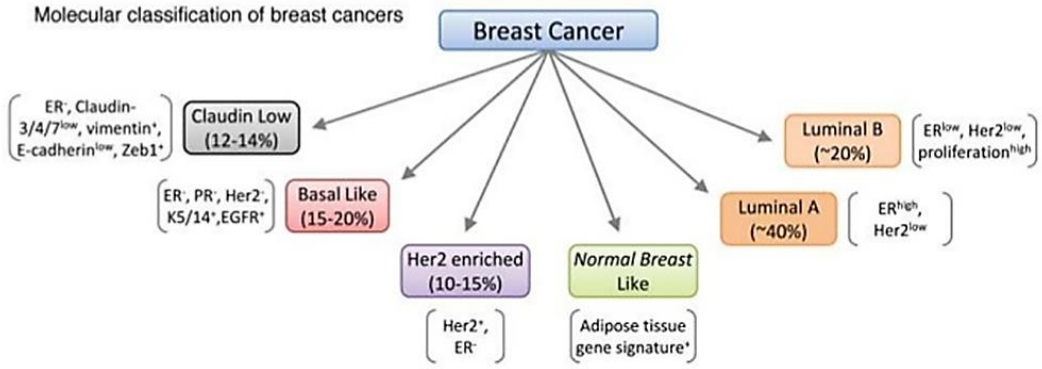

B.

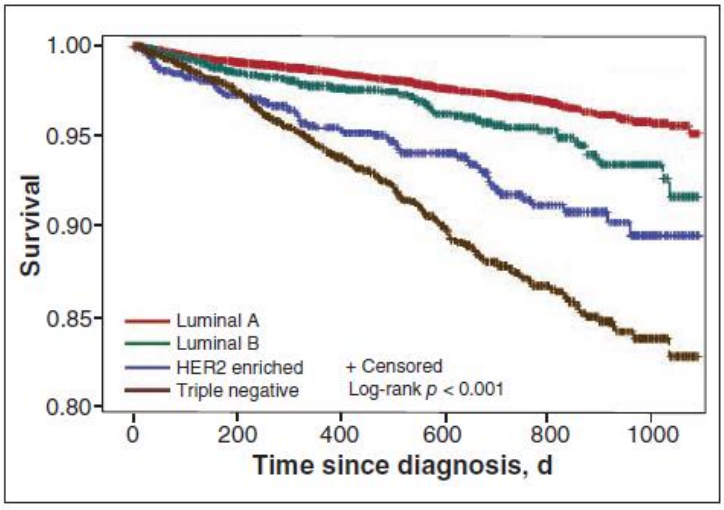

Figure 1.2: A. Molecular classification of breast cancer. (The Luminal B subtype can vary in marker expression but is generally ER-positive and HER2-positive or HER2-low with a high Ki67 ≥14%.) *Source: (Malhotra et al. 2010).* **B.** Overall breast cancer survival by molecular subtype. *Source: (Fallahpour et al. 2017).*

Both oestrogen and progesterone (**Figure 1.3**) are crucial hormones for the female organism. They are responsible for the development and correct function of the female reproductive system, menstrual cycle and secondary sex characteristics, as well as pregnancy and embryogenesis. Their receptors (ER and PR respectively) both act by binding to specific DNA regions (hormone response element – HRE) to activate target genes and regulate gene expression (Li et al. 2004; Lin et al. 2004).

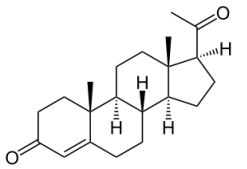

Progesterone

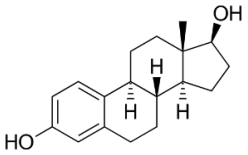

Oestrogen (17β-Oestradiol)

Figure 1.3: Chemical structures of progesterone and oestrogen

More specifically, ER can be found in tissues such as the ovary, uterus and breast, having an important role in promoting the proliferation of the tissues' cells. This receptor is also responsible for cholesterol level control and preservation of bone density. However, oestrogen could also prove harmful, since its gene expression regulatory activity could have adverse effects on the cells, increasing the chance for malignant mutations (Arsenyan et al. 2014). It is a fact that the vast majority of breast cancers present a marked dependence on oestrogen to grow, and they are characterized as hormone-sensitive or HR-positive cancers (Lin et al. 2004). The mechanism of ER activation is schematically depicted in **Figure 1.4**.

On the other hand, the human epidermal growth factor receptor (HER) family comprises tyrosine kinase receptors responsible for the growth and development of the breast, along with other organs. Ligands binding to their corresponding HER result in homo- or hetero-dimerization of the receptor, which subsequently activates downstream signalling involving trans-phosphorylation of tyrosine residues. HER2 is the most important receptor in breast tumours, since it does not have a known ligand and it acts upon cross-activation by a partner receptor bound to its ligand. Moreover, it is also the preferred heterodimerization partner for the other HERs. HER2 overexpression can lead to signal activation regardless of the ligand binding status, thus initiate the downstream signalling pathway in a ligand-independent manner. This

pathway eventually leads to cell progression, proliferation and survival, promoting tumour growth and perseverance (Creedon et al. 2014). Indeed, HER2 gene amplification is found in 15–20% of patients with invasive breast cancer, and is linked with increased risk of metastasis and death.

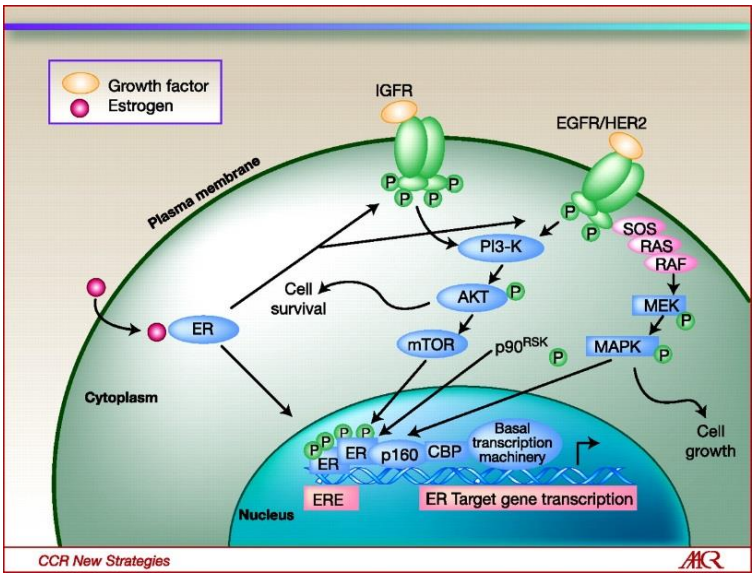

Figure 1.4: ER and HER activation mechanisms and downstream signalling pathways. *Source: (Johnston 2010).*

1.1.3 Therapeutic interventions

Breast cancer management usually depends on clinical and histopathological characteristics, such as tumour size, tumour grade, node status, age of the patient, metastasis staging and most importantly, hormone receptor expression status (Maughan et al. 2010; Reddy et al. 2012; Westbrook and Stearns 2013).

The usual treatment options combine surgery, radiation therapy and chemotherapy. The surgical treatment includes removal of the whole breast (mastectomy), removal of one quarter of the breast (quadrantectomy/ partial mastectomy) or removal of only a small part of the breast (lumpectomy).

In most cases, surgery is followed by radiation therapy, which inevitably involves exposure to radiation of normal tissues along with the tumour area. This may lead to severe side effects caused by the incidental exposure of the heart and the lungs, currently minimized by more modern precisely targeted application techniques.

Chemotherapy involves cytotoxic agents, referred to as adjuvant or neoadjuvant therapies, according to their administration simultaneously or prior to the main treatment. In that scope, there are more personalized biological treatment options including endocrine therapies for ER-positive tumours, and tissue-targeted therapies for tumours overexpressing HER2 (Maughan et al. 2010; Kaufmann et al. 2013).

However, all these therapies have potential side effects and limited efficacy in most of the cases. It is also evident that tumours lacking HR expression and HER2 overexpression are even more challenging to treat. Therefore, HR- and HER2- negative breast tumours have very few treatment options, and for these cases doctors usually exploit combination regimens (Reddy et al. 2012).

1.2 Triple negative breast cancer

1.2.1 General characteristics

Triple negative breast cancer (TNBC) is a subtype of BC defined as lacking the immunohistochemical expression of ER, PR and not showing overexpression of HER2/neu protein or HER2/neu gene amplification. It accounts for 15 – 20% of all invasive breast cancers and occurs more commonly in younger women and women of black race or Hispanic ethnicity (Andreopoulou et al. 2015). Other risk factors include higher parity, young age at the time of first birth and diagnosis, use of oral contraceptives by women less than 40 years old, lower socioeconomic status, increased body weight and the existence of metabolic syndrome (Yamamoto and Iwase 2010).

Although "triple negative" is not synonymous to "basal like", the molecular signature of TNBC frequently overlaps with basal like, in approximately 80% of the cases, based on PAM50 intrinsic subtype classification (Bertucci et al. 2008). Indeed in most cases, TNBC has a basal-like molecular phenotype by gene expression profiling, and shares clinical and pathological features with hereditary Breast Cancer 1 (BRCA1)-related breast cancers (Yadav et al. 2014; Andreopoulou et al. 2015). It is, in fact, associated with a higher probability of BRCA1 mutation (breast cancer susceptibility gene). The clinical and molecular characteristics of TNBC subtype are summarized in **Table 1.1**.

Clinical

- Accounts for ~ 15% of all breast cancers
- More common in women of black race and/or Hispanic ethnicity
- Younger age at presentation (<40 years old)
- Higher risk of visceral metastases, including brain metastasis
- Associated with germ-line BRCA mutations in ~ 50% of patients with a strong family history of breast and/or ovarian cancer, and up to 20% of unselected patients

Molecular

- Basal-like subtype and claudin-low subtypes are the most common 'intrinsic subtypes' by gene expression
- When present, BRCA mutations are associated with defective DNA repair and sensitivity to DNA damaging agents and poly-ADP-ribose-polymerase inhibitors
- Sporadic cancers not associated with BRCA mutations are often BRCA-like due to methylation-induced silencing of BRCA1 and/or loss of other DNA repair proteins
- Commonly associated with somatic p53 mutations, but 'clinically actionable' aberrations occur in < 20% (BRAF V600E, high-level EGFR amplifications, and ERBB2 and ERBB3 mutations) and may not be driver aberrations
- PI3K pathway activation, despite the low PI3K mutation rate, due to PTEN and INPP4B loss and/or amplification of PIK3CA

Table 1.1: Summary of clinical and molecular characteristics of TNBC. *Adapted from (Andreopoulou et al. 2015).* Abbreviations used: BRCA: Breast cancer 1, human tumour suppressor gene. BRAF V600E: Serine/threonine-protein kinase B-Raf gene. EGFR: Human epidermal growth factor receptor. ERBB2: Human epidermal growth factor receptor 2. ERBB3: Human epidermal growth factor receptor 3. PI3K: Phosphatidylinositol-4,5-bisphosphate 3-kinase. PTEN: Phosphatase and tensin homolog gene. INPP4B: Inositol polyphosphate- 4-phosphatase gene. PIK3CA: Phosphatidylinositol-4,5-bisphosphate 3-kinase, catalytic subunit alpha.

Although sensitive to chemotherapy, TNBC has an intrinsic aggressive clinical course associated with a 4-fold increased risk of distant recurrence, high rates of visceral (84 vs 61%, $p<0.001$) and central nervous metastases and worse prognosis after recurrence than HR-positive subtypes. The actual risk of recurrence increases rapidly in the first three years, peaking between one and three years after diagnosis, and mostly occurs within five years of diagnosis (Dent et al. 2007; Mayer et al. 2014; Andreopoulou et al. 2015; Marmé and Schneeweiss 2015). More specifically, the expected survival of patients with metastatic TNBC is rarely over 12 months, and eventually all women with this disease will die of it, despite systemic therapy (Fosu-Mensah et al. 2015).

In fact, TNBC represents a highly heterogeneous group characterized by extreme genomic alterations and instability. A recent study has revealed at least seven distinct molecular subtypes defined by their gene expression profiles, which differ in important biological pathways and prognosis. Basal-Like 1 and 2 (BL1 and BL2) show higher expression of cell cycle and DNA response gene damage; Immunomodulatory

(IM), Mesenchymal (M) and Mesenchymal Stem-Like (MSL) are enriched with epithelial mesenchymal transition (EMT) genes; Luminal Androgen Receptor (LAR) highly expresses genes involved in androgen receptor (AR) signalling; while the unclassified is based on gene ontology analysis (Lehmann et al. 2011; Marmé and Schneeweiss 2015) (**Table 1.2**). Distinguishing the different subtypes from one another remains a challenging task at clinical histologic examination, and as a result of this heterogeneity, it is inappropriate to treat all TNBCs in a uniform fashion, as variations in morphology and biological characteristics result in differences in clinical presentation and response to therapy (Fosu-Mensah et al. 2015).

Tumours of this subtype are almost all ductal invasive adenocarcinomas, mostly categorized as grade 3, with a high rate of p53 mutations. TNBCs are less likely to be diagnosed at screening mammography because of the age distribution, and tend to be diagnosed at a higher stage (Guarneri et al. 2013).

TNBC tumour subtype	After neoadjuvant chemotherapy pathological complete response rates (%)	Candidate therapeutic targets
Basal – like (BL2)	8	EGFR, MET, EPHA2, mTOR
Luminal androgen receptor (LAR)	10	AR, Hsp90, PI3K, FGFR4
Mesenchymal stem – like (MSL)	23	SRC, PI3K, MEK1/2, mTOR, PDGFR, NFKβ, IGF1R, FGFR, TGFBRIII
Immunomodulatory (IM)	30	JAK1/2, LYN, STATs, IRF1/7/8, BTK, NFKβ
Mesenchymal (M)	31	SRC, PI3K, Mtor, IGF1R, PDGFR,
Unstable (UNS)	33	PARP1, TTK, PLK1, CHEK1, AURKA/B, RAD51
Basal – like (BL1)	52	PARP1, TTK, PLK1, CHEK1, AURKA/B, RAD51

Table 1.2: Nomenclature and classification of TNBC. TNBC is molecularly heterogeneous and has been subdivided into seven definable molecular subclasses governed by distinct sets of genes and pathways. Each of these subclasses shows varying pathological complete response rates following neoadjuvant chemotherapy and may be amenable to targeted therapies using different molecular targets. *Adapted from (Kalimutho et al. 2015).*

1.2.2 Current therapeutic options

Management of TNBC remains challenging because of the lack of approved therapies, its aggressive behaviour and its relatively poor prognosis. There are no specific treatment guidelines for patients with TNBC and, unlike other molecular subtypes of breast cancer, there is no validated specific biomarker for TNBC, so they are just managed with standard chemotherapy treatments (as discussed below) (Sagara et al. 2017). Although it has been evidenced that these tumours are more sensitive to chemotherapy than other subtypes and in some cases, complete pathological response (pCR) is achieved, the results remain unsatisfactory. This is because even though pCR to the neoadjuvant chemotherapy is higher in the TNBC subset of patients, the disease free survival (DFS) and overall survival (OS) are still lower than in the non-TNBC patient group. The high biological heterogeneity within the TNBC subtype represents the major challenge for new drug development, and has clear implications for clinical trial design. A better understanding of its pathogenesis onset and progression, including the still unclear association with BRCA1 mutations, and the causes of phenotypic heterogeneity will be the key to a new treatment for this disease. Several experiments are being carried out and while some have failed, others have led to an improved understanding of the biology of the disease and the tumour cell environment, helping to find new biomarkers and potential targeted treatments. However, finding an effective treatment for TNBC is still urgently needed. The following are the therapeutic options currently available in TNBC (Guarneri et al. 2013; Mahamodhossen et al. 2013; Yadav et al. 2014; Zhang et al. 2015) (**Figure 1.5**):

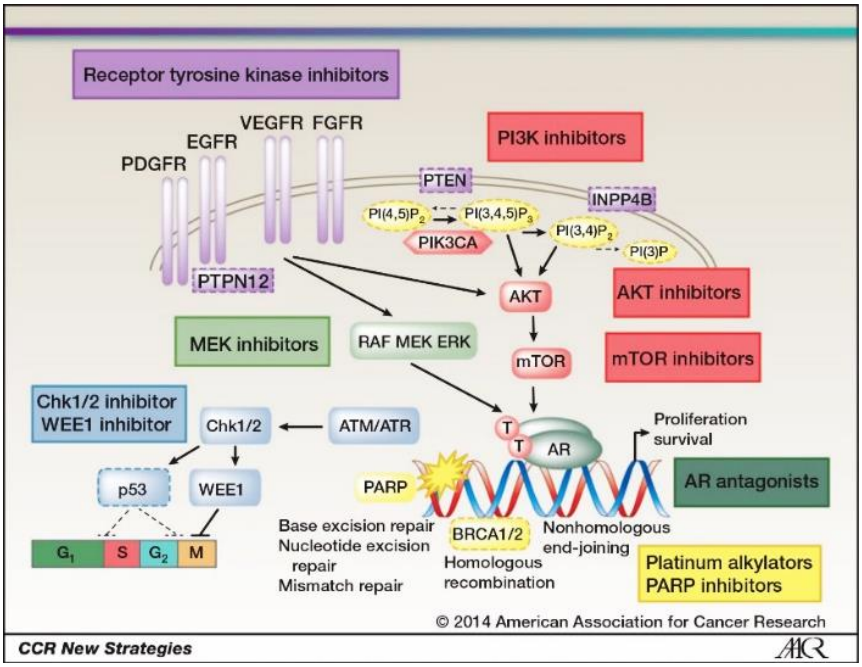

Figure 1.5: Potential therapeutic targets for TNBC. Current and future potential targets in TNBC include inhibitors of the impaired homologous recombination repair mechanism, modulation of the p53 signalling, antagonists of the androgen receptor and inhibitors of its pathway and inhibitors of the MAPK/MEK pathway. *Source: (Mayer et al. 2014).*

- **Systemic cytotoxic chemotherapy**

Due to the fact that TNBC is characterized by the loss of target receptors such as ER, PR and HER2, patients do not benefit from hormonal or trastuzumab-based therapies. Surgery, where applicable, and cytotoxic chemotherapy remain the mainstay of treatment for TNBC, despite the lack of long-term effectiveness. Early stage TNBC is usually addressed by a combination of cytotoxic agents used as an adjuvant or neoadjuvant therapy. Standard adjuvant and neoadjuvant regimens typically involve an anthracycline (doxorubicin or epirubicin) plus an alkylating agent (cyclophosphamide), administered either simultaneously with a taxane (docetaxel) or sequentially before or after a taxane (docetaxel or paclitaxel). As for their mechanism of action, anthracyclines can inhibit DNA and RNA synthesis obstructing the replication of the rapidly proliferating cancer cells, inhibit topoisomerase II enzyme hindering DNA transcription and provoking double-strand breaks, enhance the production of reactive oxygen species and deregulate DNA damage response (Pang et al. 2013). Cyclophosphamide has a different mechanism of action, causing toxicity due to its metabolite phosphoramide mustard. This metabolite is produced only in cells expressing low levels of aldehyde dehydrogenase, such as cancer cells. The mustard

can form DNA crosslinks between and within the DNA strands, leading to cell apoptosis (Hall and Tilby 1992). On the other hand, taxanes are mitotic inhibitors, disrupting microtubule function during cell division by hindering their depolymerisation (McGrogan et al. 2008). Unlike other types of breast cancer, few studies have been specifically designed for evaluating novel treatments against TNBC and their results remain inconclusive. Although the recurrence rate of TNBC is higher than other subtypes, it initially has an increased sensitivity to conventional chemotherapy than HR-positive breast cancers, as mentioned above (Yamamoto and Iwase 2010; Andreopoulou et al. 2015; Fosu-Mensah et al. 2015).

- **Platinum – based chemotherapy**

Platinum agents are one of the established drug classes that are considered in the treatment of TNBC. Platinum-based compounds, including carboplatin and cisplatin, are DNA interacting agents that lead to intra- and inter-strand cross links of double stranded DNA, prevent the formation of the replication fork and produce double strand breaks and replication lesions. These breaks result in impairment of DNA synthesis, especially in cells whose DNA repair cascade is non-functional, like when deficient in homologous recombination repair mechanisms, such as BRCA1/2-mutated cells, including the majority of TNBC cases. This deficiency leads to an increased sensitivity to chemotherapeutic agents that cause DNA damage, because when a cell has reparatory defects, error-prone compensatory repair mechanisms step in and lead to a high degree of genomic instability, finally leading to its death. At present, platinum agents, as a component of neoadjuvant chemotherapy, cannot be recommended over established regimens outside of a clinical trial because none of the studies was able to detect disease-free or overall survival benefit (Mayer et al. 2014). Therefore, they should always be used in combination with taxanes or anthracyclins to increase response and survival rates. However, patients with BRCA1 mutation tend to have maximum benefit in the neoadjuvant setting (Yamamoto and Iwase 2010; Mayer et al. 2014; Yadav et al. 2014; Andreopoulou et al. 2015; Fosu-Mensah et al. 2015; Marmé and Schneeweiss 2015).

- **Poly adenosine diphosphate ribose polymerase (PARP)-1 Inhibitors**

A relatively novel therapeutic target for TNBC is the enzyme PARP-1. As mentioned above, cells with abnormal repair mechanisms, like BRCA1/2-deficient cells, are over-sensitized to the effects of other DNA repair mechanisms-targeting agents, a concept known as synthetic lethality (Fosu-Mensah et al. 2015). PARP-1 is essential for DNA single-strand breaks repair through regulating the DNA base excision pathway. DNA single-strand breaks are subsequently accumulated upon PARP-1 inhibition by RNA interference or with chemical inhibitors (Mayer et al. 2014). In cells with normal BRCA function, this leads to the activation of the homologous recombination pathway. However, tumour cells with BRCA dysfunctions are unable to deal with this break accumulation, therefore undergo apoptosis (Yamamoto and Iwase 2010).

Some of the anticancer PARP inhibitors described in preclinical and clinical models are iniparib, olaparib, veliparib and rucaparib. Although PARP inhibitors have shown clinical activity in TNBC patients, there are still issues to be addressed such as the still limited experience, the selection of appropriate combinations with other drugs, the optimal route of administration, the duration of the therapy and the possible toxicities following the combination therapy (Yadav et al. 2014). PARP inhibitor resistance in BRCA-associated tumours has also been reported (Marmé and Schneeweiss 2015).

- **Tyrosine kinase Inhibitors**

A wide variety of cell surface receptors include a tyrosine kinase domain, whose enzymatic activity is to transfer a phosphate group from ATP to a tyrosine residue on a protein. These receptor tyrosine kinases (RTKs) are critical regulators of important cellular processes, such as cell proliferation, differentiation, survival, metabolism, migration and cell cycle control. Many cancers and their metastatic progression are characterized by the deregulation of RTKs, therefore, they present a useful anticancer target. In this scope, several RTK inhibitors have been developed which block or constrict RTK activity to target TNBC (Fosu-Mensah et al. 2015). A few of them are listed below:

- Epidermal Growth Factor Receptor (EGFR) Inhibitors

Epidermal growth factor receptor (EGFR), along with its downstream signalling pathway, is important for cell growth, survival and apoptosis. Since the majority of TNBC tumours overexpress EGFR and this high expression is linked to a poor prognosis, attempts have been made towards using approved EGFR inhibitor drugs. Gefitinib, erlotinib, lapatinib and neratinib are under investigation, however recent studies indicate that EFGR inhibition alone is not enough, therefore a combination therapeutic strategy comprising of more RTK pathways-inhibitors seems more likely to be successful (Guarneri et al. 2013; Fosu-Mensah et al. 2015). Monoclonal antibodies towards EGFR itself have also been designed, including cetuximab and panitumumab, but clinical data has again pointed to a modest effect on a TNBC subset (Marmé and Schneeweiss 2015).

- Vascular Endothelial Growth Factor (VEGF) Inhibitors

The majority of data on inhibition of angiogenesis in TNBC by targeting the vascular endothelial growth factor (VEGF) comes from clinical trials with the monoclonal antibody bevacizumab. However, more details on this category of anti-cancer agents can be found in section 1.3.3.

- Fibroblast Growth Factor Receptor (FGFR) Inhibitors

Fibroblast growth factor receptors (FGFRs) are a subfamily of RTKs that regulate several cellular and developmental processes, including apoptosis, proliferation, migration and angiogenesis. FGFR can promote angiogenesis along with other receptors, such as vascular endothelial growth factor receptor 2 (VEGFR2). The rationale for FGFR targeting is due to the amplification of both FGFR1 and FGFR2 in TNBC. There are currently no selective FGFR inhibitors in clinical testing, although FGFR expressing TNBC cell lines were sensitive to PD173074, a dual FGFR/VEGFR inhibitor, and to RNAi silencing of FGFR2 (Turner et al. 2010). The structural similarity between FGFR and VEGFR kinase domains may lead some inhibitors of both receptors to clinical investigation against TNBC. For example, lucitanib is an inhibitor of FGFR1/2/3, VEGFR1/2/3 and PDGFR (Fosu-Mensah et al. 2015; Papa et al. 2015).

- PI3K/AKT/mTOR pathway Inhibitors

Phosphoinositide-3-kinase (PI3K) is part of a large family of lipid kinases that phosphorylate the 3-hydroxyl group of phosphoinositides, involved in cell regulation, proliferation and survival. Mutations in *PIK3CA*, the gene encoding PI3K, are among the most frequent in BC. Downstream of PI3K there are protein kinase-B (AKT), which affects downstream molecules such as mammalian target of rapamycin (mTOR), and 3-phosphoinositide-dependent kinase-1 (PDPK1). The phospholipid produced by PI3K activates AKT, triggering a cascade of events responsible for cell growth and proliferation that can also drive tumour progression (Vivanco and Sawyers 2002). Apart from that, the actions of PI3K and its downstream proteins are opposed to the tumour suppressor gene phosphatase and tensin homolog (PTEN) (Papa et al. 2015). Across all TNBC subtypes, there is an elevated frequency of loss/mutation of PTEN expression leading to an activation of the AKT/mTOR signalling pathway. It has also been shown that mutation or upregulation of this pathway affects almost all its downstream components, resulting in resistance and cancer progression (Fosu-Mensah et al. 2015). Moreover, phosphorylation of mTOR in early TNBC is associated with an adverse prognosis (Marmé and Schneeweiss 2015). Therefore, inhibition of the PI3K/AKT/mTOR pathway has been recognized as a promising therapeutic target.

There are many modifiers of this pathway under ongoing research on a breast cancer subset, mainly as parts of a combination therapy. Temsirolimus and everolimus are prodrugs of rapamycin (sirolimus) and they are specific inhibitors of mTOR. Temsirolimus proved quite effective when combined with other anti-neoplastic modulators. For example, a combination of temsirolimus with letrozole for the treatment of advanced breast cancers was tested under a Phase III clinical trial, but had to be discontinued due to non-enhanced efficacy compared to letrozole alone (Wolff et al. 2013). Everolimus and other rapalogues seem to activate AKT in patients with breast carcinomas and also induce the mitogen-activated protein kinase (MAPK) signalling pathway leading to a shorter progression time. Therefore, a combination of rapalogues with AKT or MAPK inhibitors may prove more effective than the rapalogues alone (Cloughesy et al. 2008). Since everolimus showed mediocre results in breast cancer patients, other novel analogues are currently under investigation.

There is one clinical trial setting up to study the safety and efficacy of MLN0128, a selective competitive inhibitor of mTOR, in combination with hormone-therapeutics to treat metastatic breast cancer patients. AZD2014, another selective inhibitor of mTOR, is undergoing evaluation alone or in combination with AZD8186, a small-molecule inhibitor of PI3K, in a TNBC subset (Basu et al. 2015). In addition, the mTOR inhibitor DHM25 was found to efficiently inhibit the growth and metastasis of TNBC cells *in vivo* (Fouqué et al. 2015). Buparlisib, a PI3K inhibitor, induced only partial response in patients with TNBC but no response in those with ER-positive breast cancer, so in another clinical trial it was studied in combination with olaparib, showing enhanced activity (Rodon et al. 2014; Matulonis et al. 2017). Finally, pictilisib, another PI3K and mTOR inhibitor, showed strong antitumour activity against xenografts of TNBC in combination with a dual EGFR and HER3 inhibitor (Tao et al. 2014).

In summary, the mTOR inhibitors which exhibit antitumor effects in breast cancer patients emphasise the necessity for the development of novel selective and efficient compounds. A combination of PI3K/mTOR inhibitors with classical chemotherapeutic agents may be helpful in the treatment of TNBC patients and remains an attractive therapeutic approach (Fouqué et al. 2016).

- Proto-oncogene tyrosine-protein kinase Src Inhibitors

SRC gene is a proto-oncogene encoding a non-receptor protein tyrosine kinase (Src), responsible for many downstream effects of RTKs, including the EGFR family. It is involved in several signal transduction pathways, controlling biological functions such as cell growth, differentiation, migration and survival, as well as angiogenesis (Fosu-Mensah et al. 2015; Papa et al. 2015). Cytoplasmic and membrane Src's increased frequency in TNBC has been linked to a higher invasiveness towards metastasis and tumour progression (Guarneri et al. 2013). Gene expression studies and preclinical data suggested that TNBC might be susceptible to growth inhibition by the Abl/Src/c-kit inhibitor dasatinib (Qian et al. 2017). Despite encouraging preclinical results, clinical trials were disappointing, with dasatinib showing only modest efficacy. Thus, it was deemed ineffective as a single agent in TNBC. However a gene expression profile is currently under investigation as a predictive marker for response to dasatinib and some preclinical studies suggest a synergistic effect of the combination between

dasatinib and chemotherapy or other RTK inhibitors. Therefore, the re-evaluation of this agent is still ongoing (Fosu-Mensah et al. 2015; Marmé and Schneeweiss 2015).

- Mitogen-activated protein kinase (MAPK) Inhibitors

The Raf/MEK/ERK pathway, otherwise known as the mitogen-activated protein kinase (MAPK) pathway, is involved in directing cellular responses to a diverse array of stimuli, thus important for normal human physiology (MEK=mitogen-activated protein kinase kinase, ERK=extracellular signal-regulated kinase). Although Ras and Raf oncoproteins are not frequently mutated at the gene expression level in TNBC, dysregulations of this pathway are common in several human cancers, including BC, through activation of upstream RTKs, and/or activating mutations in proteins upstream, such as EGFR and HER2. TNBC has been linked to higher expression of several gene sets related to the Raf/MEK/ERK pathway. Therefore, MAPK pathway inhibitors may be useful against TNBC. Trametinib, a MEK1/2 inhibitor, and cobimetinib, a MEK inhibitor, are currently under investigation. One of the pathways activated in response to MEK inhibition is PI3K/AKT, thus the efficacy of MEK inhibitors in combination with PI3K/mTOR pathway inhibitors is also being evaluated in TNBC (Andreopoulou et al. 2015; Fosu-Mensah et al. 2015). Apart from that, a recent study suggested that in TNBC MEK inhibition may improve recruitment of tumour-infiltrating lymphocytes increasing tumour immunogenicity thus having a synergistic effect with the immune system (Dushyanthen et al. 2017).

- **Androgen receptor antagonists**

The androgen receptor (AR) is a particularly interesting target for TNBC. The association between AR pathway and TNBC is based on gene expression profiling, which pointed a subset of TNBCs, despite lacking ER and PR expression, being driven by AR expression (Andreopoulou et al. 2015). TNBC cell lines with AR-positive phenotype may respond to therapy with androgen antagonists (Marmé and Schneeweiss 2015). The androgen antagonist bicalutamide is currently under investigation. In a phase II study, bicalutamide was tested in a subset of AR-positive, ER-negative, PR-negative metastatic breast cancer and it was shown to have a 19% clinical benefit rate within 6 months, as well as a progression-free survival of 12 weeks

(Gucalp et al. 2013). Further studies of the inhibitor abiraterone in ER-positive and ER-negative AR expressing breast cancers are ongoing. Thus, further evaluation of anti-androgen therapies for the AR-positive TNBC is needed (Guarneri et al. 2013; Marmé and Schneeweiss 2015).

It is therefore obvious that the research on novel therapies against TNBC has currently been very active and we hope to see some successful approaches arising soon. Despite the many interesting strategies proposed by researchers though, angiogenesis remains a very promising area of research in relation to TNBC, and many groups still try to better understand and tackle this process that seems to be so vital for TNBC progression and metastasis.

1.3 Angiogenesis

Angiogenesis is a multi-step process of new capillary formation from pre-existing blood vessels. It plays a pivotal role in physiological processes, but it has also been recognized as a prerequisite for tumour growth, progression and metastasis (**Figure 1.6**). Especially for tumours, the ability to create new vasculature and expand the host vascular bed enables them to tap into the body's blood supply and draw on oxygen and nutrients essential for survival, growth, progression and metastasis. Without angiogenesis many tumours cannot grow beyond a limited size (1 – 2mm^3), and so tumour angiogenesis becomes a necessary and required step for the transition from a small cluster of faster dividing cells to a larger tumour (Carmeliet and Jain 2011; Bishayee and Darvesh 2012).

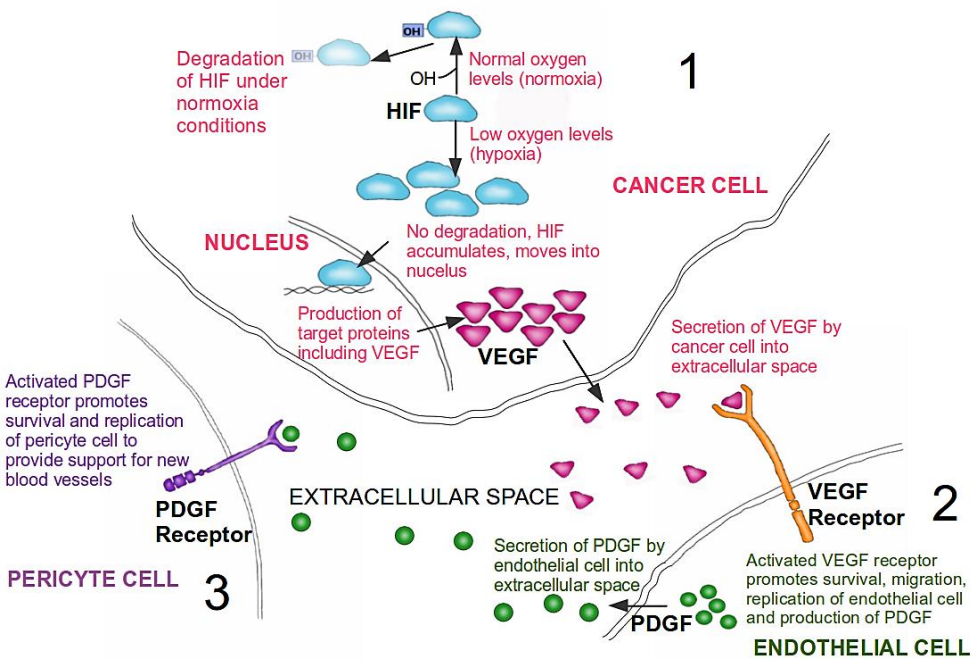

Figure 1.6: Activation of angiogenesis. Several stimuli can induce angiogenesis, including hypoxic conditions. Under these conditions higher VEGF levels are produced and excreted from the cancer cell into the extracellular environment where they bind to VEGF receptors on the surface of endothelial cells. This binding results in the survival, migration and replication of endothelial cells, ultimately promoting the formation of new blood vessels. *Source: https://blogs.scientificamerican.com/guest-blog/the-hallmarks-of-cancer-5-sustained-angiogenesis/*

Angiogenesis is a complex process, which is related to the function and life cycle of endothelial cells, involving processes such as activation, adhesion, proliferation and migration from the origin blood vessels to the newly formed ones. Physiological angiogenesis is tightly controlled by several pro-angiogenic and inhibitory molecules that exist in a highly regulated balance. Imbalance of this system leads to pathological angiogenesis involved in tumour progression. Sprouting angiogenesis is the most common phenomenon that participates in tumour neovascularization (Hillen and Griffioen 2007; Gacche and Meshram 2014).

1.3.1 Neovascularization process

As mentioned before, during angiogenesis new capillaries sprout from pre-existing vessels via the neovascularization process, and several steps are involved.

Adult blood vessels consist of a polarized streamlined monolayer of quiescent endothelial cells (ECs), called phalanx cells. At first, under multiple stress factors such

as ischemia and inflammation, cancer cells can activate these quiescent ECs via several growth factors. These factors act as stimulators of angiogenesis, activating respective receptors on ECs of pre-existing blood vessels, inducing more chemotaxis at the same time. These activated ECs initiate the production of proteases, that have the ability to degrade the extracellular matrix and basement membrane to allow for the migration and invasion of cells. These proteases include matrix metalloproteinases (MMPs), the most important for angiogenesis being MMP-2 and MMP-9, which can degrade all kinds of extracellular matrix proteins and play a vital role in cellular behaviour (Hillen and Griffioen 2007; Missiaen et al. 2017).

After the degradation of the extracellular matrix, and along with an increased vascular permeability driven by cancer produced growth vactors such as VEGF, ECs can proliferate and migrate to form solid sprouts from neighbouring vessels. The selection of an EC as a tip cell is important, since it becomes polarized and creates numerous filopodia and lamellipodia, that enable the migration of this cell towards the angiogenic signal. The tip cell is followed by trailing proliferative stalk cells, which are mainly able to form tubes and branches. The sprout extends towards the angiogenic source and forms loops which will develop a new vessel lumen and basement membrane, consisting of stalk cells. As the sprouting evolves, it enables the new still immature vessels to grow across gaps in the vasculature and through many processes, such as recruitment of pericytes and deposition of basement membrane, vessel maturation is achieved. The now mature vessels finally reach the tumour site, where they will deliver nutrients and oxygen and help in the detoxification of the rapidly splitting cancer cells, acting as a waste pathway (Hillen and Griffioen 2007; Gacche and Meshram 2014; Missiaen et al. 2017). However, it must be noted that the tumour blood vessels have many differences compared to normal vessels in that they are hyperpermeable and highly heterogeneous with regards to morphology and efficiency of tissue perfusion (Falcon et al. 2016). A summary of the neovascularization process is depicted in **Figure 1.7 A-D**.

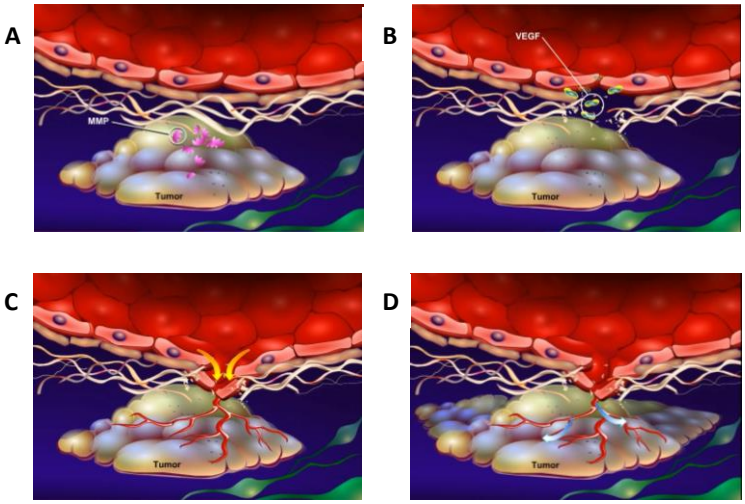

Figure 1.7: The dinstinct steps of angiogenesis. A: Activated ECs excrete proteases (MMPs) that degrade the extracellular matrix. **B:** VEGF secreted from cancer cells reaches the vasculature and activates signalling pathways promoting new vessel formation. **C:** New immature vessels sprout towards the tumour site. **D:** Mature vessels connect the tumour with the host vasculature and promote its growth. *Adapted from Youtube video "Introduction to Cancer Biology", channel of Mechanisms in Medicine.*

Angiogenesis is also important for the ability of a tumour to spread and metastasize. There is growing evidence that single cancer cells can be detached from an original established tumour site and circulate through the blood vessels towards areas where they can implant and begin a secondary tumour site. In fact, tumour blood vessels are suggested to be mosaic vessels, with irregular shapes, including both endothelial and cancer cells, which is also called mimicry. This heterogeneity and mosaicity may assist circulating tumour cells to reach distant areas and establish new tumour sites. If this process could be inhibited, there would be less possibility for tumour metastasis and possibly the primary tumour would also shrink in size (Shan et al. 2014).

1.3.2 Angiogenic activators – Growth factors

As discussed, tumours have the ability to induce blood vessel growth by secreting several growth factors. The first angiogenic growth factor to be identified in the early 1980s was the fibroblast growth factor (bFGF or FGF-2). This family of growth factors includes 23 members along with four FGF tyrosine kinase receptors. aFGF (FGF-1) and bFGF (FGF-2) are the most well-known members and they can stimulate the angiogenic cascade and induce capillary growth into the tissue when expressed by different cell types, including cancer cells (Hillen and Griffioen 2007; Bodner-Adler et al. 2016; Cai et al. 2016).

Other pro-angiogenic growth factors which control angiogenesis physiologically but also during cancer include members of the vascular endothelial growth factor (VEGF) family, the platelet-derived growth factor (PDGF), the transforming growth factor (TGF), the placental growth factor (PLGF), the hepatocyte growth factor (HGF), and chemokines such as follistatin and angiopoietins. However, VEGF family has been recognized as the most potent contributor to angiogenesis, activating the basic signalling required for neovascularization (Gacche and Meshram 2014).

1.3.2.1 Vascular endothelial growth factor

Vascular endothelial growth factor (VEGF) or vascular permeability factor is the basic mediator of both physiological and pathological angiogenesis. It affects many endothelial related functions, such as proliferation and mobility, and it also provokes vessel dilatation and increased permeability of the vessel wall. Moreover, it is an inducer for all the steps of angiogenesis as described above, namely the expression of matrix metalloproteinases and other activators of the degradation of the basal membrane and the subsequent EC migration and new vessel establisment (Hillen and Griffioen 2007).

The family of VEGF includes seven members, namely VEGF-A, VEGF-B, VEGF-C, VEGF-D, VEGF-E, VEGF-F and the PLGF. VEGF-A seems to be the homologue that is responsible for EC survival and growth and is also hypoxia-inducible. It is an N-glycosylated 35–45kDa homodimeric glycoprotein, where the two monomers assemble in an anti-parallel fashion with four interchain disulfide bonds that form a characteristic 'cystine knot' (Ulyatt et al. 2011; Gacche and Meshram 2014) (**Figure 1.8**). There are five different isoforms of VEGF-A, namely $VEGF_{121}$, $VEGF_{145}$, $VEGF_{165}$, $VEGF_{189}$ and $VEGF_{206}$, deriving from the alternative splicing mechanism in exon 8 of the VEGF-A gene (Gacche and Meshram 2014) (**Figure 1.9**).

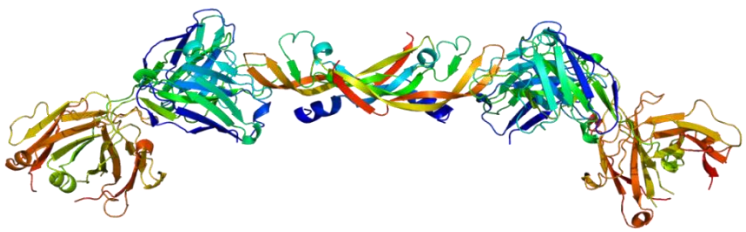

Figure 1.8: Structure of homodimeric VEGF-A. *Source: RCSB PDB.*

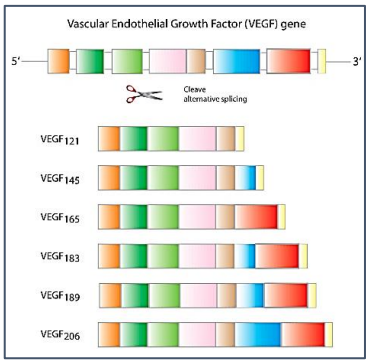

Figure 1.9: Alternative splicing of VEGF-A gene and the isoforms produced

The receptors related to the VEGF growth factor family are cell surface RTKs and there are three of them: VEGFR-1 (Flt-1), VEGFR-2 (KDR/Flk-1) and VEGFR-3 (Flt-4). There is also a second class of non-signalling co-receptors named neuropilins (Ferrara et al. 2003; Hillen and Griffioen 2007) (**Figure 1.10**).

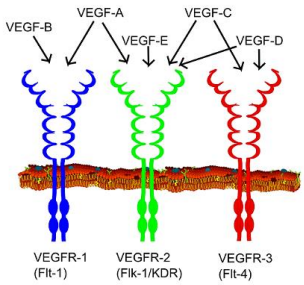

Figure 1.10: Main receptors of VEGF family and their ligands. *Source: cancerpublications.com.*

VEGFR2 is the major signal transducer for the mitogenic, angiogenic and permeability-enhancing effects of VEGF and is activated by VEGF-A, with a binding affinity as Kd of approximately 75-125pM, whereas VEGF-E is a selective agonist for this receptor (Ferrara et al. 2003; Shibuya 2004; Cudmore et al. 2012) (**Figure 1.11**). It is abundantly expressed in vascular ECs and lymphatic ECs, as well as neuronal cells, megakaryocytes and hematopoietic stem cells. It consists of an extracellular part with seven immunoglobulin–like domains, a transmembrane domain, and an intracellular part with two tyrosine kinase domains. A kinase-insert domain lies between the two tyrosine kinase domains (Zhu and Zhou 2015).

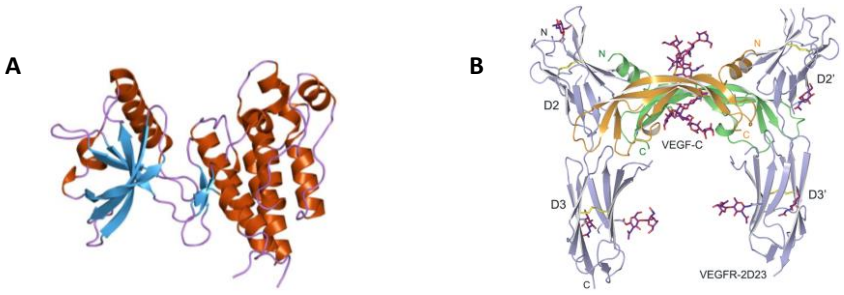

Figure 1.11: Structures. A: Structure of VEFGR2. *Adapted from RCSB PDB.* **B:** Crystal structure of VEGFR2 in complex with one of its ligands, VEGF-C. *Source: (Leppänen et al. 2010).*

Binding of VEGF-A to VEGFR2 triggers the dimerization of two monomers of the receptor and the trans-autophosphorylation and activation of the kinase domain, with subsequent ligand-dependent activation of the downstream signalling cascade leading to proliferation and migration of ECs and pro-angiogenic signal transduction. The autophosphorylation of VEGFR2 occurs in two phosphorylation sites, tyrosines-1054/1059 (Y1054/Y1059) in the tyrosine kinase domain, and this event is one of the earliest and most critical for the activation of the receptor upon VEGF binding. Another major phosphorylation site on human VEGFR2 is tyrosine-951 (Y951), which is in the kinase-insert domain and mediates EC permeability and migration. There are also two other major phosphorylation sites on VEGFR2, that are tyrosines-1175 (Y1175) and -1214 (Y1214) in the C-terminus area (Zhu and Zhou 2015). Y1175 is responsible for EC proliferation and migration and Y1214 for EC migration (Falcon et al. 2016). Especially phospho-Y1175 binds the p85 subunit of PI3K and PLC-γ leading to the initiation of the PLC-γ-PKC-Raf-MEK-MAPK pathway (PLC-γ=phosphoinositide phospholipase C-γ, PKC=protein kinase C) responsible for the proliferation of ECs. Some of the main downstream proteins related to VEGFR2 activation in ECs are the Src kinase, the focal adhesion kinase (FAK), PI3K, AKT, PLC-γ and mTOR. The EC growth is related to the activation of the Raf-MEK-ERK pathway, whereas the prosurvival effects are mediated by the PI3K/AKT pathway (Ferrara et al. 2003; Koch et al. 2011; Shibuya 2013; Gacche and Meshram 2014) (**Figure 1.12**).

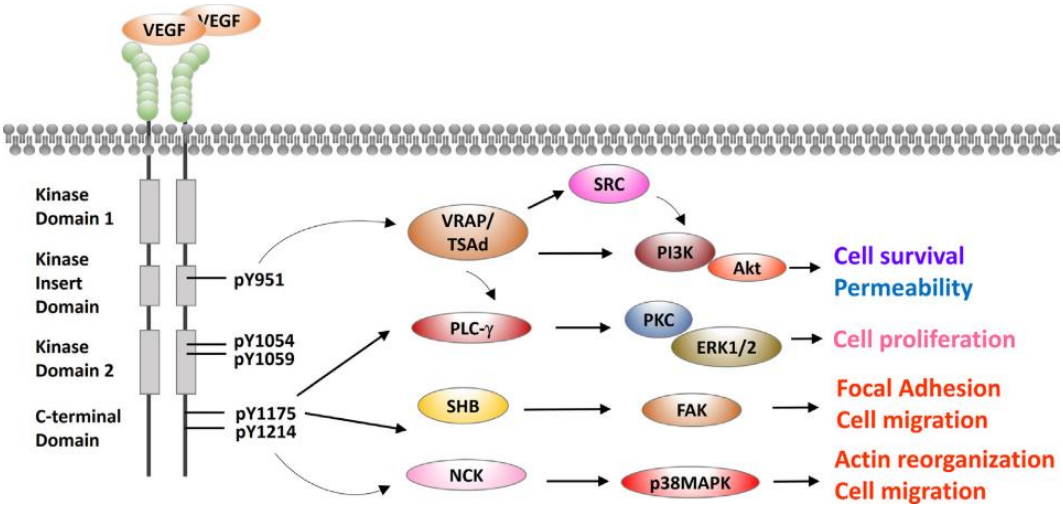

Figure 1.12: Cross talks between VEGFR2 and other signalling pathways in ECs. VEGFR2 is depicted with an extracellular domain, a juxtaposed transmembrane domain and intracellular kinase domains. Extracellular domain of VEGFR2 is composed of seven IgG-like domains to bind to its cognate ligand VEGF. Intracellular domain has two tyrosine kinase domains, which are split by a kinase-insert domain of 70 amino acids. Five major phosphorylation residues Y951, Y1054, Y1059, Y1175, and Y1214 are highlighted. SH2 domain-containing adaptor proteins are recruited by these phosphorylated tyrosine residues, including VRAP/TSAd, PLC-γ, SHB, and NCK. These adaptors mediate the downstream effects of VEGFR2 including cell proliferation, permeability, cell survival, and cell migration. *Source: (Zhu and Zhou 2015).*

The other main receptor, VEGFR-1, is also a substrate for VEGF-A, but has much lower expression levels compared to VEGFR2 (Cudmore et al. 2012). VEGFR-1 is a signalling receptor critical for the activation of the endothelial nitric oxide synthase (eNOS) and the *in vitro* angiogenesis. It can promote EC differentiation into vascular tubes via nitric oxide (NO) production and the two VEGF receptors seem to be in a continuous cross-talk for the regulation of angiogenesis (Bussolati et al. 2001; Ahmad et al. 2006). The main specific ligands of this receptor is placental growth factor (PLGF), a secreted dimeric protein of the VEGF family, and VEGF-B, and it has been shown that PLGF can promote branching angiogenesis by interacellular signalling through VEGFR-1 (Cai et al. 2003). Although VEGFR-1 shows a many-fold higher affinity for VEGF-A than VEGFR2, it has poor intracellular signalling capability and weaker ligand-dependent tyrosine kinase activation than VEGFR2. It is thought to be mainly involved in inflammatory responses for the migration of monocytes, as well as the hematopoietic pathway and the recruitment of endothelial progenitors. VEGFR-1 expression is also tightly related to oxygen levels, with hypoxic conditions severely upregulating this receptor via a hypoxia-inducible factor 1a (HIF-1a) –dependent manner (Hornig et al. 2000; Ferrara et al. 2003; Shibuya 2004; Ulyatt et al. 2011).

In addition to the homodimerization necessary for these receptors to be activated, there has also been reported a heterodimerization process between VEGFR-1 and VEGFR2. The heterodimer can negatively regulate the signalling and cellular response following VEGFR2 homodimer stimulation, especially during the angiogenic process, which adds even more complexity to the understanding and manipulation of the VEGF/VEGFR system (Cudmore et al. 2012).

The last receptor VEGFR-3 is the least studied one and it does not show any affinity for VEGF-A, binding instead to VEGF-C and VEGF-D. It seems to play an important role in lymphangiogenesis (Ferrara et al. 2003).

Another important receptor related to the angiogenic process is the soluble form of VEGFR-1 (sVEGFR-1). This soluble variant of VEGFR-1 is generated by differential splicing of the VEGFR-1 mRNA and is descibed as a natural antagonist of the VEGF and PLGF activity, by reducing the levels of active VEGF-A (Hornig et al. 2000; Al-Ani et al. 2010). This splice variant that was described by Kendall et al. back in 1993 (Kendall and Thomas 1993), consists of 6 out of the 7 extracellular immunoglobulin-like domains of the full-length receptor and a C-terminal extension of 31 amino acids derived from an intron. Soluble VEGFR-1 has been shown to form heterodimers with full-length VEGFR2, leading to a dominant negative regulator complex which inhibits angiogenesis *in vivo* by eliminating receptor autophosphorylation. In specific, sVEGFR-1 can form a VEGF-stabilized ternary complex with the extracellular ligand-binding region of VEGFR2 leading to inhibition of the signal transduction (Kendall et al. 1996; Hornig et al. 2000; Ahmad and Ahmed 2004). This receptor most probably participates in a paracrine regulation of local angiogenesis also ensuring a more normalized response to abundant VEGF presence. Furthermore, sVEGFR-1 is regulated by hypoxic conditions, which lead to its overexpression, whereas hyperoxia has the opposite effect. Therefore, sVEGFR-1 comprises a naturally expressed endogenous antagonist that can halt the activation of VEGFR-1 and VEGFR2 acting anti-angiogenically (Kendall et al. 1996; Hornig et al. 2000).

Up to date evidence shows that the VEGF-A/VEGFR2 interaction may be the most important one for sprouting angiogenesis promoting cancer growth, progression and metastasis. It has also been shown that many human tumours show an upregulation

of the VEGF mRNA, and the VEGFR2 expression levels in ECs surrounding tumours seemed to be elevated (Shibuya 2004; Hillen and Griffioen 2007; Gacche and Meshram 2014). This is the main reason why targeting the VEGF-A/VEGFR2 system directly deemed as a promising anti-cancer approach and still attracts a lot of research interest.

Especially for TNBC, the VEGF-A/VEGFR2 system seems to be upregulated and correlated with worse prognosis and a more aggressive phenotype. VEGFR2 expression is crucial for breast cancer cells with mutant p53 and the activation of the receptor increases mammospheres and enzymatic activity in TNBC cells (Pfister et al. 2015). Elevated VEGF-A expression was also associated with more aggressive cancer, as happens also with increased VEGFR2 production, which was linked to a decreased 5-year breast cancer specific survival in TNBC patients. VEGFR2 expression, EGFR expression and the gene copy numbers were all significantly associated with TNBC (Rydén et al. 2010a; Rydén et al. 2010b).

Targeting VEGFR2 and downstream kinases might not only help in developing better therapies for TNBC, but also overcome the chemo- and radiation resistance in TNBC, which are more common in this unique subtype (Bousquet et al. 2017).

1.3.3 Anti-angiogenic agents

As noted already, targeting the process of angiogenesis involved in tumour progression could provide a new therapeutic approach against cancer and especially against TNBC, where there are much fewer treatment options. Considering the importance of the VEGF-A/VEGFR2 system in angiogenesis, it is logical that this system is one of the most vital targets against carcinogenesis (Li et al. 2016).

In the absence of neovascularization, tumour growth is limited and so is the potential of metastasis. Anti-angiogenic agents could potentially reduce the size of the primary tumour and also tumour vascularity, thus limit the number of tumour cells that can metastasize and the vascular surface available for extravasation. Anti-angiogenic treatment may normalize tumour vasculature and the resulting vessels, which now have a closer resemblance to the normal ones, might be harder for tumour cells to penetrate than the chaotic and disorganized tumour blood vessels (Falcon et al. 2016).

Several studies have proved that combining existing anti-VEGF agents with chemotherapy or radiation therapy could result in a better effect compared to monotherapies (Ferrara et al. 2003). Several pharmaceutical companies undertake research in developing small molecular inhibitors of the tyrosine kinase activity of VEGFR2, even though there is also an unrelated blockade of VEGFR-1, due to the high structural homology. Other potential targets related to VEGFR2 are the autophosphorylation sites and its downstream cascade (Shibuya 2004; Hillen and Griffioen 2007).

There are three main categories of anti-angiogenic agents currently in clinical trials: 1. monoclonal antibodies against specific pro-angiogenic growth factors and their receptors, 2. tyrosine kinase inhibitors (TKIs) of several growth factor receptors and 3. inhibitors of the mTOR pathway (Gacche and Meshram 2014).

The most widely studied and currently prescribed as combination therapy for many cancer types is the monoclonal antibody against VEGF-A bevacizumab, which will be discussed in the next section. Other antibodies approved include cetuximab (target: EGFR), trastuzumab (target: HER2) and panitumumab (target: EGFR). Many other antibodies are still under research, such as HuMV833 (targets: $VEGF_{121}$ and $VEGF_{165}$), IMC-18F1, IMC-1121B and ImClone (target: VEGFR-1 or 2). The antibody MIL60 is also currently being developed, which has similar VEGF-neutralizing activity to bevacizumab and has shown promising clinical results (Gacche and Meshram 2014). Since bevacizumab remains quite expensive for developing countries, alternative antibodies were identified, and MIL60 seems to have similar antigen binding activity and affinity for VEGF as bevacizumab. It has also been suggested to share the same epitopes on VEGF with bevacizumab, therefore it could potentially have a similar toxicity profile. Many other candidates with stronger affinity for VEGF proved more toxic than the parent antibody (Yang et al. 2014).

Approved TKIs for anti-angiogenic combination therapies are axitinib, cabozantinib, pazopanib, regorafenib, sorafenib, sunitinib and vandetanib. Unfortunately, most of the first generation anti-angiogenic TKIs such as sunitinib, sorafenib and pazopanib, have adverse effects unrelated to the blockade of VEGF, as they also inhibit a wide range of kinase targets such as PDGFRs and B-Raf in addition to the VEGFRs. The

second generation anti-angiogenic TKIs such as axitinib, tivozanib and cediranib though, have improved potency and selectivity for VEGFRs. Several of these TKIs have been approved by the Food and Drug Administration (FDA) in solid tumours, including metastatic renal cell carcinoma, gastrointestinal stromal tumours, pancreatic neuroendocrine tumours, unresectable hepatocellular carcinoma, advanced soft tissue sarcoma and advanced medullary thyroid cancer (Falcon et al. 2016).

The majority of the ongoing clinical trials on anti-VEGF based therapies are focused on expanding their benefit in other approved indications, either by trying combinations with agents that inhibit alternative pro-angiogenic pathways or by combining them with cancer immunotherapy agents. In any case, the amount of clinical trials targeting angiogenesis (over 3000) reflects the consistent scientific and therapeutic interest in inhibiting this process and remains a major active area in the mainstream of anti-cancer research (Gacche and Meshram 2014; Falcon et al. 2016; Li et al. 2016).

However, although anti-VEGF therapy for breast cancer specifically was initially welcomed with great enthusiasm, there are many side problems that need to be dealt with if higher efficacy is desired. Even though inhibition of pathological angiogenesis could be the answer, there should be extra consideration on the potential blockade of the physiological process as well. There is also the paradox that limiting the blood supply of the whole tumour body hinders the access of anti-cancer drugs to the tumour, reducing their efficacy. There are also numerous compensatory angiogenic feedback loops that may prevail, along with off-target toxicities and adverse effects that might decrease the therapeutic benefit. In any case, blocking a single pro-angiogenic molecule or pathway may have little impact on the total tumour angiogenesis and growth, since there are many angiogenic factors that can be vital for each different development stage of a tumour.

Other challenges include the ability of tumours to acquire resistance against anti-angiogenic agents and aggressively recur after withdrawal of the anti-angiogenic treatment. The limited availability of angiogenesis-specific biomarkers for TNBC in the current clinical practice is also a halting factor for the success of any anti-angiogenic agent. Finally, different angiogenic mechanisms might be involved in the different

tumour subtypes and at various stages, making anti-angiogenic drug development even more challenging, as a combination of many agents targeting different tumour signalling pathways may be necessary (Ferrara et al. 2003; Gacche and Meshram 2014).

1.3.3.1 Anti-VEGF-A antibody (Bevacizumab)

The first anti-angiogenic drug to be marketed was bevacizumab (Avastin®). It is a recombinant humanized monoclonal antibody that binds all isoforms of VEGF-A extracellularly, inhibiting their binding to VEGFRs, which would otherwise activate the angiogenic downstream signalling cascade (**Figure 1.13 A**).

Bevacizumab was initially approved as a combination therapy with chemotherapy by FDA in 2004 against a variety of cancer subtypes, with metastatic colorectal cancer being the first indication. Currently bevacizumab has been approved as a monotherapy for recurrent glioblastoma, in combination with chemotherapy for metastatic colorectal cancer, metastatic non-squamous non-small cell lung cancer, platinum resistant ovarian cancer and metastatic cervical cancer and in combination with IFNα for metastatic renal cell carcinoma (Hillen and Griffioen 2007; Rini 2007; Falcon et al. 2016) (**Figure 1.13 B**). It was initially on FDA "fast track" approval process for metastatic breast cancer (HER2-negative), for which it actually received approval in 2008, but it was eventually revoked due to non-significant improvement in the overall survival rates as first line treatment for patients with advanced breast cancer in November, 2011.

Avastin® caused several side effects, such as high blood pressure and hemorrhaging. Other potential side effects include gastrointestinal perforations, thromboembolysis and impaired wound healing (Hillen and Griffioen 2007; Ebos et al. 2009a; Thomssen et al. 2012; Gacche and Meshram 2014; Zhu and Zhou 2015). There was evidence that it could slow the progression of metastatic breast cancer when combined with paclitaxel, but the quality of life was not enhanced and the life expectancy remained the same. On the contrary, some preclinical studies proved that bevacizumab could promote a more aggressive and metastatic behaviour of breast cancer cells. There is also much evidence suggesting possible acquired resistance. It has also been proposed

that the reduced blood supply to the tumour affects drug penetration and increases hypoxic stimulation with subsequent VEGF elevation in the tumour (Ebos et al. 2009b).

As evident from the above case, it seems more likely that a future efficient cancer therapy will be composed of a combination of chemotherapy and one or several other agents that can inhibit multiple pathways with reduction of the acquired resistance, as well as minimal implications to the physiological process. Novel combination approaches also include simultaneously targeting multiple pro-angiogenic factors that impact tumour growth at different stages and affect the different steps of blood vessel maturation. New agents in these combinations could also help in reducing the necessary dose of approved drugs with dose-related adverse effects. Other strategies, such as intermittent dosing schedules, sub-maximum tolerated dosaging to delay hypoxia onset thus improving oxygenation and delivery of co-administered drugs, seems to be the way forward for anti-angiogenic therapies. In summary, the future of anti-angiogenic treatment depends on identifying predictive biomarkers to monitor response and novel combination approaches that can overcome innate resistance, avoid induction of acquired resistance and provide a significant survival benefit to the patients (Falcon et al. 2016).

A

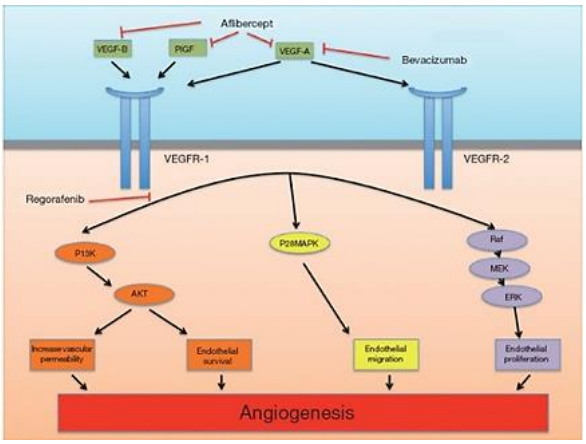

B

Figure 1.13: Bevacizumab. A: Pro-angiogenic targets of bevacizumab, aflibercept and regorafenib. Bevacizumab binds to VEGF-A and interrupts the interaction with VEGFR-1 and -2. Apart from VEGF-A, aflibercept binds to and interrupts also the function of VEGF-B and PGF. Regorafenib is a small molecule, multi-kinase inhibitor, whose targets include VEGFR-1, -3, RAF, TIE-2, and mutant oncogenic kinases KIT, RET and BRAF. *Source: (Jitawatanarat and Ma 2013).* **B:** FDA approves bevacizumab for recurrent ovarian cancer. *Source: Medscape.*

1.3.4 Reactive oxygen species in angiogenesis

Another vital mechanism taking part in angiogenesis is the production and homeostatic maintenance of reactive oxygen species (ROS). Cancer cells are known to have a different redox status compared to normal cells in most cancer types. Due to the high metabolic rates and signalling aberrations, cancer cells usually exhibit elevated levels of ROS. Therefore, modulating redox potential with new drugs could prove helpful in the fight against cancer (Gorrini et al. 2013).

Recent research has shown that the angiogenic cascade is tightly interweaved with ROS production and signalling, and ROS can be critical regulators of angiogenic homeostasis (Ushio-Fukai 2006; Ushio-Fukai and Nakamura 2008; Kim and Byzova 2014). The main sources of ROS in ECs are NAPDH oxidases (NOX) that maintain basal ROS levels, and the mitochondrial respiratory chain. In ECs, the production of ROS is continuous in low levels and different isoforms of NOX can enhance ROS production, which leads to stimulation of VEGFR2 auto-phosphorylation and protein kinases activation, therefore promoting EC migration and proliferation. ROS can also increase EC permeability and enhance cell adhesion surface molecule expression. The stimulation of VEGF itself can also increase their production in low levels, an important event for the subsequent VEGF-induced c-Src activation and phosphorylation of VE-cadherin. Thus, ROS can support growth factor signals and promote angiogenesis in various *in vivo* and *in vitro* tests by upregulating the synthesis of many molecules (such as MMPs) and transcription factors. In addition to these actions, NOX can also stimulate redox-sensitive signalling cascades independently (for example PI3K/AKT, ERK, Ras, c-Src pathways). Finally, even exogenous ROS can stimulate VEGF expression, which can be used as a marker of the angiogenic switch, and they can promote proliferation, migration, cytoskeletal reorganization and tubular morphogenesis in ECs (Lamalice et al. 2007; Radomska-Lešniewska et al. 2016).

However, the effects of ROS on vascular function depend drastically on the amount of ROS present. Low doses of ROS were shown to promote angiogenesis via cell membrane damage and subsequent basic FGF-2 release. This initiates the intracellular production of ROS through NOX and initiation of downstream signalling for

proliferation, migration and tube formation. On the other hand, high doses of ROS can provoke oxidative stress and subsequent death of cells necessary for angiogenesis, thereby inhibiting the whole process. In addition to dose, timing and application method can also determine the pro- or anti-angiogenic potential of ROS. The complex role of ROS in angiogenesis is also outlined by the fact that antioxidant therapies were sometimes unsuccessful in inhibiting conditions characterized by over-activated angiogenic events (Radomska-Lešniewska et al. 2016; Kruk and Aboul-Enein 2017).

Cellular hypoxia is a key regulator of ROS production. During hypoxic events, the electron transport chain in mitochondria becomes uncoupled, leading to leakage of electrons and formation of oxygen species. Hypoxia can also upregulate NOX and activate hypoxia-inducible factor-1 (HIF-1), which induces proangiogenic genes. Cancer has been associated with abnormal ROS production and a variety of cells derived from human tumours demonstrate elevated ROS levels. Cancer cells themselves are an abundant source of ROS via their defective respiration and oxidative metabolism. These elevated levels are also responsible for the upregulation of HIF-1a and VEGF expression through activation of the PI3K/AKT pathway or the MEK/ERK pathway (Radomska-Lešniewska et al. 2016).

It should be noted though, that ROS are primarily formed during normal physiological processes such as the aerobic metabolism of molecular oxygen, inflammation and immune response. They act as regulators of signalling pathways, secondary messengers and inducers of mitogenic responses. Their involvement in carcinogenesis and pathological angiogenesis is coincidental and strongly related to other dysregulated processes and mechanisms of defence that are so common in cancer cells (Kruk and Aboul-Enein 2017).

1.4 Carbon monoxide

1.4.1 General characteristics and toxicity

Carbon monoxide (CO) is an inert gas, colourless, odourless, tasteless and non-irritating. It is a low molecular weight diatomic molecule (M.W. 28.01), slightly less dense than air and with relatively poor water solubility. The bond length between the carbon atom and the oxygen atom is 112.8 pm, consistent with a triple bond, making

it a chemically stable molecule. Its ground electronic state is a singlet state, with no unpaired electrons, and the oxidation state of carbon is +2, since all the bonding electrons are attributed to the more electronegative oxygen (Wu and Wang 2005).

CO has long been known as a "silent killer", with CO intoxication potentially fatal due to its 210 – 250 times higher affinity for iron atoms in haemoglobin than oxygen, eventually forming carboxyhaemoglobin (HbCO) (Wu and Wang 2005; Ryter et al. 2006; Maruyama et al. 2012). This binding significantly reduces the oxygen-storage function and the oxygen-carrying capacity of haemoglobin, consequently leading to tissue hypoxia and CO poisoning in humans. Most common symptoms of CO poisoning include headaches, dizziness, nausea, vomiting and visual confusion, eventually leading to coma and death, if remaining untreated (Wu and Wang 2005; Foresti et al. 2008). The most important organs to be severely damaged by CO would be the brain and the heart, as proved by the increased rates of lipid peroxidation and apoptotic cell death (Piantadosi et al. 1997).

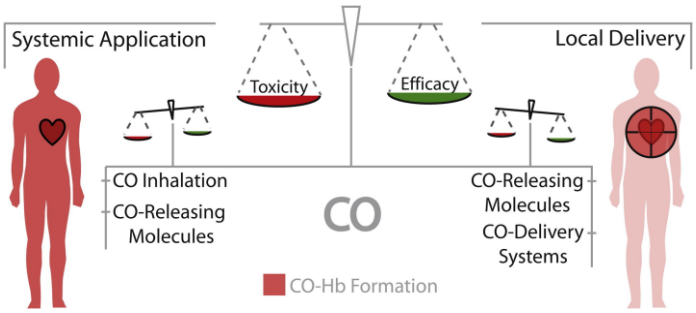

Figure 1.14: Therapeutic use of CO. The therapeutic use of CO is impeded by safety challenges following non-targeted, systemic administration and the use of toxicologically critical transition metals. An emerging number of local delivery approaches addressing these issues have recently been introduced and provide exciting new starting points for translating the fascinating preclinical potential of CO into a clinical setting. *Source: (Steiger et al. 2016).*

However, the binding of CO to haem iron centers in haemoglobin functions more like a detoxification mechanism than being the major reason of the observed CO poisoning (Schatzschneider 2015). The increase in the concentration of CO in tissues is more responsible for these symptoms, since elevated tissue levels lead to disruption of the mitochondrial function by inhibiting their respiratory system. More specifically, CO can bind to proteins of the mitochondrial electron transfer chain including haem,

such as the mitochondrial cytochrome c oxidase (complex IV), hence harm cellular respiration. Since the mitochondria are affected, membrane permeability is increased and electron leakage is consequently observed, mainly from complex III, leading to the formation of ROS (Lo Iacono et al. 2011; Gullotta et al. 2012; Long et al. 2014).

1.4.2 Endogenous production and physiological functions – Haem oxygenases

It was not only until early 1950s when CO was found in the exhaled air of healthy humans as a metabolite (Sjöstrand 1949b,a; SjöStrand 1951). It appears that there is an endogenous CO production process in every healthy human organism. This CO is generated as a by-product of the enzymatic degradation of haem, catalysed by the family of enzymes called haem oxygenases (HOs). As a consequence, there is a small amount of HbCO normally present in healthy human organisms. In reality, the rate of endogenous CO production was estimated around 0.42mL/h (18.7μmol/h), so the majority of blood HbCO comes from the endogenous production process, corresponding to blood CO levels of 0.4 –1%, which is a normal range for non-smoker humans (Wu and Wang 2005; Ryter et al. 2006).

Haem oxygenases (HO) can be found as two isoforms: HO-1 is redox-sensitive-inducible (32.8kDa), and HO-2 is a constitutive form (36kDa), controlled by post-translational modifications and expressed mainly in the brain, endothelium and testis (Wu and Wang 2005; Bannenberg and Vieira 2009; Chigaev et al. 2014). There has been a third isoform identified, HO-3, but its physiological role still remains unclear. This enzyme catalyses the conversion of haem to ferrous iron, CO and biliverdin, which is subsequently reduced to bilirubin by biliverdin reductase (Motterlini et al. 2002) (**Figure 1.15**).

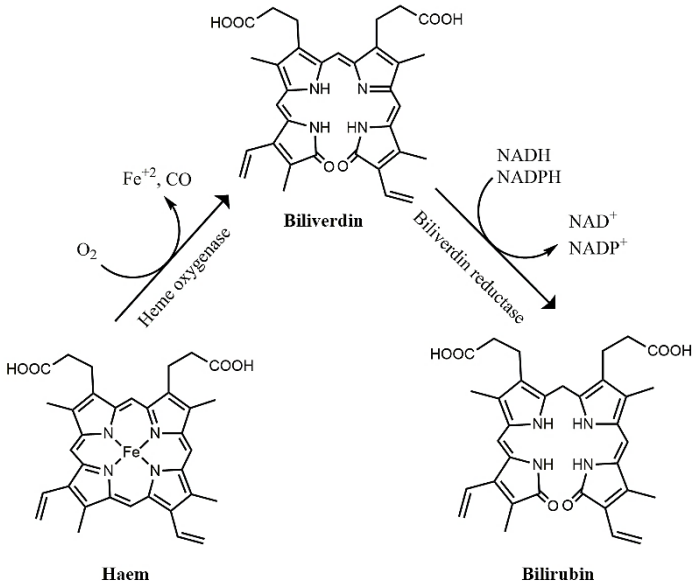

Figure 1.15: Endogenous production of CO from the enzymatic degradation of haem. *Source: (Kourti et al. 2017).*

Haem oxygenase-1 (HO-1) is a well-characterized cytoprotective enzyme, which is widely upregulated during cellular responses to pro-oxidative and pro-inflammatory stimuli. These stimuli include haem, growth factors (especially VEGF), NO, fluctuations in oxygen levels, cytokines and peroxynitrite ($ONOO^-$) among others. HO-1 has different basal expression levels in the various cell types and tissues and is responsible for the maintenance of cellular homeostasis, by controlling oxidative injury, attenuating inflammation and affecting cell proliferation. Its by-products, biliverdin and bilirubin, form a system that has a high antioxidant capacity, through scavenging ROS (Dulak et al. 2008; Ferrando et al. 2011; Loboda et al. 2015b).

Haem oxygenase-1 is known to offer pleiotropic protection to ECs *in vitro*, enhancing their proliferation and cell cycle progression. Several human tumours, such as renal and prostate cancer, may overexpress HO-1 and lead to an enhanced cell survival and anticancer drug resistance. As a result, inhibition of HO-1 was proposed as another potential anticancer strategy, especially since HO-1 may also have pro-angiogenic effects in inflammatory conditions associated with cancer (Dulak et al. 2008; Loboda et al. 2015b).

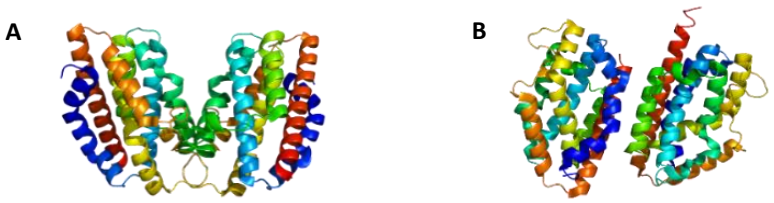

Figure 1.16: Structures of Haem oxygenase-1 (**A**) and -2 (**B**). *Source: RCSB PDB.*

Although recognised as a normal metabolite, the physiological role of the endogenously produced CO was yet to be identified until 1993 when CO was eventually proved to act as a molecular mediator, a neurotransmitter (Verma et al. 1993). Since then, researchers classified CO with two other biologically active diatomic molecules, that is NO and hydrogen sulphide (H_2S), forming the group of gaso-transmitters (Romão and Vieira 2015).

The primary cellular binding targets for CO have not been clearly identified yet, but haem proteins seem to be the main targets, especially soluble guanylate cyclase (sGC). sGC is a haem protein, which has a covalent haem co-factor anchored via a histidine ligation to the iron, and the *trans* position to the histidine is able to bind either NO or CO. This leads to a two- to four-fold increase in cGMP production from GTP by CO, far lower than the activation induced by NO, posing a question if this is indeed its real primary cellular target (Poulos 2006; Schatzschneider 2015). Other functions of CO, apart from haem catabolism and increase in cGMP production, involve activation of Ca^{2+}-dependent potassium channels and MAPKs (Kaczara et al. 2015; Gessner et al. 2017).

A well-reported regulatory activity of CO regards the cardiovascular system. The vasorelaxant properties observed are justified by the elevated cGMP levels in the vascular smooth muscles and aorta, and have been proved to be non-endothelium mediated (Bannenberg and Vieira 2009). The vasodilatory mechanisms may implicate ion-dependent channels, as well. Additionally, blood platelet aggregation was reported to be inhibited by endogenous and exogenous CO (Wu and Wang 2005; Ryter et al. 2006; Olas 2014). As with other observations, though, the anti-coagulative functions of CO seem to be contradicting, since earlier research reported opposite outcomes (Marshall and Hess 1981).

The anti-inflammatory effects of CO have been well established by various studies. The possible mechanisms include the inhibition of lipopolysaccharide (LPS)-dependent pro-inflammatory cytokine expression (such as tumour necrosis factor-α (TNFα), interleukin-1b (IL-1b), IL-2, macrophage inflammatory protein-1b (MIP-1b)), and the augmentation of anti-inflammatory cytokines, such as IL-10 (Otterbein et al. 2000; Wu and Wang 2005; Ryter et al. 2006; Olas 2014). This property of CO is probably mediated by p38 MAPK and MKK3, independently of the cGMP pathway, as demonstrated for RAW264.7 macrophages (Otterbein et al. 2000). CO gas administration or CO-releasing molecules (CORMs) treatment reduces macrophages' activation by LPS and promotes expression and stabilization of HIF-1, which regulates inflammatory and apoptotic genes (Motterlini et al. 2005a).

The combination of the vasodilatory and anti-inflammatory effects of CO may contribute to the indicated CO protection of myocardial cells against ischemia-reperfusion injury, myocardial infarction and cardiac rejection cases (Clark et al. 2003; Guo et al. 2004; Wu and Wang 2005).

Recent research has also revealed anti-apoptotic and anti-proliferative activities of CO on different cell types. Brouard et al. demonstrated that reduction in TNFα expression leads to inhibition of TNFα-initiated apoptosis in fibroblasts and ECs through p38 MAPK and NF-κB activation (Brouard et al. 2000). Increased levels of cGMP and HO-1 activity may play an important role in this inhibitory effect on apoptosis, as well. Anti-apoptotic effects have also been reported in vascular smooth cells and hepatocytes. The anti-proliferative properties, on the other hand, were mainly observed in smooth muscle cells and are mediated through the activation of guanylyl cyclase and p38 MAPK, contributing to the general protective actions of CO (Bannenberg and Vieira 2009). However, anti-apoptotic effects are not observed in all cell types studied and this is also true for the reported anti-proliferative effects (Wu and Wang 2005; Ryter et al. 2006; Olas 2014).

Another physiological effect mediated by CO is the inhibition of hypoxia-induced VEGF expression (Goldberg and Schneider 1994). CO can also inhibit the cytochrome P450 family of enzymes, since the level of P450 is affected by the availability of cellular haem. In addition, CO is indirectly related to oxidative stress, although it is not a free

radical itself. CO can bind to haem proteins and alter their role in oxidative stress control, hence indirectly change the cellular redox status. The pro-oxidant effects of CO were demonstrated in the vascular endothelium and other cell types (Wu and Wang 2005). However, as with most of the effects of CO, the pro-oxidant activity remains controversial, since many publications suggest opposite results. In a recent study by Wilson et al. (Wilson et al. 2017), CO was found to increase VEGF in LPS-activated BV2 microglial cells after 3h of treatment with a novel CORM, namely CORM-401, although the levels return to normal after 6h. It is also implied to have an anti-oxidant effect, contradicting many publications stating the pro-oxidant activity of CO. These opposite results are very common in the case of CO and CORMs, as highlighted also in other recent publications (Kourti et al. 2017).

Finally, CO also affects some nervous system functions and expresses neuroprotective and neurotherapeutic properties, potentially mediating memory and circadian rhythm (Mahan 2012; Wilson et al. 2017).

The range of systems physiologically affected by and responding to CO is wide as evident above and in many publications. Some of these systems and organs are listed below, just to demonstrate the complexity of the HO/CO-related signalling networks:

A. Circulatory System

B. Nervous System

C. Respiratory System

D. Reproductive System

E. Gastrointestinal System

F. Liver

G. Kidneys

H. Pancreas

As anticipated from the above list, the physiological functions of CO are various, but the clearer image still remains elusive. This is due to the contradicting results acquired for different tissues, cell types and *in vivo* models.

1.4.3 Therapeutic applications

- Inflammatory diseases

The anti-inflammatory potential of CO observed *in vitro* was also tested in *in vivo* models of inflammatory diseases, such as sepsis and asthma. CO-pre-treated mice injected with LPS showed decreased TNFα levels and increased IL-10 production. This result was mediated by MKK3 and suggested a protective role for CO in sepsis via inflammatory cytokine production modulation (Ryter et al. 2006). In asthma, CO pre-treatment in mice resulted in modest increase in the total number of all inflammatory cells involved, such as macrophages, eosinophils and neutrophils. Exogenous CO was also able to reduce IL-5 production, indicating that CO potentially regulates inflammation in asthma too (Ryter et al. 2006). CORM-2 reduced the histamine release under immunological conditions, suggesting another potential use of CORMs for the treatment of allergies. In a study where UV irradiation was employed for its ability to provoke immunosuppression, CO, in the form of CORM-2, could provide protection. Finally, neuro-inflammation also seems to be suppressed by CO in a variety of conditions, such as autoimmune encephalomyelitis and multiple sclerosis (Motterlini et al. 2005a).

- Cardiovascular diseases

Several cardiovascular system-related conditions have been tested for treatment via CO administration. In myocardial infarction models a CO-donor molecule, CORM-3, included in the reperfusion media after ischemia, had a beneficial effect on cardiac performance and reduced infarct size. In systemic hypertension *in vivo* models, CO managed to reduce blood pressure. In addition, in vascular injury conditions, CO showed an inhibitory effect on the proliferation of smooth muscle cells and lowered leukocyte infiltration activity (Ryter et al. 2006). Finally, CORM-2 prevented the increase in mean arterial pressure in a rat model of acute hypertension and CORM-3 and CORM-A1 succeeded in vasorelaxing an isolated aortic ring pre-contracted with phenylephrine (Motterlini et al. 2005a).

- Ischaemia/Reperfusion

Ischemia-Reperfusion (I/R) during lung surgery and transplantation can potentially lead to tissue injury. CO showed protection against liver and lung I/R injuries by exerting antiapoptotic effects through p38, MKK3 and c-Jun N-terminal kinase (JNK) activity modulation. The inhibition of apoptosis is also related to a downregulation in the expression of apoptosis-related factors, such as caspase-3 (Ryter et al. 2006).

- Organ transplantation

Increasing the probability of survival after organ transplantation still remains a medical need. Despite the fact that HO-1 expression has mostly been tested against organ transplantation models, CO was also proved to have a beneficial effect in suppressing graft rejection in a mouse to rat cardiac transplant model. It seems that the anti-inflammatory and inhibitory action on platelet aggregation abilities of CO contribute to this result (Sato et al. 2001). It has been shown that CO can be useful in lung transplantation xenografts, as well. Inhalation of CO reduced lung injury and rejection due to the anti-apoptotic and anti-inflammatory properties of CO (Song et al. 2003).

However, all the publications regarding the potential therapeutic applications of CO in various disease models raise concerns over the usage of gas mixtures in humans. CO must be administered in a controlled and directed manner, which is quite problematic, in addition to the difficulties in storing and handling this gas with special equipment and in specialized hospital settings. Moreover, the prolonged inhalation of CO may lead to intoxication of the oxygen transport and delivery system, hence making this approach of limited therapeutic use (Motterlini et al. 2005a).

1.5 Carbon monoxide – releasing molecules

1.5.1 General characteristics

Since CO attracts such major scientific interest in terms of its therapeutic potential, large efforts have been made in the past decade to develop safer ways for delivering CO to specific body tissues. The direct administration of CO by inhalation could be considered in cases of targeting the respiratory tract and the lungs, or for the

treatment of a transplant donor or *ex vivo* treatment of an organ to be transplanted. However, as the inhalation of large doses of CO required for sufficient diffusion of therapeutically effective concentrations can prove dangerous, interest has turned to alternative approaches, the most important being CO-releasing molecules (CORMs) (Motterlini et al. 2005a; Bannenberg and Vieira 2009).

CORMs were first introduced as industrial catalysts and for purification purposes. These complexes include a transition metal atom in low oxidation state as core, which is surrounded by a certain number of carbonyl groups as coordinated ligands. CORMs are capable of releasing CO upon activation. Apart from serving as an alternative to the inhalation of CO gas, they have also provided further mechanistic insight into the behaviour of CO in biological systems (Ryter et al. 2006).

The CORM comprises of three parts. First is the *metal centre*, responsible for the main features and toxicity profile of the molecule. The second part is the *coordination sphere* (or CORM sphere – CO groups and ancillary ligands), for determining the responsiveness towards specific stimuli and the CO-release mechanism. More specifically, this part modulates the number of CO groups that can be released, the kinetics of the release process and the trigger mechanism for initiation. The final part is the *drug sphere*, referring to modifications of the periphery of the ancillary ligands pointing away from the metal centre, for tuning the pharmacological parameters of the whole molecule, that is solubility, biocompatibility, targeting and ADME (absorption, distribution, metabolism and excretion) characteristics (**Figure 1.17**). The ability to manipulate the pharmacological characteristics of the molecule is the most important advantage of CORMs over simple CO gas, since it determines the allocation between the different body fluids and tissues and the ability of a CORM to actively or passively target specific cell subpopulations (García-Gallego and Bernardes 2014; Schatzschneider 2015). Furthermore, CORMs also offer a more precise control of the concentration of CO even at low levels, compared to CO gas, whose main obstacle in *in vitro* and *ex vivo* preparations is atmospheric oxygen (Lo Iacono et al. 2011).

The design and synthesis of novel enhanced CORMs has become the main focus in the field recently, however there are still unresolved issues about the appropriate features of these molecules. For example, there is still no consensus whether a high

or low number of CO ligands per metal complex unit would be more useful and what is the optimal speed for the CO release. There is probably not a single profile that these molecules should comply with, but instead, different groups of CORMs should be designed with favourable properties according to the targeted diseases (García-Gallego and Bernardes 2014; Schatzschneider 2015).

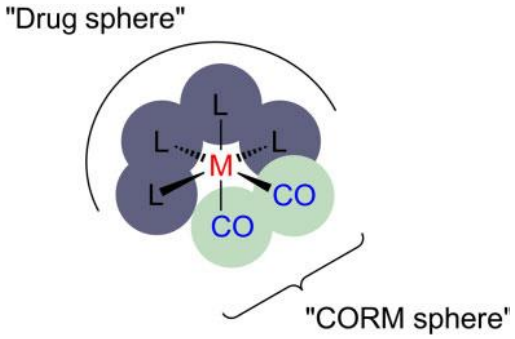

Figure 1.17: The distinct parts of a CORM. In the middle there is the metal centre, responsible for the main features and toxicity profile of the molecule. The second part is the coordination sphere (or CORM sphere) referring to CO and ancillary ligands, for determining the CO-release mechanism and kinetics. The third part is the drug sphere including the periphery of ancillary ligands, for tuning the pharmacological parameters of the whole molecule. *Source: (Schatzschneider 2015).*

1.5.2 Mechanisms of CO release

There are several reviews dealing with the potential trigger mechanisms for the CO release from CORMs. CORMs have been classified in three groups according to the mechanism of CO release: 1) molecules that release CO due to ligand exchange reactions with the medium, 2) molecules that need a proper internal or external stimulus to induce the release, for example light and 3) molecules that explore the differences in cellular microenvironments, such as enzyme expression or pH, to be used as alternative trigger mechanisms (**Figure 1.18**) (Zobi 2013; Simpson and Schatzschneider 2014; Schatzschneider 2015).

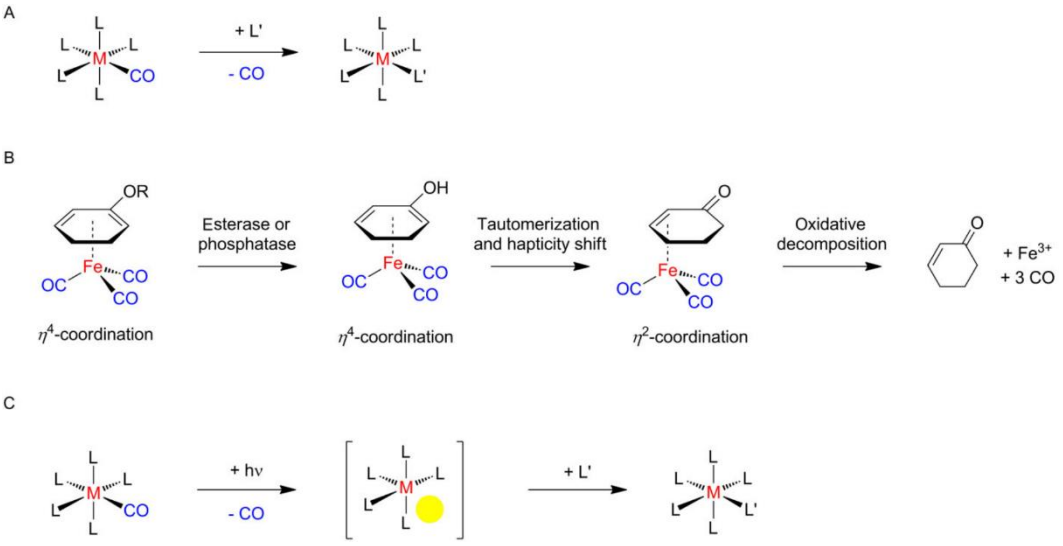

Figure 1.18: Potential trigger mechanisms for CO release from CORMs. *Source: (Schatzschneider 2015).*

An appropriate selection of the metal atom, the number and spatial arrangement of CO groups around it and the nature of the ligands completing the outer coordination sphere of the molecule allows the tuning of the CO-release properties. Compounds with one labile CO group have the simplest release kinetics. In the case of more labile groups per molecule, the profile might be entirely different, therefore making kinetic analysis and identification of potential intermediates much more complicated.

Most of the initial metal-carbonyl complexes release CO upon ligand exchange reactions with the medium, undergoing thermal activation or hydrolysis. This is the case for CORM-2 and CORM-3 (thoroughly discussed in the next section). However, these molecules lack a well-defined and assignable pharmacokinetic (PK) profile, which becomes the main obstacle for their further clinical development. More recent development explores alternative trigger mechanisms for the CO release, such as light or magnetic field, generating more drug-like CORMs. These prodrug compounds would be stable towards the potential biological ligands, allowing for the CO release to occur only upon appropriate internal or external stimulus application (García-Gallego and Bernardes 2014; Schatzschneider 2015).

Since light can be well-focused and offer a precise spatial and temporal control of the release of CO, it would be a very attractive external stimulus only when and where the biological activity is required. An overview of this group of CORMs is discussed in section 1.5.4 (Schatzschneider 2011,2015).

Another potential stimulus would be magnetic fields, previously described by Kunz et al. (Kunz et al. 2013). Kunz and colleagues discovered that biocompatible magnetic iron oxide nanoparticles (Fe_2O_3) (IONPs) can act as carriers for CORMs, which are covalently bound to their surface. For example, a derivative of CORM-3 was anchored to the surface of the IONPs, where the ruthenium carbonyl fragment ligates to a dioxy-phenylalaninato instead of a glycinato group. These particles can be triggered to release CO via heating in an alternating magnetic field (**Figure 1.19**).

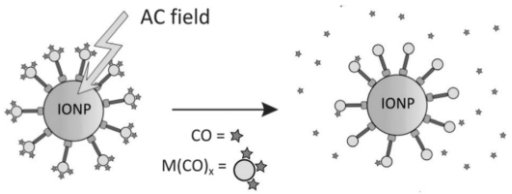

Figure 1.19: Induced CO-release from CORM-functionalized IONPs with the application of magnetic field. *Source: (Kunz et al. 2013).*

Other recent work focuses on the differences in cellular microenvironments for a more localized control of the CO release. Several parameters like cellular pH and redox environment can be exploited in this context. The group of Schmalz explored an alternative approach based on the differences in cellular enzyme expression rates in the various tissues (Romanski et al. 2011). The metal carbonyl complexes synthesized exploit the two possible tautomeric forms of the organometallic ligand, after the exposure of the sensitive group to esterases or phosphatases. A change in the hapticity results in increased sensitivity of the molecule to oxidative decomposition and subsequent CO release (Schatzschneider 2015).

1.5.3 First and second generation CORMs

As mentioned earlier, CORMs were used as an alternative source of CO, because the gas itself was proven to be really toxic and unsuitable for patient use. This idea evovled when it was shown that CO covalently bound to a metal could be carried and released under certain physiological conditions.

The first CORM to be developed was CORM-1, with the molecular formula $[Mn_2(CO)_{10}]$. The limitations of CORM-1 mostly refer to its insolubility in aqueous media and the requirement for photo-activation in order to release its CO groups from

the manganese metal core. In such context, we can classify CORM-1 to the photo-CORM group, mentioned in the next section.

Unlike iron and manganese carbonyl complexes though, which require exposure to light to release CO, ruthenium based CORMs could transfer CO spontaneously, even in the absence of light, and exerted an almost identical pharmacological effect to that observed with CO gas (García-Gallego and Bernardes 2014).

As a result, the second CORM to be developed was CORM-2, with the molecular formula $[Ru(CO)_3Cl_2]_2$. CORM-2 has a ruthenium core and is insoluble in aqueous media, requiring organic solvents such as dimethyl sulfoxide (DMSO) to be dissolved. The loss of CO groups occurs upon ligand exchange reactions with the solvent. CORM-2 has been widely used as a 'prodrug' of CO and has been involved in numerous studies aiming to elucidate the mechanism of action of CO or its various effects on different cellular systems and disease models. However, the water insolubility remains an unresolved matter posing limitations and restrictions to its clinical applications. The rapid loss of CO upon dissolution in DMSO (< 1min) is also a problem to consider of before conducting experiments with CORM-2 (Motterlini et al. 2002).

Further research of these lipid-soluble systems led to the synthesis of a second generation of more water-soluble CORM analogues, which behave more favourably in biological systems and confer different CO-release profiles and biological properties. One of them includes the amino-acid glycine and a ruthenium core, and is named CORM-3 $[Ru(CO)_3Cl(glycinate)]$. CORM-3 is air-stable, water-soluble and rapidly releases CO via a hydrolytic mechanism, so upon water exchange reaction (Clark et al. 2003). However, due to its instability in aqueous solutions, CORM-3 was excluded from further clinical research, despite its benefits in several disease models (Kunz et al. 2013; García-Gallego and Bernardes 2014). In more detail, while a distilled water solution of CORM-3 at 37°C has a half-life of 98h, this is reduced to just 3.6min in human plasma (Schatzschneider 2015). However, studies of the interaction of CORM-3 with proteins revealed that this complex reacts rapidly with plasma proteins such as human haemoglobin and albumin, hence leading to ruthenium species bound to these proteins (Santos-Silva et al. 2011). These species lose one equivalent of CO in the form of CO_2, thus yielding protein–$[Ru(CO)_2]$ adducts. These adducts, which are

carried throughout the body via blood circulation, are responsible for the differential CO distribution to organs and tissues, through slow loss of CO. This mechanistic approach is consistent with the therapeutic versatility of CORM-3 (García-Gallego and Bernardes 2014).

The other prototype water-soluble CORM to be synthesized by the group of Motterlini was a borano-carbonate analogue, namely CORM-A1 [$Na_2H_3BCO_2$]. This CORM displays a pH-dependent CO release profile, with a half-life in normal pH conditions of ~21min (Foresti et al. 2004; Motterlini et al. 2005b) (**Figure 1.20**).

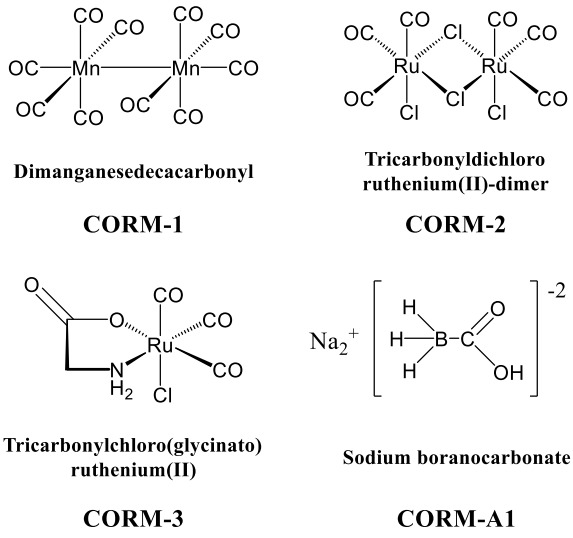

Figure 1.20: Structures of first and second generation CORMs

After extensive discussion (Foresti et al. 2008; Zobi 2013; Romão and Vieira 2015; Kourti et al. 2017), the field has reached a notion that there are a number of prerequisites for an ideal CORM. First of all, it should be effective at low doses, non-toxic for normal cells, soluble and stable in biological fluids and also biocompatible. Moreover, it should have well-defined CO-release kinetics, tissue specificity, stability in aerobic aqueous media and appropriate ADME properties.

The release of CO groups from CORMs is validated mainly by the monitoring of the formation of carboxymyoglobin (MbCO) from deoxymyoglobin (Mb) spectroscopically (Motterlini et al. 2002; García-Gallego and Bernardes 2014; Schatzschneider 2015). In this so-called "myoglobin assay" the conversion of MbCO is followed spectrophotometrically by measuring the reduction in intensity of the band of Mb at 557nm and the increase in intensity of the band of MbCO at 540nm and 577nm, until

the measurements reach a plateau value. Although the myoglobin assay remains the most popular procedure for the initial screening of the release properties of a novel CORM, there are some limitations regarding this assay, which should be taken into consideration if an alternative is not possible (Schatzschneider 2015). For example, strongly coloured CORMs can interfere with the absorption bands of myoglobin and complicated deconvolution techniques would be required for analysis. Another limitation is the reducing atmosphere needed to keep the Fe in the +II state (ferrous iron), which would be inappropriate for oxidation-activatable CORMs like the ones synthesized by the Schmalz group (Romanski et al. 2011). The aqueous sodium dithionite required for the reduction of myoglobin can easily interact with the CORM or other components, causing additional issues. Finally, the undefined mechanism of interaction between the CO of the CORM with the myoglobin poses extra limitations to this technique. So, alternative methods such as gas chromatography (GC) are chosen over the traditional method (Schatzschneider 2015).

1.5.4 Overview of the family of photo-CORMs

From the first moment that CORMs were considered aspotential pharmaceutical agents, the problem of uncontrolled and unspecific delivery of CO arose. For a CORM to be used clinically, there should be a well-defined and controlled way of CO release, preferably after an appropriate trigger is applied. It was 2008 when the first groups started reporting an alternative approach to this problem, and this approach was photo-activatable CORMs. Light has been the main and most preferable external trigger suggested, because it is usually non-toxic in the used wavelengths and there are various devices for light manipulation with a quite straightforward way of triggering the release of the carbonyl groups as CO gas into the biological fluids. These photo-activatable CORMs, later named photo-CORMs, have the advantage of releasing CO in a specific tissue with temporal control, according to where the light source is targeted.

However, there are limitations and challenges for these compounds, as well. An ideal photo-CORM should be activated at long wavelengths, with complete stability in darkness. The first member of this group was reported by Motterlini and co-workers, and it was CORM-1, as described above. Since then, several groups are active in this

area, with numerous successful attempts being reported. For instance, the group of Schatzschneider have recently developed a novel class of macromolecular photo-CORMs, namely $Mn(CO)_3$ functionalized metallo-dendrimers, which release CO upon activation with light at 410nm (Govender et al. 2013). They have also successfully coupled $[Mn(CO)_3(R\text{-}tpm)]^+$ complexes with target molecules, without affecting the photochemical CO-release properties of the complexes (Dördelmann et al. 2012).

Using light as an external trigger for the internal release of CO in a controlled way remains a very active area of CORM research. Most photo-CORMs share common characteristics, such as being metal-based, stable in the dark in aqueous solutions and able to accumulate in the target tissue before the activation with light. The main strategies in the design of new photo-CORMs are three: 1) to shift the release wavelength of the photo-CORM towards the infrared area of the spectrum through appropriate metal and co-ligand combinations (that is ligands with extended aromatic p systems), 2) to attach a photosensitizer for the CO release process to a metal-carbonyl moiety, such as an organic dye or metal complex, and 3) to use two-photon absorption to achieve photolytic liberation of CO from a photo-CORM prodrug. These strategies have been applied in order to generate a new generation of photo-CORMs which can be activated by visible light (García-Gallego and Bernardes 2014).

1.5.5 Carbon monoxide and CORMs as anti-cancer agents

The potential application of CO and CORMs in anti-cancer therapy is still under investigation. The relevant findings in the literature showed rather contradictory results (Loboda et al. 2015b; Romão and Vieira 2015; Kourti et al. 2017). The molecular targets and specific signalling pathways affected by CO remain unclear, being the main difficulty in an anti-cancer application of CO (Li Volti et al. 2005; Chatterjee 2007; Ahmad et al. 2015). The most plausible scenario is that CO causes opposite effects in different biological systems. CO and CORMs have been studied for their effects on cell proliferation, apoptosis and angiogenesis, primary processes involved in cancer initiation and progression, and the conclusion until now is that this effect is variable and seems to be cell–type specific (Loboda et al. 2015a,b). As mentioned already though, the anti-cancer potential of CO is a highly active area of research and the near

future will be decisive in the elucidation of the exact mechanism of action of this gas and its prodrugs, as well as any potential benefits against cancer.

Examples of a few promising studies are reported here, which could be of interest for further development, as they seem to implicate agents that inhibit various aspects of cancer and with a diversity of mechanisms and pharmacological profiles. However, before any clinical trials are initiated, there should be a more detailed mechanism of action elucidated for CO and CORMs. For instance, in his study Lee et al. (Lee et al. 2014) suggested that CO could attenuate the activity of heat shock protein 90 (HSP90), as well as its client proteins, possibly inhibiting cancer progression. The same group (Chakraborty et al. 2015) also applied a novel technique for drug delivery, utilizing Al-MCM-41 mesoporous silica nanoparticles (MSNs) loaded with a newly synthesized photo-CORM, namely fac-$[Re(CO)_3(pbt)(PPh_3)](CF_3SO_3)$, (ReCO), for the selective delivery of the photo-CORM to breast cancer cells. The anti-cancer activity of the endocytosed particles after light-induced CO release in MDA-MB-231 cells measured via the MTT assay reached an 80% eradication of the cancer cells. This was a much stronger effect than that after the application of the photo-CORM alone, due to the extravasation of nano-sized particles occurring in a tumour-selective manner (Chakraborty et al. 2015).

However, the HO-1/CO system is still under investigation and not fully understood. This may be the reason why there are so many contradicting publications regarding the real role of this system in tumorigenesis and angiogenesis (Kourti et al. 2017). It is a possibility that the cytoprotective activities of HO-1 and its by-products could offer cancer cells an advantage over the elevated oxidative conditions participating in tumorigenesis, but the antioxidant and protecting activities may delay tumour initiation (Loboda et al. 2015b).

The most important aspect to be elucidated is the true role of HO-1 in angiogenesis and tumour progression. This role might very well depend on the specific tissue and conditions under investigation and if revealed, will also help in the correct application of the CO/CORMs in the fight against cancer. The complexity might be related to the many products that derive from the enzymatic activity of HO-1 and the plethora of interactions of not only the protein itself but also of all the products with the

surrounding pathways (Loboda et al. 2015b). Moreover, it seems that the oxidation conditions in the relevant area affect the pro- or anti-angiogenic properties of HO-1, as the induction of this protein under oxidative stress suggest an involvement in angiogenesis linked to inflammation. On the other hand, LPS-induced inflammation initiates an angiogenic process that may be inhibited by HO-1 activity (Dulak et al. 2008). Studies on prostate cancer prove an inhibition of various cell functions by HO-1, identifying MMP-9 as a potential downstream target of HO-1, whereas the opposite results were evident in pancreatic cancer. The general conclusion from all these studies was that HO-1 activity is context-dependent and that different steps of the angiogenic process may be differentially affected by this system. Other factors such as the relative expression levels might also affect the synergistic or antagonistic interactions with other signalling pathways. The proposed dual role is that VEGF-induced angiogenesis may require HO-1 activity but inflammation-derived angiogenesis might be inhibited by HO-1 overexpression. Especially in cancer, the role is dependent on the type of tumour and other undefined factors (Ferrando et al. 2011). The only certain prediction is that when the role of HO-1 is elucidated, CO could truly be studied and applied as a potent anti-cancer approach.

1.5.6 CO and CORMs in relation to reactive oxygen species production

The cellular pathways targeted by CO and CORMs have been shown to be affected by the generation of ROS (Bilban et al. 2008). Elevated ROS levels were evident in many cancers and associated with increased malignance and regulatory effects on angiogenesis (Ushio-Fukai and Nakamura 2008). For example, ROS can mediate cell proliferation and migration, including cancer and ECs, by acting as important signalling molecules. Furthermore, elevated ROS levels have also been implicated in the production and regulation of HIF1α and VEGF, affecting tumour angiogenesis (Tertil et al. 2010; Ferrando et al. 2011).

Two of the main activities of CO, the anti-oxidant and cytoprotective, are through ROS generation and signalling, and induce endogenous cellular mechanisms of defence linked to anti-inflammatory events (Zuckerbraun et al. 2007; Bilban et al. 2008). It is well-known that cancer cells undergo metabolic changes, preferentially using glucose and the glycolytic pathway for energy production, which favours their proliferative

capacity (Hanahan and Weinberg 2011). The mild uncoupling of mitochondrial respiration is a way of avoiding excessive ROS production, especially under stress conditions. Mitochondria seem to be the main target of CO, which therefore affects cellular metabolism and energy production. Previous studies by Lo Iacono et al. (Lo Iacono et al. 2011) showed that low concentrations of CORM-3 are capable of increasing mitochondrial respiration, potentially affecting the Warburg effect. Also, as it has been suggested that a mild increase in ROS production can activate the cellular anti-oxidant machinery, a recent study showed that low CO levels provoke mitochondrial ROS generation, inducing the anti-oxidant pathway of glutathione (Queiroga et al. 2010). Taken together, it is logical to explore CO-mediated cellular metabolism as a potential cancer intervention.

However, it is well known that the CO/HO-1 system is trivial and has a complex relation to cancer initiation and progression. For example, HO-1 was found overexpressed in many tumours and was associated to their intrinsic resistance (Yin et al. 2014). Contradictory results regarding the regulatory roles of CO/HO-1 levels were reported in different cancer types. In particular, the CO/HO-1 system-related chemoresistance may depend on the tumour stage and type (Chau 2015; Tan et al. 2015). Therefore, the effects of CO in tumour development might be tumour type-specific.

In summary, the activity of CO, endogenously or exogenously applied, can manipulate cell metabolism and favour oxidative phosphorylation. CO can also increase mitochondrial respiration and therefore the related ROS production. However, when in high amounts, ROS levels can exceed the basal threshold, leading to oxidative stress and leak of Ca^{+2} from the sarcoplasmic reticulum (André et al. 2011). This is indicative of how the concentration of CO reaching the cells and the duration of exposure can alter the physiological relevance of this small molecule and complicate its study in a cancer related environment.

1.5.7 Designing new CORM analogues

Over the last decade, the increasing number of publications regarding CO and its prodrugs suggest that there is a growing interest in developing novel CO-based

therapeutics. As CO biological activities are gradually revealing, we hope that CORMs would become a new class of therapeutic agents against various pathological conditions in the near future. However, before reaching this goal, we are facing many obstacles. In particular, the three parts of a CORM, namely the metal centre, the coordination sphere and the drug sphere, play a major role in determining the pharmacochemical features as well as the kinetics and toxicity of the molecule.

As for the metal centre, it has a decisive contribution in the toxic effects observed, due to potential uncontrolled distribution and accumulation into unrelated areas. Each metal used in CORM designing has unique characteristics that will allow for special CO arrangement and a defined number of other ligands, according to its coordination number. Choosing a well-characterized metal with reported pharmacokinetics and minimum side effects will benefit the whole development process and establish a more predictable toxicological profile.

The ligand coordination sphere determines the kinetics of the molecule, as well as all the properties that are related to the CO itself, such as stoichiometry, in terms of number of CO groups that can be coordinated, and the mechanism of CO release. This would also affect stability against plasma proteins and reactivity with various stimuli, namely biologically related ligands, light and magnetic field. To be allowed to manipulate not only the mechanism and kinetics of CO release but also the appropriate trigger for its initiation, is an additional advantage of CORMs over CO gas.

Finally, the drug sphere is the most versatile part of a CORM, and can provide the whole complex with favourable ADME characteristics and maybe tissue or cell-type targeting elements. The pharmacological features of the molecule are a direct consequence of the structure of ancillary ligands, which are responsible for important drug properties such as solubility in water and biocompatibility. Choosing appropriate ligands can benefit the complex with specific tissue spatial distribution and targeting moieties. By exploring differences in the distribution of CORMs between normal and disease/foreign cells numerous possibilities for therapeutic purposes unravel, with a few examples listed below (García-Gallego and Bernardes 2014; Romão and Vieira 2015; Schatzschneider 2015).

During the last decade, a number of different molecules have been reported to be able to release CO under certain conditions and their cores belong to a wide variety of metals (Ru, Fe, Mn, V, Co, Ir, Cr, Mo, W). This new generation of complexes have improved properties over CORM-3, which is often chosen as the lead structure. ALF492 and ALF794 are two examples from this new generation of CORMs, which present some favourable characteristics (**Figure 1.21**). ALF492 was synthesized to have strong affinity for the liver, and it proved really successful against malaria. It is a water-soluble molecule that can transfer CO groups to haem proteins in circulation without increasing the amount of HbCO formed (Pena et al. 2012). ALF794 was also designed to have high liver specificity, along with other favourable ADME properties, as a drug against overdose of paracetamol. It has low acute toxicity *in vivo* and the release of CO is accelerated in the presence of liver microsomes. It can rescue the liver after paracetamol intoxication, and is effective even after the 8h initial response period (Romão and Vieira 2015). These example show that CORMs can be designed to have pharmaceutical profiles and properties similar to those of other regular drugs or prodrugs, therefore overcoming most of the problems usually related to metal-based drugs.

One other complex that belongs to the new generation of CORMs is ALF186, which has been employed as a good model for the study of the main interactions of organometallic complexes with biological fluids. It seems that the CO equivalents of ALF186 are released upon O_2 trigger, and they are then transported through the circulation partly bound to haemoglobin, while the metal by-product forms interact weakly with other proteins (García-Gallego and Bernardes 2014) (**Figure 1.21**).

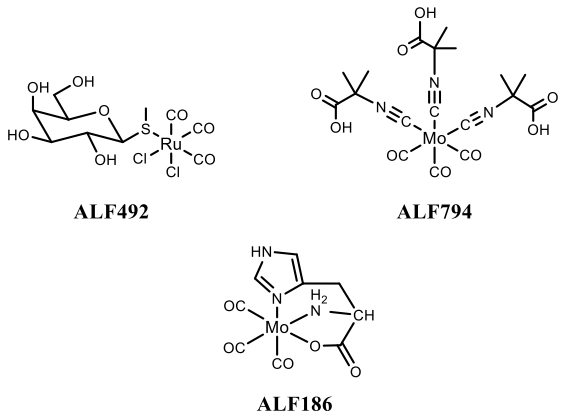

Figure 1.21: Structures of next generation CORMs

The main representative of the external stimuli application for initiation of CO release approach is the group of photo-CORMs. As discussed previously, by controlling the initiation of CO release, any therapeutic effects they may have focus only in the area where appropriate light excitation occurs, minimizing off-site effects and inadequate CO concentration due to systematic circulation of the complex with subsequent loss of a signification proportion of the carried CO. For example, in early work, Schatzschneider and co-workers synthesized a versatile photo-CORM with a $[Mn(CO)_3(tpm)]^+$ scaffold (where tpm =tris(pyrazolyl)methane) that undergoes photo-induced CO release upon irradiation with UV light of 365nm in aqueous buffer. The molecule is capable of releasing two out of the three CO ligands and has shown photo-induced cytotoxicity against human colon cancer cells (Niesel et al. 2008). Based on that scaffold, the same group explored the installation of an alkynyl group for further functionalization with short peptides, such as part of the transactivation domain of p53 with mouse double minute 2 homolog (MDM2), which would give the molecule the capability of targeting specific proteins (Pfeiffer et al. 2009) (**Figure 1.22**).

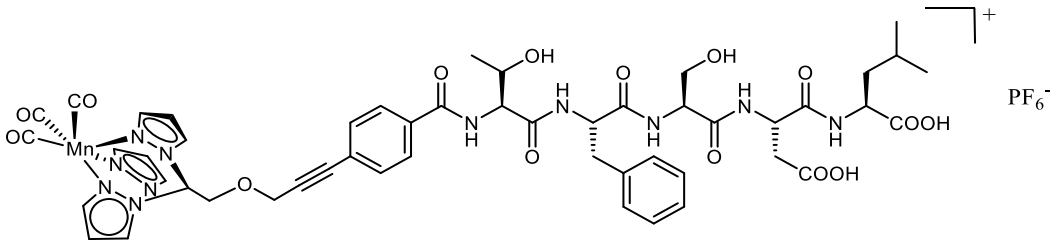

Figure 1.22: Example of $[Mn(CO)_3(tpm)]^+$–peptide conjugate. *Source: (Pfeiffer et al. 2009).*

Another example of designing new generation CORMs is the photoCORP-1 (**Figure 1.23**), which is the first example of a CO-releasing hydrogel that can release CO upon

remote low power visible light excitation and has been proven cytotoxic against adenocarcinoma cells. This photoactivatable CORM also employs the approach of controlled release of CO, this time with an even more precise way, by using optic fibre technology to initiate the release via visible light. Through a specially designed optical fibre-based CO catheter, CO can be specifically released in a controlled manner to malignant targets in inaccessible cavities and body parts where CO can induce cancer cell apoptosis (Pinto et al. 2017).

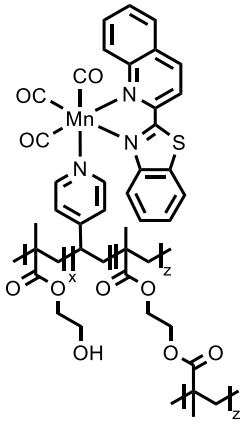

Figure 1.23: Photo-CORP-1. *Source: (Pinto et al. 2017).*

Apart from the photo-CORM group, Zobi and co-workers described a family of Re-based CORMs whose CO release can be modulated by pH and ligand variation on the basis core. These cyanocobalamin (vitamin B12) derivatives show some useful features such as water solubility, biocompatibility, aqueous stability and release of a minimally toxic metal fragment after the dissociation of CO. These molecules have been tested against ischemia-reperfusion injury and can increase cardiomyocyte cell survival by up to 83% (Zobi et al. 2012) (**Figure 1.24**).

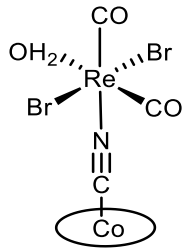

Figure 1.24: B_{12}-ReCORM-2. *Source: (Zobi et al. 2012).*

There are many other examples of new generation CORMs, most of the research being focused on the group of photo-CORMs. Notable examples are the work of Mascharak

(Chakraborty et al. 2014), Fairlamb (Ward et al. 2016) and Westerhausen (Mede et al. 2016) who all try to overcome the main problems of CORMs. However, there are also other advances in CORM designing that focus on different releasing mechanisms, with the redox-triggered possibility being a novel and highly promising one.

It is obvious that as with every drug development process, there are many obstacles that need to be overcome before a pharmaceutical agent can be clinically useful. The development of CORMs is even more challenging, as most of them are still water insoluble, unstable in aerobic and aqueous conditions and carry a metal core that needs to be thoroughly examined for potential toxicity and favourable pharmacokinetics. It is mostly intriguing to design a CORM with the ability of targeting the appropriate disease site where CO can be released upon a specific stimulus and at the proper concentration and timeframe. Motterlini and Otterbein conclude in a number of requirements for CORMs which refer to 1) water solubility and biocompatibility, 2) stability in aqueous aerobic environment, 3) slow decay of the $M(CO)_x$ fragment in the circulation and finally 4) low toxicity and quick metabolism and excretion of the remaining metal scaffold after the release of the CO (Motterlini and Otterbein 2010). As for the special class of photo-CORMs, additional properties are required, such as photoreactivity at specific wavelengths where the penetration depth is optimal, that can only be achieved by suitable metal and co-ligand combinations (Kourti et al. 2017).

The final issue that remains unresolved despite the efforts of many research groups over the last twenty years, is what exact characteristics are considered desirable for such molecules in each disease case. For example, how many CO ligands per metal complex unit should be released and should the release be slow or fast, rapid or steady? CORMs that dissociate CO rapidly could be beneficial in the study of ion channel kinetics, whereas for therapeutic interventions, a more steady and controlled release may be desired. Therefore, there are probably more than one profile that these molecules should demonstrate, and the different groups of CORMs should be designed with specific properties according to the medical application each time in mind (García-Gallego and Bernardes 2014; Schatzschneider 2015).

1.6 Hypothesis, purpose and aims of the study

Invasive breast cancer affects more than 1.3 million women worldwide each year, with more than 55,000 reported cases in the UK only in 2015. Although some breast cancers overexpress HER2, there is a distinct subtype called triple-negative breast cancer (TNBC) that does not express ER, PR or HER2. Clinical surveys reveal that approximately 15% of all breast cancers are diagnosed as TNBC, which occurs more frequently among younger women (<40 years old) and is characterized by high histological grade, high risk of recurrence and shorter disease-free survival, alongside a more frequent metastasis to bone, lung and brain.

This unique subtype of breast cancer has yet no established effective therapeutic regimens, and the most frequently prescribed drugs are a combination of chemotherapeutic agents and RTK inhibitors. However, the results remain disappointing and lack long-term effectiveness. The highly regulated process of angiogenesis has recently emerged as a promising target for TNBC, where it seems to be significantly over-activated and supports the growth and metastasis of the primary tumour. It is well established that one of the main growth factors regulating angiogenesis is VEGF. VEGF itself is abundantly secreted by breast cancer cells in order to promote differentiation and an aggressive phenotype. By overexpressing VEGF, cancer cells succeed in stimulating angiogenesis and providing further nourishment for the growing tumour. Recent investigations into the use of anti-VEGF therapies such as bevacizumab alongside chemotherapy have ultimately proved long-term ineffective for patients with invasive breast cancer. Given the status of anti-VEGF drugs as one of the few available targeted therapies for TNBC, there remains an urgent and unmet need for improving their efficacy.

For a long time, carbon monoxide (CO) has been best known for its potent toxic effect as an air pollutant because of its strong affinity (>220 fold greater than that of oxygen) for haemoglobin. Endogenously produced CO was found to regulate various endogenous signalling pathways related, among others, also to cellular metabolism, and was therefore characterized a gasotransmitter. However, since the administration of CO gas can be dangerous and poorly regulated, the discovery of

transition metal carbonyls that can act as CO-releasing compounds (CORMs) has provided a safer way to control CO release *in vivo* in a spatial and temporal manner. Previous studies suggested that CO can have various and even opposite effects on different subtypes of cancer and in the form of its pro-drugs, CORMs, might act as a new therapeutic entity. Additional to the observed heterogeneous effects on different systems and cell types, recent research has also demonstrated that a first generation CORM, that is CORM-2, can exhibit anti-VEGF and anti-angiogenic activity through the released CO (Ahmad et al. 2015).

Therefore this project aimed to determine any potential cytotoxic and anti-angiogenic properties of four commercially available CORMs against TNBC. Based on the produced results, one of the four CORMs would be chosen for further structural modifications following classic medicinal chemistry principles, in order to produce a small subset of novel compounds. The new compounds would also be tested for any anti-angiogenic potential and one compound would emerge as a proposed leading structure for future studies.

The specific aims of this study were:

1. To test the cytotoxicity of four currently commercially available CORMs against two TNBC cell lines (MDA-MB-231 and MDA-MB-436), one epithelial cell line (MCF-10A) and one endothelial cell line (HECV).
2. To check for alterations in the metabolic activity of TNBC cells upon treatment with these compounds using the Seahorse Extracellular Flux Analyser.
3. To screen for potential anti-angiogenic properties of these compounds by quantifying relevant proteins and identifying subsequent effects on EC function.
4. To select one compound, which would be subjected to structural modifications in order to synthesize novel analogues.
5. To carry out the synthesis of a small subset of new compounds.
6. To test the new analogues for anti-angiogenic properties and effects on ECs. From the observations throughout this process, one lead compound would eventually be proposed for further studies in the future.

Chapter II

Materials & Methods

2.1 Materials

2.1.1 Standard reagents and solutions

Solutions for cell culture

- *0.05M Ethylenediaminetetraacetic acid (EDTA) in PBS*

One gram of KCl (Fisons Scientific Equipment, Loughborough, UK), 5.72g Na_2HPO_4 (BDH Chemical Ltd., Lutterworth, UK), 1g KH_2PO_4 (BDH Chemical Ltd.), 40g NaCl (Sigma-Aldrich, Dorset, UK) and 1.4g EDTA (Duchefa Biochemie, Haarlem, the Netherlands) were dissolved in distilled water and made up to 5L. The solution was adjusted to pH 7.4 before it was autoclaved and stored for future use.

- *Trypsin (25mg/mL)*

Five hundred milligrams of trypsin were dissolved in 20mL 0.05M EDTA. The solution was mixed and filtered through a 0.2µm minisart filter (Sartorious, Epson, UK), aliquoted in 250µL samples and stored at -20^{o}C until required. For routine cell culture usage, one aliquot was diluted further in 10mL 0.05M EDTA solution and used for cell detachment.

- *100x Antibiotic cocktail mix*

Five grams of streptomycin, 3.3g penicillin and 12.5g amphotericin B were dissolved in 5mL DMSO and then diluted with 495mL of PBS and filtered. In each 500mL media bottle, a 5mL aliquot was added.

- *Phosphate buffered saline (PBS)*

Fifty millilitres of 10x stock PBS (Sigma-Aldrich) were diluted in 500mL with distilled water, autoclaved and aliquoted in 25mL samples for future use.

Solutions for cytotoxicity assays

- *3-(4,5-dimethylthiazol-2-yl)-2,5-diphenyltetrazolium bromide (MTT) solution (5mg/mL)*

One hundred milligrams of MTT (Sigma-Aldrich) were dissolved in 20mL of sterile PBS and stored at -20^{o}C, protected from light, until required.

- *Acidified isopropanol (0.04M)*

Five millilitres of 2M hydrochloric acid solution (HCl) were diluted in isopropanol (2-propanol) at a final volume of 250mL and the solution was left into the fume hood at room temperature for at least one month before usage.

- *5x Stock solutions of CO-releasing molecules to be tested*

The calculated milligrams of each compound were weighed and dissolved in 1mL DMSO to create a 10mM stock solution. 100µL of this 10mM stock solution were further diluted with 1.9mL of normal media to a final volume of 2mL to create a 500µM stock solution. 100µL of this 500µM solution were added in each well of the first two columns of a 96-well plate (triplicates for each different compound or DMSO), omitting the outer wells, and columns 2 – 10 were serially diluted with 100µL of normal media to obtain 5x the concentration range desired for the experiments. From this 5x stock solution, 30µL were transferred into each well of the test plate.

The calculation of the required milligrams for each compound was based on the equations: n= m/MW and 1M= 1mol/L. For example, for CORM-2: $n = \frac{5.1201mg}{512.01g/mol} = 0.01mmol$. If it is diluted in 1ml of solvent it becomes 0.01mmol/ml= 0.01M= 10mM.

- *3x Stock solutions of CO-releasing molecules to be tested in IncuCyte™ Cytotox reagent*

One IncuCyte™ Cytotox reagent vial (Essen Bioscience, Hertfordshire, UK) was diluted with 45µL of full normal media to provide a stock concentration of 100µM, and the 50µL solution was then transferred to 6.6mL full media to yield a Cytotox reagent working solution of 750nM. The 10mM compound stocks prepared as described above were diluted at 3x final assay concentrations in the Cytotox reagent working solution and 50µL were transferred into each well of the test plate.

- *3x Stock solutions of CO-releasing molecules to be tested in CellPlayer Kinetic Caspase-3/7 reagent*

The CellPlayer 96-Well Kinetic Caspase-3/7 reagent (Essen Bioscience) was diluted with full normal media to provide a stock solution of 15μM. The 10mM compound stocks prepared as described above were diluted at 3x final assay concentrations in the caspase-3/7 stock solution and 50μL were transferred into each well of the test plate.

Solutions for cell biomass quantification

- *4% v/v Formalin solution*

To prepare a 4% v/v formalin solution, 500mL of 10% v/v formalin solution (Sigma-Aldrich) were diluted with 750mL of distilled water to prepare a 1.25L solution of 4% v/v.

- *0.5% v/v Crystal violet solution*

To prepare a 0.5% v/v crystal violet solution, 500mL of 1% v/v crystal violet solution (Sigma-Aldrich) were diluted with 500mL of distilled water to prepare a 1L solution of 0.5% v/v.

Solutions for metabolic dysfunction detection

- *1mM Glutamine solution in Seahorse XF Base Medium (Glycolysis medium)*

A 100mM glutamine solution was prepared by dissolving 29.23mg of glutamine (Sigma-Aldrich) in 2mL of Seahorse XF Base Medium (Seahorse Bioscience, Agilent Technologies, Cheshire, UK). This was further diluted by transferring 500μL of the 100mM solution to 50mL of Seahorse XF Base Medium (1mM). The Glycolysis medium was kept in a warm bath at 37^{o}C for the rest of the experiment.

- *7x Stock solutions of CO-releasing molecules to be tested*

The calculated milligrams of each compound were weighed and dissolved in 1mL DMSO to create a 10mM stock solution. From this high stock, appropriate dilutions were performed to obtain a 700μM stock solution for the 100μM treatment, a 350μM

stock for the 50μM treatment, a 175μM stock for the 25μM treatment and a 87.5μM stock for the 12.5μM treatment. 75μL for the 24-well XF Microplate, or 25μL for the 96-well XF Microplate were injected to each well during the experiment (working concentrations of 100-50-25-12.5μM). *Port A for 96-well plate.*

- *80mM Glucose injection solution*

The glucose injection was prepared as a 8x working concentration solution of 80mM. 43.23mg of glucose (Sigma-Aldrich) were dissolved in 3mL of Seahorse XF Base Medium. 75μL for the 24-well XF Microplate, or 25μL for the 96-well XF Microplate, were injected to each well during the experiment (working concentration of 10mM). *Port A for 24-well plate, Port B for 96-well plate.*

- *9μM Oligomycin injection solution*

The oligomycin injection was prepared as a 9x working concentration solution of 9μM. 1.35μL of a 20mM oligomycin stock solution (Sigma-Aldrich) was diluted in 3mL of Seahorse XF Base Medium. 75μL for the 24-well XF Microplate or 25μL for the 96-well XF Microplate were injected to each well during the experiment (working concentration of 1μM). *Port B for 24-well plate, Port C for 96-well plate.*

- *1000mM 2-Deoxy-Glucose injection solution*

The 2-Deoxy-Glucose injection (2-DG) was prepared as a 10x working concentration solution of 1000mM. 492.48mg of 2-DG (Sigma-Aldrich) were dissolved in 3mL of Seahorse XF Base Medium and the pH was calibrated to 7.35. 75μL for the 24-well XF Microplate or 25μL for the 96-well XF Microplate were injected to each well during the experiment (working concentration of 100mM). *Port C for 24-well plate, Port D for 96-well plate.*

Solutions for protein assays

- *Lysis Buffer*

Two millimolar (221.96mg) $CaCl_2$, 0.5% Triton X-100, 10μL of 1mg/mL leupeptin, 10μL of 1mg/mL aprotinin and 10μL of 10mM stock sodium orthovanadate solution were

dissolved in distilled water (final volume 1mL) and stored at 4^{o}C until required. Extra phosphatase inhibitors were added right before each experiment.

- *10% w/v Ammonium Persulfate (APS)*

One gram of ammonium persulfate (Melford Laboratories Ltd., Suffolk, UK) was dissolved in 10mL of distilled water and stored at 4^{o}C until required.

- *10x Running Buffer*

The 1L 10x Tris-Glycine-SDS buffer stock solution (T7777) (Sigma-Aldrich) was diluted with 9L of distilled water to prepare a 1x running buffer solution.

- *10x Transfer buffer*

The 1L 10x Tris-Glycine concentrate stock solution (T4904) (Sigma-Aldrich) was diluted with 2L of methanol and 7L of distilled water to prepare a 1x transfer buffer solution.

- *10x Tris – Buffered Saline (TBS)*

A 10x stock solution (0.2M Tris, 1.38M NaCl) was prepared by dissolving 121g Tris (Sigma-Aldrich) and 403.2g NaCl (Melford Laboratories Ltd.) in distilled water up to 5L final volume and adjusted to pH 7.4 with HCl. The solution was stored at room temperature until required.

- *TBS-Tween 0.1% v/v (TBS-T)*

A 500mL solution was prepared by adding 0.5mL of Tween 20 (Sigma-Aldrich) in 499.5mL of TBS and left to stir for 10min until complete homogenization.

Solutions for ELISA

- *1x Wash buffer for VEGF ELISA kit*

The 25x Wash Buffer Concentrate (Life Technologies Ltd., Paisley, UK) was allowed to reach room temperature and then diluted 25 times with deionized water (25mL of 25x solution diluted with deionized water up to a final volume of 625mL). This Working wash buffer was stored at 4^{o}C until required, within 14 days of preparation.

- *Reconstituted human VEGF standards for VEGF ELISA kit*

One vial of Human VEGF Standard (Life Technologies Ltd.) was reconstituted in 1.51mL of deionized water (final concentration of 10,000pg/mL), mixed gently and allowed to sit for at least 10min to ensure complete reconstitution. 90µL of the reconstituted standard were added to a clean Eppendorf tube containing 510µL of Standard Diluent Buffer (Life Technologies Ltd.) and this was labelled as 'standard 1500pg/mL'. This standard was serially diluted as follows: 300µL at a time added to a fresh Eppendorf tube containing 300µL of Standard Diluent Buffer. The final concentration range created was 1500pg/mL – 23.4pg/mL of Hu VEGF.

- *Streptavidin-HRP solution for VEGF ELISA kit*

The 100x Streptavidin-HRP solution (Life Technologies Ltd.) was diluted in HRP Diluent, 15min prior to usage. For each 8-well strip used in the assay, 10µL Streptavidin-HRP 100x solution were pipetted, the pipette tip was wiped to remove any excess solution, and dispensed into a tube containing 990µL of HRP Diluent. The solution was mixed thoroughly.

- *1x Lysis Buffer for pVEGFR2 ELISA kit*

The 10x Cell Lysis Buffer (Cell Signalling Technology, Leiden, The Netherlands) was allowed to reach room temperature and then diluted 10 times with deionized water (120µL of 10x solution diluted with deionized water up to a final volume of 1.2mL). This 1x cell lysis buffer was used to prepare the cell lysates for the pVEGFR2 detection with the commercial ELISA kit. The final concentration of the components is as follows: 20mM Tris-HCl, 150mM NaCl, 1mM Na_2EDTA, 1mM EGTA, 1% Triton, 2.5mM sodium pyrophosphate, 1mM β-glycerophosphate, 1mM Na_3VO_4 and 1µg/mL leupeptin. Extra phosphatase and protease inhibitors were added right before each experiment.

- *1x Wash buffer for pVEGFR2 ELISA kit*

The 20x Wash Buffer (Cell Signalling Technology) was allowed to reach room temperature and then diluted 20 times with deionized water (5mL of 20x solution

diluted with deionized water up to a final volume of 100mL). This 1x Wash buffer was prepared fresh before each experiment.

- *Detection antibody solution for pVEGFR2 ELISA kit*

The Phospho-VEGF Receptor-2 (Tyr1175) Rabbit Detection mAb (Cell Signalling Technology) was diluted in 1mL of Detection Antibody Diluent and incubated for 5min at room temperature with occasional gentle mixing. The final working solution was prepared by adding this 1mL of reconstituted Detection Antibody to 10mL of Detection Antibody Diluent and stored at 4^{o}C until required.

- *HRP-linked antibody solution for pVEGFR2 ELISA kit*

The Anti-rabbit IgG, HRP-linked Antibody (Cell Signalling Technology) was diluted in 1mL of HRP Diluent and incubated for 5min at room temperature with occasional gentle mixing. The final working solution was prepared by adding this 1mL of reconstituted HRP-Linked Antibody to 10mL of HRP Diluent and stored at 4^{o}C until required.

Solutions for ISO Broth Microdilution method

- *Mueller-Hinton broth*

The original formulation was prepared from dehydrated infusion of 300g beef, 17.5g of acid digest of casein and 1.5g of corn starch, all made up to 1L QSP distilled water and adjusted to pH 7.2-7.4.

- *Mueller-Hinton broth for campylobacter testing*

The formulation was prepared by supplementing the original broth with 5% lysed horsed blood (TCS Biosciences, Buckingham, UK) and 20mg/L β-NAD (Sigma-Aldrich).

- *Stock solutions of CO-releasing molecules for testing*

The compounds were provided in sealed containers, protected from light, and kept at a -20^{o}C freezer until the day of the experiment. These precautionary measures were taken as humidity, light, pH imbalances and high temperature can tamper the compounds provoking untimely CO release from the stocks. All stock solutions were

made up in either sterile water (in house) or DMSO (Sigma-Aldrich) according to provided guidelines. The range of concentrations used was 0.008mg/L – 128mg/L. All solutions were prepared freshly on the day of the experiment and they were protected from light throughout the handling procedure until in contact with the microorganisms.

2.1.2 Equipment for chemical synthesis and identification

Analytics

^{1}H NMR spectra were measured on a Bruker AVANCE 500 UltraShield NMR spectrometer (500 MHz) at ambient temperature. Data was recorded as follows: chemical shifts in ppm from internal tetramethylsilane, multiplicity (s =singlet; d =doublet; t =triplet; m =multiplet), coupling constant (Hz), integration and assignment. ^{13}C NMR spectra were measured on a Bruker AVANCE UltraShield NMR spectrometer (125 MHz) at ambient temperature. Chemical shifts were recorded in ppm from the solvent resonance employed as the internal standard ($CDCl_3$ at 77.16ppm, MeOD at 49.00ppm, deuterated DMSO at 39.52ppm, THF-d_8 at 67.21ppm and 25.31ppm). Thin layer chromatography (TLC) was conducted on pre-coated silica gel 60 GF_{254} plates. Preparative TLC plates (20x20cm, 500-2000 silica) were purchased from Merck (Southampton, UK). Mass spectrometry analysis (LC-ESI-MS) was performed on a Bruker micro-TOF spectrometer. High-resolution mass spectrometry (ESI-HRMS) was performed at the School of Chemistry.

Solvents and chemicals

All the anhydrous solvents and reagents were purchased from Sigma-Aldrich and they were used without further purification. The amino acids and their derivatives used as starting materials were purchased from Alfa Aesar (Heysham, UK). Fluka silica gel (35-70mm) (Bucharest, Romania) was used as the stationary phase for column chromatography.

2.1.3 Cell lines

All cell culture work was carried out in class II microflow cabinets. Pipette tips, culture medium and all other cell culture equipment were either purchased sterile or autoclaved prior to use. All cells were cultured at 37^{o}C in a humidified incubator containing 5% CO_2.

In this study, five different cell lines were used, listed in **Table 2.1.** First, the two human TNBC cell lines MDA-MB-231 and MDA-MB-436, obtained from the America Type Culture Collection (ATCC, Middlesex, UK), were used. Non-tumorigenic human epithelial breast cells MCF-10A (LGC Standards, Lancashire, UK), the human umbilical cord endothelial cell line HECV (InterLab, Genova, Italy) and the vascular endothelial primary cell line HUVEC (ATCC) were also part of the study.

Cell line	Origin	Cell morphology	Tissue type	Metastatic site	Hormone receptors
MDA-MB-231	51-year-old Caucasian female	Epithelial	Adenocarcinoma (tumorigenic)	Pleural effusion	ER-/PR-/HER2-
MDA-MB-436	43-year-old Caucasian female	Epithelial	Adenocarcinoma (tumorigenic)	Pleural effusion	ER-/PR-/HER2-
MCF-10A	36-years-old Caucasian female	Epithelial	Fibrocystic disease	-	-
HECV	Caucasian female	Endothelial	Umbilical cord – Normal immortalized	-	-
HUVEC	New-born babies	Endothelial	Umbilical vein – Primary	-	-

Table 2.1: Cell lines used in this study

2.1.4 Antibodies

Full details of primary antibodies used in this study are provided in **Table 2.2.** The secondary antibodies used for Western blotting were horseradish-peroxidase (HRP)-conjugated goat derived anti-rabbit IgG or rabbit derived anti-mouse IgG, all supplied by Sigma-Aldrich (Product codes: A-9044 and A-0545 respectively).

Antibody name	Molecular weight (kDa)	Phosphorylation site	Final concentration used	Product code
Mouse anti-GAPDH	37	-	0.2 µg/mL	SC-32233
Mouse anti-pERK1/2	42/44	Y204	0.4 µg/mL	SC-7383
Mouse anti-pAKT	62/56/60	S473	0.4 µg/mL	SC-81433
Rabbit anti-pVEGFR2	152	Y1175	1.49 µg/mL	Ab-194806
Rabbit anti-p-p38	38	T180+Y182	1.0 µg/mL	Ab-4822
Rabbit anti-pSrc	60	Y419	0.538 µg/mL	Ab-185617
Rabbit anti-HO-1	32	-	1.0 µg/mL	HC3001
Rabbit anti-pFAK	119	Y397	1.0 µg/mL	Ab-81298

Table 2.2: Primary antibodies used in this study

2.2 Methods

2.2.1 Cell culture

MDA-MB-231, MDA-MB-436 and HECV cell lines were routinely maintained in Dulbecco's Modified Eagle's medium (DMEM/Ham's F-12 with L-Glutamine) (Sigma-Aldrich) supplemented with 10% heat-inactivated foetal bovine serum (FBS) (Sigma-Aldrich) and 1% of antibiotic cocktail mix (working concentrations of 100IU/mL penicillin (=0.5988mg/mL), 0.1mg/mL streptomycin and 0.25µg/mL amphotericin B, 100x stock solution, obtained from Sigma-Aldrich).

MCF-10A cells were routinely maintained in Mammary Epithelial Basal Medium (MEBM, Lonza, Gloucestershire, UK) supplemented with the following growth supplements (MEGM kit) (Lonza): 2mL BPE, 0.5mL hEGF, 0.5mL Hydrocortisone, 0.5 mL GA-1000 and 0.5mL insulin. The medium also contained 1% antibiotic cocktail mix (Sigma-Aldrich) and 100ng/mL cholera toxin (Sigma-Aldrich).

HUVEC cells were routinely maintained in Endothelial Cell Growth Basal Medium-2 (EBM-2, Lonza) supplemented with 1% antibiotic cocktail mix (Sigma-Aldrich), 2% FBS (Lonza) and the following growth supplements (EGM-2 BulletKit) (Lonza): 0.5mL hEGF, 0.2mL Hydrocortisone, 0.5 mL GA-1000, 2mL hFGF-B, 0.5mL VEGF, 0.5mL R3-IGF-1, 0.5mL ascorbic acid and 0.5mL heparin.

All the cells were grown to confluence in $25cm^3$ or $75cm^3$ culture flasks loosely capped (Greiner Bio-One Ltd., Gloucestershire, UK) at 37^oC in 5% CO_2 and 95% humidity. The flasks were left to reach adequate confluence before starting each experiment, unless

otherwise stated. Full media (or normal media) referrs to the optimal media for each cell line supplemented with the recommended percentage of FBS.

2.2.1.1 Trypsinization and counting of cells

Cells were grown until they reached approximately 80 – 90% confluence, as assessed visually evaluating the coverage of cells over the surface of the culture flask using an inverted light microscope. The culture medium was aspirated and the cells washed once with 1mL of sterile PBS. 1mL of trypsin-EDTA solution (0.01% w/v trypsin-0.05% w/v EDTA in PBS buffer) was added and the cells were left in the normal incubator for 5min to detach. Cells were visualized under a microscope in order to verify if they had detached and the flask was also gently tapped to help detachment. The detached cell suspension was neutralized with 4mL of normal serum media and transferred to a 20mL universal container (Greiner Bio-One Ltd.), where it was centrifuged at 1700rpm for 5min for the cells to pellet. The supernatant was aspirated and the pellet was resuspended in 5mL of normal cell culture medium. The cells were then re-cultured by transferring 1/5 of the cell suspension into new culture flasks, counted for experimental work or stored under liquid nitrogen for future use.

For cell counting, a haemocytometer counting chamber was used. Briefly the cell pellet after centrifugation was resuspended in 1mL of medium and appropriate volume was loaded into the counting chamber. An inverted light microscope was used to count the cells for further *in vitro* cellular assays. The dimensions of each 16 square area of the counting chamber was 1mm x 1mm x 0.1mm which allowed the number of cells per mL to be determined using the following equation:

Cell number/mL= (sum number of cells counted in 4 corner squares/4) x 10^4 cells/mL

2.2.1.2 Cell storage in liquid nitrogen

The cell lines were stored in liquid nitrogen after detached from a small T25 flask and pelleted as described above. The freezing medium was prepared by supplementing standard culture medium with 10% v/v DMSO (Sigma-Aldrich). The cell pellet was resuspended in freezing medium at a cell density of 10^6 cells/mL and aliquoted into 1.0mL cryopreservation tubes CRYO.S (Greiner Bio-One). The cryo vials were stored

for 2h at -20^{o}C before being transferred at a -80^{o}C deep freezer overnight. The vials were then stored in liquid nitrogen tanks for long term storage.

2.2.1.3 Recovery of cells from liquid nitrogen

Frozen cells were removed from liquid nitrogen and left at room temperature for 2-3min to facilitate rapid thawing. After complete thawing, the cell suspension was transferred to a universal container with 10mL of pre-warmed medium and allowed to sit for 2min before centrifugation at 1700rpm for 5min. The supernatant was aspirated, the pellet resuspended in 5mL of pre-warmed normal medium and placed into a fresh T25 culture flask, followed by normal incubation at 37^{o}C in 5% CO_2 and 95% humidity. Following incubation for 24h, the medium was aspired, the flask washed with 1mL of sterile PBS and 5mL of fresh normal medium were added before leaving the cells to grow normally.

2.2.2 Cytotoxicity assays

2.2.2.1 MTT assay

Upon reaching adequate confluence (~90%), cells of a T25 flask were trypsinized and counted as described above. The cell pellet was resuspended at 500,000cells/12mL normal media and 120µL of this suspension were seeded on each well of a 96-well plate (Greiner Bio-One Ltd.) leaving the outer wells empty to fill up with 120µL of sterile PBS. Another 96-well plate was seeded with 120µL of normal media but no cells, following the same layout. The plates were left in a normal incubator for 24h.

24h after seeding, the treatments were added in the wells as 30µL of 5x stock solutions. The final concentration range of the treatments was 100µM – 0.390625µM, triplicates each sample and the same concentrations were used for the DMSO treatments, which served as controls. The blank plate was treated the same way. The plates were then left in a normal incubator for 72h.

72h after treatment, 20µL of 5mg/mL MTT solution were added in each well of both plates and left in a normal incubator for 4h. After that, the medium was aspirated and the plates blotted against clean tissue. The remaining purple crystals were dissolved in 100µL of acidified isopropanol and the absorbance of both plates was read at

540nm using an ELx800 plate reading spectrophotometer (Bio-Tek, Wolf laboratories, York, UK). The blank plate absorbance was subtracted from the plate that contained cells, in order to eliminate the background interference within the absorbance readings.

2.2.2.2 IncuCyte™ Cytotoxicity assay

A similar experimental preparation as for the MTT assay was followed in this experiment. Confluent T25 flasks were used to obtain a cell pellet, which was resuspended at 500,000cells/10mL normal media and 100µL of this suspension were seeded on each well of a 96-well plate. The plate was left in a normal incubator overnight for cells to adhere.

24h after seeding, the treatments were added in the 96-well plate wells as 50µL of the 3x stock solutions in IncuCyte™ Cytotox reagent. The final concentrations of the treatments were 100 – 50 – 25 – 12.5µM, triplicates each sample and the same concentrations were used for the DMSO treatments, which served as controls. The final assay concentration of the Cytotox reagent was 250nM. The plate was then placed into the IncuCyte™ ZOOM® instrument with a 10x objective using the Standard Scan Type. The images were captured every 2h until the assay was completed (72h).

2.2.2.3 IncuCyte™ Caspase-3/7 assay (Apoptosis assay)

Confluent T25 flasks were used to obtain a cell pellet, which was resuspended at 1,000,000cells/10mL normal media and 100µL of this suspension were seeded on each well of a 96-well plate. The plate was left in a normal incubator overnight for cells to adhere.

A few hours after seeding and upon reaching the desired confluence of 10-20%, the treatments were added in the 96-well plate wells as 50µL of the 3x stock solutions in CellPlayer™ Caspase 3/7 reagent. The final concentrations of the treatments were 100 – 50 – 25 – 12.5µM, triplicates each sample and the same concentrations were used for the DMSO treatments, which served as controls. The final assay concentration of the Caspase 3/7 reagent was 5µM. The plate was then placed into

the IncuCyte™ ZOOM® instrument with a 10x objective using the Standard Scan Type. The images were captured every 2h until the assay was completed (72h).

2.2.3 Cell biomass quantification

2.2.3.1 Crystal violet assay

To calculate the cell biomass as an indirect way to quantify the number of viable cells, a crystal violet assay was performed. The normal media of pre-seeded cells in a multiwell plate was aspirated and 100μL of 4% formalin solution were added to each well for 15min. After the fixation of the cells, the formalin solution was removed and 100μL of 0.5% crystal violet solution were added to each well for another 15min. The solution was then aspirated and the plate was carefully washed under the tap. The plate was left overnight to dry and then the crystal violet dye was resuspended in 200μL of 10% acetic acid solution (Sigma-Aldrich). The plate was read at 540nm using an ELx800 plate reading spectrophotometer (Bio-Tek).

2.2.4 Metabolic dysfunction detection with the Seahorse Extracellular XF^e Flux Analyser

The glycolysis levels of the cells were measured using the Seahorse Extracellular XF^e Flux Analyser. The cells were seeded in a Seahorse XF24 or XF96 Cell Culture Microplate the day before the experiment or as otherwise stated. For the 24-well plate 40,000 cells/well were seeded, whereas for the 96-well plate 10,000 cells/well were seeded.

After the supplementation of the Seahorse Base medium with 1mM glutamine, the pH was calibrated to 7.35 and the media was kept in a 37^{o}C warm bath after filtration through a 0.2μm minisart filter (Sartorious).

XF24 Cell Culture Microplate: The normal media of the cells was removed and 525μL of Glycolysis media were added in each well of the XF Microplate. The plate was then left in a CO_2-free incubator for 1h.

Meanwhile, the injections were prepared as indicated in the solution preparation section. All the injections were loaded on the injection plate at volumes of 75μL each.

After finishing the experiment, the wells were washed with PBS twice and 11µL of lysis buffer were added to each well. A protein quantification of the cell lysates was performed right after.

XF96 Cell Culture Microplate: The normal media of the cells was removed and 150µL of Glycolysis media were added in each well of the XF Microplate. The plate was then left in a CO_2-free incubator for 1h.

Meanwhile, the injections were prepared as indicated in the solution preparation section. All the injections were loaded on the injection plate at volumes of 25µL each.

After finishing the experiment, the wells were washed with PBS twice and a crystal violet assay was performed right away for the quantification of the cell biomass.

2.2.5 Protein detection

2.2.5.1 Sodium dodecyl sulphate – Polyacrylamide gel electrophoresis (SDS-PAGE) and Western blotting

Cell lysis and protein extraction

Upon reaching adequate confluence (~90%), the normal media was removed and the cell monolayer of a T25 flask was washed two times with ice-cold sterile PBS. 100µL of lysis buffer supplemented with 1µL of 500mM sodium orthovanadate (working concentration of 5mM, phosphatase inhibitor) and 1µL of 2.5M sodium fluoride (working concentration of 25mM, phosphatase inhibitor) were added on the cell monolayer. When preparing the cell lysates for the pVEGFR2 ELISA kit, apart from using the 1x Cell Lysis Buffer mentioned previously, 1µL of 1mg/mL aprotinin was also added (working concentration of 10µg/mL, serine protease inhibitor). The cells were scraped from the base using a disposable cell scraper and everything was kept in ice during that procedure. The detached cells were transferred to a 0.5mL Eppendorf tube (A laboratories, Hampshire, UK) and placed in ice for 30min in order to extract the cell lysate. The Eppendorf was vortexed every 10min on a Vortex-Genie 2 (Scientific Industries, Cole-Parmer, UK) to enhance the lysis of the cells. The lysed cells were then centrifuged at 13,000rpm for 15min at 4^{o}C in an AccuSpin Micro 17R microcentrifuge (Fisher Scientific) to remove cellular debris and collect the protein in

the supernatant. The supernatant was transferred to a clean Eppendorf tube and protein quantification was performed before sample usage in Western blotting or the samples were stored at -20^{o}C until future use.

Protein quantification of cell lysates

For the standardisation of protein samples when loading on to the SDS-PAGE gel, the concentration of protein in each sample was quantified and standardised. This was done using the Bio-Rad DC Protein Assay kit (Bio-Rad Laboratories, Hemel Hempstead, UK). First, a serial dilution of bovine serum albumin (BSA) standard samples (Sigma-Aldrich) with known concentrations of protein was prepared in the same cell lysis buffer used in protein extraction, to give a working concentration range between 10mg/mL – 0.156mg/mL. 5µL of either the sample or the standard were pipetted into a 96-well plate in duplicate before adding 25µL of "working reagent A/S", followed by 200µL of "working reagent B" (a dilute Folin Reagent). "Working reagent A/S" was prepared by mixing each mL of reagent A (an alkaline copper tartrate solution) with 20µL of reagent S. If the samples do not contain detergent, this step can be skipped and reagent A can be used as supplied. The mixture was left in the dark at room temperature for 15min allowing the colorimetric reaction to occur. The absorbance of both the samples and the standards was measured at 630nm using an ELx800 plate reading spectrophotometer (Bio-Tek). A standard protein curve was constructed for the BSA standards and used to correlate the absorbance of each sample with a protein concentration.

All protein concentrations were adjusted to desired working concentrations of 1 – 2mg/mL by diluting the samples with the same cell lysis buffer used for the protein extraction. This was followed by further dilution 1:1 (v/v) with 2x Laemmli sample buffer concentrate (Sigma-Aldrich). Samples were then boiled at 100^{o}C for 5min allowing the denaturation of the proteins before loaded on an SDS-PAGE gel or stored at -20^{o}C until required.

Loading the samples and running the gel

SDS-PAGE was carried out using an OmniPAGE VS10 vertical electrophoresis system (OmniPAGE, Wolf laboratories). Acrylamide gels were made up at a concentration

appropriate to the molecule being analysed. They were prepared in a universal tube and added between two clean, dry glass plates and assembled on a casting stand. The TEMED was added to the mixture just before loading, as this causes the gel to polymerise and set. The amount of each ingredient required to make up 10mL of 10% resolving gel (proteins with molecular weight in the range of 30 – 220KDa) are shown in the table below:

Component	mL
Distilled water	4.0
30% acrylamide mix	3.3
1.5M Tris (pH 8.8)	2.5
10% SDS	0.1
10% ammonium persulfate	0.1
TEMED	0.004

Table 2.3: Recipe for 10mL of 10% resolving gel

Using a disposable plastic pipette, the resolving gel was applied between the glass plates and immediately covered with isopropanol (Sigma-Aldrich) to ensure a smooth surface for the gel and minimum interaction with the environmental oxygen which can cause oxidation of the gel. The gel was left to polymerise at room temperature on a flat surface. After approximately 30min the resolving gel was set, the isopropanol layer was removed and 3mL of 5% stacking gel were added on top. A well forming Teflon comb was placed gently at the top of the stacking gel and the gel was allowed to polymerise at room temperature for further 30min. The components and amounts used for the 5% stacking gel are indicated below:

Component	mL
Distilled water	2.1
30% acrylamide mix	0.5
1.5M Tris (pH 8.8)	0.38
10% SDS	0.03
10% ammonium persulfate	0.03
TEMED	0.003

Table 2.4: Recipe for 3mL of 5% stacking gel

Once the stacking gel had set after approximately 30min, the comb was carefully removed without tearing the edges of the wells and the loading cassette was placed into an electrophoresis tank filled up with 1x running buffer until the wells were completely covered.

The samples were loaded into the wells using a 20µL pipette at equal volumes of approximately 15µL. Control wells with 10µL of molecular weight marker SDSH2 (Sigma-Aldrich) were always used to indicate the molecular weight of the bands.

The proteins were then separated according to their molecular weight using electrophoresis at 120V, 80mA and 500W for 1.5h.

Preparation of membrane and Western Blotting

Following SDS-PAGE, the protein samples were transferred onto an Immobilon®–P PVDF membrane (Merck Milipore, MA, USA) by Western blotting. The electrophoresis system was disassembled and the glass plates separated. The gel was removed and separated from the glass plates after removing the stacking gel with a plastic edge. The nitrocellulose membrane and four sheets of filter paper (Whatman International Ltd., Maidstone, UK) were cut (7.5cm x 7.5cm) and immersed into 1x transfer buffer for 10min to ensure correct binding of the protein to the membrane. The PVDF membrane was then activated by immersing into methanol for 30 seconds and transferred immediately back to transfer buffer. Two sheets of filter paper were placed on top of the (+) pole of a SD10 SemiDry Maxi System blotting unit, then the activated membrane on top, the gel on top of the membrane and finally another two sheets of filter paper. The surface of the "sandwich" of papers-nitrocellulose membrane-gel-papers was carefully smoothed out to remove air bubbles which may interfere with the protein transfer. The (-) pole lid was attached and the sandwich was set up for protein transfer from the gel to the membrane via electroblotting at a constant current of 15V, 500mA, 8W for 50min – 1h.

Once completed, the membrane was removed and by forming a roll, it was transferred facing upwards into a clean 50mL falcon tube (Nunc, Fisher Scientific). It was then incubated in 50mL of 10% milk blocking solution (500mg skimmed milk in 5mL TBS-T) for 1h with agitation on a roller mixer (Stuart, Wolf Laboratories) at room temperature. This solution blocks the proteins on the membrane, disallowing non-specific binding of the primary antibody. The blocking solution was then discarded and 5mL of specific primary (1^{o}) antibody (appropriate dilution) made up in 5% milk solution (250mg skimmed milk in 5mL TBS-T) were added to the tube and the

membrane was left to probe overnight at 4^{o}C with agitation on a roller mixer. After this, the 1^{o} antibody solution was discarded and the membrane was washed three times for 10min each wash, with 15mL of TBS-T, to ensure complete removal of any unbound 1^{o} antibody. The membrane was then incubated in 5mL of HRP-conjugated secondary (2^{o}) antibody solution (dilution 1:1000) (Sigma-Aldrich; dependent on the species of the primary antibody) made up in 5% milk solution with agitation for 1h at room temperature. The 2^{o} antibody solution was discarded and the membrane was washed again as previously described.

Chemiluminescent detection of protein

The EZ-ECL system (Biological Industries, Cromwell, USA), a highly sensitive chemiluminescent substrate for the HRP used for the Western blotting procedure, was used for protein detection on the membrane. The two substrates, A and B, were mixed in a 1:1 ratio with a final volume of 1mL/membrane and left in the dark for 4min to allow the reaction to develop. Once the mixture was ready, the washing solution was decanted from the membrane and it was placed on a tray and covered with the solution. The membrane was left in the dark for 1 – 3min, any excess solution was drained over a piece of clean tissue paper and the chemiluminescent signal was captured and visualized on a computer monitor connected to a G:Box Chemi XRQ imager (Syngene, Cambridge, UK). Semi-quantitative analysis was undertaken using the ImageJ software (National Institutes of Health, NY, USA) in order to assess the protein levels in the samples.

2.2.6 Enzyme – linked immunosorbent assay (ELISA)

2.2.6.1 ELISA for VEGF quantification

All the solutions and diluents included in this assay were purchased from Life Technologies Ltd., Paisley, UK, unless otherwise stated. The ELISA technique was used to detect human VEGF levels in the supernatant of confluent cells. Protein concentration of each flask was used to normalize the results of the ELISA.

Upon reaching adequate confluence (60-70%), the normal media from a culture at a T25 flask was collected into Eppendorf tubes and centrifuged at 13,000rpm for 5min

in a microcentrifuge to remove cellular debris and cells. The supernatant was transferred to clean Eppendorf tubes and kept at a -80^{o}C freezer until required for ELISA.

All the reagents were allowed to reach room temperature before use. 50µL of the Incubation Buffer were added to all wells of the provided pre-coated 96-well plate except chromogen blanks. 100µL of standards were added to the appropriate microtiter wells. For samples and controls, 50µL of Standard Diluent Buffer were added to each appropriate well, followed by 50µL of the sample or control. The plate was covered and incubated for 2h with constant agitation at room temperature. The solution was then thoroughly aspirated and the wells were washed 4 times with 300µL diluted (1x) Wash Buffer.

After the washing, 100µL of the Human VEGF Biotin Conjugate solution were added to each well except chromogen blanks. The plate was covered and incubated for 1h with constant agitation at room temperature. After this time, the same washing procedure described above was followed. 100µL of Streptavidin-HRP solution were then added into each well except the chromogen blanks and the plate was covered and incubated for further 30min with constant agitation at room temperature. The same washing procedure already described was then followed. 100µL of Stabilized Chromogen were added to each well and the substrate solution begun to turn blue. The plate was covered and incubated for 30min at room temperature in the dark. Finally, 100µL Stop Solution were added to each well and all the contents were gently mixed until the solution in the wells turns from blue to yellow.

The absorbance was then read at 450nm using an ELx800 plate reading spectrophotometer (Bio-Tek), within 2h of adding the Stop Solution. The standard curve was generated using a curve-fitting software (Microsoft Excel 2013) and used to associate an absorbance reading with a standard VEGF concentration. The background absorbance was subtracted from all data points prior to plotting, and the values obtained for the samples (and controls) were multiplied by the appropriate factor to correct for the sample dilution.

2.2.6.2 ELISA for pY1175 (pVEGFR2) quantification

All the solutions and diluents included in this assay were purchased from Cell Signalling Technology (Leiden, The Netherlands), unless otherwise stated. The sandwich ELISA technique was used to detect pVEGFR2 (Tyr1175) levels in the lysate of pre-treated cells as described in the corresponding sections.

Upon reaching adequate confluence (70-80%), the normal media of a culture at a T25 flask was aspirated and the cells were lysed as described previously. The supernatant of the lysate was transferred to a clean Eppendorf tube and kept at a -80^{o}C freezer until required for ELISA.

All the reagents were allowed to reach room temperature before use. Cell lysates were diluted before the experiment with the Sample Diluent at a working concentration of around 0.2mg/mL. 100µL of each sample were added to the corresponding wells of the provided pre-coated 96-well plate. The plate was covered and incubated for 2h at 37^{o}C. The solution was then thoroughly aspirated and the wells were washed 4 times with 200µL diluted (1x) Wash Buffer.

After the washing, 100µL of reconstituted Detection Antibody solution were added to each well. The plate was covered and incubated for 1h at 37^{o}C. After that, the same washing procedure described above was followed. 100µL of reconstituted HRP-Linked secondary antibody solution were then added into each well and the plate was covered and incubated for further 30min at 37^{o}C. The same washing procedure already described was then followed. 100µL of 3,3’,5,5’-Tetramethylbenzidine (TMB) substrate were added to each well and the substrate solution begun to turn blue. The plate was covered and incubated for 10min at 37^{o}C. Finally, 100µL of the Stop Solution were added to each well and all the contents were gently mixed until the solution in the wells turns from blue to yellow.

The absorbance was then read at 450nm using an ELx800 plate reading spectrophotometer (Bio-Tek), within 30min of adding the Stop Solution. The values obtained for the samples (and controls) were multiplied by the appropriate factor to correct for the sample dilution and compared to each other.

2.2.7 Tube formation assay

2.2.7.1 Tube formation assay using conditioned media

Fifty microliters of Matrigel (BD Biosciences, Oxford, UK) were added in each well of a 96-well plate and the plate was left in a normal incubator for the Matrigel to set for 30min. A 70% confluent T75 flask was used to obtain a cell pellet, which was resuspended in normal full media and 35,000cells/100µL were seeded on top of the Matrigel in each well. The plate was then left in the normal incubator for 30 – 40min for the cells to adhere to the Matrigel. After this, the full media was removed and 100µL of serum free media were added on top of the cells. 60µL of conditioned media from treated MDA-MB-231 cells were also added in each well and the plate was left in the incubator for 6h. After 6h the wells were imaged using a Leica DM 1000 LED microscope (Leica Microsystems, Milton Keynes, UK) (5x objective) capturing at least 3 images/well in random areas. Images were analysed using the ImageJ Software (National Institutes of Health) and the percentage of total tube length compared to the cells that received conditioned media from vehicle treated MDA-MB-231 cells was calculated.

2.2.7.2 Tube formation assay with instant treatments

Fifty microliters of Matrigel (BD Biosciences) were added in each well of a 96-well plate and the plate was left in a normal incubator for the Matrigel to set for 30min. A 70% confluent T75 flask was used to obtain a cell pellet, which was resuspended in normal full media and 35,000cells/100µL were seeded on top of the Matrigel in each well. The plate was then left in the normal incubator for 30 – 40min for the cells to adhere to the Matrigel. After this, the full media was removed and 100µL of serum free media were added on top of the cells. 11.2µL of 10mM CORM stock or 1% DMSO stock (diluted in serum free media) or serum free media were added in the corresponding wells and the plate was left in the incubator for 6h. After 6h the wells were imaged using a Leica DM 1000 LED microscope (Leica Microsystems) (5x objective) capturing at least 3 images/well in random areas. Images were analysed using the ImageJ Software (National Institutes of Health) and the percentage of total tube length compared to the vehicle treated cells was calculated.

2.2.8 Migration assays

2.2.8.1 Traditional Scratch wound healing assay

Cells were seeded into a 24-well plate at a concentration of 10^5 cells/well/1mL in normal media. Cells were allowed to attach and reach confluence for 3 days in a normal incubator. When having reached adequate confluence (>90%), the medium was aspirated and the wells were washed with 200µL sterile PBS. A 100µL pipette tip was used to scratch down a straight line in the centre of the well. The wells were carefully washed again with 200µL PBS and 1.5mL of media supplemented with the corresponding treatments of 100µM CORMs or 1% DMSO were added in each well, triplicates for each different treatment, and the plate was followed up for 24h. Cells were imaged using a Leica DM 1000 LED microscope (Leica Microsystems) (5x objective) at 0h, 8h, 12h and 24h, in an area determined by blue lines drawn across each well. Images were analysed using the ImageJ Software (National Institutes of Health) and the percentage of wound closure (wound confluence) was calculated.

2.2.8.2 IncuCyte™ Scratch wound assay

Confluent T25 flasks were used to obtain a cell pellet, which was resuspended in normal media and 50,000cells/100µL were seeded on each well of a 96-well ImageLock plate (Essen Bioscience). The plate was then left in the IncuCyte™ ZOOM® instrument with a 10x objective using the Standard Scan Type. The images were captured every 2h until the cells reached adequate confluence of >90% (usually overnight).

Upon reaching adequate confluence, the ImageLock plate was removed from the instrument and the Wound Maker was used to scratch all the wells of the plate following the manufacturer's instructions. The wells were immediately washed twice with 100µL normal media and then 100µL of normal media supplemented with treatments was added to each well for 48h. The ImageLock plate was returned to the instrument, where images were captured every 1h or 2h with specific parameters set for the experiment. The concentrations used were 100 – 50 – 25 – 12.5µM CORMs or corresponding percentages of DMSO, quadruplicates for each different treatment.

Images were analysed using the IncuCyte ZOOM 2016A software (Essen Bioscience) and the percentage of wound confluence was calculated.

2.2.9 Antibacterial activity assessment – ISO Broth Microdilution method (Described in the Appendix)

Working solutions of the compounds to be tested were dispensed into microdilution trays at 50µl per well with double the desired final concentrations of antimicrobial agent. At least one well containing 50µl of antimicrobial agent-free medium was included as a growth control for each strain tested. Likewise, a well containing 100µl of antimicrobial agent-free medium was included as an uninoculated negative control well for each strain tested. The trays were inoculated within 30min of standardizing the bacterial suspension, in order to maintain viable cell number concentration. To each well containing 50µl of diluted antimicrobial agent in broth, a volume of 50µl of bacterial suspension was added.

Viable counts were performed on the test suspension to ensure that test wells contain approximately 5×10^5 CFU/mL (the inoculum is expressed as colony-forming units per millilitre (CFU/mL)). This was done by removing 10µl from the growth control well immediately after inoculation and diluting it in 10mL of broth. 100µl of the diluted growth control were spread over the surface of a suitable agar plate, which was then incubated overnight. Twenty to eighty colonies would be expected from an acceptable test suspension. If this is not achieved, the results for this strain cannot be used.

After the addition of the bacterial suspension, microdilution trays were sealed in polyethylene bags before incubation, in order to prevent desiccation. In order to avoid uneven heating, microdilution trays were not to be stacked more than five high. The trays were incubated at 37^{o}C in ambient air for (18 ± 2)h. A CO_2-enriched atmosphere should not be used.

Results shall only be read when there is sufficient growth of the test organism (that is obvious button or definite turbidity in the positive growth control), when there is no growth in the uninoculated or negative growth control and when purity and the appropriate cell number concentration of the inoculum has been established. The

amount of growth in each well is compared with that in the positive growth control, and the MIC recorded is the lowest concentration of the agent that completely inhibits visible growth.

2.2.10 Statistical analysis

Statistical analysis was performed using GraphPad Prism (GraphPad Software, Inc., CA, USA). Each experiment was performed at least three times and the data presented shows the mean of the three repeats (unless otherwise stated), with error bars showing the standard deviation (SD) or standard error of the mean (SEM). Student's *t*-test (for rank comparison between two groups) and two-way ANOVA (for more than two groups and two factors comparison) were performed to check for statistical significance, with a p-value of <0.05 considered statistically significant. Asterisk notation (*) was used to identify significances: * $p<0.05$, ** $p<0.01$, *** $p<0.001$ and **** $p<0.0001$.

Chapter III

Screening of available CORMs

3.1 Cytotoxicity Assessment

3.1.1. Introduction

In vitro cell-based assays are often used for the screening of anti-cancer compounds to determine if they have effects on cell proliferation or show direct cytotoxic effects that eventually lead to cell death (Ganot et al. 2013). The preclinical toxicity testing is recognised as an essential process during the screening of new molecules by the US FDA, in order to reveal any toxic effects of an investigational product on various biological systems (Berridge and Tan 1993; Parasuraman 2011). Since the compounds related to this project are able to release CO, a potentially lethal gas, the investigation of any potential cytotoxicity for the four commercially available CORMs is a useful and decisive first analysis. Apart from that, there is a bias among researchers against metal-based drug candidates, by assuming that heavy metals cause more harmful effects than lighter metals (Egorova and Ananikov 2017). This has not been conclusively established in any investigation yet. Nevertheless the screening for cytotoxicity was deemed important.

Meanwhile, previous studies have shown that CORM-2 at 50μM antagonised the proliferation of endothelial HUVEC cells after stimulation with increasing concentrations of VEGF (Ahmad et al. 2015). Furthermore, Lee et al. revealed that HO-1 induction or exogenous CO delivered by CORM-2 decreased the proliferation of breast cancer cell lines, such as MCF-7 and MDA-MB-231 cells (Lee et al. 2014). Finally, anti-proliferative effects of CO in the form of CORM-2 were also demonstrated by the group of Vitek et al. (Vítek et al. 2014). Taken together, these studies suggested the necessity of a cytotoxicity assessment of the compounds chosen against the different cell lines used.

Tetrazolium dye assays can be used to identify cytotoxicity (loss of viable cells) or cytostatic activity (shift from proliferation to quiescence) of potential medicinal agents and toxic materials (Berridge et al. 2005). The MTT assay is a colorimetric assay for measuring the activity of NAD(P)H–dependent MTT–reducing enzymes (located mainly into the mitochondria, but also in the cytosol) to reduce the tetrazolium dye 3-(4,5-dimethylthiazol-2-yl)-2,5-diphenyltetrazolium bromide (MTT) to its insoluble

formazan, which has a purple colour (**Figure 3.1**). MTT is positively charged and readily penetrates viable eukaryotic cells. The formazan form of the MTT accumulates as an insoluble purple precipitate inside the cells as well as near the cell surface and in the culture medium.

When cells die, they lose the ability to convert MTT into formazan, thus colour formation serves as a useful and convenient indirect marker of the number of viable cells. The quantity of formazan (presumably directly proportional to the number of viable cells) is measured as absorbance at 540nm in a plate spectrophotometer reader. By all means, the formazan must be solubilized prior to the absorbance readings, and for the experiments of this chapter, a solubilisation solution of acidified isopropanol has been used, as described in section 2.2.2.1.

The amount of signal generated is dependent on several parameters including the concentration of the MTT, the length of the incubation period, the number of viable cells and their metabolic activity. All of these parameters should be considered when optimizing the assay conditions to generate a sufficient amount of product that can be detected above background. The conversion of MTT to formazan by cells in culture is also time dependent.

However, it is worth noting that since MTT reduction is fulfilled by NAD(P)H–dependent oxidoreductases, it is a marker reflecting viable cell metabolism and not specifically cell proliferation or cell number. Cells with low metabolic rates obviously reduce MTT much less compared to rapidly diving cells, such as breast cancer cells. An important drawback of this assay is that it could be affected by a number of conditions that can alter the metabolic activity and thus MTT reduction, not directly reflecting cell viability.

The IncuCyte® Live-Cell Analysis System enables a real-time, automated viability assay. The IncuCyte® Cytotox reagent is an inert, non-fluorescent cyanine nucleic acid dye that crosses the cell membrane, when the cells become unhealthy and their membrane integrity diminishes. This yields a 100-1000 fold increase in fluorescence upon binding to the cell DNA. In this way, cell membrane integrity and cell death in response to pharmacological agents can be detected.

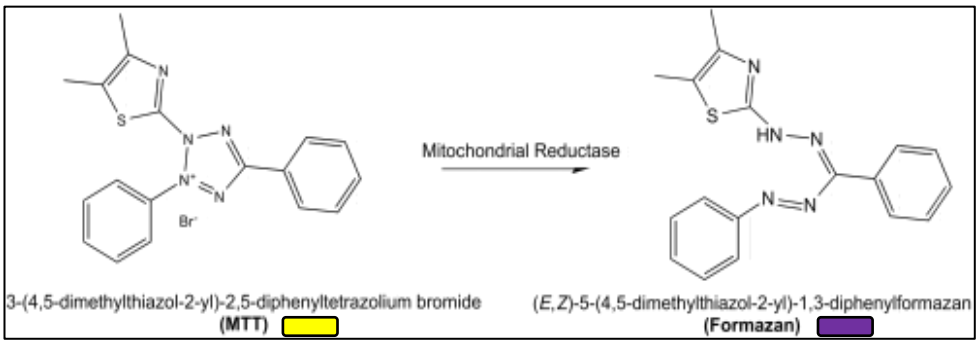

Figure 3.1: Tetrazolium bromide dye reduction to purple formazan. *Adapted from (Mosmann 1983).*

Caspases are a family of cysteine-dependent aspartate-directed proteases which take part in the execution phase of programmed cell death, apoptosis. Their name originates from their specific activity to nucleophilically attack and cleave a target protein after an aspartic acid residue. Activation of caspases initiates and highly regulates apoptosis, which enables the degradation of cellular components in a least affecting manner for the surrounding tissues and microenvironment (Porter and Jänicke 1999) (depicted in **Figure 3.2**).

Caspases are synthesised and exist as inactive pro-enzymes (pro-caspases, zymogens), which are activated upon receiving relevant stimuli. Their activation following apoptotic signals involves the dimerization of the pro-caspase followed by the proteolytic cleavage at inter domain linker regions with conserved aspartic residues producing a small and a large subunit. These subunits associate with each other to form an active heterotetramer and take up a conformation favourable for enzymatic activity (Riedl and Shi 2004).

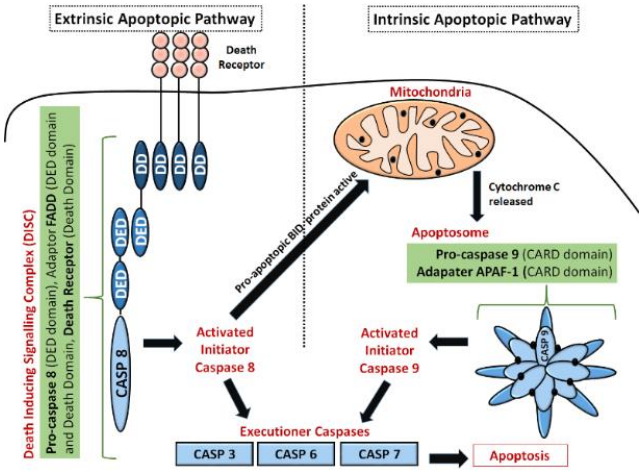

Figure 3.2: Apoptotic pathways mediated by caspases.
Source: https://en.wikipedia.org/wiki/Caspase.

More specifically, caspases are subcategorized into initiator (caspases-2, 8, 9, 10, 11 and 12) and executioner or effector caspases (caspases-3, 6 and 7). The activation of initiator caspases requires the binding to oligomeric activator proteins, and then the dimerization can take place. Both initiator caspases of the formed dimer undergo cleavage by autocatalysis. The heterotetramer can then proteolytically cleave the executioner caspases, which may exist as a homodimer constitutively. The resulting small and large subunits associate to form a heterotetramer. The activated effector caspase tetramer can then degrade intracellular proteins via proteolysis, in order to trigger cell death (McIlwain et al. 2013) (**Figure 3.3**).

Caspase-3 is a member of the caspase family and is an effector caspase. When activated by caspases-8 or 9 or 10, it can cleave and subsequently activate caspases-6 and 7. Caspase-3 has a typical role in apoptosis, where it controls chromatin condensation and DNA fragmentation. It is also responsible for the cleavage of many key cellular proteins that control the process of apoptosis and for some typical hallmarks of it (Porter and Jänicke 1999).

Caspase-3 has also been implicated in tumorigenesis, where increased levels of the enzyme cause apoptosis and secretion of paracrine factors, especially in breast cancer tissues. This enables compensatory proliferation from the surrounding stromal tissues and even tumour cell re-population through increased secretion of prostaglandin E2 (PGE2), thus complicating effective therapeutic interventions such as radiotherapy (O'Donovan et al. 2003; Shalini et al. 2015).

Caspase-7 is subsequently activated by caspase-3 and belongs to the effector caspases, too. Apart from caspase-3, it can also be cleaved and activated by caspases-9 and 10. Caspase-7 mediates the cleavage of proteasomes, contributing to the reduction of proteasome activity and the accumulation of ubiquitinated proteins within the cell. Caspases-3 and 7 are structurally related and present overlapping substrate specificity. However, they have distinct roles during apoptosis and are differentially regulated, with specific subcellular localizations (Jang et al. 2007; Lamkanfi and Kanneganti 2010).

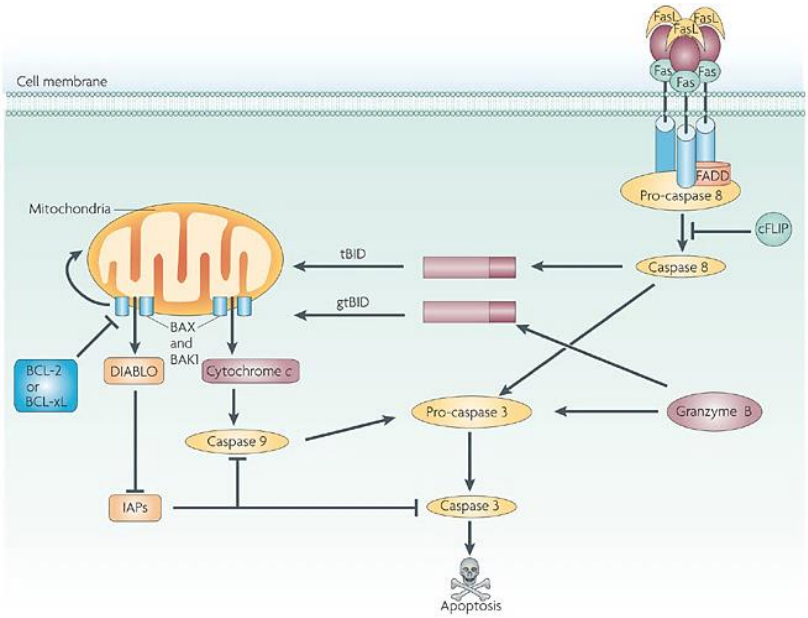

Figure 3.3: Caspase-dependent cell death. *Source: (Clarke and Tyler 2009).*

The IncuCyte® Live-Cell Analysis System enables a real-time, automated apoptosis assay using the IncuCyte® Caspase-3/7 reagent which is an inert, non-fluorescent (DEVD) substrate that freely crosses the cell membrane, where it can be cleaved by activated caspase-3 or 7 to release either a green or red DNA-binding fluorescent label. Apoptotic cells are identified by the appearance of fluorescently-labelled nuclei.

In this part of the screening of the four available CORMs the aim was to identify any cytotoxic activities of these CORMs against two TNBC, one epithelial and one endothelial cell lines. A further aim was to quantify the number of cells undergoing apoptosis after treatments with CORMs in different concentrations. These experiments were carried out using the MTT assay and the automated IncuCyte® Live-Cell Analysis System.

3.1.2 Materials & Methods

Cell lines and treatments

MDA-MB-231, MDA-MB-436 and HECV cell lines, maintained in DMEM media with 10% FBS and antibiotics, were used for the MTT assay. In addition, MCF-10A cells were used and maintained in MEBM media with the necessary MEGM supplements, cholera toxin and antibiotics. All cells were maintained at 37°C with 5% CO_2. The cells were treated with different concentrations of CORMs or DMSO for 72h, when they were supplemented with MTT and the absorbance read at 540nm in a plate reading spectrophotometer.

For the IncuCyte™ assays, MDA-MB-231, MDA-MB-436 and MCF-10A cells were used, maintained as previously described. The cells were treated with increasing concentrations of CORMs or DMSO (12.5 – 25 – 50 – 100μM) diluted in the suggested concentration of IncuCyte™ Cytotox reagent or CellPlayer™ Caspase 3/7 reagent for 72h and the manufacturer's instructions were followed in each protocol.

MTT assay

$5x10^3$ cells were seeded in 120μL of normal medium per well in a 96-well plate. The number of cells was chosen after appropriate optimisation experiments. Three replicates were undertaken per treatment concentration and an identical plate was also prepared with no cells (blank). The cells were left to attach overnight and then cells were treated with increasing concentrations of CORMs or DMSO. The concentration range used was a serial dilution between 100μM and 0.39μM, and the vehicle treated cells were used as controls. The blank plate received the same treatments. The cells were left in an incubator for 72h and then MTT solution was added and both plates were left in the incubator for further 4h. The medium was removed and acidified isopropanol was used to dissolve the purple formazan crystals. The absorbance of both plates was read at 540nm and the blank plate was used to subtract any background absorbance from the test plate absorbance. The method is detailed in section 2.2.2.1.

IncuCyte™ Cytotoxicity assay

$5x10^3$ cells were seeded in 100μL of normal medium (supplemented with FBS) per well in a 96-well plate. The layout of the experiment is the same as in the MTT assay, except for the concentration range used, 100 – 12.5μM, and the addition of the Cytotox reagent in a final concentration of 250nM in each well, as detailed in section 2.2.2.2. Again, vehicle treatments served as controls and the treatment time was 72h.

IncuCyte™ Caspase-3/7 assay (apoptosis assay)

$10x10^3$ cells were seeded in 100μL of normal medium per well in a 96-well plate. The plate was left overnight for the cells to adhere and next day the same treatment pattern as the one used in the IncuCyte™ cytotoxicity assay was followed. The CellPlayer™ Caspase 3/7 reagent was added along with the CORM or vehicle treatments, in a final concentration of 5μM in each well. The method is described in section 2.2.2.3. The experiment was followed for 72h.

IC_{50} calculation

Absorbance was normalized to the corresponding absorbance of the vehicle treated cells prior to plotting. Data was statistically analysed using non-linear regression (curve fit) to calculate the IC_{50} of each compound against each cell line in GraphPad Prism (www.graphpad.com).

IncuCyte™ data analysis

The IncuCyte™ data was analysed using the IncuCyte ZOOM 2016A software, kindly provided by Essen Biosciences and according to the manufacturer's guidelines.

Statistical analysis

Statistical analysis was performed using GraphPad Prism. Two-way ANOVA was performed to check for statistical significance, with a p-value of <0.05 considered statistically significant. Asterisk notation (*) was used to identify significances: * $p<0.05$, ** $p<0.01$, *** $p<0.001$ and **** $p<0.0001$.

3.1.3 Results

The effect of CORM treatments on the viability of different cell lines using the MTT assay

Two TNBC cells, MDA-MB-231 and MDA-MB-436, treated with CORM-1, CORM-2, CORM-3 or CORM-A1 in different concentrations, were assessed for their viability using the MTT colorimetric assay. No major cytotoxicity compared to the vehicle was observed against these cell lines and the calculated IC_{50} values exceeded 100μM. The MCF-10A breast epithelial cells representing the healthy cells in a normal breast environment were also assessed. Only CORM-2 appeared to be cytotoxic against these cells, with a calculated IC_{50} of 31.87μM. Finally, the ECs HECV were used, as vasculature is mainly lined by ECs. Again, no major cytotoxicity was observed, with only CORM-2 having an IC_{50} just above 100μM (**Figure 3.4 A** shows the average figures for all concentrations and cell lines tested; **Figure 3.4 B** shows the cytotoxicity of the highest concentration tested for all compounds; **Figure 3.4 C** shows the calculated IC_{50} values for these compounds and cell lines).

In **Figure 3.4 C**, a red box was used to highlight the CORM with the most favourable ratio of cytotoxicity between the cancer and normal cells. CORM-3 was more cytotoxic against the two TNBC cell lines than MCF-10A (IC_{50} not converged, which means that a common value could not be generated by the results, but very low cytotoxicity suggested by the graph in **Figure 3.4 B**) or HECV (more than three times higher).

A.

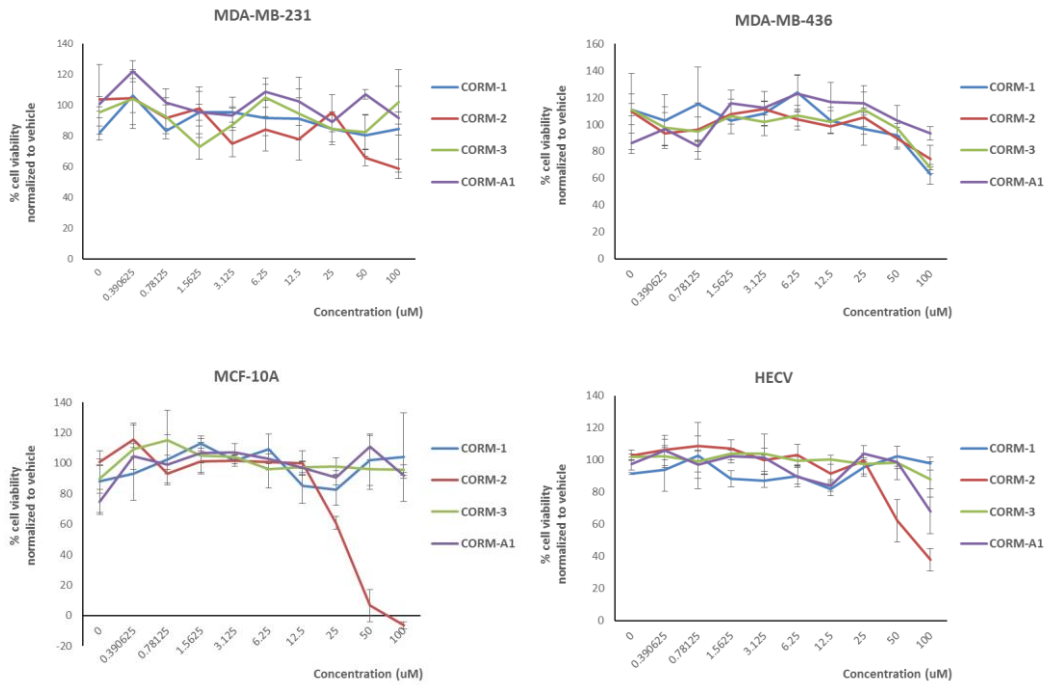

B.

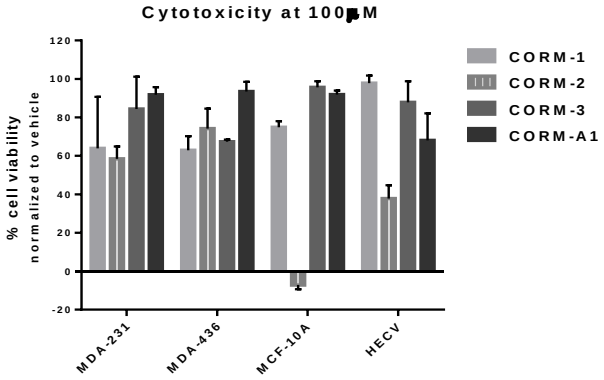

C.

IC_{50} (µM)	*CORM-1*	*CORM-2*	*CORM-3*	*CORM-A1*
MDA-MB-231	170.4±11.90	116.8±7.79	312.5±31.57	1529±286.01
MDA-MB-436	288.8±28.32	400.1±28.82	358.8±33.96	Not converged
MCF-10A	387.6±40.18	31.87±2.40	Not converged	8251±500.53
HECV	2141±530.46	108.3±5.35	996.3±104.58	327.3±19.26

Figure 3.4: Cytotoxicity of CORMs. A. Percentage of cell viability for each concentration of CORM tested for all four cell lines used. (Graphs show average % of cell viability normalized to vehicle ±SEM; n=3, N=4). **B.** Percentage of cell viability for the highest concentration of CORM tested. **C.** Calculated IC_{50} values ±SD for all compounds (as calculated in GraphPad Prism).

The effect of CORM treatments on the viability of different cell lines using the IncuCyte™

MDA-MB-231, MDA-MB-436 and MCF-10A cells were assessed for their viability using the IncuCyte™ cytotoxicity assay, following treatments with CORM-1, CORM-2, CORM-3 or CORM-A1 in four different concentrations. The same result as in the MTT assay was observed for all cell lines, that is no major cytotoxicity of the CORM treatments compared to vehicle treatments apart from CORM-2 against MCF-10A cells (representative images from the experiments in **Figures 3.5 A**, **3.6 A** and **3.7 A**). However, given the abilities of the IncuCyte™ and its software, an analysis of the confluence throughout each experiment was conducted and a difference between the treated and untreated cells was observed for some of the treatments.

More specifically, for the MDA-MB-231 cells, it appeared that 1% DMSO reduced the confluence of the cells throughout the experiment in a statistically significant manner ($p=0.0349$). Following the same pattern as their vehicle, all CORMs at 100μM concentration reduced the confluence of these cells compared to media treatment, with CORM-2 and CORM-3 reaching statistical significance ($p=0.0111$ and $p=0.0225$, respectively) (**Figure 3.5 B** shows the average increase of confluence for the 100μM CORMs, the 1% DMSO and the media treated cells, N=3). For lower concentrations, no such effect was observed (data not shown).

For MDA-MB-436 cells, there was no observed statistically significant reduction in confluence between the 1% DMSO and the media treated cells ($p>0.05$). Only CORM-1 and CORM-2 appeared to reduce the confluence of the cells compared to media treatment reaching statistical significance ($p=0.0383$ and $p=0.0258$, respectively) (**Figure 3.6 B** shows the average increase of confluence for the 100μM CORMs, the 1% DMSO and the media treated cells, N=3).

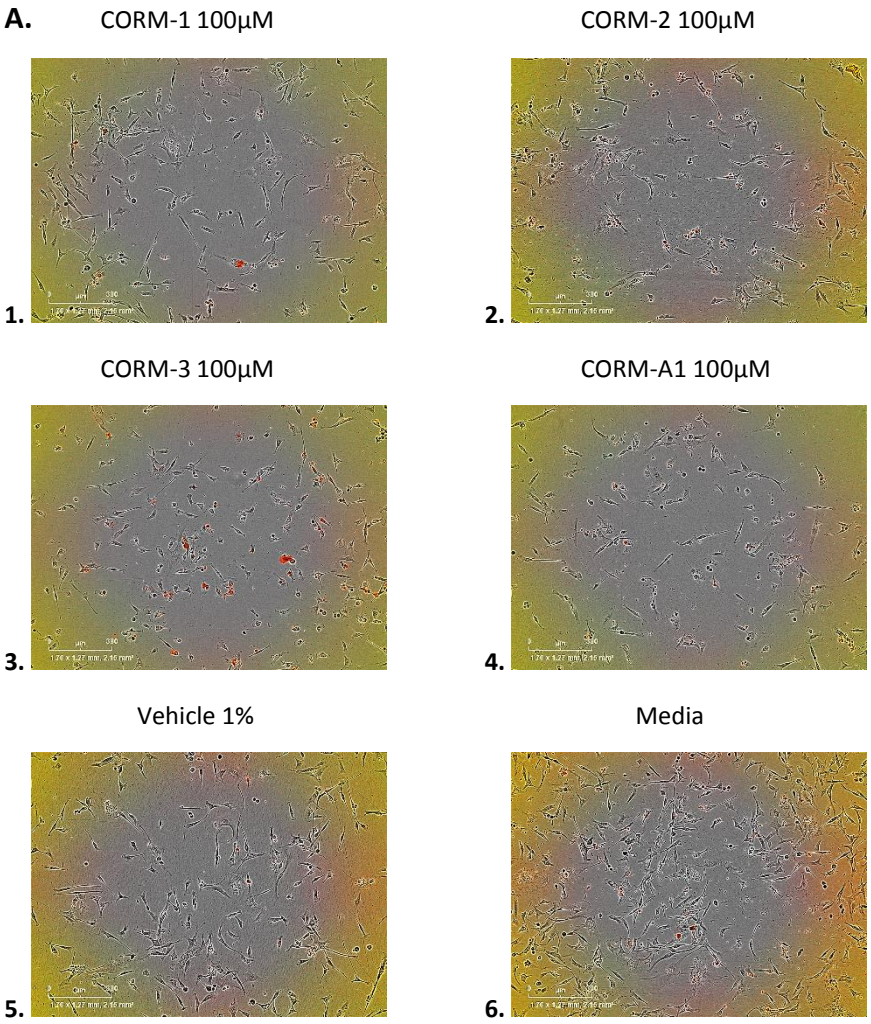

Figure 3.5: Cytotoxicity and confluence of MDA-MB-231 after CORM treatments at IncuCyte™. **A.** Representative images from the IncuCyte™ cytotoxicity assay in MDA-MB-231 cells, 64h after treatment with the highest concentration of CORMs (100µM). 1= CORM-1, 2= CORM-2, 3= CORM-3, 4= CORM-A1, 5= Vehicle 1%, 6= Media. Objective 10x bar=300µm. **B.** Confluence change rate for the 100µM treatment of CORMs followed for 64h after the treatment. (Average ±SEM; n=4, N=3) (All data was statistically analysed against media treated cells using two-way ANOVA: * $p<0.05$).

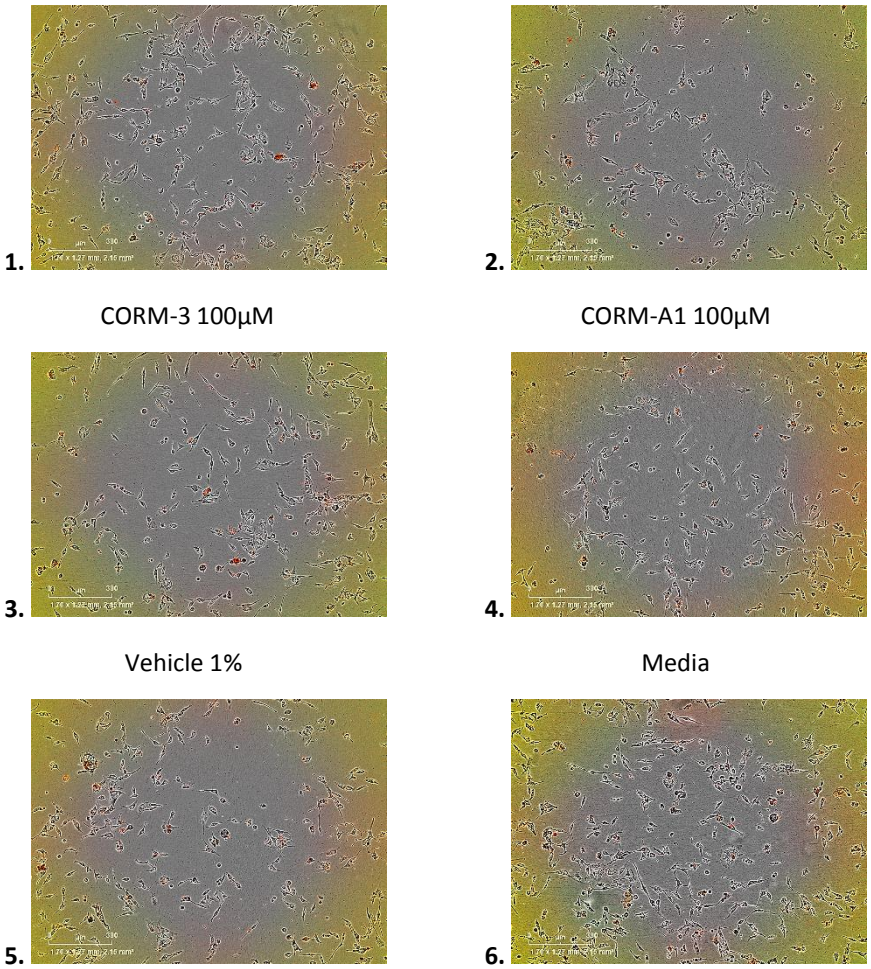

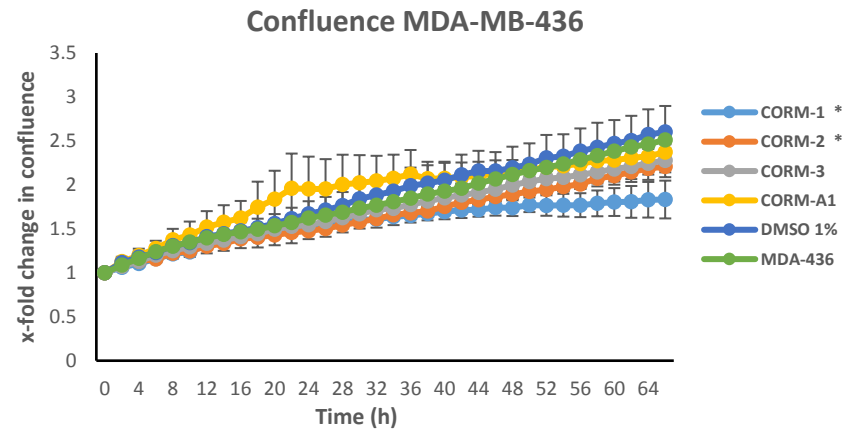

Figure 3.6: Cytotoxicity and confluence of MDA-MB-436 after CORM treatments at IncuCyte™. **A.** Representative images from the IncuCyte™ cytotoxicity assay in MDA-MB-436 cells, 72h after treatment with the highest concentration of CORMs (100µM). 1= CORM-1, 2= CORM-2, 3= CORM-3, 4= CORM-A1, 5= Vehicle 1%, 6= Media. Objective 10x bar=300µm. **B.** Confluence change rate for the 100µM treatment of CORMs followed for 64h after the treatment. (Average ±SEM; n=4, N=3) (All data was statistically analysed against media treated cells using two-way ANOVA: * $p<0.05$).

There was no observed statistically significant difference in confluence of the MCF-10A cells between the 1% DMSO and the media treated cells ($p>0.05$). Only CORM-2 significantly lowers the confluence of the cells compared to media treatment, but this is undoubtedly connected to the toxicity of this compound towards these cells ($p=0.0452$). However, there was no statistical difference between CORM-2 100μM and DMSO 1% treated groups ($p>0.05$) (**Figure 3.7 B** shows the average increase of confluence for the 100μM CORMs, the 1% DMSO and the media treated cells, N=2).

The effect of CORM treatments on breast cancer apoptosis

Following the cytotoxicity assessment with both the MTT assay and the IncuCyte™ cytotoxicity assay, caspase 3/7 levels were measured for the two TNBC cell lines following the IncuCyte™ caspase 3/7 assay. Since the MTT is an indirect way of quantifying the number of viable cells by measuring the metabolically active ones, it was deemed worthy trying different tests in order to validate the cytotoxicity of these compounds.

None of the cell lines showed any significant differences between the vehicle treated and the CORM treated groups. This result confirms the previous observations from the MTT and the IncuCyte™ cytotoxicity assays, establishing that the four commercially available CORMs show almost no cytotoxicity against the cell lines tested. The images also reflect the other observation discussed, that is the reduced confluence for the MDA-MB-231 cell line after treatment, especially with CORM-2 and CORM-3. (Representative images from the experiments in **Figures 3.8 A** and **3.9 A. Figures 3.8 B** and **3.9 B** show the change in the number of apoptotic cells for the 100μM CORMs, the 1% DMSO and the media treated cells for the two TNBC cell lines, N=2).

A.

CORM-1 100µM

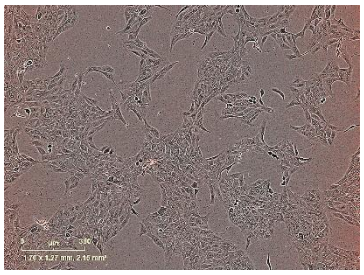

1.

CORM-2 100µM

2.

CORM-3 100µM

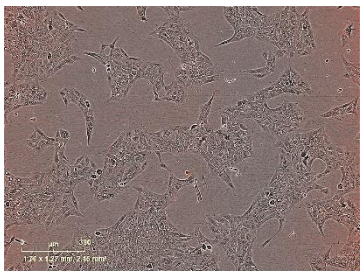

3.

CORM-A1 100µM

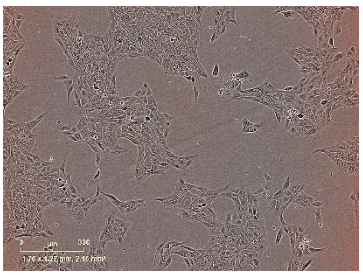

4.

Vehicle 1%

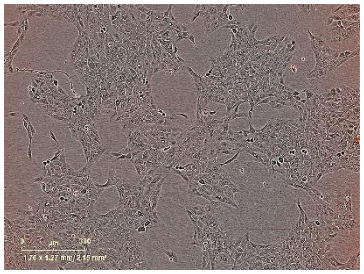

5.

Media

6.

B.

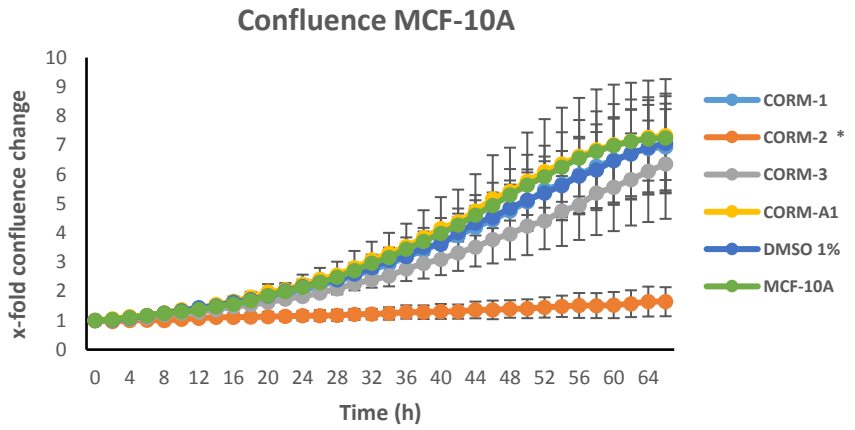

Figure 3.7: Cytotoxicity and confluence of MCF-10A after CORM treatments at IncuCyte™. **A.** Representative images from the IncuCyte™ cytotoxicity assay in MCF-10A cells, 72h after treatment with the highest concentration of CORMs (100µM). 1= CORM-1, 2= CORM-2, 3= CORM-3, 4= CORM-A1, 5= Vehicle 1%, 6= Media. Objective 10x bar=300µm. **B.** Confluence change rate for the 100µM treatment of CORMs followed for 64h after the treatment. (Average ±SEM; n=4, N=2) (All data was statistically analysed against media treated cells using two-way ANOVA: * $p<0.05$).

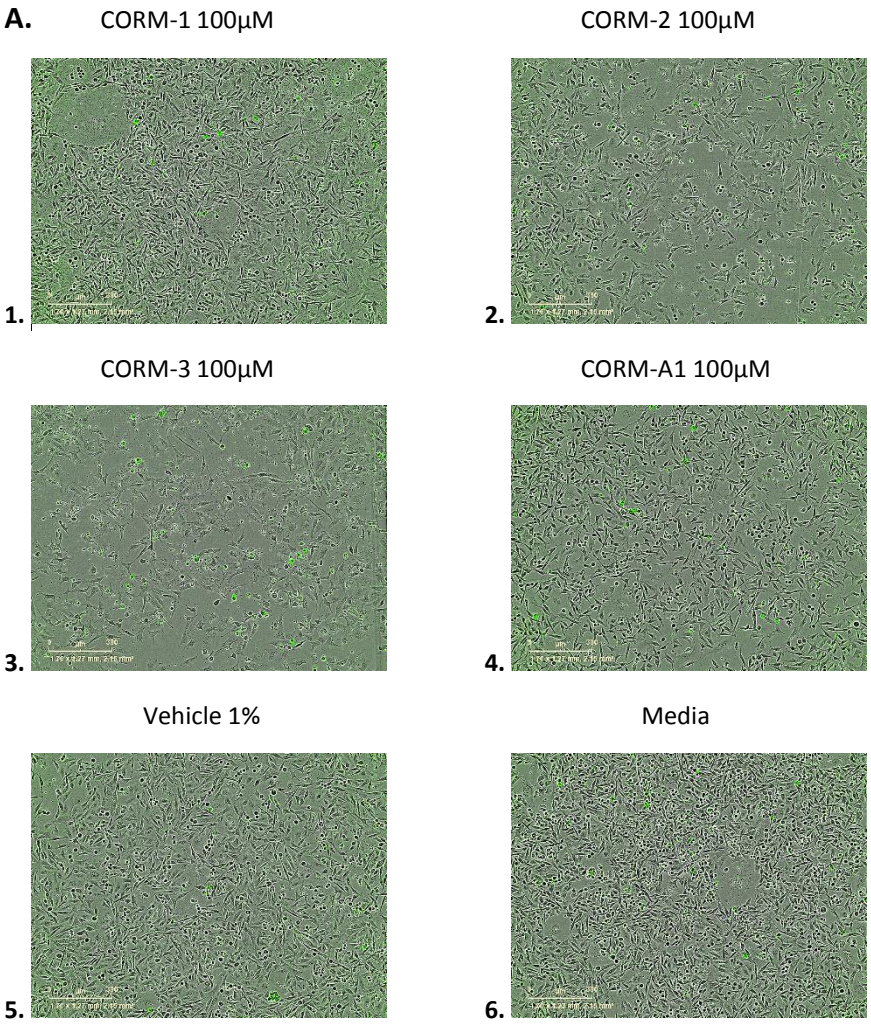

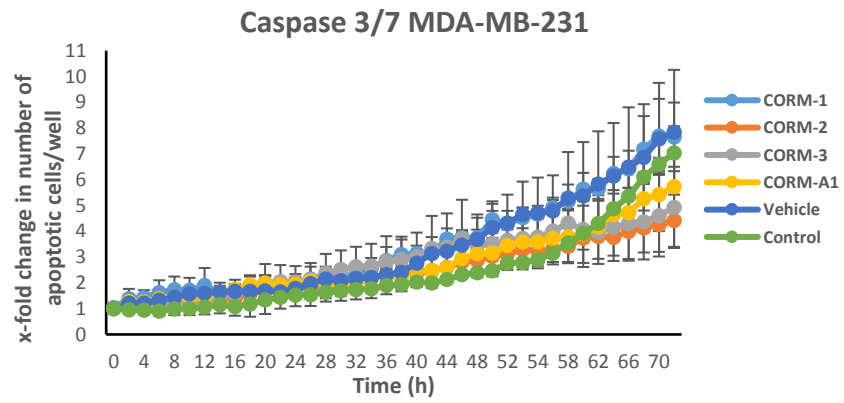

Figure 3.8: Caspase 3/7 quantification after CORM treatments in MDA-MB-231 at IncuCyte™. **A.** Representative images from the IncuCyte™ caspase 3/7 assay in MDA-MB-231 cells, 72h after treatment with the highest concentration of CORMs (100µM). 1= CORM-1, 2= CORM-2, 3= CORM-3, 4= CORM-A1, 5= Vehicle 1%, 6= Media. Objective 10x, scale bar=300µm. **B.** Change in the number of apoptotic cells per well for the 100µM treatment of CORMs followed for 72h after the treatment. (Average ±SEM; n=3, N=2) (All data was statistically analysed against media treated cells using two-way ANOVA: * $p<0.05$).

A.

CORM-1 100µM

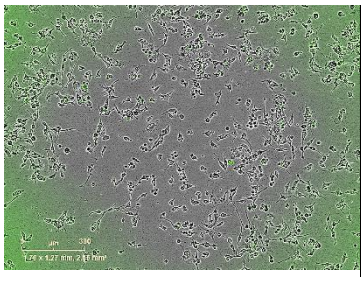

1.

CORM-2 100µM

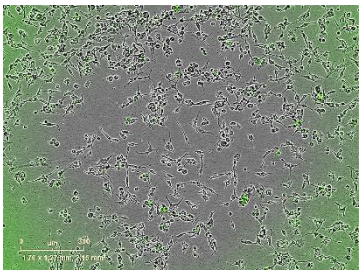

2.

CORM-3 100µM

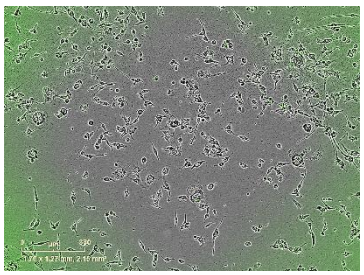

3.

CORM-A1 100µM

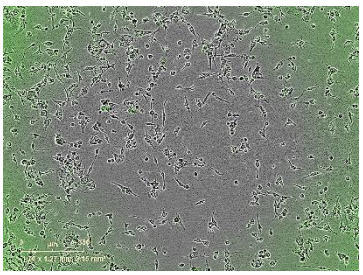

4.

Vehicle 1%

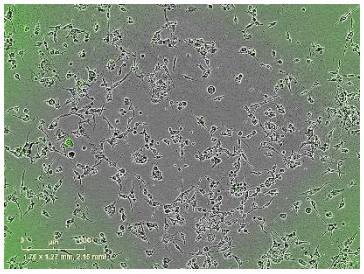

5.

Media

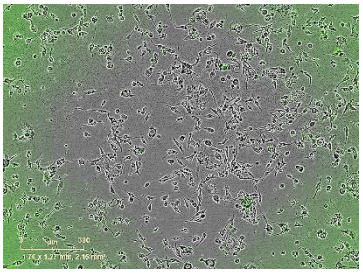

6.

B.

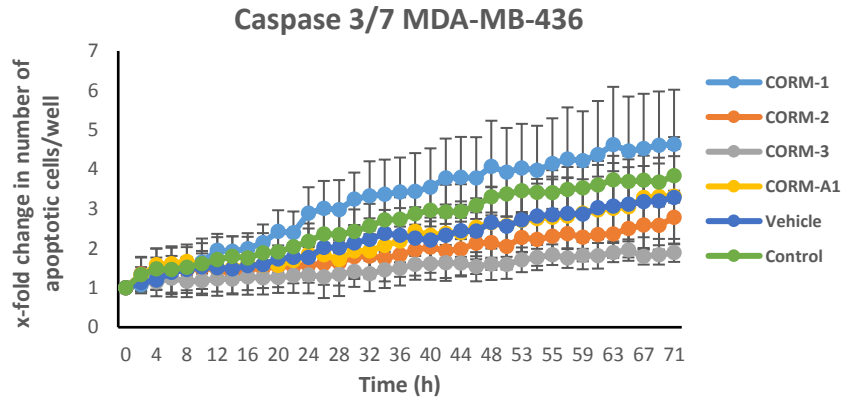

Figure 3.9: Caspase 3/7 quantification after CORM treatments in MDA-MB-436 at IncuCyte™. **A.** Representative images from the IncuCyte™ caspase 3/7 assay in MDA-MB-436 cells, 72h after treatment with the highest concentration of CORMs (100µM). 1= CORM-1, 2= CORM-2, 3= CORM-3, 4= CORM-A1, 5= Vehicle 1%, 6= Media. Objective 10x, scale bar=300µm. **B.** Change in the number of apoptotic cells per well for the 100µM treatment of CORMs followed for 71h after the treatment. (Average ±SEM; n=3, N=2) (All data was statistically analysed against media treated cells using two-way ANOVA: * $p<0.05$).

3.1.4 Discussion

According to general opinion, heavy metals and drugs based on them may present toxicological concerns not only to the environment in general, but also to different cells and organisms. It is generally believed that metals such as palladium and platinum are more harmful than lower molecular weight metals such as nickel or cobalt. Metal toxicity, however, is tightly correlated with the form in which the metal is present, as pure elements may differ greatly from their compounds, that might have solubility, oxidation state and bioavailability variations. The same applies to organometallic compounds with different metals bound, as the toxic effects derive mainly from the intrinsic characteristics of each one, such as the oxidation state, ligand sphere or the counter-ion present (Egorova and Ananikov 2017). The prejudice against metal-based drugs was partially lifted when cisplatin was discovered, which led to numerous other candidates for metal-based drugs (Wang and Lippard 2005). Nevertheless, the common conception that the composition of a compound can be directly linked to its toxicity is still misleading, especially for metal-based drugs. Organometallic compounds consist a special class of compounds and it should be acknowledged that it is probably impossible to confidently correlate structure with toxicity and metals should not be seen as purely toxic components, but their toxicity is rather correlated with the oxidation state, the ligands, the solubility and the stereochemistry of each molecule (Egorova and Ananikov 2017).

Both CORM-2 and CORM-3 are ruthenium (Ru)-based molecules that eventually release Ru-bound species to the microenvironment of the tissues (Winburn et al. 2012). As a matter of fact, Ru-based agents have undergone clinical trials with the first one to be tested being NAMI-A with gemcitabine in 2008 (phase I/II) (Alessio 2017). Ru compounds are believed to cause fewer and less severe side effects compared to other organometallic drugs, due to certain reasons: 1) they have low toxicity because Ru can mimic iron (Fe); 2) they have slow ligand exchange rates; 3) they are activated by reduction; 4) they may preferably accumulate in cancer tissues and 5) their transfer and uptake are mediated by transferrin. However, Ru compounds have eventually shown broad diversity in their activity, toxicity and mechanisms of action, surprising both their supporters and opponents, and many researchers challenge these

attributed advantages (Page 2012; Alessio 2017; Ndagi et al. 2017). In any case, if a metal-based compound is designed to be highly selective towards an enzyme and the metal core is not toxic itself, then they will probably afford non-toxic compounds that are also safer to the general environment (Allardyce and Dyson 2016).

Similarly, manganese (Mn) is an essential and biocompatible metal. Mn complexes have various medicinal applications. The most significant therapeutic value of Mn complexes is their antioxidant application in biological systems, and due to this, three Mn-based complexes (AEOL-10150, EUK-134, and M40403) are already under clinical trials (Ali et al. 2017).

In the assessment of cytotoxicity for the four commercially available CORMs, two TNBC cell lines were chosen to be tested, MDA-MB-231 and MDA-MB-436, because this is the targeted cancer subtype, along with a control epithelial breast cell line, MCF-10A and an endothelial cell line, HECV. As shown in the graphs (**Figure 3.4**), these compounds had a moderate cytotoxicity against the cell lines, with the most potent compound in general being CORM-2.

As discussed earlier, CORM-2 has been previously shown to exert toxicity against different cell subtypes at around 50μM (Lee et al. 2014; Vítek et al. 2014; Ahmad et al. 2015). Similar to these results, CORM-2 at 100μM reduced the viability of MDA-MB-231 by ~50% and of MDA-MB-436 by ~30%, with calculated IC_{50} values of 117μM and 400μM, respectively. However, CORM-2 was also the most toxic CORM against the control MCF-10A cell line, with a low IC_{50} of 32μM. The toxicity of CORM-2 against the ECs along with the TNBC cells might be desired, but the quite high toxicity against the breast epithelial cells is definitely a drawback.

Since the MTT assay offers an indirect measurement of cell viability that might be affected by the interference of CORMs with the mitochondria, another more direct assay was also conducted. When considering the results of the IncuCyte cytotoxicity assay, even though the cell viability results were very similar to the previous ones, CORM-2 obviously affects the proliferation of MDA-MB-231, pointing towards a cytostatic rather than a cytotoxic profile. Even though there was no statistical significance upon a two-way ANOVA analysis between the vehicle and the CORM-2

group, when comparing CORM-2 with the media treated group, significance could be obtained with a p-value of 0.0111. Furthermore, the vehicle itself reduced the confluence of the cells after 44h, and when comparing with media treated cells, this trend reached significance (p=0.0349). Anyway, CORM-2 remains the only one with such low confluence after 72h of treatment in MDA-MB-231. Similar results were reported also in MDA-MB-436, where again CORM-2 was not very cytotoxic, but reduced cell confluence significantly when compared with media treated cells (p=0.0258). Finally, the high toxicity of CORM-2 against MCF-10A was most probably responsible for the inhibition of their proliferation in a notable manner.

CORM-3 on the other hand, even though sharing many common features with CORM-2, such as the Ru core and the similar ligand sphere, exerted a considerably lower toxicity against the tested cells. It appeared to be more potent against MDA-MB-231 with an IC_{50} value of 312.5μM, closely followed by MDA-MB-436, and almost no cytotoxicity was reported against epithelial or ECs. It was the only CORM with such as big difference (almost three times) between the toxicity against TNBC cells and normal cells, which suggests a kind of selectivity for this CORM. CORM-3 did not affect the proliferation of the cells at significant levels, apart from MDA-MB-231, where p=0.0225 when compared to media treated cells.

CORM-1 was the only Mn CORM tested, which also belongs to the photo-CORM family. Even though no specific light excitation was used for this compound, the stock solutions were prepared and kept in the dark until they reached the cells, under ambient daylight. For this compound, a desirable toxicity profile was reported, where the two TNBC cells were more sensitive compared to the epithelial or endothelial ones. However, the toxicity against MCF-10A was very close to the toxicity against MDA-MB-436. The lowest IC_{50} was measured for the MDA-MB-231 cells, although a little higher than CORM-2's. CORM-1 significantly reduced the proliferation of only MDA-MB-436 cells when compared to media (p=0.0383).

Finally, CORM-A1 did not show any cytotoxicity against these cells or any inhibition of their proliferation rates. It is also the only one without a heavy metal core, potentially responsible for the total lack of toxicity.

Since the highest concentration tested for the MTT assay was 100μM, all the calculated IC_{50} values exceeding 100μM are extrapolated values, which poses certain limitations. The safest way to determine an IC_{50} value is by experimental testing of all the relevant concentrations until the half point is reached. However, due to time restrictions only a few concentrations were explored, and the calculation was performed by the statistical software Graphad, which means that the true experimental value could be a lot different than the calculated one. It is also worth considering that the projected sigmoid curves could follow another pattern after the 100μM concentration, but since this was not experimentally determined, the extrapolated calculated IC_{50} values could not be used as a concluding result but rather as an indication of where the IC_{50} could lie. Nevertheless, for the purposes of this study, these values were used to imply potential selectivity of some CORMs and for comparison reasons, even though they should be viewed rather sceptically.

At this point, another relevant issue must be addressed, and that is the solvent used in these experiments. Dimethyl sulfoxide (DMSO) is a common chemical solvent for pharmaceutical preparations, although it has certain disadvantages compared to water. As discussed in many publications, low concentrations of DMSO have no deleterious effects on cell viability or cytology, however when the concentration goes up to 1% (used as the highest concentration in my experiments) the effects become more significant and increased apoptosis is reported (Winburn et al. 2012). Although many studies try to deal with this problem, by using both a low and a high concentration of DMSO and comparing their results with both as well as the media itself, most of the studies seem to deliberately ignore this phenomenon and use a much lower concentration of DMSO as control compared to the one used to dissolve the CORMs (Winburn et al. 2012). In my experiments I chose to use the correct concentration of DMSO, that is 1%, as the highest one, since this is exactly how much is needed to dissolve the CORMs. Even then though, CORM-1 was challenging, because even in pure DMSO it is not completely or easily soluble.

The caspase 3/7 quantification experiment showed no statistically significant difference between the treated groups, even though the trend could be seen for increased apoptosis following DMSO 1% treatment in MDA-MB-231.

In summary, the metal core may be partly responsible for the moderate toxicity associated with CORMs -1, -2 and -3, although no major cytotoxicity was reported for any of the cells tested. This is also an indication that the heavy metal core is not necessarily toxic in all potential forms, and that other characteristics may affect this behaviour.

3.2 Metabolic dysfunction detection

3.2.1. Introduction

In 1924 Otto Warburg realized that cancer cells depend on aerobic glycolysis to metabolize glucose and generate ATP. This is a less efficient pathway to produce energy, since with oxidative phosphorylation the yield is 36 molecules of ATP per glucose molecule, but with aerobic glycolysis the yield falls to only 2 molecules of ATP. This is also the case for cancer cells with plenty of oxygen and no apparent oxygen deprivation, which is more common in the cores of solid tumours. This phenomenon is referred to as the “Warburg effect” (Gatenby and Gillies 2004). The up to 200 times higher rate of glycolysis in cancer cells is followed by lactic acid fermentation in the cytosol, unlike normal cells which oxidize pyruvate in mitochondria (Kim and Dang 2006).

The Warburg effect was initially thought as a cause for the transition of normal cells to cancerous ones, but today it is viewed more as a consequence of damaged mitochondrial function or a simple adaptation of the cancer cells to unfriendly environments with low oxygen concentrations and nutrient supply (López-Lázaro 2008; Alfarouk et al. 2014). This metabolic switch is useful for the tumour also for other reasons, one of them being the generation of a unique pH gradient between the low extracellular pH and the alkaline or near neutral pH environment within the tumour, that serves as a determining factor for the ability of the tumour to invade and metastasize, surpassing the immune system (Alfarouk 2016).

Nevertheless, this observation of high glycolysis levels of cancer cells compared with normal cells, which produce energy via the oxidation of pyruvate in mitochondria, was deemed a promising target for new anti-cancer therapies (Alfarouk et al. 2014; Alfarouk 2016). Inhibition of glycolysis would deprive cancer cells of energy, reducing

their rapid growth and proliferation. Cancer cells seem to be completely dependent on the glycolytic pathway for energy production, and oxidative phosphorylation was found to be suppressed in them. Thus, activating the mitochondrial respiration back could be a potential alternative approach for anti-cancer therapy, leading cancer cells to apoptosis (Upadhyay et al. 2013). In that scope, it has also been reported that aerobic glycolysis seems more efficient during rapid cell growth – as in cancer cells – compared with normal glycolysis linked to the tricarboxylic acid (TCA) cycle and oxidative phosphorylation, therefore switching to an oxidative metabolism could lead cancer cells to ineffective growth and death (Shyh-Chang et al. 2013).

There are many publications dealing with the alterations in cell metabolism caused by the administration of exogenous CO. One study in astrocytes reports a reduction in the ratio between lactate production and glucose consumption, while oxygen consumption and mitochondrial population were increased. This could indicate a CO-induced enhancement of oxidative phosphorylation for these cells, promoting cytoprotection (Almeida et al. 2012). Moreover, the group of Wegiel has demonstrated an inhibition in prostate cancer progression by CO, which seems to induce an anti-Warburg effect also promoting chemotherapeutic effectiveness. Mitochondria seem to be the main target of CO, as assessed by higher oxygen consumption levels and elevated ROS generation, leading to mitochondrial dysfunction and cell growth inhibition induced by the combined chemotherapy (Wegiel et al. 2013). Finally, another study supports the ability of CORM-A1 to induce differentiation in neurons due to increased mitochondrial population and enhanced oxidative phosphorylation levels, which suggest a metabolic modulation driven by CO towards a more oxidative profile (Almeida et al. 2016).

With these in mind, investigation into whether this metabolic modulation was evident in TNBC cells and if different treatment options and durations would affect these observations was desired. A way to measure glycolysis levels in treated and untreated cells is by using the Seahorse XF Glycolysis Stress Test. This test illustrates the three key parameters of glycolytic function: glycolysis, glycolytic capacity and glycolytic reserve. The Seahorse XF^{e} Extracellular Flux Analyser can measure glycolytic levels by measuring the extracellular acidification rate (ECAR) of cells inserted in the

instrument. These cells can be previously treated for a certain time period with agents that can potentially alter their metabolism, or the treatment can be injected during the experiment directly on the cells (instant treatment).

In this section, the aim was to identify if 72h pre-treated or instantly treated cancer cells show differences in their glycolytic metabolism compared to untreated or vehicle treated cells. There was also a desire to spot any differences the co-treatment with 10μg/mL or 100μg/mL of Avastin® could induce to their glycolysis levels.

In order to achieve that, the cells were either pre-treated with increasing concentrations of CORMs for 72h prior to the experiment or the treatments were injected during the experiment. Glycolysis levels can be calculated after the increase in glycolysis induced by the precursor glucose injected directly on the cells. Glycolytic capacity is measured after injecting the antibiotic oligomycin, which is well known for its inhibitory activity on the ATP synthase. This way, cells are forced to use glycolysis only for the production of energy. Finally, the glucose competitor 2-deoxy-D-glucose (2-DG) is injected to stop glycolysis and cells return to their original levels, which indicates the glycolytic reserve.

3.2.2 Materials & Methods

Cell lines and treatments

MDA-MB-231 cells maintained in DMEM media with 10% FBS and antibiotics were used for these experiments. All cells were maintained at 37°C with 5% CO_2 prior to the assay. Cells were treated with increasing concentrations of CORMs or DMSO and standard concentrations of Avastin® in the corresponding experiments.

Glycolysis Stress test with the Seahorse Extracellular XF^e Flux Analyser

The glycolysis levels of the cells were measured using the Seahorse Extracellular XF^e Flux Analyser. For the Seahorse XF24 Cell Culture Microplate, 40,000 cells/well were seeded. The Seahorse Base medium included 1mM glutamine, had a pH of 7.35 and was kept at 37^{o}C after filtration. The normal media of the cells was removed and 525μL of Glycolysis media were added before the plate was left in a CO_2-free incubator for 1h. All the injections prepared meanwhile were loaded on the injection plate at

volumes of 75μL each. After the experiment, wells were washed with PBS twice and 11μL of lysis buffer were added to each well. A protein quantification assay was performed right after.

For the Seahorse XF96 Cell Culture Microplate, 10,000 cells/well were seeded. The procedure was the same apart from changes in concentrations and volumes: the normal media of the cells was removed and 150μL of Glycolysis media were added in each well. All the injections were loaded on the injection plate at volumes of 25μL each. After finishing the experiment, the wells were washed with PBS twice and a crystal violet assay was performed right away for the quantification of the cell biomass.

Statistical analysis

Statistical analysis was performed using GraphPad Prism. Two-way ANOVA was performed to check for statistical significance, with a p-value of <0.05 considered statistically significant. Asterisk notation (*) was used to identify significances: * $p<0.05$, ** $p<0.01$, *** $p<0.001$ and **** $p<0.0001$.

3.2.3 Results

Glycolysis Stress test for pre-treated MDA-MB-231 (72h)

MDA-MB-231 cells were pre-treated with three different concentrations of CORMs or 1% DMSO for 72h and then subjected to a glycolysis stress test in the Seahorse Analyser. As observed in **Figure 3.10 A**, no statistically significant difference between the CORM and vehicle treated groups was measured in this experiment for any of the concentrations tested.

Glycolysis Stress test for instant treatments on MDA-MB-231

MDA-MB-231 cells were subjected to a glycolysis stress test in the Seahorse Analyser. The treatments were added directly on the cells as the first injection, and then the protocol was followed as previously described. Four different concentrations of CORMs were tested, along with matching vehicle concentrations and media treatments as controls. As observed in **Figure 3.10 B**, for the highest concentration tested (100μM), only CORM-2 raised a statistically significant reduction in the

glycolysis change rate compared to the vehicle group (p=0.0006). Again for the 50μM treatment, only CORM-2 reduced the levels of glycolysis significantly, with a p-value of 0.0184. However, for both lower concentration treatments, nearly all CORMs produced such an effect, with the media treated group also appearing to perform glycolysis in a significantly lower level than the vehicle group (p=0.0108 for the 25μM treatment and p<0.0001 for the 12.5μM treatment). More specifically, for the 25μM treatment, CORMs -1, -2 and -3 reduced glycolysis compared to vehicle with p-values of 0.0326, 0.0399 and 0.046, respectively. Finally, for the 12.5μM treatment, CORMs -1, -3 and -A1 significantly decreased glycolysis with p-values of 0.0297, 0.0133 and 0.0018, respectively.

A.

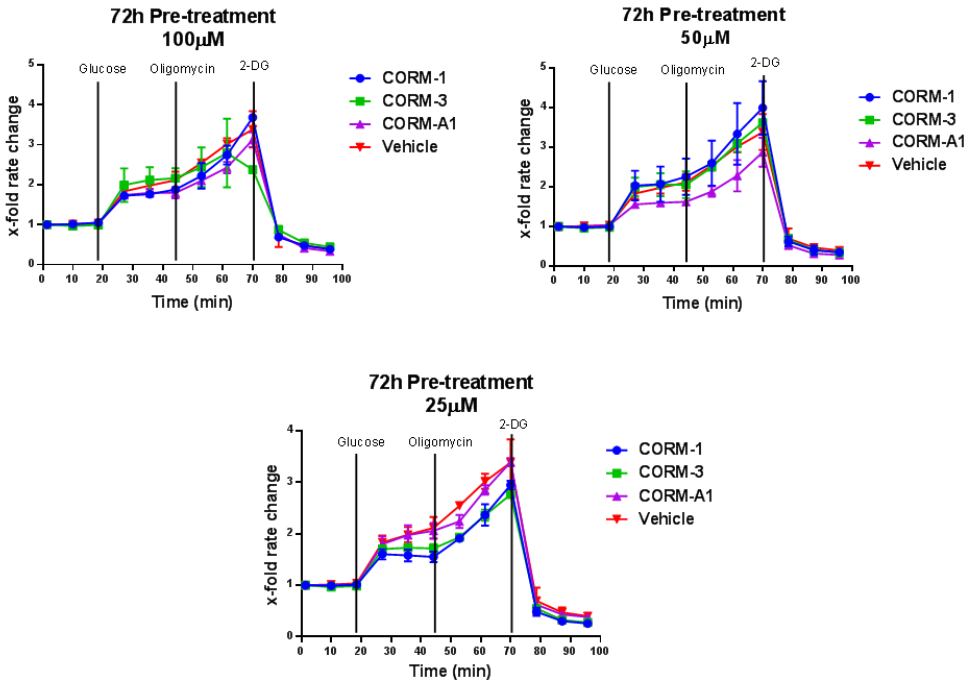

B.

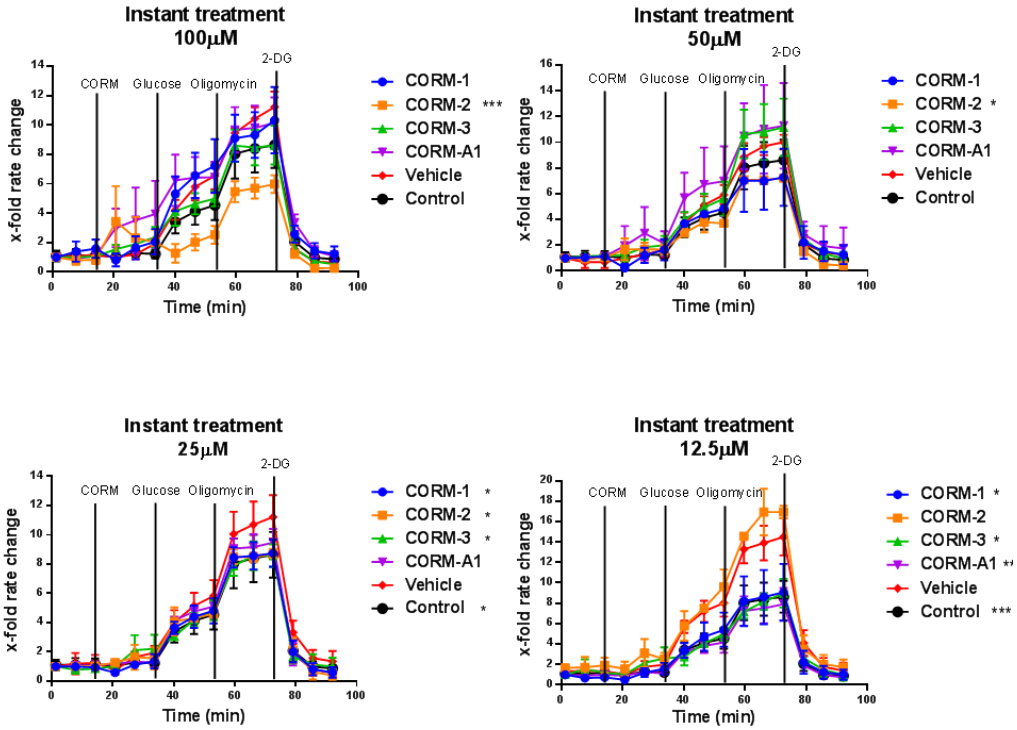

Figure 3.10: Glycolysis stress test in MDA-MB-231 after CORM treatments. A. Change rate in the glycolysis levels of pre-treated MDA-MB-231 cells, measured as ECAR (mpH/min). (Average ±SEM; n=3, N=2). **B.** Change rate in the glycolysis levels of instantly treated MDA-MB-231 cells, measured as ECAR (mpH/min). (Average ±SEM; n=3, N=2) (All data was statistically analysed against vehicle treated cells using two-way ANOVA: * $p<0.05$, ** $p<0.01$ and *** $p<0.001$).

Glycolysis stress test for CORM combined with Avastin® 10μg/mL treatments on MDA-MB-231

Avastin® was the first anti-angiogenic drug to be marketed as discussed earlier in section 1.3.3.1. Since the general aim was to examine if these four CORMs had any anti-angiogenic effects against TNBC and could be eventually combined with Avastin® in order to enhance its efficacy, it was considered interesting to look for any differences in the glycolytic levels of MDA-MB-231 cells after treatment with CORMs and a standard concentration of Avastin®. Two concentrations of Avastin® were chosen for this study, 10μg/mL and 100μg/mL, although the highest one (100μg/mL) interfered with the experiment and no useful results were obtained.

As shown in **Figure 3.11**, the addition of Avastin® (10μg/mL) dissimulated the previously observed decrease in the glycolytic levels of these cells, reducing any differences between the vehicle and CORM treated groups. Only CORM-A1 managed to raise statistical significance in the highest concentration tested ($p=0.0349$), whereas CORM-3 was the only different in the 50μM treatment group ($p=0.0246$).

Glycolysis stress test for CORM combined with Avastin® 100μg/mL treatments on MDA-MB-231

Unfortunately, the results of this experiment were not appropriate for analysis, since after the addition of this high concentration of Avastin®, the pH of the wells was severely derailed, not allowing for the detection of changes. Most of the wells showed pH values in the sub-zero area, so the results were not deemed worth of analysis, and the experiment was not repeated.

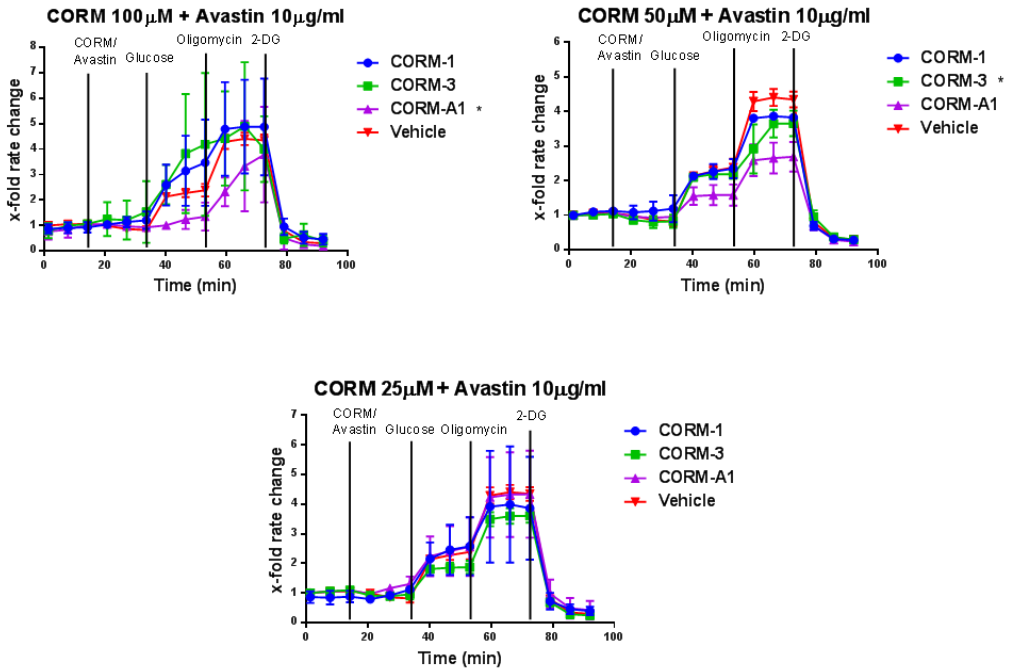

Figure 3.11: Glycolysis stress test in MDA-MB-231 after CORM treatments combined with Avastin®. Change rate in the glycolysis levels of instantly treated with combination of CORMs and Avastin® (10μg/mL) MDA-MB-231 cells, measured as ECAR (mpH/min). (Average ±SEM; n=3, N=2) (All data was statistically analysed against vehicle treated cells using two-way ANOVA: * $p<0.05$).

3.2.4 Discussion

Cancer has been linked to mitochondrial dysfunctions even from studies carried out many years ago. Several studies have shown decreased mitochondrial number and the reduced efficiency of Krebs' cycle compels cancer cells to use glycolysis for the production of energy. Aerobic glycolysis (Warburg effect) can be more efficient in supporting the rapid growth of cancer cells, compared to normal glycolysis linked to the TCA cycle and oxidative phosphorylation. In addition, diminishing mitochondrial activity offers cancer cells a way to reduce apoptosis, therefore provides an evolutionary advantage. The reprogramming of cellular metabolism and the shift of the environmental pH towards the acidic region during malignant transformation suppresses the growth of normal cells and potentially supports cancer cell growth and migration (Shyh-Chang et al. 2013; Alfarouk 2016).

Carbon monoxide has been shown to exert a variety of effects on mitochondrial function and cell metabolism, depending on its concentration, the duration of exposure and the specific cell subtype studied. It is generally accepted that CO can inhibit cellular mitochondrial respiration via inhibition of complex IV (cytochrome c oxidase). CO has also been implicated with increased ROS production, which is also a mechanism for its signalling activity. Even though low concentrations can activate survival pathways, high concentrations of CO can increase mitochondrial oxidative stress, inhibit mitochondrial electron transport chain and protein synthesis and maybe activate apoptotic pathways in predisposed cells (Alonso et al. 2003; D'Amico et al. 2006; Piantadosi et al. 2006; Zuckerbraun et al. 2007; Winburn et al. 2012; Szabo 2016).

As shown in many studies, exogenous CO reduces glucose consumption and at the same time increases oxygen consumption, indicating a CO-induced improvement in oxidative phosphorylation levels (R. Oliveira et al. 2016). CO can also limit prostate cancer progression by manipulating cell metabolism, thus sensitizing cancer cells to chemotherapy via promoting an anti-Warburg effect. Indeed, CO can target the mitochondrial activity, inducing higher oxygen consumption levels and free radical generation, thus leading to mitochondrial collapse, cancer cell growth inhibition and maybe apoptosis, induced potentially by chemotherapy (Wegiel et al. 2013). Finally,

in another study by Kaczara et al. (Kaczara et al. 2015), it has been demonstrated that CO released from a novel CORM (CORM-401) induced uncoupling of mitochondrial respiration and repression of glycolysis, which could lead to the inhibition of pathological angiogenesis.

In the first experiment, a 72h pre-treatment with CORMs was tested for any effects on the metabolism of MDA-MB-231 in three different concentrations. As expected, no major differences were observed between the CORM and vehicle treated cells. This was probably due to the long treatment, where all CO released would have the time to escape from the cell media, therefore no long-time effects would be measurable. If indeed the CO is responsible for any inhibition of the glycolytic metabolism of the cancer cells, this would be an instantaneous incident and a shorter treatment would be more appropriate to measure it. It should also not be forgotten that the CORMs chosen for this study have a very short half-life, except for CORM-A1 (~21min).

Thus, a different scheme was also tested, that is an instant treatment with CORMs as the first injection during the experiment. As shown in **Figure 3.10 B**, in the highest concentration tested, only CORM-2 managed to raise a statistically significant reduction in the glycolysis levels of TNBC cells compared to vehicle treatment, and more specifically in the actual glycolysis and the glycolytic capacity. However, an anomaly during the first measurements could be seen, which would probably diminish if the experiment was repeated further and may be linked to changes in the pH due to the addition of the treatment in such high concentration.

When the concentration halved (50μM), again only CORM-2 reduced the metabolism of the cancer cells in a significant manner, although less compared to the higher concentration. Again the reduction was reported in the glycolysis and the glycolytic capacity of the TNBC cells.

On the contrary, when the concentrations of the treatments decreased, a difference between the vehicle and media treated cells was observed, where the vehicle seemed to increase the glycolytic metabolism of the cells, and especially their glycolytic capacity. All CORMs in the 25μM treatment, apart from CORM-A1, managed to reduce

this reported increase and resembled the media treated cells, raising statistical significance over the vehicle.

Finally, in the lowest concentration used (12.5μM), again the vehicle and the media treated cells showed a highly statistically significant difference in the glycolysis and glycolytic capacity ($p<0.0001$), and all CORMs, apart from CORM-2 this time, managed to reduce this increase and resemble the media treatment. This unexpected effect of low concentrations of the vehicle might be due to the limited time of repeats for this experiment or due to other unidentified reasons. In any case, if such observations are close to the truth, then CORMs managed to reduce the glycolytic levels of TNBC cells even against the increasing influence of their vehicle, which suggests a notable reduction.

It has been previously shown that CO release from low concentrations of CORM-3 interact with the mitochondrial respiratory chain by uncoupling proteins and also with adenine dinucleotide transporters leading to disruption of the membrane potential. Ruthenium compounds have demonstrated significant mitochondrial toxicity suggesting that the Ru core of CORM-2 and CORM-3 might also be responsible for the impairment of complex I and IV activity (Lo Iacono et al. 2011; Winburn et al. 2012; Long et al. 2014; Kaczara et al. 2015). Therefore, these results could be explained, especially for CORM-2 and CORM-3, by supporting the hypothesis that the Ru core along with the CO reduce the glycolytic metabolism of TNBC cells by interfering with the mitochondrial activity, inhibiting proteins of the respiratory chain and leading to electron leakage and ROS production.

Avastin® is a well-known anti-VEGF-A monoclonal antibody, which has been approved for different cancer subtypes. Since CORMs were studied for any anti-angiogenic effects for a potential combination with Avastin® in TNBC, the glycolytic levels of MDA-MB-231 cells after instant treatment with CORMs in combination with a standard concentration of Avastin® (10μg/mL) were also tested.

The same concentrations of CORMs were chosen (100μM, 50μM 25μM), and as depicted in **Figure 3.11**, no major differences were reported between the CORMs and the vehicle treated cells. Only CORM-A1 managed to significantly reduce the glycolysis

and glycolytic capacity of the cells compared to vehicle. This has also been shown for neuronal cells, that CORM-A1 can enhance their mitochondrial metabolism by increasing oxidative phosphorylation and decreasing lactate production per molecule of glucose consumed (Almeida et al. 2016). In the 50μM, only CORM-3 was different from the vehicle, although CORM-A1 showed the same trend but barely missed significance (p=0.0563). Finally in the lowest concentration tested, no differences were observed between the CORM treatments and the vehicle.

In principle, all experiments should be repeated at least three times in order to be statistically analysed safely. However, due to restrictions in the use of the Seahorse equipment, as well as other unforeseen circumstances, these experiments were only repeated twice, which might partially explain the few inconsistencies observed and the noticeable error bars for some of them. In the 72h pre-treatment and in the combination with Avastin® experiments, no media treated group was included, which largely affects the overall picture, as a very interesting increasing trend was reported for the low concentrations of vehicle during the instant treatments, which could not be assessed for the other experiments too. Especially in the combination of CORMs with Avastin®, it would be very interesting to study the change in glycolysis levels for normal media treated cells and compare with the vehicle and other treatments. This may have indicated a similar increasing trend for the vehicle, which would explain the lack of reduction in glycolysis after CORM treatments. All in all, CORMs seem to have effects on the glycolytic ability of TNBC cells, but more experiments and various protocols would be needed in order to safely reach conclusions.

3.3 Protein expression quantification

3.3.1. Introduction

In order for tumour angiogenesis to take place, two important steps must be accomplished. First, the tumour cells should be able to express high concentrations of VEGF and other growth factors, in order to induce pro-angiogenic signals. Second, ECs around the tumour area should express effective VEGFRs (RTKs) that upon binding with VEGF will initiate the pro-angiogenic signal through activation of their downstream signalling pathways. This activation cascade involves the

phosphorylation of several kinases that manipulate EC survival, proliferation, migration and vessel formation. Therefore, an anti-angiogenic agent could potentially inhibit several different steps of this process that is either the ability of cancer cells to express elevated stimulant levels or the ability of ECs to execute an efficient signal transduction that will lead to new vessel formation.

Endothelial cells are equipped with surface VEGFRs that upon stimulation with VEGF activate their downstream signalling pathway. This pathway is quite complicated, as depicted in **Figure 3.12**. Numerous proteins are involved in the successful signalling towards EC survival, proliferation, migration and capillary formation, but in this study the focus was on a few of them, depicted more clearly in **Figure 3.13**.

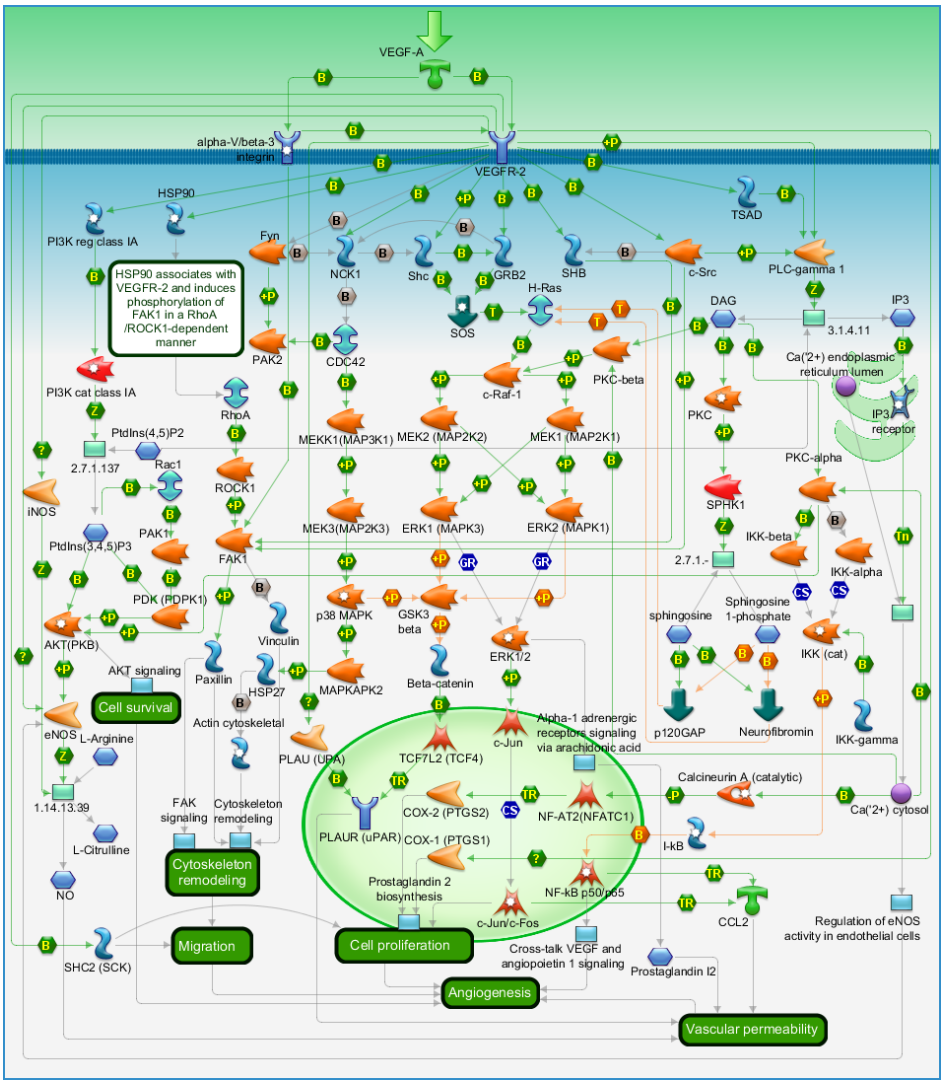

Figure. 3.12: VEGFR2 signalling cascade upon stimulation with VEGF-A. Source: *http://www.bio-rad.com/en-cn/prime-pcr-assays/pathway/development-vegf-signaling-via-vegfr2-generic-cascades.*

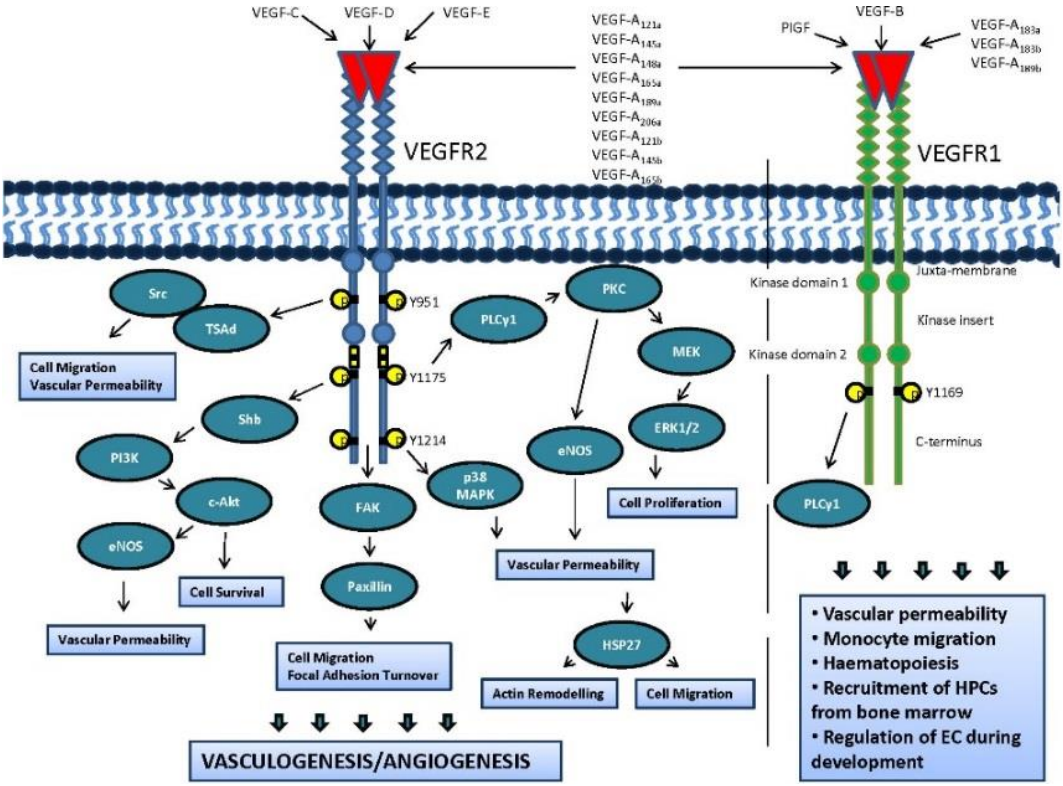

Figure. 3.13: Summarized version of VEGFR2 signalling cascade upon stimulation with VEGF. Source: *http://www.oapublishinglondon.com/article/471#*

Upon VEGFR2 stimulation with VEGF, diverse signalling proteins are activated in ECs, including the non-catalytic region of tyrosine kinase adaptor protein (NCK), Shc-related adaptor protein (SCK), phospholipase C-γ (PLC-γ), protein kinase C (PKC), protein kinase B (PKB/AKT), p38 mitogen-activated protein kinases (p38 MAPK), focal adhesion kinase (FAK) and extracellular signal-regulated kinases (ERK). The cross talk between these molecules successfully modulates the process of angiogenesis. Upon activation with VEGF, VEGFR2 undergoes autophosphorylation and seven important phosphorylation sites have been identified; Y1054, Y1214, Y801, Y1175, Y951, Y1059 and Y996. Each of them is correlated with a different downstream signalling pathway towards a specific EC function. More specifically, Y1214 phosphorylation modulates signalling events towards cell migration. Y801 phosphorylation regulates cell survival. Y1175 is linked to cell proliferation and migration. Y951 and Y1059 phosphorylation regulates cell survival, migration and proliferation. Finally, Y1054 interacts with integrins and regulates signalling events involved in cell migration (Wu et al. 2000; Abhinand et al. 2016).

An important pathway linked to EC proliferation appears to be correlated with the p-Y1175-PLC-γ mediated activation of PKC and downstream induction of the ERK through the PLC-γ-PKC-Raf-MEK-ERK pathway. The VEGF-mediated activation of ERK depends on the activation of Ras and both are important for EC proliferation (Bruce and Tan 2011; Shibuya 2013). Cell survival is mainly regulated by the VEGFR2-dependent activation of the PI3K-AKT signalling pathway. AKT is a serine/ threonine-specific protein kinase involved in multiple cellular processes such as cell metabolism, apoptosis, proliferation, transcription, permeability and migration. It has three isoforms, AKT1, AKT2 and AKT3. AKT1 is mainly involved in the PI3K/AKT/mTOR pathway (Wu et al. 2000; Somanath et al. 2006; Abhinand et al. 2016). On the other hand, several signalling pathways downstream of VEGFR2 are induced by VEGF and contribute towards EC migration, but particularly important is the complementary role of the signalling through the p38 MAPK for actin polymerization and stress fibre reorganisation and the FAK for focal adhesion turnover. FAK is activated through two complementary downstream pathways, one involving the Src kinase (Bruce and Tan 2011; Abhinand et al. 2016).

In that scope, CORMs were subjected to relevant experiments in order to assess their ability to affect the two required steps for successful angiogenesis. First, TNBC cells were treated with CORMs and the expression levels of VEGF were quantified at three different time points. Any reduction in the expressed VEGF could lead to a decreased pro-angiogenic signal towards the surrounding ECs. Complementary to this, HO-1 levels of TNBC cells were also quantified after treatment with CORMs, in order to detect any potential decrease in the levels of this anti-oxidant and cyto-protective enzyme. Reduced HO-1 could lead to more sensitive cancer cells that are more prone towards oxidative stimuli. Finally, ECs were subjected to CORM treatments and phosphorylation levels of Y1175 and other relevant downstream proteins were assessed both upon and without VEGF stimulation.

The concentration of CORMs chosen to be tested in these experiments was the 100μM based on previous literature. CORM-related papers use a wide range of concentrations according to the activity to be explored, but the 50μM and 100μM were the most common. A few examples can be found in these references (Megías et

al. 2007; Vadori et al. 2009; Winburn et al. 2012; Lee et al. 2014; Patterson et al. 2014; Vítek et al. 2014; Ahmad et al. 2015).

3.3.2 Materials & Methods

Cell lines and treatments

MDA-MB-231 and MDA-MB-436 maintained in DMEM media with 10% FBS and antibiotics (full media), were used for the quantification of VEGF expression after CORM treatments. All cells were maintained at 37°C with 5% CO_2. Cells were treated with 100μM CORMs or 1% DMSO or normal media for 6h, 12h or 24h before collecting the supernatant.

MDA-MB-231 maintained in DMEM media with 10% FBS and antibiotics (full media), were used for the quantification of HO-1 expression after CORM treatments**.** All cells were maintained at 37°C with 5% CO_2. Cells were treated with 100μM CORMs or 1% DMSO or normal media for 12h before collecting the cell lysate.

HECV maintained in DMEM media with 10% FBS and antibiotics (full media), were used for the quantification of pVEGFR2 and other downstream phosphorylated proteins after CORM treatments. All cells were maintained at 37°C with 5% CO_2. Cells were treated with 100μM CORMs or 1% DMSO or normal media for 6h, 12h or 24h before collecting the cell lysate.

HUVEC maintained in serum free EBM-2 media (SFM) were stimulated with 50ng/mL or 100ng/mL VEGF for 5min or 20min and the levels of their phosphorylated proteins were assessed in order to find the best protocol for VEGFR2 pathway stimulation. Upon finding the appropriate protocol, HUVEC were treated with CORM-2 or CORM-3 or 1% DMSO and then stimulated with 100ng/mL VEGF in order to be used for the quantification of pY1175 of VEGFR2 and other downstream phosphorylated proteins. All cells were maintained at 37°C with 5% CO_2. Cells were treated with 100μM CORM-2 or CORM-3 or 1% DMSO or serum free media (SFM) for 15min and then stimulated with 100ng/mL VEGF for 5min. After that, the cell lysate was collected. An unstimulated sample was also obtained.

VEGF expression after treatment with CORMs

Upon reaching adequate confluence (~70%), the normal media of a T25 flask was removed and the flask washed twice with PBS. Fresh media containing the corresponding concentration of CORMs or 1% DMSO or no treatment was added to each flask and the cells were left in the normal incubator for 6h, 12h or 24h. After the indicated incubation time, the supernatant of the flask was collected, centrifuged and aliquoted in 1mL Eppendorf tubes that were kept at -80^{o}C until required. Protein was also extracted from each flask using 100µL lysis buffer, quantified using the Bio-Rad DC Protein Assay kit (Bio-Rad laboratories) and used for normalization of the results. Each aliquot was thawed and used only once and the VEGF content was quantified using the human VEGF ELISA kit (Life Technologies Ltd.) following the manufacturer's instructions. The assay is described in section 2.2.6.1

HO-1 expression in MDA-MB-231 after treatment with CORMs

Upon reaching adequate confluence (~70%), the normal media of a T25 flask was removed and the flask washed twice with PBS. Fresh media containing 100µM CORMs or 1% DMSO or no treatment was added to each flask and the cells were left in the normal incubator for 12h. After that, the supernatant of the flask was discarded and the total protein was extracted from each flask using 100µL lysis buffer and was quantified using the Bio-Rad DC Protein Assay kit. After the SDS-PAGE, the proteins were transferred onto nitrocellulose membrane which was then blocked and probed with the relevant primary and the corresponding peroxidase-conjugated secondary antibodies. All of the antibodies used in this study are listed in **Table 2.2**. The protein bands were eventually visualized using the chemiluminescence detection system EZ-ECL (Biological Industries).

Expression of phosphorylated proteins in HECV after treatment with CORMs

Upon reaching adequate confluence (~70%), the normal media of a T25 flask was removed and the flask washed twice with PBS. Fresh media containing 100µM CORMs or 1% DMSO or no treatment was added to each flask and the cells were left in the normal incubator for 6h, 12h or 24h. After that, the supernatant of the flask was discarded and the total protein was extracted from each flask using 100µL lysis buffer

and was quantified using the Bio-Rad DC Protein Assay kit. After the SDS-PAGE, the proteins were transferred onto nitrocellulose membranes which were then blocked and probed with the specific primary and the corresponding peroxidase-conjugated secondary antibodies. The protein bands were eventually visualized using the chemiluminescence detection system EZ-ECL.

Expression of phosphorylated proteins in VEGF stimulated HUVEC after treatment with CORMs

HUVEC cells were seeded in 6-well plates and upon reaching adequate confluence (~80%), the normal media was replaced with serum free media for 12h. 50ng/mL or 100ng/mL VEGF was added to each well for 5min or 20min. The supernatant of the well was then discarded, and the total protein was extracted from each well using 100µL lysis buffer and quantified. The lysate was used for Western blot analysis.

For the CORM treatments, HUVEC cells were seeded in 6-well plates and upon reaching adequate confluence (~80%), they were serum starved for 12h. Treatments of 100µM CORMs or 1% DMSO or no treatment were added to each well and the cells were left in the normal incubator for 15min. After that, 100ng/mL VEGF was added for further 5min. The supernatant of the well was then discarded and the total protein was extracted from each well using 100µL lysis buffer and quantified. The lysate was used either for ELISA (diluted 1:3 with Sample Diluent) or for Western blot analysis.

Statistical analysis

Statistical analysis was performed using GraphPad Prism. Unpaired Student's *t*-test with Welch's correction and nonparametric Mann-Whitney *t*-test were performed to check for statistical significance, with a p-value of <0.05 considered statistically significant. Asterisk notation (*) was used to identify significances: * $p<0.05$, ** $p<0.01$, *** $p<0.001$ and **** $p<0.0001$.

3.3.3 Results

VEGF expression in MDA-MB-231, MDA-MB-436 and MCF-10A cells

Before studying the effect of CORM treatments on the expression of VEGF from TNBC cells, an initial experiment aiming to estimate a rough concentration of VEGF in the supernatants of confluent cultures of the two TNBC cell lines along with the control breast cell line MCF-10A was conducted. As evident from the graph and table shown in **Figures 3.14 A** and **B** respectively, MDA-MB-231 cells expressed a much higher amount of VEGF compared to the other two cell lines. This was an expected observation, since these cells are known to be quite aggressive and highly metastatic (Browne et al. 2016; Takeda et al. 2017). Hence, this cell line was used for most of the further studies.

A.

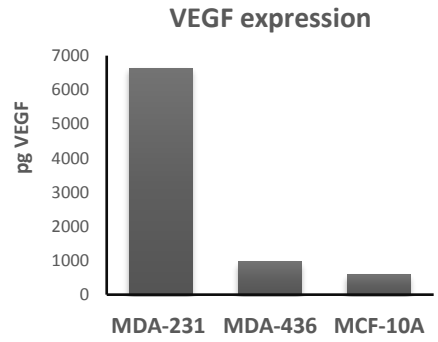

B.

Cell line	VEGF (pg)
MDA-MB-231	6634.4729
MDA-MB-436	970.3879
MCF-10A	585.8851

Figure 3.14: VEGF expression in different cell lines. A. Quantification of VEGF levels in the supernatants of confluent cultures of MDA-MB-231, MDA-MB-436 and MCF-10A cells. **B.** Levels of VEGF expressed in picograms (pg) in the supernatants of confluent cultures of MDA-MB-231, MDA-MB-436 and MCF-10A cells quantified using the human VEGF ELISA kit.

VEGF expression in MDA-MB-231 cells after CORM treatments

In order to investigate any potential anti-angiogenic properties of the four commercially available CORMs, MDA-MB-231 cells were treated with 100μM CORMs for three different time periods and the concentration of VEGF excreted in the cell supernatants was then quantified. As established in the previous experiment, MDA-MB-231 cells express a high concentration of VEGF, so any decrease in this concentration might make them less aggressive and metastatic. Taking this into consideration, three different treatment periods were chosen to be tested, that is 6h, 12h and 24h, as any changes in the expression of VEGF were expected to be fast and last for a limited time.

As observed in **Figure 3.15 A**, all four CORMs indeed reduced the excreted VEGF. More specifically, in the 6h treatment, CORM-3 reduced VEGF by more than 55%, reaching high statistical significance ($p=0.0017$). For other CORMs the significance was slightly lower, with p-values of 0.0141 for CORM-1, $p=0.0171$ for CORM-2 and $p=0.0278$ for CORM-A1.

At this point, it is useful to point out that all these values were calculated comparing the CORM treated cells with normal media treated ones. In all other experiments, the treatments were compared to the vehicle, as was logical from the plan of each experiment. Due to unforeseen circumstances and uncertain reasons though, in this experiment, the vehicle treated cells presented a highly variable expression of VEGF, especially for the 6h treatment. The experiment was repeated many times, but the outcomes were very similar and many values were excluded in order for the graphs to be designed. Hence, it was decided to include the corresponding values for the vehicle treated cells, but compare the treatments with media treated cells instead (control). Here, it has to be noted that the values obtained and depicted for the vehicle treated cells are not statistically different from the control, with $p>0.05$.

The reduction in the expression of VEGF in MDA-MB-231 cells remained evident even in the longer time treatments. As depicted in the same graph for the 12h treatment, CORM-2 managed to reduce VEGF by 60% with the greatest statistical significance among the others ($p=0.0012$). For other CORMs the p-values also indicated high

statistical significance, that is p=0.0303 for CORM-1, p=0.0025 for CORM-3 and p=0.0098 for CORM-A1.

Finally, in the 24h treatment, the pattern was similar, with CORMs -2 and -3 reducing VEGF expression by 65% and 50%, respectively, with statistical significance (p=0.0255 and p=0.0055, respectively). For the other CORMs -1 and -A1, the reduction was between 30% and 40% and they were also different from the control (p=0.0258 and 0.0139, respectively).

With these above encouraging results, it was also decided to test these CORMs at a higher concentration (250μM), to seek for concentration-dependent effects (**Figure 3.15 B**). However, only CORM-2 appeared to reduce VEGF expression vastly more compared to its lower concentration, but this could also be linked to a higher cytotoxicity of this concentration. This experiment was only conducted once, as concentrations much higher than 100μM are not clinically relevant, so just a potential pattern was pursued. Nevertheless, it should be noted that CORM-2 managed to reduce VEGF expression in MDA-MB-231 cells at all time points by more than 90% compared to control. Especially for the 12h treatment, there was a very high statistical difference between these two groups, with p=0.001.

VEGF expression in MDA-MB-436 cells after CORM treatments

The other TNBC cell line, MDA-MB-436, was also studied for similar reduction effects of the CORMs in the concentration of excreted VEGF. The results of 100μM treatments at three different time points are depicted in **Figure 3.15 C**. All four CORMs reduced the excreted VEGF, as observed also in the other TNBC cell line. In the 6h treatment, only CORM-2 managed to reach statistical significance, reducing VEGF by 80% (p=0.0485). In the 12h treatment, CORM-1 was statistically different compared to control and decreased the expression by 70% (p=0.0234). Finally, in the 24h treatment, CORM-3 had the greatest effect, with an observed reduction of more than 65% (p=0.0121). For other CORMs, even though the reduction pattern was still evident, the results did not reach significance, and this might have been a consequence of the fewer repeats and the higher SEMs observed for all the treatments and time points.

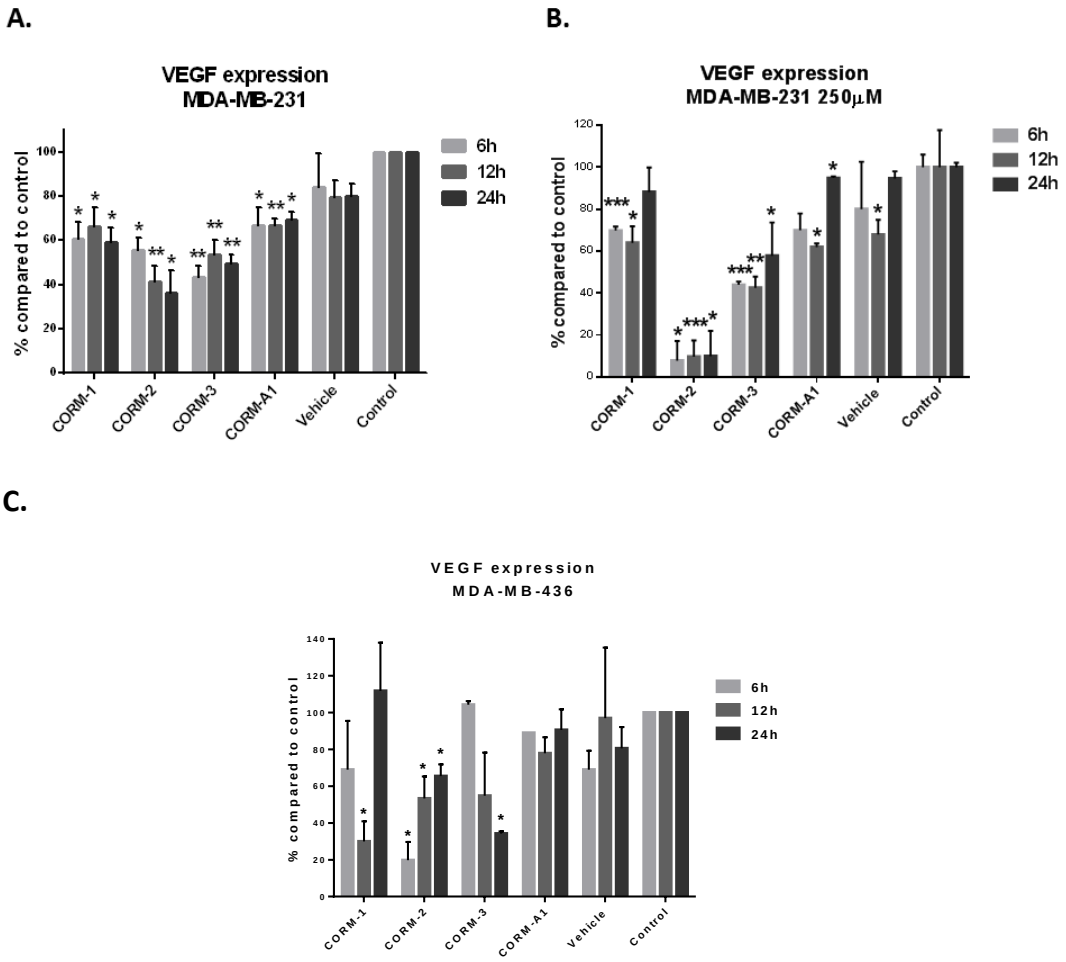

Figure 3.15: VEGF expression after CORM treatments. A. Quantification of VEGF levels in the supernatants of treated MDA-MB-231 cells with 100μM CORMs or 1% DMSO or normal media for 6h, 12h or 24h. (% compared to media treated cells (control) +SEM; n=3, N=4). **B.** Quantification of VEGF levels in the supernatants of treated MDA-MB-231 cells with 250μM CORMs or 1% DMSO or normal media for 6h, 12h or 24h. (% compared to media treated cells (control) +SD; n=3, N=1). **C.** Quantification of VEGF levels in the supernatants of treated MDA-MB-436 cells with 100μM CORMs or 1% DMSO or normal media for 6h, 12h or 24h. (% compared to media treated cells (control) +SEM; n=3, N=3) (All data was statistically analysed against media treated cells using unpaired *t*-test with Welch's correction: * $p<0.05$, ** $p<0.01$, *** $p<0.001$).

HO-1 expression in MDA-MB-231 cells after CORM treatments for 12h

As discussed previously, HO-1 is a well-characterised cytoprotective enzyme that defends the cell in conditions of oxidative stress and excessive ROS production. CORMs have been reported to increase ROS production, especially in bacterial, but also in eukaryotic cells. Therefore, this study aimed to investigate if CORMs could potentially alter the expression of this enzyme, affecting the redox status of the cancer cells and their antioxidant defending systems. MDA-MB-231 cells were treated with 100μM CORMs for 12h and the expression of HO-1 was quantified via Western blot analysis.

As observed in **Figures 3.16 A** and **B**, CORMs -1 and -2 could reduce the expression of HO-1 after 12h of treatment, reaching statistical significance ($p=0.0079$ and $p=0.0179$), whereas CORM-3 failed to reach this level. On the other hand, CORM-A1 increased the expression of this enzyme by 40% ($p=0.0079$), indicating a different mechanism of interaction from the other CORMs.

A.

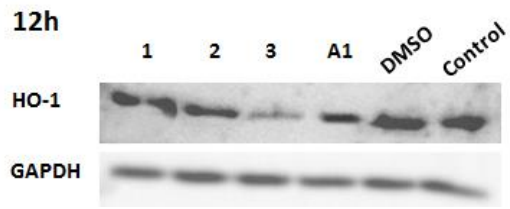

B.

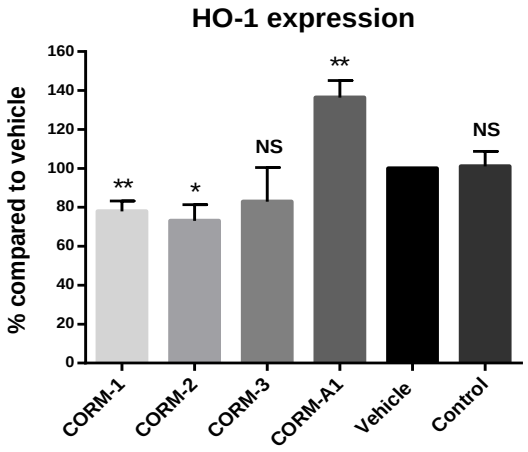

Figure 3.16: HO-1 expression after CORM treatments. A. Western blot of HO-1 expression following CORM or vehicle or media treatment for 12h in MDA-MB-231 cells. (Blot shows representative data; N=4). **B.** Assessment of HO-1 levels in MDA-MB-231 cells following 12h of treatment with CORM or vehicle or media (control) treatment. (Graph shows % compared to vehicle +SEM; N=4) (Data statistically analysed using nonparametric (Mann-Whitney) *t*-test with * $p<0.05$, ** $p<0.01$).

Downstream proteins of the VEGFR2 signalling pathway in HECV cells after CORM treatments

Before investigating the ability of the four available CORMs to inhibit the phosphorylation and activation of downstream molecules of the VEGFR2 signalling pathway following VEGF stimulation, an initial study was conducted, to determine the relative expression levels of phosphorylated Y1175 of VEGFR2, p38, Src, AKT and ERK1/2 proteins in unstimulated CORM treated ECs.

The experiment was carried out once for each different time point, but it was evident in the corresponding Western blots in **Figures 3.17 A** and **B**, that there was a trend for all CORMs to reduce the phosphorylation of some these proteins in unstimulated ECs. More specifically, the phosphorylation of VEGFR2 at Y1175 was investigated in cell lysates of CORM treated HECV cells and compared to vehicle treated cells at three different time points (**Figure 3.17 A**). CORM-3 appeared to be the most potent, reducing the activation of VEGFR2 at all time points by more than 40%. CORM-2 also showed similar effects, whereas CORM-A1 significantly increased the phosphorylation of this tyrosine residue on VEGFR2, especially after 24h of treatment (representative bar graph in **Figure 3.17 C**).

Different trends were observed for the other downstream proteins tested, including p-p38 (T180/Y182), p-Src (Y419), p-AKT (S473) and p-ERK1/2 (S473) (**Figure 3.17 B**). The levels of these proteins were quantified after 6h of treatment with CORMs or vehicle or normal media (control). In the case of p-p38, CORM-1 reduced its expression by more than 50%, closely followed by CORM-2, whereas CORM-A1 increased the activation of this protein to some extent (**Figure 3.17 C**).

For Src, all CORMs seemed to slightly increase its phosphorylation, whereas p-AKT was reduced after treatment with CORM-1 (**Figure 3.17 C**).

Finally, CORM-1 remained the one with the highest effect on p-ERK1/2 in HECV cells, although all CORMs seemed to reduce the levels of p-ERK1/2, as well (**Figure 3.17 C**).

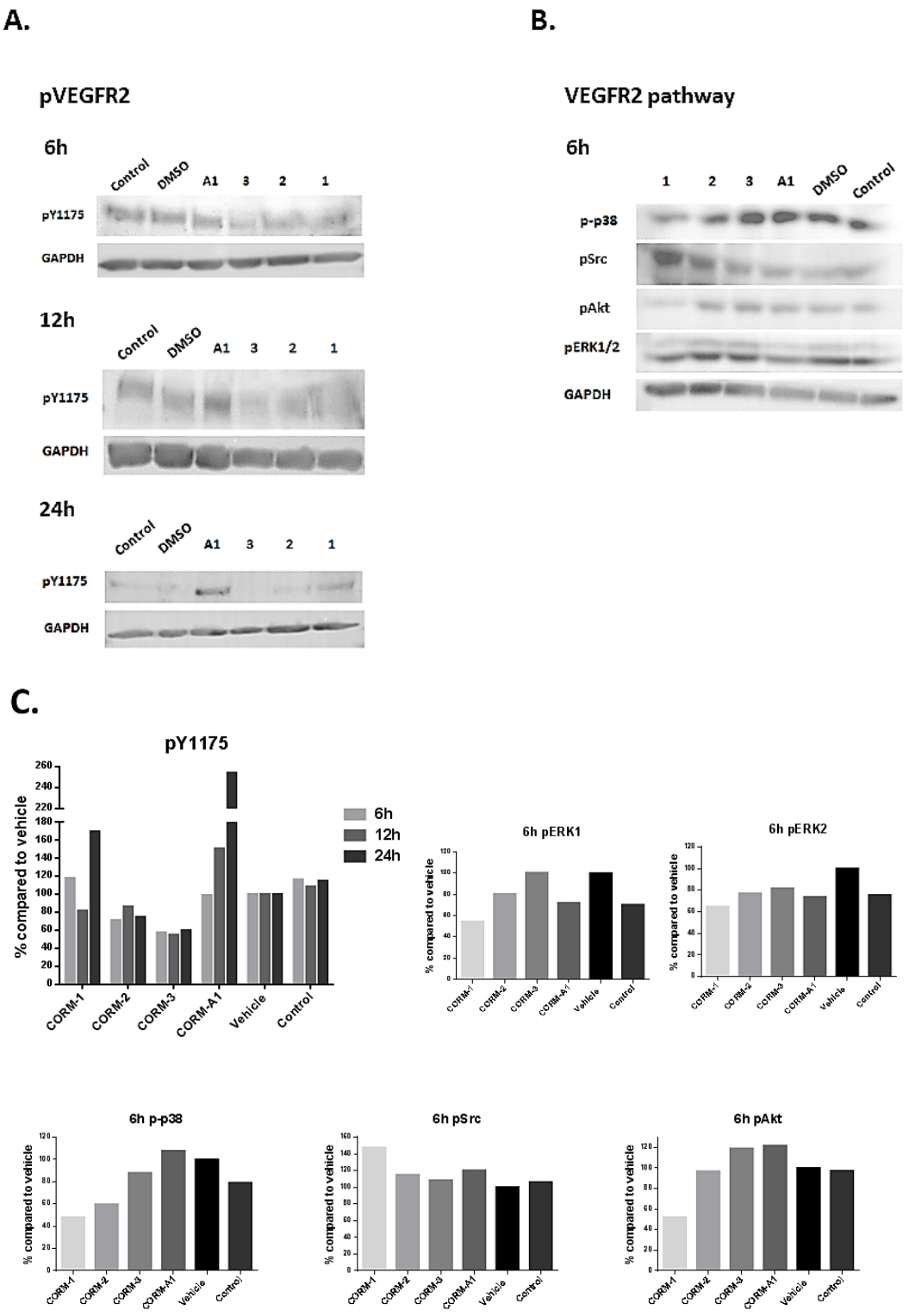

Figure 3.17: Expression of VEGFR2 pathway proteins in HECV after CORM treatments. A. Western blots of pY1175 expression following CORM or vehicle or media treatment for 6h, 12h or 24h in HECV cells. **B.** Western blots of VEGFR2 pathway protein expression following CORM or vehicle or media treatment for 6h in HECV cells. (All blots show the obtained data; N=1). **C.** Assessment of pY1175, pERK1, pERK2, p-p38, pSrc and pAKT levels in HECV cells following the indicated duration of treatment with CORM or vehicle or media (control) treatment. (Graphs show % compared to vehicle; N=1).

Downstream proteins of the VEGFR2 signalling pathway in VEGF stimulated HUVEC cells

As evident from the previous experiment, even unstimulated EC seemed to react to CORM treatments by altering the activation levels of several proteins of the VEGFR2 pathway. Since within the tumour microenvironment the concentration of VEGF is significantly elevated compared to normal tissues, more relevant results would be obtained if VEGF stimulated ECs were treated with CORMs and any differences in the activation of proteins of the VEGFR2 pathway were assessed.

The first few attempts were made with HECV cells. However, the few protocols tried with these cells seemed not to produce the expected stimulation for all the tested proteins, therefore other ECs were adopted, where the differences would be more profound. These ECs were HUVEC, that have been vastly explored in the literature for similar purposes, for example (Ahmad et al. 2015).

The main difference between primary ECs and EC lines is the limited lifespan of the primary cells, that can be grown for up to 10 serial passages. Thereafter they enter a senescence stage halting their proliferation and changing their morphology (Bouïs et al. 2001). Even within the same primary ECs though, a disparate behaviour during experiments can be observed, since the different donor origin for their harvest can alter several responses, for example the response towards IL-8 stimulation (Watson et al. 1995).

Moreover, the molecular characteristics of the cells can vary greatly, as for example some EC lines such as the HMEC-1 (human microvascular endothelial cells), have been shown to express growth factors including VEGF and bFGF, but others do not express these factors (for example the telomerase-immortalized human microvascular endothelial cell line, TIME) (Ng et al. 2015). HECV is an EC line that secretes high concentrations of VEGF-A even under normal conditions (643.3 ± 72.37pg/ml secreted in the supernatant of a 24h confluent cell culture (Puddu et al. 2016)), whereas HUVEC express very low concentrations of VEGF. This leads to a divergent growth factor dependence, as also suggested by the different optimal growth media for each cell line. Following this, another very relevant point to be made is the differential

expression of VEGFRs by primary ECs and EC lines, as for example HUVEC have been shown to express elevated levels of VEGFRs (300%-1000% increase) compared to HECV (Martin T.A., unpublished data). These observations of different growth factor dependence and uneven VEGFR expression might be the reason why HECV did not respond to VEGF stimulation as much as HUVEC did in this study.

The different conditions reported in literature vary in the concentration of VEGF and the duration used for stimulation, therefore relevant experiments were conducted to find the appropriate protocol. Results are depicted in **Figure 3.18** for four different protocols. After 12h serum starvation, both 50ng/mL and 100ng/mL VEGF were used for either 5min or 20min stimulation. As shown in the Western blot data, the best protocol was obtained with 100ng/mL VEGF for 5min. Although pAKT was very mildly activated under these conditions, this protocol was used anyway for further experiments. A longer time treatment might have been useful for pAKT, but all other proteins tested responded at the expected level.

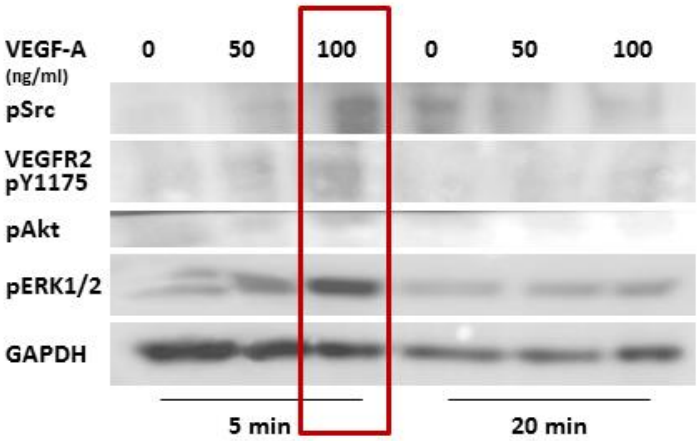

Figure 3.18: Western blot analysis for the different conditions tested. The chosen condition is highlighted in the red box.

For the next experiment, 100μM CORMs or 1% DMSO or serum free media treatments were added to the cells for 15min prior to stimulation. After the 5min stimulation period, cell lysate was isolated and used either for ELISA for pY1175 of VEGFR2 or for Western blot analysis for pSrc (Y419), pERK1/2 (Y204), pFAK (Y397) and pAKT (S473) proteins.

As shown in **Figures 3.19 A** and **C**, all proteins were activated by VEGF at different levels. CORM-2 and CORM-3 downregulated both pERK1 and pERK2 at baseline levels, very close to the unstimulated control (**Figure 3.19 A**). This reduction reached significance for both CORMs (pERK1; p=0.079 for CORM-2 and p=0.0317 for CORM-3, pERK2; p=0.0173 for CORM-2 and p=0.0079 for CORM-3). On the contrary, pSrc was not affected by the two CORMs, which failed to lower the phosphorylation levels of this protein, although upon stimulation with VEGF only a moderate increase in the phosphorylation of ~50% for the control and ~25% for the vehicle was observed (**Figure 3.19 B**).

The other two proteins, pAKT and pFAK also responded mildly to the stimulation with VEGF, and due to the experiment having been repeated only twice, no quantification was performed. However, an obvious reduction in the phosphorylation levels of both proteins was observed for CORM-2, whereas CORM-3 decreased only pAKT and did not affect pFAK levels (**Figure 3.19 C**).

Finally, ELISA quantification was performed for the phosphorylation levels of VEGFR2 at Y1175, and as shown in **Figure 3.20 A**, only CORM-2 managed to return the phosphorylation at the baseline levels of the unstimulated control. This reduction reached statistical significance with p=0.0067. CORM-3 failed to decrease these levels, and the same result was also verified with a Western blot analysis, where it was obvious that only CORM-2 can inhibit the phosphorylation and activation of Y1175 of VEGFR2 (**Figure 3.20 B**).

A.

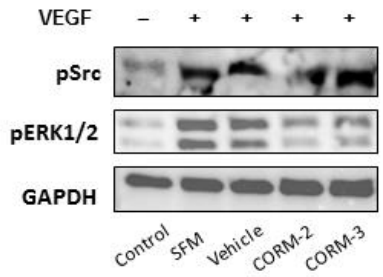

B.

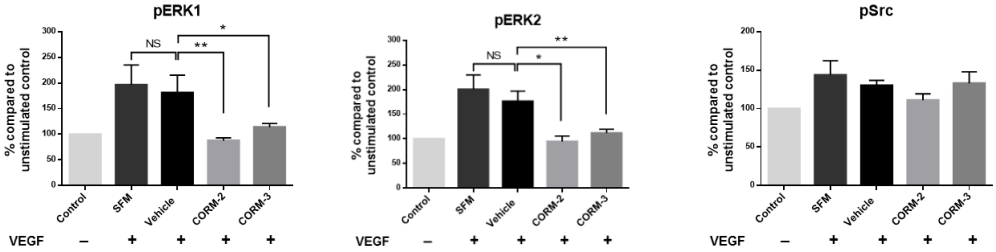

C.

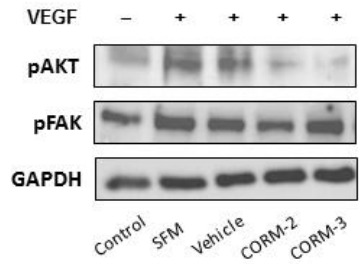

Figure 3.19: Expression of VEGFR2 pathway proteins in HUVEC after CORM pre-treatments and VEGF stimulation. A. Western blot of pSrc and pERK1/2 following 15min of CORM or vehicle pre-incubation and then stimulation with VEGF (100ng/ml) for 5 min. The first sample is the unstimulated control (Control) and the second is the stimulated control (SFM=serum free media). (Blots show representative data; N≥4). **B.** Quantitative assessment of pERK1/2 and pSrc levels in HUVEC following the same protocol. (Graphs show % compared to Control +SEM; N≥4) (Data statistically analysed using nonparametric (Mann-Whitney) *t*-test with * $p<0.05$, ** $p<0.01$). **C.** Western blot of pAKT and pFAK following the same protocol. (Blots show representative data; N=2).

A.

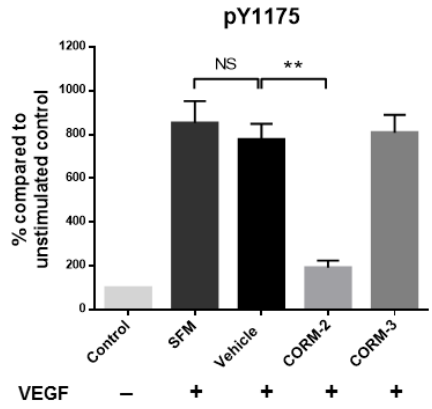

B.

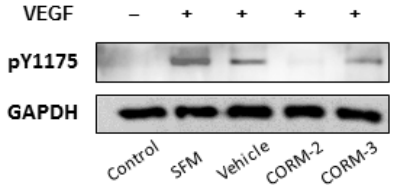

Figure 3.20: pY1175 levels. A. Expression levels of pY1175 of VEGFR2 in HUVEC after 15min of CORM or vehicle pre-incubation and then stimulation with VEGF (100ng/ml) for 5 min, as measured with the human pY1175-VEGFR2 ELISA kit. The first sample is the unstimulated control (Control) and the second is the stimulated control (SFM=serum free media). (Graph shows % compared to Control +SEM; N=3) (Data statistically analysed using unpaired Student's *t-test* with Welch's correction * $p<0.05$, ** $p<0.01$). **B.** Western blot of pY1175 of VEGFR2 following 15min of CORM or vehicle pre-incubation and then stimulation with VEGF (100ng/ml) for 5 min, which verifies the results of the ELISA. (Blot shows the obtained data; N=1).

3.3.4 Discussion

Angiogenesis is linked to the expression of several proteins, both by the cancer cells themselves and by the ECs that line the surrounding blood vessels and execute the process of neovascularization. In that scope, the next step of the screening of the four commercially available CORMs was to measure the expression of proteins related to angiogenesis and are responsible for its successful accomplishment.

As suggested by other studies, several chemotherapeutics may have a complementary anti-angiogenic activity, along with any other *in vitro* and *in vivo* effects. For example, paclitaxel, doxorubicin and thalidomide can also inhibit VEGF expression, bisphosphonates may also reduce VEGF serum levels and celecoxib can also decrease circulating angiogenic markers. A logical approach would be to combine agents that can reduce the expression of angiogenic factors with ones that target these factors *per se*, or their receptors. The principle behind this combination involves the potential enhancement of the delivery of cytotoxic agents to the tumour site, as well as the possible interference with the ability of the tumour to recover from the effects of the accompanying chemotherapeutic agent (Wang et al. 2015).

The main pro-angiogenic factor, VEGF, participates in the angiogenic process by increasing vascular permeability and stimulating EC survival, proliferation, migration and expression of MMPs, among others (Abhinand et al. 2016). Previous literature suggested an increase in VEGF expression induced by CORMs in several *in vitro* models. More specifically, ECs seemed to stimulate their VEGF expression upon treatment with CORMs, CORM-2 and CORM-3 in most studies, and this pointed towards an increased angiogenic potential for these cells (Jözkowicz et al. 2003; Li Volti et al. 2005). Other cells showed a similar behaviour, that is CORM-2 caused an increase in VEGF secretion in astrocytes (Choi et al. 2010) and CORM-401 and CORM-A1 led to an enhanced expression of VEGF in microglia cells after 3h of treatment, whereas after 6h the levels returned back to normal (Wilson et al. 2017). However, there are also studies contradicting these results, such as the study from Ahmad et al. (Ahmad et al. 2015) where HUVEC – primary vascular ECs – were reported to downregulate the phosphorylation and activation of both VEGFR2 and AKT upon treatment with CORM-2, suggesting a potential anti-angiogenic ability of this

compound. Nevertheless, none of these studies used cancer cells, and since CO and CORMs have extensively been reported to have contradicting effects that are cell and tissue-type specific, it was deemed useful to study the effects of the commercially available CORMs on the expression of VEGF from TNBC cells.

As shown in the relevant figures, MDA-MB-231 cells are more aggressive, thus express a higher concentration of VEGF compared to MDA-MB-436. When MDA-MB-231 cells were treated with CORMs for 6h, 12h and 24h, VEGF secretion was reduced, especially for CORM-2 and CORM-3 treatments. The reduction reached a level of 50-60%, suggesting a very promising profile for these complexes that can potentially halt the elevated expression of VEGF by TNBC cells, possibly also decreasing the angiogenic stimulation reaching the surrounding ECs. It would be important to mention that these results were significant, and all four CORMs seemed to share the same tendency to reduce the VEGF expression of TNBC cells at the used concentration of 100μM.

The same pattern was observed also for a higher concentration of CORMs, where CORM-2 was surprisingly effective at reducing the expression of VEGF. However, it should be considered whether this reduction was a direct effect of CORM-2 or it was linked to potential toxicity of this compound against MDA-MB-231 at higher concentrations than 100μM.

The more sensitive TNBC cell line, MDA-MB-436, seemed to be erratically affected by the four CORMs, with patterns not complying to the increase in the treatment duration and CORM-A1 showing ineffectiveness. This might have been a consequence of small differences in the confluence of the flasks during the treatments and between the experiments, the different passage numbers of the cells used or other unidentified factors. MDA-MB-436 cells are less aggressive and resilient compared to MDA-MB-231, therefore a more unpredicted behaviour might be observed. More repeats of this experiment would help in establishing a more robust pattern for the effects of the four CORMs on VEGF expression by MDA-MB-436 cells.

Thus, the main observation of this experiment was the reduction in the excreted VEGF from TNBC cells at all time points tested, leading to potentially decreased angiogenic stimulation towards ECs. These complexes were shown to interfere with the

expression pathway of VEGF in TNBC cells, possibly leading to lower stimulation signals to the surrounding tissues. Observing that these results contradict previous literature, it should be again pointed out that the *in vitro* models of none of these studies were cancer cells, and CO and CORMs have repeatedly been reported to have cell and tissue-type specific effects. There are differences in the physiological procedures of normal and TNBC cells, hence this result might be a consequence of a divergent VEGF expression mechanism in TNBC cells that is prone to CORM interference.

It has been previously shown that suppression of HO-1 expression can impede the proliferation and viability of pancreatic cancer cells (Berberat et al. 2005), as well as the survival and growth of hepatocellular carcinoma (Sass et al. 2008) and prostate cancer cells (Li et al. 2011). However, in other studies HO-1 silencing was oppositely reported to increase tumour growth (Zou et al. 2011), pointing towards a rather complex and tumour type-specific role. Most of the increasing evidence though, suggest a link between lower expression of HO-1 and higher sensitivity of cancer cells (Szabo 2016). Therefore, it would be useful to study the effect of CORMs on HO-1 expression in TNBC cells. A study by Taillé et al. (Taillé et al. 2005) suggested no change in HO-1 expression after 24h treatment with up to 10μM CORM-2 in airway smooth muscle cells, so a shorter incubation time was chosen, that is 12h.

The result of the study showed a downregulating activity of CORMs towards HO-1 that was significant for CORMs -1 and -2, but failed to reach significance for CORM-3. However, the pattern observed for these complexes was not shared by CORM-A1, which markedly increased HO-1 expression in TNBC cells. These observations suggest two different concepts: 1) that transition-metal based CORMs can decrease the expression of HO-1 in TNBC, a mechanism not followed by the non-transition metal based CORM-A1, and 2) that this downregulation might lead to a higher sensitivity of these cells towards other chemotherapeutic or anti-angiogenic agents, based on previous observations for other tumour types.

Another important aspect of angiogenesis is the successful pro-angiogenic signal transduction from the surface receptor VEGFR2 to its complicated network of downstream proteins. As discussed in Chapter 1, VEGF has a higher affinity for VEGFR-

1, but the effects of activation are much more profound for VEGFR2, regulating EC functions. VEGFR2 has also been found upregulated in TNBC. As an RTK, VEGFR2 undergoes dimerization and oligomerization, which results into auto- and trans-phosphorylation on specific tyrosines in the cytoplasmic domain. Two of the most important tyrosine residues (autophosphorylation sites) are Y1175 and Y1214 (Lamalice et al. 2007; Jansson et al. 2014). Therefore, CORMs were studied for their ability to reduce the phosphorylation of one of these tyrosine residues of VEGFR2, in order to investigate any inhibitory activity on the activation of this major receptor. The ELISA technique is more sensitive than a Western blot analysis, therefore it was chosen for measuring the phosphorylation levels of Y1175 after appropriate stimulation with VEGF.

The effective concentration (EC_{50}) of VEGF for the stimulation of VEGFR2 has been reported to be around 650pM (≈27ng/mL) (Akeson et al. 2010). However, most published papers utilise this or higher concentrations of VEGF, as a cell line is only an *in vitro* model that can represent the *in vivo* situation with modest accuracy and usually requires higher concentrations of stimulants to induce a measurable activation. Following this, the optimization experiment for the stimulation of the VEGFR2 pathway in HUVEC aimed to determine the best concentration and duration of stimulation between 50ng/mL and 100ng/mL concentrations and 5-minute and 20-minute stimulation durations. These values were chosen based on previous literature, for example the published work of Cai et al. (Cai et al. 2003) and Ahmad et al. (Ahmad et al. 2015), whereas a very comprehensive study was conducted by Akeson et al. (Akeson et al. 2010) where several concentrations and durations were explored and the 50ng/mL for 4-6min was shown to stimulate most of the proteins tested. In more detail, a good ratio between phospho-VEGFR2/VEGFR2 was shown for stimulatory concentrations of VEGF ≥20ng/mL, with 50ng/mL for 4min being the most effective. Moreover, for PLC-γ and MAPK the best stimulation was achieved with 50ng/mL of VEGF for 6min, whereas for AKT the longer the duration the higher stimulation was observed. It must be noted here that 50ng/mL was the highest concentration tested in the cited study (Akeson et al. 2010). Therefore, 50ng/mL was chosen as the reference concentration and the higher 100ng/mL was used for comparison purposes,

even though it proved to be more effective in the conducted experiments and used further. The 20-minute stimulation was tested mostly to prove that VEGF achieves significant stimulation very quickly that fades with time, as also shown by the obtained results.

Only CORM-2 appeared to inhibit the activation of this receptor on Y1175, reducing the phosphorylation almost to baseline levels, whereas CORM-3 failed to produce such an inhibition. This was a particularly interesting finding that correlates well with previous literature (Cudmore et al. 2007; Ahmad et al. 2015) and suggests an impairment of the angiogenic signal transduction after treatment with CORM-2, even upon stimulation with a high dose of VEGF.

As a proof of concept, more downstream proteins were investigated upon stimulation with VEGF, in order to shed light on any potential targets of CORM-2 and CORM-3 (Abhinand et al. 2016). Different studies reported contradictory results. The work by Otterbein et al. (Otterbein et al. 2000) and Brouard et al. (Brouard et al. 2000) suggested an upregulation of pERK1/2 in stimulated macrophages, fibroblasts and ECs upon treatment with CO gas, whereas a study by Song et al. (Song et al. 2011) showed an inhibition of ERK phosphorylation in stimulated human gingival fibroblasts upon treatment with CORM-3. The group of Taillé et al. (Taillé et al. 2005) found decreased ERK1/2 phosphorylation in airway smooth muscle cells upon treatment with CORM-2, which implicated ROS production. Therefore, HUVEC cells were studied for the phosphorylation levels of different proteins of the VEGFR2 pathway upon VEGF stimulation and it was found that both CORM-2 and CORM-3 had an inhibitory activity.

CORM-3 seemed to be more effective towards pERK1/2 whereas CORM-2 was effective against all tested proteins. This suggested a different mechanism of action for the two similar CORMs, but anyway confirmed their potential as anti-angiogenic agents. Not all proteins were affected by the two CORMs though, for example Src phosphorylation was not downregulated upon treatment. This observation proved some type of preferential inhibition on ERK activation and maybe also on AKT activation for CORM-3, but not on the whole pathway, whereas for CORM-2 a more holistic inhibition might be the case.

3.4 Migratory ability assessment

3.4.1 Introduction

Angiogenesis is directly linked to the capability of ECs to proliferate and migrate in response to growth factor activation (Potente and Carmeliet 2017). As discussed in the introduction, there is a fine balance between pro- and anti-angiogenic factors that determines the formation of new blood vessels, not only in a normal environment but also in a cancerous one. In this process, migration of capillary ECs plays a main role and it follows the stimulation induced by the secreted and circulating VEGF. ECs are equipped with VEGFRs and VEGFR2 is the most potent of them. The next step is the selection of an EC as a tip cell, which will lead the vascular sprout towards the angiogenic signal produced by avascular tissue. The tip cell is followed by trailing proliferative stalk cells that will subsequently form a vascular lumen, create links between adjacent cells and build the basement membrane (Lamalice et al. 2007; Missiaen et al. 2017). The angiogenic cascade is also tightly correlated with ROS production and signalling, as discussed earlier (Lamalice et al. 2007).

Finding agents that can disrupt the migration of ECs would be a promising alternative approach towards the inhibition of cancer-mediated angiogenesis. Since ECs are the major contributors to the formation of new blood vessels that can sustain the growth of tumours, targeting their vital functions could prove helpful.

In that scope, the four available CORMs were tested for their ability to inhibit the migration of ECs following a wound formation on their monolayer.

3.4.2 Materials & Methods

Cell lines and treatments

HECV cells maintained in DMEM with 10% FBS and antibiotics, were used for the scratch wound assay. All cells were maintained at 37°C with 5% CO_2 prior to and during the experiments. Cells were treated with 100μM of CORMs or 1% DMSO or normal media.

MDA-MB-231 cells maintained in DMEM with 10% FBS and antibiotics, were used for the IncuCyte™ Scratch wound assay. All cells were maintained at 37°C with 5% CO_2 prior to and during the experiments. Cells were treated with increasing concentrations of CORMs or vehicle.

Scratch wound assay

$1x10^5$ cells were seeded in 1mL of normal media per well in a 24-well plate and left to form a confluent monolayer. Three replicates were undertaken per different treatment tested. The cells were washed with PBS, wounded with a pipette tip and then treated with 100μM of CORMs or 1% DMSO or normal media for 24h. Photos were taken at 0h, 8h, 12h and 24h after wounding. Migration distances were measured using ImageJ software. The process is detailed in section 2.2.8.1.

IncuCyte™ Scratch wound assay

$5x10^4$ cells were seeded in 100μL of normal media per well in a 96-well ImageLock plate (Essen Bioscience) and left to reach >90% confluence (usually overnight). Four replicates were undertaken per different treatment tested. The Wound Maker was used to make the scratches. The wells were washed twice with media and then treatments were added to each well for 48h. Images were taken every 2h after wounding. The process is detailed in section 2.2.8.2.

IncuCyte™ data analysis

The IncuCyte™ data was analysed using the IncuCyte ZOOM 2016A software, kindly provided by Essen Biosciences.

Statistical analysis

Statistical analysis was performed using GraphPad Prism. Unpaired Student's *t*-test with Welch's correction and two-way ANOVA were performed to check for statistical significance, with a p-value of <0.05 considered statistically significant. Asterisk notation (*) was used to identify significances: * $p<0.05$, ** $p<0.01$, *** $p<0.001$ and **** $p<0.0001$.

3.4.3 Results

Endothelial cell migratory ability tested with the Scratch Wound assay

In order for angiogenesis to take place, migration of ECs must occur, so that the new blood vessels will start to form. As extensively discussed in section 1.3.1, the migration of a tip cell towards the angiogenic signal is the initiating step allowing for the formation of immature tubes and branches between pre-existing blood vessels. Therefore, it was worth investigating if the treatment of ECs with CORMs could affect their ability to migrate. Inhibiting this process would prove very useful in the blockade of the neovascularization process as a whole.

Figures 3.21 A – C present the results of a scratch wound assay in ECs after CORM, vehicle or normal media treatments, as quantified from images captured 8h, 12h and 24h after the scratch. As observed, CORMs -1, -2 and -3 blocked the migration of ECs, leaving the induced wound still open, even 24h after the scratch (**Figure 3.21 A**). More specifically, although after treatment of ECs with normal media, vehicle and CORM-A1, the wound managed to close due to successful migration of ECs, the result was totally different after treatment with CORMs -1, -2 and -3. These differences reached statistical significance with p-values of 0.0092, 0.0003 and 0.0045, respectively (**Figure 3.21 B**). It should be noted though, that the vehicle treated cells showed slower migration than the media treated ones, and this difference was significant with p=0.0056, as calculated in a two-way ANOVA test. **Figure 3.21 C** depicts the percentage of wound confluence in the final time point tested (24h), and again these three CORMs reached significance (p=0.0323, p=0.0003, p=0.0092 for CORMs -1, -2 and -3). In this time point, vehicle and control treatments did not show statistically different results, as calculated in an unpaired *t*-test with Welch's correction.

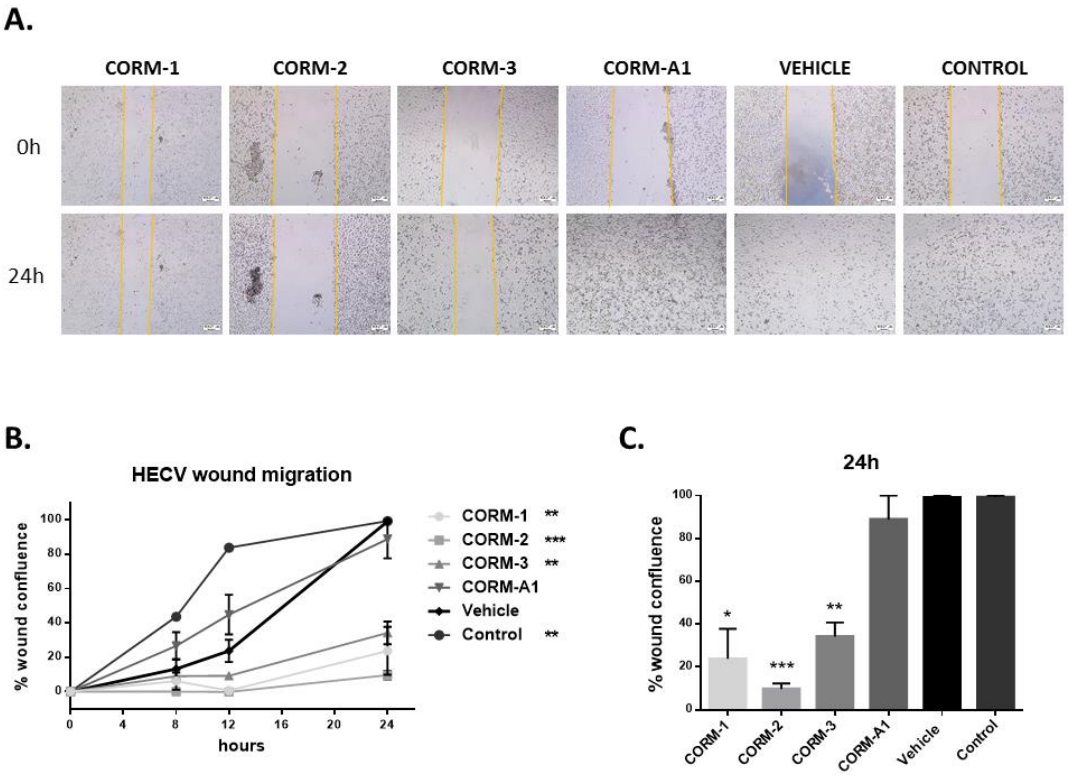

Figure 3.21: Migratory ability of HECV after CORM treatments. A. Representative images from the scratch wound assay in HECV cells, at 0h and 24h after treatment with 100µM CORMs or 1% DMSO or normal media. Objective 5x. **B.** Assessment of the healing, expressed as % wound confluence, at three time points after treatments. (% wound confluence ±SEM; n=3, N=3) (All data was statistically analysed against vehicle treated cells using two-way ANOVA: * p<0.05, ** p<0.01, *** p<0.001). **C.** Average % wound confluence at the final time point (24h) for all treatments. (All data was statistically analysed against vehicle treated cells using un-paired *t*-test with Welch's correction: * p<0.05, ** p<0.01, *** p<0.001).

Cancer cell migratory ability tested with the IncuCyte™ Scratch Wound assay

MDA-MB-231 cells are capable of migrating, hence their metastatic and aggressive nature. Therefore, any inhibitory activity of CORMs on the migration of these cells was tested, as well. Blocking their capability to travel long distances might help in reducing their aggressive phenotype.

In an IncuCyte™ Scratch Wound assay, MDA-MB-231 cells were treated with 100μM CORMs following a scratch induced by a wound maker. As observed in **Figure 3.22 A**, none of the CORMs succeeded in blocking the migration of these TNBC cells, allowing the wound to close 48h after the scratch. However, as depicted in the corresponding images 26h after the scratch, for CORMs -1, -2 and -3 treated cells the migration was slightly slower compared to vehicle or media treated cells. The overall result may not have raised statistical significance in a two-way ANOVA test (**Figure 3.22 B**), but it could imply a negative effect on the migratory ability of these cells, that could possibly reach significance in higher concentrations.

When the results for the intermediate time point (26h) were plotted separately (**Figure 3.22 C**) though, a significant difference between the percentage wound confluence of the vehicle versus the media treated group in an unpaired *t*-test with Welch's correction ($p=0.0108$) could be observed. None of the CORM treatments raised significance compared to the vehicle group, but when compared to the media treated group, CORMs -2, -3 and -A1 were shown to be very significantly different ($p=0.0037$, $p=0.0009$ and $p=0.0010$, respectively).

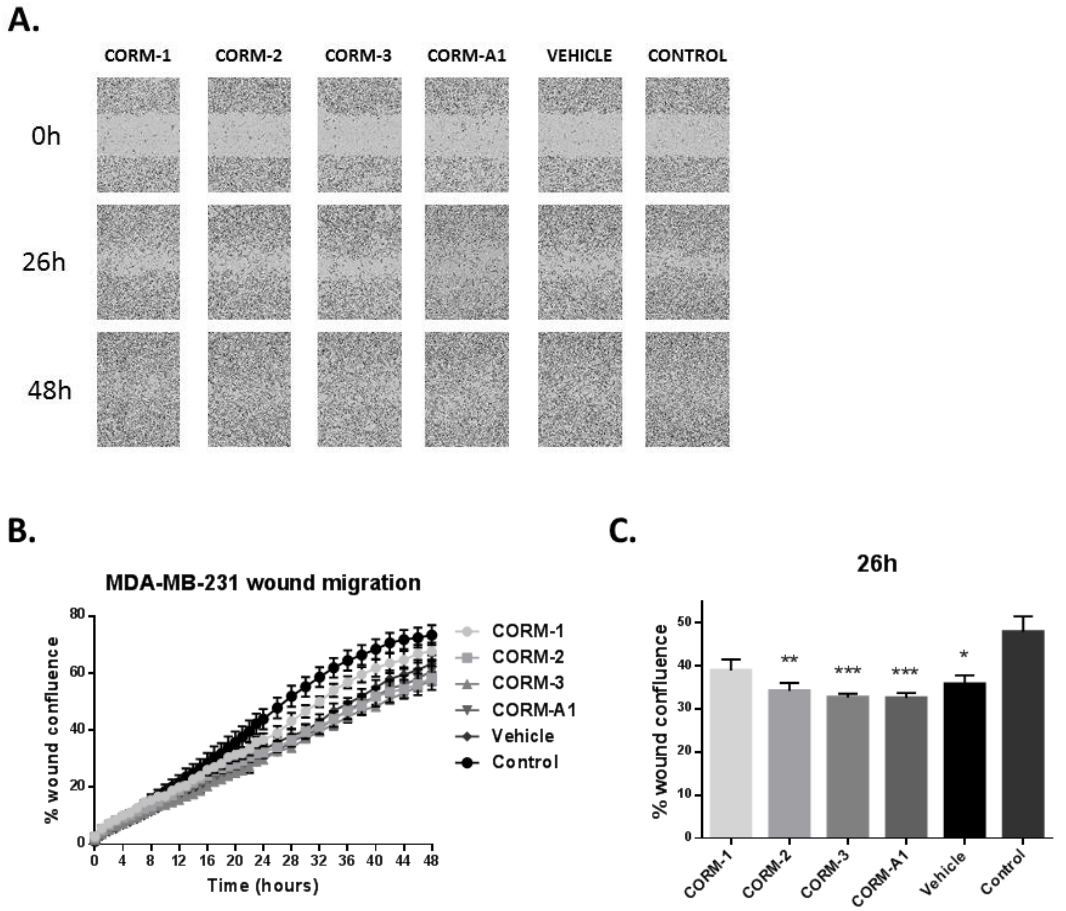

Figure 3.22: Migratory ability of MDA-MB-231 after CORM treatments. A. Representative images from the IncuCyte™ scratch wound assay in MDA-MB-231 cells at 0h, 26h and 48h after treatment with 100μM CORMs or 1% DMSO or normal media. Objective 10x. **B.** Assessment of the healing, expressed as % wound confluence, at all time points tested after treatments. (% wound confluence ±SEM; n=4, N=2) (All data was statistically analysed against vehicle treated cells using two-way ANOVA: * $p<0.05$). **C.** Average % wound confluence at an intermediate time point (26h) for all treatments. (All data was statistically analysed against control treated cells using un-paired *t*-test with Welch's correction: * $p<0.05$, ** $p<0.01$, *** $p<0.001$).

3.4.4 Discussion

Angiogenesis refers to the highly organized process of the formation of new blood vessels from pre-existing ones. A whole cascade of events take part in this process, but capillary EC migration is one of the most decisive components. Angiogenesis has traditionally been viewed from the perspective of how ECs coordinate migration and proliferation in response to growth factors, in order to form new vessel branches, and molecules that are capable of inhibiting EC migration were deemed promising for novel anti-angiogenic therapies (Lamalice et al. 2007; Missiaen et al. 2017; Potente and Carmeliet 2017). In the widely used experiment of scatch wound assay (Menyhárt et al. 2016), ECs are grown in a monolayer and when confluent, a scratch is induced on their surface. Molecules that can inhibit the closure of this wound, thus the migration of ECs, could be considered for anti-angiogenic therapies.

However, since the effects of proliferation cannot be excluded from this experiment a more useful assay to explore would have been a trans-well migration assay. Especially when considering the fast proliferation of HECV, it is not clear whether the obtained results represent just the impairement of the migratory ability of the cells or effects on their proliferation also contribute to the observed inhibition of wound closure. This poses a limitation on interpreting the results.

According to the obtained results for HECV, all CORMs apart from CORM-A1 managed to inhibit the closure of the wound in a statistically significant manner. Even though the vehicle treated ECs were slower in closing the wound compared to control, eventually both groups, vehicle and control, succeeded in providing a fully confluent monolayer of ECs. On the contrary, ECs treated with CORMs -1, -2 and -3 never recovered from the wound and almost no EC migration took place during the 24h of the experiment. Especially for CORM-2, this result was highly significant when compared to the vehicle group. Even when plotting the end point results (24h) and performing a different statistical test, the result was the same, that is CORMs -1, -2 and -3 managed to inhibit the migration of ECs in a notable level.

Although the delay in EC migration induced by the vehicle itself should not be overlooked, CORMs seem to have a strong inhibiting effect on EC migration that raised

significance over the vehicle. This points towards a potentially anti-aniogenic profile of these molecules, since EC migration is key process for the formation of new blood vessels.

MDA-MB-231 are a well-characterized aggressive and highly metastatic TNBC cell line, which has the ability to migrate and invade distant areas, such as the bones and the brain, where secondary tumour niches can be formed (ECACC catalogue No. 92020424). Therefore, it was considered interesting to look for potential anti-migratory effects of CORMs on MDA-MB-231 cells. For this experiment, the IncuCyte™ ZOOM® instrument and the Wound Maker were used, that provide higher consistency in the produced wounds and in the areas from where the photos can be captured.

The results showed a minimal inhibition of the migration of TNBC cells that did not reach significance when compared to the vehicle group in a two-way ANOVA analysis. However, the plotted results for the intermediate time point (26h) revealed a difference between the vehicle and control groups, strongly resembling the one for HECV cells, suggesting a delay in the migration of the tested cells caused by the vehicle itself. This effect was even greater with CORM treatments, and more specifically with CORMs -2, -3 and -A1. This result might have been enhanced by the vehicle at some level, but CORMs reduced the percentage wound confluence even more and in a statistically significant manner when compared to the control group. This suggests a modest inhibition in the migration of MDA-MB-231 cells that is short-lived and may have been even more profound if the dosing was repeated every 24h.

In summary, a strong inhibition in the migration of ECs was observed, that could potentially point towards an anti-angiogenic profile for CORMs -1, -2 and -3 but should be re-tested with more relevant assays. The slight but significant inhibition of migration of TNBC cells for the first 26h could also indicate an impairment of their aggressive nature, and it would be interesting to study if there would be an additional effect if the dosing was repeated, since TNBC cells are far more aggressive and less sensitive than ECs and they have the ability to overcome malfunctions caused by inhibitors.

3.5 Angiogenic potential

3.5.1. Introduction

As outlined thoughout this study, angiogenesis is central to many normal physiological processes, but has also been linked to tumour growth, progression and metastasis. It is essential for the rapidly dividing cancer cells to be able to draw oxygen and nutrients from the body's blood supply in order to support their survival and growth. Malignant angiogenesis has been recognised as a required step for the transition from a small cluster of faster dividing cells to a primary tumour (Carmeliet and Jain 2011; Bishayee and Darvesh 2012). The prevalent form of pathological angiogenesis is sprouting angiogenesis, which participates in tumour neovascularization (Hillen and Griffioen 2007).

Mature blood vessels are the main type of vessels formed during pathological angiogenesis, although they have many differences compared to normal vessels, such as hyperpermeability, heterogeneous morphology and reduced efficiency in tissue perfusion (Gacche and Meshram 2014; Falcon et al. 2016; Missiaen et al. 2017). Moreover, angiogenesis has a contributory role in the ability of a tumour to spread and metastasize. Single cancer cells can be detached from an original established tumour site and circulate through the blood vessels towards a secondary tumour site. Considering the morphology of tumour vessels, which are mosaic vessels with irregular shapes and consist of both endothelial and cancer cells, tumour cells may be facilitated in circulating towards distant areas and establishing new tumour sites (Shan et al. 2014).

Since VEGF is the basic mediator of pathological angiogenesis and arising evidence shows that the interaction between VEGF and its receptors facilitates angiogenesis and promotes tumour growth especially in TNBC, the study could not ommit a test for the ability of ECs to form tubes after VEGF stimulation and CORM treatments. Therefore, conditioned media from MDA-MB-231 cells which had been treated with CORMs or vehicle or media for different durations, was used to stimulate tube formation in HECV cells. In addition, a separate experiment was conducted, where

HECV cells were directly treated with CORMs and assessed for their ability to create tube-like formations.

3.5.2. Materials & Methods

Cell lines and treatments

HECV cells maintained in DMEM with 10% FBS and antibiotics, were used for the tube formation assay. All cells were maintained at 37°C with 5% CO_2 prior to and during the experiments. Cells were treated with conditioned media from MDA-MB-231 cells incubated with 100μM of CORMs or 1% DMSO or normal media for 6h, 12h or 24h. For the instant treatments, the same cells and conditions were used, and the cells were directly treated with 100μM of CORMs or 1% DMSO or normal media.

Tube formation assay using conditioned media

$3.5x10^4$ cells were seeded on top of a pre-set layer of Matrigel in each well of a 96-well plate. The plate was left in the normal incubator for cells to adhere and then the full media was replaced with serum free media containing conditioned media from treated MDA-MB-231 cells. After 6h, the wells were imaged using a Leica DM 1000 LED microscope capturing at least 3 images/well in random areas. The images were analysed using the ImageJ Software and the percentage of total tube length compared to the wells that received conditioned media from vehicle treated MDA-MB-231 cells was calculated.

Tube formation assay with instant treatment

$3.5x10^4$ cells were seeded on top of a pre-set layer of Matrigel in each well of a 96-well plate. The plate was left in the normal incubator for cells to adhere and then the full media was replaced with serum free media containing 100μM of CORMs or 1% DMSO or serum free media. After 6h, the wells were imaged using a Leica DM 1000 LED microscope capturing at least 3 images/well in random areas. The images were analysed using the ImageJ Software and the percentage of total tube length compared to the vehicle treated cells was calculated.

Statistical analysis

Statistical analysis was performed using GraphPad Prism. Unpaired Student's *t*-test with Welch's correction was performed to check for statistical significance, with a p-value of <0.05 considered statistically significant. Asterisk notation (*) was used to identify significances: * p<0.05, ** p<0.01, *** p<0.001 and **** p<0.0001.

3.5.3. Results

Tube formation after treatment with conditioned media from cancer cells

As the main objective of this study was to search for potential anti-angiogenic properties of commercially available CORMs, a tube formation assay was considered very useful towards this aim. The previous observation that these compounds can possibly decrease the expression of VEGF from TNBC cells, in conjunction with the fact that VEGF is the main inducer of angiogenesis in tumour environments, directed the search for any possible reduction in the formation of tube-like structures by ECs treated with cancer conditioned media.

Isolated media from CORM or vehicle or full media treated MDA-MB-231 cells was used to supplement ECs and check for angiogenic capability. As shown in **Figure 3.23 A**, all CORMs managed to reduce the formation of tubes by ECs to some extent. More specifically, conditioned media from CORM-2 treated MDA-MB-231 cells for 6h, 12h or 24h, stimulated fewer and longer tubes compared to conditioned media from vehicle and media treated cells. These differences reached statistical significance with p-values of 0.00486, 0.0313 and 0.0279 for 6h, 12h and 24h, respectively (**Figure 3.23 B**).

Conditioned media from 12h CORM-3 treated cancer cells reduced the formation of tube-like structures by 30%, whereas the conditioned media from 24h treatment reduced it by only 20%, although reaching higher significance (p=0.0169 and p=0.0006, respectively).

Finally, conditioned media from CORM-1 and CORM-A1 treatments did not induce statistically different tube formation capability, with only the media from 24h treatment with CORM-A1 causing a reduced response with p=0.0158.

Tube formation after treatment with CORMs

To investigate if the observed reduction was due to lower concentrations of VEGF contained in the conditioned media from CORM treated cancer cells or due to the compounds themselves, a separate tube formation experiment was conducted, where ECs were directly treated with the CORMs (100μM) or vehicle or serum free media and their tube formation capability was assessed by quantifying total tube length in images taken 6h after treatments.

As shown in **Figure 3.23 C**, treatments did not affect the tubes as much as previously observed, and only CORM-2 had a vastly different result compared to the former one, which reached high statistical significance (p=0.0026) (**Figure 3.23 D**).

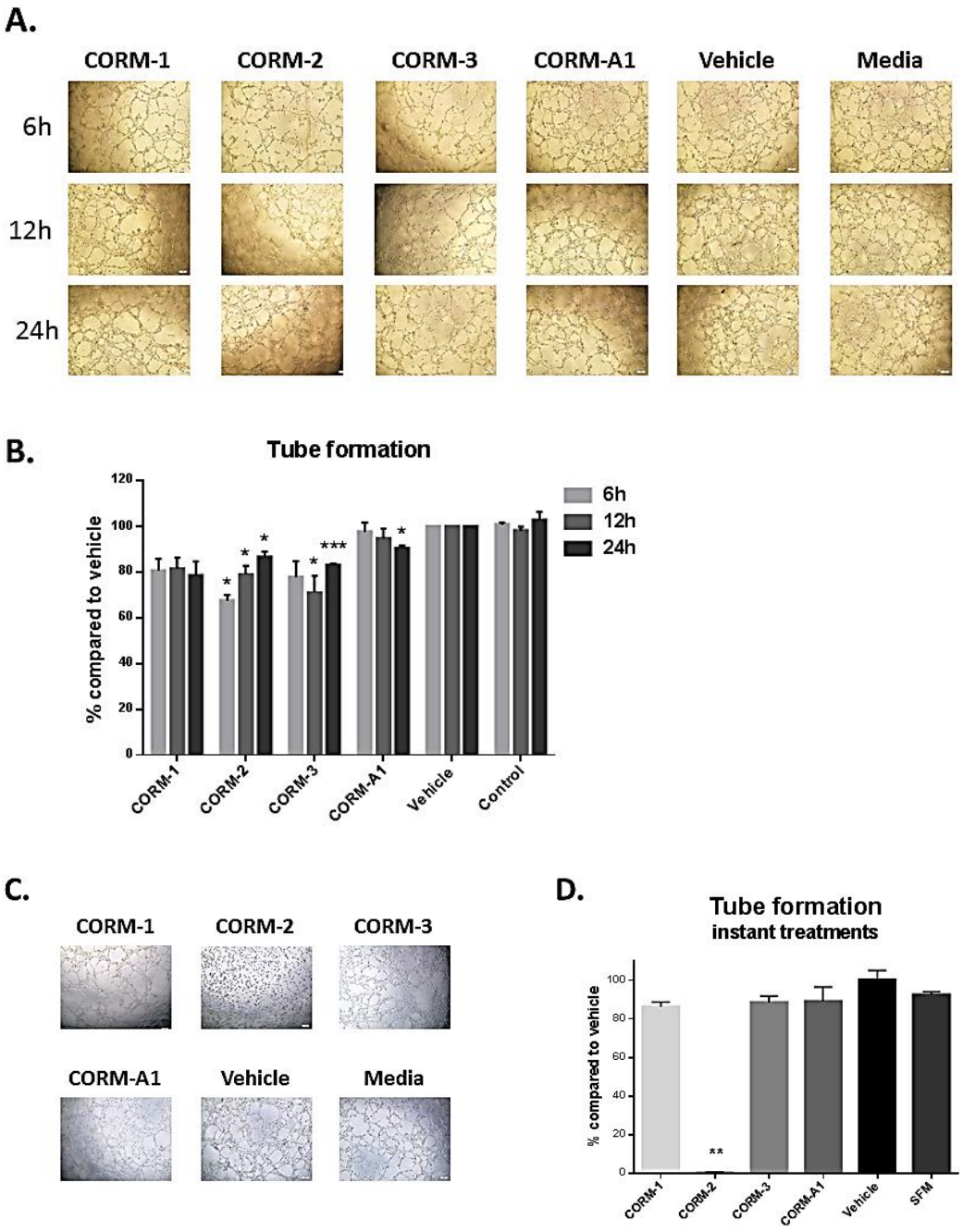

Figure 3.23: Tube formation ability of HECV after conditioned media or CORM treatments. **A.** Representative images from tube formation assay with HECV cells treated with conditioned media from variable duration incubation of MDA-MB-231 cells with 100µM CORMs or 1% DMSO or normal media. Objective 5x. **B.** Tube formation capacity of HECV cells after treatment with conditioned media from variable duration incubation of MDA-MB-231 cells with 100µM CORMs or 1% DMSO or normal media. (% total tube perimeter compared to vehicle +SEM; n=3, N=3) (All data was statistically analysed against the conditioned media from corresponding duration vehicle treated MDA-MB-231 cells using un-paired *t*-test with Welch's correction: * $p<0.05$, ** $p<0.01$, *** $p<0.001$). **C.** Representative images from tube formation assay with HECV cells treated with 100µM CORMs or 1% DMSO or serum free media. Objective 5x. **D.** Tube formation capacity of HECV cells after treatment with 100µM CORMs or 1% DMSO or serum free media. (% total tube perimeter compared to vehicle +SEM; n=3, N=2) (All data was statistically analysed against vehicle treated cells using un-paired *t*-test with Welch's correction: * $p<0.05$, ** $p<0.01$).

3.5.4 Discussion

Pathological angiogenesis has been found to support tumour growth, progression and metastasis via the supplementation of oxygen and nutrients to the rapidly diving cancer cells. The formation of the primary tumour itself has been linked to the potential of cancer cells to induce angiogenesis, and from a pathophysiological point of view, in the absence of malignant neovascularization, tumour size cannot exceed certain limits or undergo metastasis. Malignant angiogenesis has been deemed an appropriate target and there are several benefits attributed to anti-angiogenic therapies, which are well-established for different tumour subtypes (Bishayee and Darvesh 2012; Gacche and Meshram 2014).

The formation of capillary-like structures by ECs has been used as a clinically relevant and solid indication of the potential of different factors to affect angiogenesis. ECs rapidly form tube structures when plated on top of a basement membrane extracellular matrix. In this experiment, Matrigel was used, which stimulated the attachment, migration and differentiation of ECs into capillary-like structures, resembling the *in vivo* environment (Menyhárt et al. 2016).

As presented in the relevant figures, commercially available CORMs seemed to induce a mild reduction in the levels of VEGF expressed by TNBC cells. Following this, it was speculated that these decreased levels of growth factor would have a subsequent decreasing effect on the ability of ECs to form tubes. Therefore, conditioned media from CORM treated TNBC cells was used to stimulate angiogenesis on ECs and was compared to vehicle and normal media treatments. The media from all CORMs stimulated angiogenesis in a lower level compared to vehicle or media treated cells, suggesting a potential inhibition of the capability of ECs to form tubes.

CORM-2 had the most profound effect, since conditioned media from 6h CORM-2 treated TNBC cells lowered the length and complexity of the formed tubes by more than 30% compared to the vehicle. This did not mirror the results from the relevant VEGF expression experiment though, where CORM-2 seemed to lower the expression of VEGF in a time-dependent manner in treated MDA-MB-231 cells and the reduction reached 65%. However, this opposite trend might have just been coincidental, due to

the small differences between the levels of expressed VEGF at the different times checked.

The second best CORM was CORM-3, which reduced the formation of tubes by 25-30%, depending on the duration of cancer cell treatment. The best result was obtained with the 12h conditioned media, once again opposing the VEGF expression pattern, although the differences in the expressed VEGF were similarly small between each time point (all around 50% reduction). In any case, 12h and 24h CORM-3 conditioned media managed to significantly reduce the tube formation activity of ECs.

CORM-1 and CORM-A1 failed to reduce tube formation in a statistically significant manner, reflecting the VEGF expression results, where they had only a moderate effect in reducing the expression of the growth factor compared to CORM-2 and CORM-3 (around 35%). However, a trend of decreased tube formation was also evident for these compounds.

One limitation of this experiment that might explain the smaller reduction in tube formation compared to the significant reduction in VEGF expression was the use of normal media for the seeding of ECs on top of the Matrigel. The Matrigel used had a normal concentration of growth factors, which in combination with the normal media (10% FBS) used for the seeding, could have stimulated the tube formation process prior to the replacement with serum free media and the addition of treatments. Thus, any differences in the concentration of VEGF in the conditioned media could have been obscured. Moreover, the conditioned media was diluted almost 1:3 in each well, making the differences in VEGF concentration even more subtle. In any case, the same trend was observed, that is conditioned media from CORM treated TNBC cells stimulated a reduced angiogenic behaviour in ECs compared to conditioned media from vehicle and normal media treated TNBC cells.

When the same experiment was repeated with instant CORM treatments instead of conditioned media, the results were almost expected. CORMs -1, -3 and -A1 did not reduce tube formation in a significant manner, suggesting a minimal interference with the ECs themselves. However, CORM-2 treatment surprisingly reduced tube formation by 100% and no tubes were formed at any time point. On the contrary, the

cells remained stable and were unable to migrate and create capillary-like formations. The same phenomenon was observed in all the repetitions of the experiment and for all replicates of the treatment. This was a solid indication of the interference of CORM-2 with the ECs themselves that correlated well with the inhibition in migration previously shown for this compound. This result suggested a strong anti-angiogenic behaviour of CORM-2 when in direct contact with ECs and should not be linked to the moderate toxicity of this compound towards HECV cells, since the corresponding IC_{50} was more than 100μM and the duration of the tube formation assay was by far shorter than that of the cytotoxicity assays reported.

Another interesting protocol that could have been tested if more time was available would include the treatment of ECs with both CORMs and a high concentration of VEGF in order to identify any inhibition offered by the CORMs. However, as the main observation of the previous experiments was the downregulation of VEGF expression from TNBC cells, the protocol of using conditioned media from CORM-treated TNBC cells to stimulate tube formation in ECs was found more relevant and closer to the *in vivo* situation and was therefore explored. Nevertheless, this poses a limitation in the interpretation of the results, as a more wholistic view would have been available if that protocol would have also been included in this study.

In summary, conditioned media from CORM treated TNBC cells induced lower tube formation activity in Matrigel coated ECs, that reached significance for CORM-2 and CORM-3. The tubes formed were less and more elongated compared to the complex, highly organised tubes in the vehicle and media groups. However, when direct treatments of CORMs were administered on ECs, no significant inhibition was observed, apart from CORM-2, which managed to eliminate all tube-like structures and prevented ECs from creating a network of tubes completely.

3.6 Lead compound for structural modification and further studies

The first milestone of this study was to screen the commercially available CORMs for effects against various cell functions and any effects related to an anti-angiogenic potential they might have against TNBC. With this in mind, several experiments were conducted trying to relate these complexes to anti-angiogenic activities, such as

effects on the stimulant activity of TNBC cells *per se* or on the signalling and migratory activity of ECs that are responsible for the angiogenic process.

According to these experiments, many conclusions were drawn. First of all, none of the CORMs showed major cytotoxicity against TNBC, endothelial or epithelial cells. However, CORM-2 was significantly more toxic than the others and highly toxic towards non-tumorigenic breast epithelial cells. CORMs -1 and -3 on the other hand, had a more favourable profile, showing higher toxicity against TNBC than other cells, especially CORM-3. Moreover, CORMs -2 and -3 appeared to be cytostatic against MDA-MB-231 cells, whereas CORM-2 also inhibited the growth of MDA-MB-436 and MCF-10A cells, as expected by its inherent toxicity towards epithelial cells.

Cancer cells are known to use glycolysis over oxidative phosphorylation in order to meet their high demands in energy production, a phenomenon called the "Warburg effect". When the glycolytic activity of cancer cells was assessed, instant treatments were more effective in lowering the metabolism of MDA-MB-231. However, due to the experimental procedure itself, it might be possible that during the almost 20min period between preparing the treatments and the treatments actually reaching the cells, most of the CO would have been released, therefore instantaneous effects could not be detected following this protocol. Anyway, CORM-2 had the most profound reducing impact on the glycolysis of MDA-MB-231, whereas CORMs -1 and -3 also showed some inhibition at certain concentrations.

The main stimulatory activity on angiogenesis exhibited by cancer cells is the production of elevated levels of VEGF, which subsequently activate corresponding pathways in ECs initiating angiogenic behaviour. It was shown that upon treatment with all CORMs, but especially CORMs -2 and -3, this expression was reduced at significant levels. MDA-MB-231 cells were affected more than MDA-MB-436, but the same trend was observed in both cell lines.

The cytoprotective enzyme HO-1 is responsible for the endogenous production of CO. However, it is also responsible for the protection of cells against oxidative damage and ROS. It was found that upon 12h treatment with CORMs -1, -2 and -3, the expression of this enzyme was reduced, even though treatment with CORM-3 did not

show statistical significance. Therefore, cancer cells might be more vulnerable towards oxidative stress and increased ROS production.

Upon receiving VEGF from cancer cells, ECs execute several processes leading to vessel formation, which depend on the successful signal transduction from the surface receptor VEGFR2 to other downstream proteins. It was shown that CORM-2 inhibited both VEGFR2 activation and the activation of other downstream proteins such as ERK1/2 and FAK, whereas CORM-3 was more successful towards ERK1/2 protein.

The ability of ECs to migrate is tightly correlated with their capability to form new vessels. CORMs -1, -2 and -3 were shown to inhibit the migration of ECs, preventing the closure of the induced wound on the cell monolayer.

Finally, the tube formation ability of non-primary ECs was reported to be reduced after treatment with conditioned media from CORM-treated cancer cells. CORMs -2 and -3 had the most profound effect, followed by CORM-1 with good but not significant activity. CORM-2 on the other hand, was the only one to affect ECs directly, totally inhibiting their tube formation activity upon direct treatment.

Based on these observations, and taking into consideration previous literature, CORM-3 was chosen as the basis for the design of novel analogues based on its monomeric Ru core. This decision was a conflation of data and inherent limitations of the study. In general, a molecule that provided good results in the previous screening, is water soluble and contains modification handles with a variety of possible ligands to be explored would be desired as the parent structure. An ideal lead CORM should present several useful effects in the conducted screening: it should be selectively toxic against TNBC cells with very limited toxicity against normal breast epithelial cells, it should affect the glycolytic metabolism of these cells reducing their energy production, it should decrease VEGF expression by TNBC cells limiting the pro-angiogenic signals, it should downregulate HO-1 expression in order to limit the protection offered by this enzyme, it should inhibit the phosphorylation of VEGFR2 and downstream proteins reducing the pro-angiogenic signal transduction and it should halt EC migration and tube formation capability.

The first choice would have been to proceed with CORM-2 which presented a variety of favourable results and proved to be effective in nearly all the tested activities. However, CORM-2 is a dimer with limited handles for structural modification, as the only ligands that could be replaced are the chloride atoms pointing away from the metal centres, in order not to affect the dimeric structure. Since a strong inorganic chemical background would be necessary for the design of such modifications, this was not possible in the timeframe of this study. Apart from that, the dimeric structure itself complicates the synthetic procedure because most reactions would result in the destruction of the dimer and the formation of a monomer. Another important drawback is CORM-2's insolubility in water, which would probably lead to water insoluble derivatives that need DMSO as a solvent for their administration. Finally, its inherent toxicity against normal breast tissue as proved in the cytotoxicity assessment against MCF-10A cells, is yet another limiting factor pointing towards its inappropriacy as a lead structure for further modifications.

As discussed previously, CORM-1 was the first photo-CORM to be characterised, but was soon abandoned due to insolubility in water and uncontrolled photo-activatable release of CO. Many groups over the recent years started to explore the family of photo-CORMs and have produced notable new molecules. Nevertheless, the design of structural modifications on a photo-CORM again requires a strong background in inorganic chemistry and specific equipment would be necessary for further experiments, in order to validate the wavelength for the initiation of CO release and to use this wavelength to stimulate the release upon cell treatment, therefore CORM-1 could not be further pursued due to several limitations.

As a consequence, CORM-3 was chosen for structural modifications, because it presents several desired characteristics. First of all, it is water soluble, a feature that would be highly appreciated in the new analogues. Second, it has shown many positive results, such as selective toxicity against TNBC cells, potential reduction in glycolytic metabolism of cancer cells, decrease in VEGF expression from MDA-MB-231 cells, a trend of downregulation on HO-1 expression, inhibition of activation of ERK1/2 upon VEGF stimulation, EC migration inhibition and finally EC tube formation ability reduction. Furthermore, CORM-3 has been proven safe for *in vivo* applications, not

leading to substantial increase in carboxyhaemoglobin (HbCO) levels upon intravenous injections in mice (Davidge et al. 2009). Finally, it has a well-characterized but yet complicated aqueous chemistry, interacting extensively with blood proteins and forming Ru-adducts that have not been proven toxic *per se* (Johnson et al. 2007; Santos-Silva et al. 2011; Chaves-Ferreira et al. 2015).

Main findings and impact:

- Commercially available CORMs are moderately cytotoxic against TNBC cells with potential to be cytostatic – these cells never explored before with first and second generation CORMs.
- Glycolytic capacity of MDA-MB-231 is affected by all CORMs in a low level – CORMs known to affect metabolism but no literature on glycolysis for TNBC.
- VEGF expression of TNBC cells is significantly reduced by CORMs, especially CORMs -2 and -3 – contradicting results with other publications about upregulation of VEGF expression in shorter treatments and other cell lines.
- HO-1 expression is reduced after CORMs -1, -2 and -3 treatments – difference with other cells in literature, where upregulation of HO-1 evident.
- Reduction of pY1175 of VEGFR2 upon CORMs -2 and -3 treatments in unstimulated ECs, other downstream proteins also affected by all CORMs – no previous literature in unstimulated HECV.
- Reduction of pY1175 of VEGFR2 upon CORM-2 treatment in VEGF stimulated HUVEC, similar reduction for pERK1/2, pSrc, pAKT, pFAK – agreement with previous literature.
- Reduction of ERK1/2 and AKT activation upon treatment with CORM-3 in VEGF stimulated HUVEC – different mechanism of action with CORM-2, no similar comparison in previous literature.
- EC migration inhibited by CORMs -1, -2 and -3 – existence of previous literature for CORM-2, but not for this EC line and not for other CORMs.
- No significant inhibition in the migration of TNBC cells – no previous literature for migration of TNBC cells upon CORM treatments.
- Conditioned media from CORM -2 and -3 treated TNBC cells stimulated lower tubule formation in ECs – studies on a more aggressive EC line than previous literature, with high tube formation activity.
- Total inhibition of tubule formation in ECs by direct treatment with CORM-2 – confirmation of previous literature but with different more aggressive cell line.
- Only CORM-2 had minor antibacterial activity – contradicting results with previous literature about effectiveness of CORM-2 and CORM-3 but in higher concentrations than tested here.

Chapter IV

Design & Synthesis of new compounds

4.1 Design of new analogues

Based on the previous experiments described in Chapter 3, one of the four commercially available CORMs was selected as the parent compound for the design and synthesis of a small series of new analogues. CORM-3 was chosen as the lead structure, hence the design should be based on which Ru ligands could be replaced and which potential new ligands with desired characteristics could take their place. Since metal carbonyls are defined as organometallic complexes containing one or more CO ligands (Gasser et al. 2011), the three CO ligands could not be replaced with other groups. The same stands for the Ru core, since the attributed effects observed previously for both CORM-2 and CORM-3 may very well be a direct consequence of not only the CO released, but also the metal core *per se*. Therefore, the only ligands possible to be replaced were the chloride atom (Cl) and the amino acid moiety.

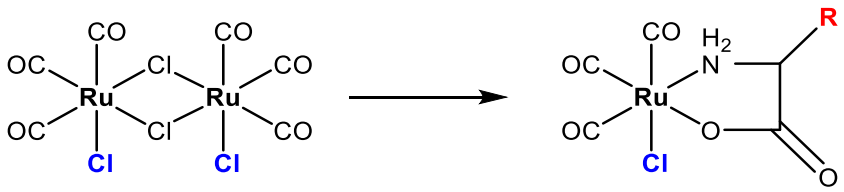

Figure 4.1: Synthetic scheme of CORM-3. *Adapted from (Clark et al. 2003).*

The synthetic scheme reported for CORM-3 and subsequently used by all relevant publications describes the synthetic reaction starting from commercially available CORM-2 (Clark et al. 2003). CORM-2 is a binuclear metal carbonyl that upon reaction with glycine forms two mononuclear adducts of the Ru core bound to the amino acid through the amine and the carboxylic groups. The two Cl ligands of each Ru are substituted by the groups of the amino acid and the last Cl remains on the molecule (**Figure 4.1**). Therefore, the most labile part of the molecule is the amino acid moiety, which can be replaced by a variety of other ligands.

In general, amino acids are favourable ligands, because they can form complexes with many transition metals and may enhance the water solubility of the resulting metal complexes (Mohr et al. 2012). Apart from that, amino acids are well-characterized and can be obtained in high chemical purity, thus make ideal starting materials. As a result, the first idea was to replace the glycine moiety of CORM-3 with other amino acids,

most of them more lipophilic than glycine, and explore differences in activity rising from their different distribution in water.

The distribution coefficient of a molecule (logP) can affect its ability to reach its target, the efficiency upon interaction with the intended target, as well as the half-life inside the body. Therefore, logP (or ClogP) is a critical feature determining the likelihood of a molecule to become a drug candidate (Leeson and Springthorpe 2007). ClogP influences the pharmacokinetics of a drug, in terms of its ADMET properties and its pharmacodynamics, in terms of the ability to reach and bind to the target receptor. It is also important in order to determine the potential toxicity of a compound, because more hydrophobic molecules tend to be retained longer, have a wider and less controlled distribution, bind extensively to blood proteins and get broadly metabolized (Pliška et al. 2008).

The topological polar surface area (tPSA) of a molecule is defined as the sum of all its polar atoms' surface, mainly oxygen and nitrogen, including their attached hydrogens. This feature is commonly used in medicinal chemistry to indicate the potential cell membrane permeability of a drug and has partially replaced the "molecular mass less than 500 Daltons" rule of Lipinski's rule of five (Veber et al. 2002).

Eight different amino acids were chosen from the 20 natural standard amino acids, and the relevant derivatives were synthesized (amino acids and properties shown in **Table 4.1**). The first of them was glycine, as in CORM-3, in order to standardize the method and determine any differences between the commercially available and the laboratory synthesized one.

Ligand	CLogP	tPSA
Glycine	-3.21	63.32
Alanine	-3.124	63.32
Serine	-2.811	83.55
Phenylalanine	-1.556	63.32
Tyrosine	-2.223	83.55
Histidine	-3.727	87.71
Tryptophan	-1.566	75.35
Aspartic acid	-2.412	100.62

Table 4.1: Common amino acids as ligands of the new CORMs and their chemical properties

The next approach was based on the substitution of glycine with uncommon amino acids, two α,α-dialkylated ones and five derivatives of tyrosine, phenylalanine and serine. The α,α-dialkylated amino acids introduce conformational constraints to the whole complex, due to the alicyclic ring and the quaternary α-carbon atom, thereby they might stabilize a pre-set conformation. In the case of 1-aminocyclopentane-carboxylic acid (ACPC) and 1-aminocyclohexane-carboxylic acid (ACHC) that will be used in this study, it has been shown that a folded conformation was preferred, that might help in creating a packed complex structure (Staykova et al. 2015). This way, both complexes will exhibit higher lipophilicity (ClogP) but similar polar surface (tPSA) with CORM-3. These two uncommon amino acids have been used extensively in research, since the strain of their rings may change the ability of the final molecule to adapt to the targeted position and the more atoms are included in the ring, the less constrained the molecule becomes (Rodríguez-Ropero et al. 2008).

More specifically, ACPC has been studied from very early on as an unnatural and antitumor amino acid. It was proven to be toxic to rats at certain small concentrations and was widely distributed in the tissues where it remained in the cellular fluid, without being incorporated into the proteins. ACPC was also shown to have a selective uptake by tumour tissue and react with amino acid transport systems A and L. Several derivatives aimed to inhibit tumour growth have been prepared from then on, based on the observation that ACPC inhibited a variety of carcinomas, such as Walker carcinoma 256 and adenocarcinoma 755 (Connors et al. 1960; Connors and Ross 1960; Berlinguet et al. 1962a; Berlinguet et al. 1962b; Hayes et al. 1976).

ACHC, similarly to ACPC, drew scientific attention due to its conformational restriction and its lipophilicity. Conformationally restricted ligands can fix the functional groups in an active conformation, therefore could be more efficient ligands for various targets. Apart from this, ACHC is also symmetric and achiral, so there is no formation of optically active compounds that need extra separation and purification. Finally, the cyclohexane ring imparts lipophilicity to the final molecule, potentially adding to its efficacy. As a consequence, there are many pharmacologically relevant derivatives of ACHC already known and some of them have also been approved by the FDA (Cyclacillin, Spiromustine, Balicatib) (Mykhailiuk et al. 2013).

The other ligands chosen were simple phenylalanine, tyrosine and serine derivatives. The nitro group seemed particularly interesting as a substituent of the aromatic ring of both phenylalanine and tyrosine, due to its innate toxicity linked also to ROS production. 4-Nitro-phenylalanine has previously been shown to inhibit amino acid activation and the transfer of phenylalanine into the microsomes during protein synthesis. The same was also observed for 3-nitro-tyrosine, and the nitro group was held responsible for these effects. Both compounds had moderate toxicity against HT-29 colorectal adenocarcinoma cells, but specifically for the 3-nitro-tyrosine, promotion of DNA degradation was observed, indicating important toxicological implications (Tamemasa et al. 1968; Prütz 1986; Zhao et al. 2015).

Therefore, some nitro ligands were chosen, including 4-nitro-phenylalanine, 3-nitro-tyrosine and 3,5-dinitro-tyrosine, in order to correlate any observed activities with the number of nitro groups on the molecule and the existence or not of the hydroxyl group. Finally, the 4-amino-derivative of phenylalanine was chosen, to compare with the corresponding nitro-derivate and the O-benzyl-serine, for comparison reasons with the simple serine analogue, as a more hydrophobic molecule.

The final designing strategy tried to exploit differences between cancer and healthy cells, in order to attribute some kind of specificity to the new molecules. As described previously, the four commercially available CORMs do not show any specificity towards certain tissues or cell subtypes, and as a consequence CO toxicity might affect healthy cells along with disease ones. Even though CORM-3 has successfully been administered to animals without elevating the concentration of carboxyhaemoglobin to toxic levels (Clark et al. 2003; Vadori et al. 2009), benefiting from the distinct characteristics of healthy and cancer cells is highly favourable in order to keep the general toxicity of a CORM health issues to a minimum.

Most cancer cells generally exhibit higher levels of ROS compared to healthy cells, which may promote tumour development and progression. In rapidly proliferating cells, the existence of oncogenic mutations promotes unusual metabolism and protein translation, resulting in elevated ROS production (Liou and Storz 2010; Gorrini et al. 2013; Li et al. 2013; Pinto et al. 2017). Usually, tumour cells also express higher levels of antioxidant defence mechanisms, however there is a relatively fragile

balance of intracellular ROS status. In general, oxidative stress-mediated signalling has been shown to affect cancer cell behaviour in processes like cell cycle progression, proliferation, survival, apoptosis, energy metabolism, adhesion, motility and angiogenesis (Liou and Storz 2010; Gorrini et al. 2013; Kruk and Aboul-Enein 2017). The threshold at which ROS can become toxic is not clear, but disproportional increase in ROS production could induce cell cycle arrest or even apoptosis (Liou and Storz 2010; Gorrini et al. 2013; Potente and Carmeliet 2017). The strategy to induce irreparable damages subsequently leading to apoptosis has been exploited by many modern chemotherapeutic agents. The apoptosis could be initiated by random damaging functions of ROS or by specific stimulation of death signalling pathways. The main advantage of this strategy is that cancer cells are already compromised by the higher inner ROS levels compared to normal cells, thus are more prone to oxidative stress than healthy cells. This characteristic offers a therapeutic window that could be explored by agents that further induce ROS production (Liou and Storz 2010; Gorrini et al. 2013).

Based on very early studies, CORMs were shown to possess antimicrobial activities based on their capability to inhibit respiratory oxidases and increase ROS production beyond manageable levels (Nobre et al. 2007). This hypothesis has not been abandoned over the more recent years, and most of the publications still agree on this mechanism of action involving ROS overproduction (Ward et al. 2017). In fact, eukaryotic cells have also been shown to respond to CORM treatments by increasing the levels of produced ROS, for example polymorphonuclear leukocytes augmented their LPS-induced ROS production upon treatment with CORM-3 (Mizuguchi et al. 2009). Taillé et al. (Taillé et al. 2005) suggested a potential target signalling pathway for CO involving NAD(P)H oxidase inhibition, leading to ERK1/2 downregulation, reduced cyclin D expression and therefore elevated mitochondrial ROS formation. Cancer cells are extensively exposed to oxidative stress as a consequence of their change in cellular redox balance. Thus, treatment of cancer cells with CORMs might lead to increased mitochondrial ROS formation that could stimulate apoptotic pathways and eventually lead to cancer cell death, due to the tip of the redox balance

towards an oxidative status (Chin et al. 2007; Piantadosi 2008; Üstün et al. 2016; Pinto et al. 2017).

CORMs sensitive to a redox environment have been explored before (Seixas et al. 2015; Aucott et al. 2017). In the work from Aucott et al. (Aucott et al. 2017), three CORMs were synthesized and fully characterized, based on the parent structure of $Mn(CO)_4$(2-phenylpyridine) photo-CORM with a ferrocenyl substitution. These compounds are yet to be tested *in vitro*, however the redox approach seems more appealing in recent years.

This study used the research done by the group of Simić et al. (Simić et al. 2007) to decide on the antioxidant and pro-oxidant activity of some natural phenolics, where molecules with first oxidation potential (Epa) value greater than 0.45 were deemed pro-oxidants and less than 0.45 antioxidants (**Table 4.2**).

Phenolics	**Epa (V)**	**Lipid peroxidation (percent inhibition)**
Salicylic acid	0.94	-12.1 ± 1.8
m-Hydroxy-benzoic acid	0.83	-10. 1± 3.0
p-Hydroxy-benzoic acid	0.87	-11.4 ± 2.0
Protocatechuic acid	0.41	+15.5 ± 0.3
Vanillic acid	0.73	-12.5 ± 1.1
Syringic acid	0.49	-5.4 ± 1.1
o-Coumaric acid	0.75	-13.0 ± 1.0
m-Coumaric acid	0.78	-10.6 ± 1.1
p-Coumaric acid	0.67	-23.3 ± 3.1
Caffeic acid	0.45	+11.2 ± 2.2
Quercetin	0.10	+67.8 ± 2.0
Rutin	0.23	+10.0 ± 3.6

Table 4.2: Epa values and antioxidant activity of phenolics. *Source: (Simić et al. 2007).*

Based on these observations, the *p*-hydroxy-benzoic acid was chosen to be used and ligated to tyrosine or serine, in order to create a hybrid molecule with the Ru core of CORM-3, a different amino acid moiety than glycine and an extra pro-oxidant moiety that might help in elevating the production of ROS, thus changing the redox status of cells potentially leading to greater toxicity for the whole complex against cancer cells. As shown in **Table 4.2**, *p*-hydroxy-benzoic acid is the second most pro-oxidant phenol, with a high Epa value and a stimulatory activity over lipid peroxidation. *o*-Hydroxy-benzoic acid is the most efficient one, but potential cyclization reactions made it more inappropriate than the *p*-derivative, therefore it was not chosen.

In summary, the uncommon amino acids chosen to replace glycine are depicted in **Table 4.3**, along with the two hybrid molecules aimed to act more pro-oxidatively than the others. One of the last two ligands (serine analogue) has an acetyl protection on its phenolic hydroxyl group, in order to delay the metabolism of the final complex and to moderate the very high polarity imparted by a free hydroxyl group. The tyrosine analogue did not need extra protection, as it is less polar.

Ligand	CLogP	tPSA
1-Aminocyclopentane-carboxylic acid	-2.254	63.32
1-Aminocyclohexane-carboxylic acid	-1.695	63.32
3-Nitro-Tyrosine	-1.844	135.36
3,5-Dinitro-Tyrosine	-1.878	187.17
4-Nitro-Phenylalanine	-1.813	115.13
4-Amino-Phenylalanine	-2.887	87.12
O-Benzyl-Serine	-0.819	72.55
O-(4-Acetoxybenzoyl)-Serine	-1.173	115.92
O-(4-Hydroxybenzoyl)-Tyrosine	-0.204	109.85

Table 4.3: Uncommon amino acids as ligands of the new CORMs and their chemical properties

For the last two analogues, the ligand had to be prepared separately before the final conjugation with CORM-2, because the amino acid derivative was not commercially available. Therefore, these ligands had to be prepared by the closest possible analogue using known reactions. For the serine analogue, the N-benzyloxycarbonyl-L-serine benzyl ester was used and conjugated with 4-acetoxybenzoic acid, whereas there was an attempt to synthesize the free hydroxyl molecule, using 4-hydroxybenzoic acid. The conjugated compound was subjected to hydrogenolysis to remove the benzyloxy protecting group. Finally, for the synthesis of the tyrosine analogue, the N-Boc-L-Tyrosine methylester was used, which after the conjugation with 4-acetoxybenzoic acid, had to be deprotected in several steps, due to the different protecting groups of the starting molecule.

4.2 Synthesis and Characterization

Procedures and spectral data

Described below are the standard procedures followed in the synthesis of new CORM analogues and the spectral data for each new compound. CORM-2 was purchased

from Sigma-Aldrich and the different amino acids from Alfa Aesar, unless otherwise stated.

Standard procedure for CORM synthesis

The new analogues were synthesized starting from the commercially available tricarbonyl dichloro ruthenium(II) dimer (CORM-2) $[Ru(CO)_3Cl_2]_2$. In general, CORM-2 (1.0mol equivalent) was dissolved in dry methanol (MeOH) in a round-bottomed flask at room temperature (r.t.) under nitrogen (N_2) atmosphere. The appropriate amino acid (2.0mol equivalent) and sodium methoxide (2.0mol equivalent) (MeONa) were suspended in dry MeOH in a separate conical flask and left to stir for a few minutes at r.t. The suspension was then added to the CORM-2 solution under N_2 atmosphere maintained by a Schlenk line, and the reaction was allowed to stir for 24h at r.t. with a N_2 balloon and protected from light. The solvent was removed in vacuo and the yellow residue re-dissolved in dry tetrahydrofuran (THF); this was precipitated with excess diethyl ether (Et_2O) or light petroleum ether (PE) 40 – 60. The new CORMs were stored in closed vials at -20°C and used fresh on the day of the experiments (Clark et al. 2003).

In some cases, all the powders (CORM-2, amino acid and MeONa) were transferred into a round-bottomed flask, which was continuously kept under N_2 and dry MeOH was added last. The reaction was allowed to stir for 24h at r.t. with a N_2 balloon and protected from light. The solvent was removed in vacuo and the yellow residue re-dissolved in dry THF; this was triturated with excess Et_2O or light PE 40 – 60 and the precipitated solid was dried under vacuum or N_2 after removal of the supernatant liquid.

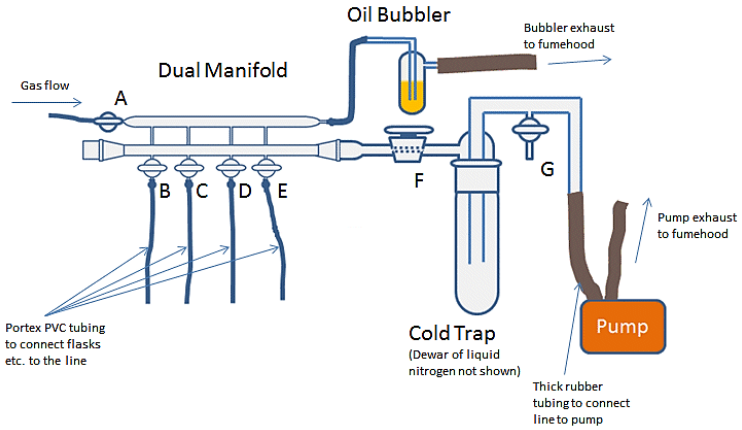

Figure 4.2: Schlenk line apparatus

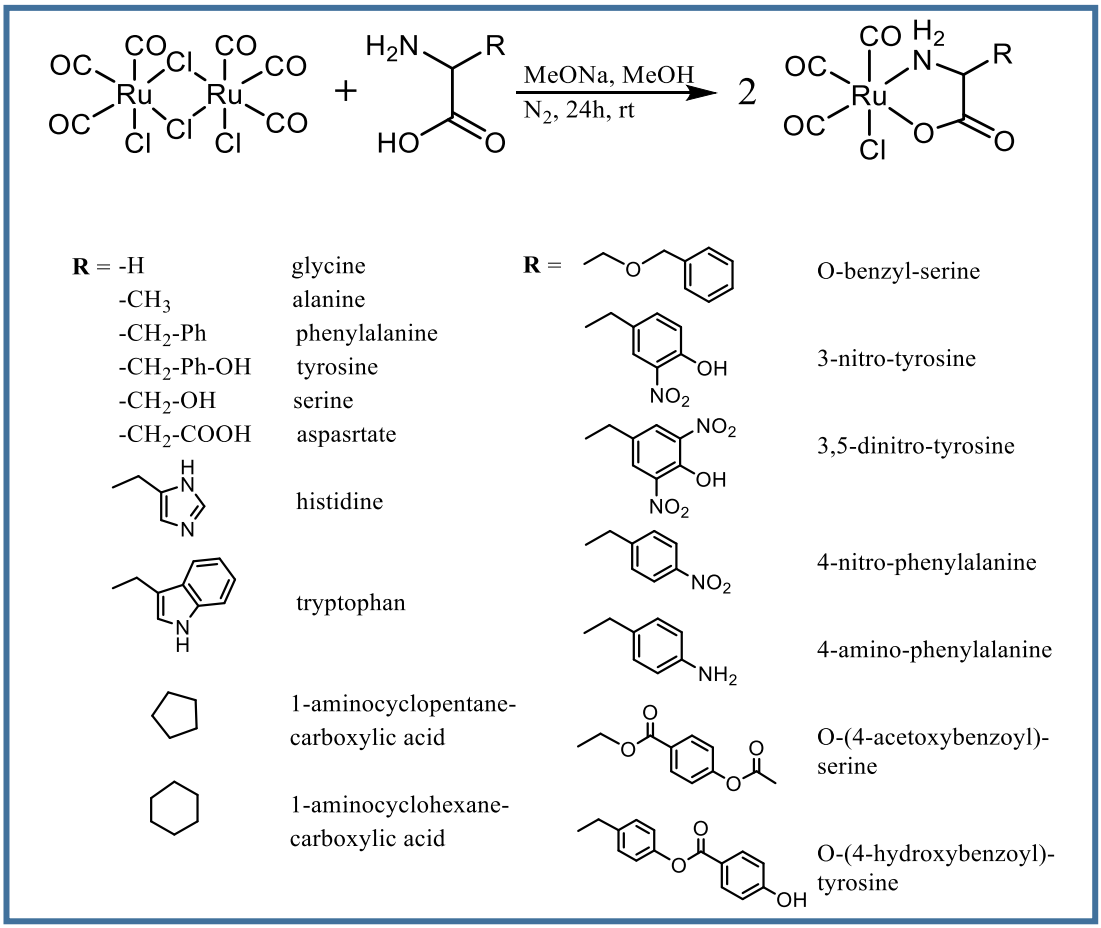

Figure 4.3: Synthetic scheme for CORM-3 analogues

Tricarbonyl chloro (glycinato) ruthenium(II) (CORM-3)

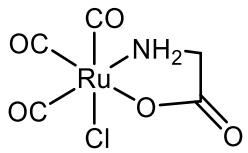

MF: $C_5H_4ClNO_5Ru$

MW: 294.61

Tricarbonyl chloro (glycinato) ruthenium(II) ([$Ru(CO)_3Cl$(glycinate)] or CORM-3) was synthesized in order to test the synthetic protocol (Clark et al. 2003), starting from the commercially available CORM-2 (Sigma Aldrich). Briefly, CORM-2 (1mol eq, 100mg, 0.195mmol), glycine (2.05mol eq, 30mg, 0.4mmol) and sodium methoxide (MeONa) (2.1mol eq, 22.16mg, 0.41mmol) were dissolved in dry MeOH (7mL) in a round-bottomed flask at r.t. under N_2 atmosphere maintained by a Schlenk line. The reaction was allowed to stir for 24h at r.t. with a N_2 balloon and protected from light. The solvent was then removed in vacuo and the yellow residue re-dissolved in dry THF (1mL); this was filtered through a syringe filter (Nylon) and excess light PE added until precipitation started. The supernatant yellow liquid was continuously transferred to another flask using a glass pipette and the remaining powder was dried under N_2 or under the vacuum pump. In the transferred liquid, more PE was added, until no solid could be further isolated. The different fractions of the solid were mixed together to yield the final CORM-3 (45mg, 39% yield). CORM-3 was stored in closed vials at -20°C, but the commercially available one was selected for use in further experiments.

For characterization purposes, ^1H and ^{13}C NMR and MS spectra were obtained and compared to the commercially available one's (reference):

^{1}H NMR (500MHz, DMSO-d_6) δ ppm 3.64 – 3.60 (m, 2H, C$\underline{H_2}$) *Reference:* 3.64 – 3.60 (m, 2H, C$\underline{H_2}$)

^{1}H NMR (500MHz, THF-d_8) δ ppm 5.81 (s broad, 1H, N$\underline{H}$) 5.14 (s broad, 1H, N$\underline{H}$) 4.70 – 4.59 (m, 1H, C$\underline{H}$) 3.90 – 3.88 (m, 1H, C$\underline{H}$) *Reference:* 5.77 – 5.54 (m, 2H, N$\underline{H_2}$) 4.00 – 3.93 (m, 2H, C$\underline{H_2}$)

^{13}C NMR (125MHz, THF-d_8) δ ppm 44.66 ($\underline{C}H_2$) 184.27 (C=O) *Reference:* 42.89 ($\underline{C}H_2$)

MS (ESI) ES+ *m/z* 317.25 [$M+Na^+$] 289.17 [$M-CO+Na^+$] 259.93 [$M-Cl^-+H^+$] 239.18 [$M-2CO+H^+$] *Reference:* 317.25 [$M+Na^+$] 289.17 [$M-CO+Na^+$] 259.93 [$M-Cl^-+H^+$]

239.17 [M-2CO+H^+] *Expected:* 317.59, 289.59, 260.16, 239.59

ES- *m/z* 293.88 [M-H^+] 265.16 [M-CO-H^+] 237.89 [M-2CO-H^+] *Reference:* 293.88 [M-H^+] 265.16 [M-CO-H^+] 237.89 [M-2CO-H^+] *Expected:* 293.60, 265.59, 237.58

Tricarbonyl chloro (alaninato) ruthenium(II) (CORM-Ala)

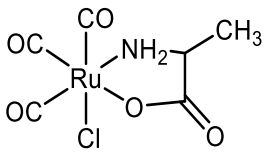

MF: $C_6H_6ClNO_5Ru$

MW: 308.64

Tricarbonyl chloro (alaninato) ruthenium(II) ($[Ru(CO)_3Cl(alaninate)]$ or CORM-Ala) was synthesized starting from the commercially available CORM-2. Briefly, CORM-2 (1mol eq, 85mg, 0.166mmol), alanine (2mol eq, 29.58mg, 0.332mmol) and MeONa (2.1mol eq, 22.16mg, 0.41mmol) were dissolved in dry MeOH (7mL) in a round-bottomed flask at r.t. under N_2 atmosphere maintained by a Schlenk line. The reaction was allowed to stir for 24h at r.t. with a N_2 balloon and protected from light. The solvent was then removed in vacuo and the yellow residue re-dissolved in dry THF (2mL) where solid started precipitating. The precipitation was enhanced with excess Et_2O. The supernatant liquid was transferred to another flask using a glass pipette and the remaining powder was dried under N_2. The remaining crude was dried and upon addition of excess Et_2O and light PE more solid could be isolated. The different fractions of the solid were mixed together to yield the final CORM-Ala (95mg, 90% yield). CORM-Ala was stored in closed vials at -20°C and used freshly on the day of the experiments.

^{1}H NMR (500MHz, DMSO-d_6) δ ppm 8.4 (broad s, 2H, $N\underline{H}_2$) 3.77 – 3.72 (q, *J*= 7Hz, 1H, C$\underline{H}$) 1.38 – 1.36 (d, *J*= 7Hz, 3H, $C\underline{H}_3$)

^{1}H NMR (500MHz, THF-d_8) δ ppm 3.62 – 3.59 (m, 1H, C$\underline{H}$) 1.40 – 1.15 (m, 3H, $C\underline{H}_3$)

^{13}C NMR (125MHz, DMSO-d_6) δ ppm 199.21, 197.74, 191.01 (3 CO), 181.24 (C=O), 50.95 (C$\underline{H}$), 20.89 ($C\underline{H}_3$)

MS (ESI) ES+ *m/z* 331.992 [M+Na^+] 303.999 [M-CO+Na^+] 268.018 [M-CO-HCl+Na^+] *Expected:* 331.891, 303.893, 267.916 (Accurate MS)

ES- *m/z* 307.90 [M-H^+] 279.91 [M-CO-H^+] 251.91 [M-2CO-H^+] *Expected:* 307.63, 279.62, 251.61

Tricarbonyl chloro (serinato) ruthenium(II) (CORM-Ser)

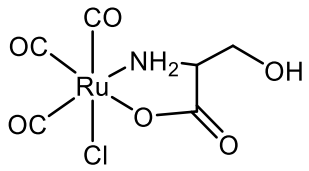

MF: $C_6H_6ClNO_6Ru$

MW: 324.64

Tricarbonyl chloro (serinato) ruthenium(II) ([$Ru(CO)_3Cl$(serinate)] or CORM-Ser) was synthesized starting from the commercially available CORM-2. Briefly, CORM-2 (1mol eq, 85mg, 0.166mmol), serine (2mol eq, 34.9mg, 0.332mmol) and MeONa (2mol eq, 17.94mg, 0.332mmol) were dissolved in dry MeOH (7mL) in a round-bottomed flask at r.t. under N_2 atmosphere maintained by a Schlenk line. The reaction was allowed to stir for 24h at r.t. with a N_2 balloon and protected from light. The solvent was then removed in vacuo and the yellow residue re-dissolved in dry THF (2mL) where solid started precipitating. The precipitation was enhanced with light PE. The supernatant yellow liquid was transferred to another flask using a glass pipette and the remaining powder was washed with light PE twice and dried under the vacuum pump. In the supernatant transferred liquid, no solid could be further isolated, even with excess Et_2O, because it kept forming a sticky and dark residue that could not be worked up any further. The solid was the final product CORM-Ser (34mg, 32% yield). CORM-Ser was stored in closed vials at -20°C and used freshly on the day of the experiments.

^{1}H NMR (500MHz, DMSO-d_6) δ ppm 8.78 – 7.80 (s broad, 2H, N$\underline{H_2}$) 3.81 – 3.69 (m, 2H, C$\underline{H_2}$)

^{13}C NMR (125MHz, DMSO-d_6) δ ppm 169.85 (C=O) 60.21 ($\underline{C}H_2$) 55.32 ($\underline{C}H$)

MS (ESI) ES+ *m/z* 325.8 [$M+H^+$] 347.8 [$M+Na^+$] 289.8 [$M-Cl^-+H^+$] 311.8 [$M-Cl^-+Na^+$]

Expected: 325.6, 347.6, 290.2, 312.17

ES– *m/z* 323.8 [$M-H^+$], 295.9 [$M-CO-H^+$] *Expected:* 323.6, 295.6

Tricarbonyl chloro (phenylalaninato) ruthenium(II) (CORM-Phe)

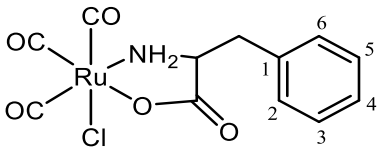

MF: $C_{12}H_{10}ClNO_5Ru$

MW: 384.73

Tricarbonyl chloro (phenylalaninato) ruthenium(II) ([$Ru(CO)_3Cl$(phenylalaninate)] or CORM-Phe) was synthesized starting from the commercially available CORM-2. Briefly, CORM-2 (1mol eq, 85mg, 0.166mmol) was dissolved in dry MeOH (2mL) in a round-bottomed flask at r.t. under N_2. Phenylalanine (2mol eq, 54.92mg, 0.332mmol) and MeONa (2.1mol eq, 18.8mg, 0.348mmol) were added in dry MeOH (5mL) in a separate flask and left to stir for a few minutes at r.t. The suspension was then added to the CORM-2 solution and the reaction was allowed to stir for 24h at r.t. connected to a Schlenk line for continuous N_2 atmosphere and protected from light. The solvent was then removed in vacuo and the yellow residue re-dissolved in dry THF (5mL); this was filtered through a syringe filter (Nylon) and excess Et_2O added. The yellow solution was evaporated down to give a pale yellow solid (99mg, 77.5% yield). CORM-Phe was stored in closed vials at -20°C and used freshly on the day of the experiments.

^{1}H NMR (500MHz, DMSO-d_6) δ ppm 7.37 – 7.22 (m, 5H, Ar-H) 3.22 – 3.09 (m, 2H, C$\underline{H}_2$) 3.03 – 2.64 (m, 1H, C$\underline{H}$)

^{13}C NMR (125MHz, DMSO-d_6) δ ppm 135.74 (Ar-C1) 129.95, 129.71, 129.00, 128.80, 127.57 (Ar-C2,3,4,5,6) 53.93 (C$\underline{H}$) 36.35 (C$\underline{H}_2$)

MS (ESI) ES+ *m/z* 408.0 [M+Na^+] 386.1 [M+H^+] *Expected:* 407.7, 385.7

ES– *m/z* 384.0 [M-H^+] *Expected:* 383.7

Tricarbonyl chloro (tyrosinato) ruthenium(II) (CORM-Tyr)

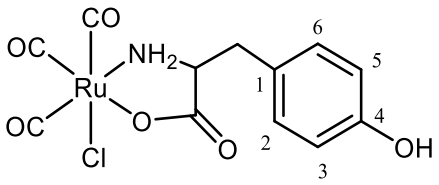

MF: $C_{12}H_{10}ClNO_6Ru$

MW: 400.73

Tricarbonyl chloro (tyrosinato) ruthenium(II) ($[Ru(CO)_3Cl(tyrosinate)]$ or CORM-Tyr) was synthesized starting from the commercially available CORM-2. Briefly, CORM-2 (1mol eq, 85mg, 0.166mmol), tyrosine (2mol eq, 60.16mg, 0.332mmol) and MeONa (2mol eq, 17.94mg, 0.332mmol) were dissolved in dry MeOH (7mL) in a round-bottomed flask at r.t. under N_2 atmosphere maintained by a Schlenk line. The reaction was allowed to stir for 24h at r.t. with a N_2 balloon and protected from light. The solvent was then removed in vacuo and the yellow residue re-dissolved in dry THF (2mL) where solid started precipitating. The precipitation was enhanced with excess light PE. The yellow suspension was evaporated down to give a yellow solid (132mg, 99.2% yield). CORM-Tyr was stored in closed vials at -20°C and used freshly on the day of the experiments.

^{1}H NMR (500MHz, DMSO-d_6) δ ppm 9.41 (s, 1H, OH), 7.07 – 7.02 (m, 2H, Ar-H2, H6), 6.73 – 6.65 (m, 2H, Ar-H3, H5), 4.15 – 4.02 (m, 1H, C<u>H</u>), 3.04 – 2.95 (m, 2H, C<u>H</u>$_2$)
^{13}C NMR (125MHz, DMSO-d_6) δ ppm 170.91 (C=O ester), 157.08 (Ar-C4), 130.96, 130.72 (Ar-C2, C6), 125.21 (Ar-C1), 115.84, 115.64 (Ar-C3, C5), 53.98 (<u>C</u>H), 35.5 (<u>C</u>H$_2$)
MS (ESI) ES+ *m/z* 402.0 [M+H$^+$] 388.1 [M-Cl$^-$+Na$^+$] 374.1 [M-CO+H$^+$] 366.1 [M-Cl$^-$+H$^+$]
Expected: 401.7, 388.3, 373.7, 366.3
ES– *m/z* 400.0 [M-H$^+$] 372.0 [M-H$^+$-CO] *Expected:* 399.7, 371.7

Tricarbonyl chloro (histidinato) ruthenium(II) (CORM-His)

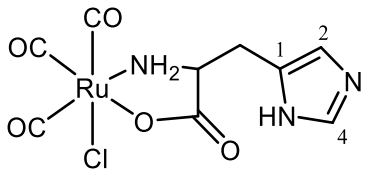

MF: $C_9H_8ClN_3O_5Ru$

MW: 374.70

Tricarbonyl chloro (histidinato) ruthenium(II) ([$Ru(CO)_3Cl$(histidinate)] or CORM-His) was synthesized starting from the commercially available CORM-2. Briefly, CORM-2 (1mol eq, 85.1mg, 0.166mmol) was dissolved in dry MeOH (2mL) in a round-bottomed flask at r.t. under N_2. Histidine (2mol eq, 51.51mg, 0.332mmol) and MeONa (2.1mol eq, 18.8mg, 0.348mmol) were added in dry MeOH (5mL) in a separate flask and left to stir for a few minutes at r.t. The suspension was then added to the CORM-2 solution and the reaction was allowed to stir for 24h at r.t. connected to a Schlenk line for continuous inert atmosphere and protected from light. The solvent was then removed in vacuo and the white residue re-dissolved in dry THF (5mL); this was filtered through a syringe filter (Nylon) and excess Et_2O added. The white suspension was evaporated down to give an off-white solid (75mg, 60% yield). CORM-His was stored in closed vials at -20°C and used freshly on the day of the experiments.

^{1}H NMR (500MHz, DMSO-d_6) δ ppm 13.15 – 13.00 (m, 1H, NH), 8.09 – 7.85 (m, 1H, Ar- H4), 7.34 – 7.10 (m, 1H, Ar-H2), 3.91 – 3.85 (m, 1H, C<u>H</u>) 3.27 – 3.19 (m, 1H, C<u>H</u>$_2$) 3.06 – 3.01 (m, 1H, C<u>H</u>$_2$)

^{13}C NMR (125MHz, DMSO-d_6) δ ppm 203.24, 202.47, 201.41 (3 CO) 180.84 (C=O ester) 140.89 (Ar-C4) 134.71 (Ar-C1) 115.31 (Ar-C2) 52.44 (<u>C</u>H) 28.27 (<u>C</u>H$_2$)

MS (ESI) ES- *m/z* 373.853 [M-H$^+$] 345.866 [M-CO-H$^+$] 309.910 [M-CO-2H^{2+}-Cl$^-$]

Expected: 373.912, 345.917, 309.939 (Accurate MS)

Tricarbonyl chloro (tryptophanato) ruthenium(II) (CORM-Trp)

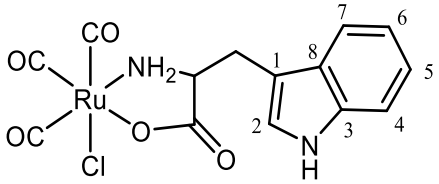

MF: $C_{14}H_{11}ClN_2O_5Ru$

MW: 423.77

Tricarbonyl chloro (tryptophanato) ruthenium(II) ([$Ru(CO)_3Cl$(tryptophanate)] or CORM-Trp) was synthesized starting from the commercially available CORM-2. Briefly, CORM-2 (1mol eq, 85.1mg, 0.166mmol) was dissolved in dry MeOH (2mL) in a round-bottomed flask at r.t. under N_2. Tryptophan (2mol eq, 67.8mg, 0.332mmol) and MeONa (2.1mol eq, 18.8mg, 0.348mmol) were added in dry MeOH (5mL) in a separate flask and left to stir for a few minutes at r.t. The suspension was then added to the CORM-2 solution and the reaction was allowed to stir for 24h at r.t. connected to a Schlenk line for continuous inert atmosphere and protected from light. The solvent was then removed in vacuo and the yellow residue re-dissolved in dry THF (5mL) where excess Et_2O was added. The yellow solution was evaporated down to give a pale yellow solid (100mg, 71% yield). CORM-Trp was stored in closed vials at -20°C and used freshly on the day of the experiments.

^{1}H NMR (500MHz, DMSO-d_6) δ ppm 11.13 – 10.93 (m, 1H, NH), 7.61 – 7.52 (m, 1H, Ar- H7), 7.40 – 7.33 (m, 1H, Ar-H4), 7.26 – 7.19 (m, 1H, Ar-H2), 7.11 – 6.96 (m, 2H, Ar-H6, H5) 4.31 – 4.00 (m, 1H, C<u>H</u>) 3.30 – 2.91 (m, 2H, C<u>H</u>$_2$)

^{1}H NMR (500MHz, THF-d_8) δ ppm 10.25 – 10.13 (m, 1H, NH), 7.66 – 7.61 (m, 1H, Ar-H7), 7.39 – 7.28 (m, 2H, Ar-H4, H2), 7.14 – 6.97 (m, 2H, Ar-H6, H5) 4.09 – 3.83 (m, 1H, C<u>H</u>) 3.61 – 3.18 (m, 2H, C<u>H</u>$_2$)

^{13}C NMR (125MHz, THF-d_8) δ ppm 135.17 (Ar-C3) 126.02 (Ar-C8) 122.07 (Ar-C2) 119.38 (Ar-C5) 116.83 (Ar-C6) 116.34 (Ar-C7) 109.18 (Ar-C4) 107.74 (Ar-C1) 53.57 (<u>C</u>H) 27.06 (<u>C</u>H$_2$)

MS (ESI) ES+ *m/z* 411.064 [M-HCl+Na^+] 419.038 [M-CO+Na^+] 361.084 [M-HCl-CO+H^+] 355.081 [M-2CO-HCl+Na^+] *Expected:* 410.952, 418.934, 360.975, 354.963 (Accurate MS) ES- *m/z* 422.95 [M-H^+] 394.95 [M-CO-H^+] *Expected:* 422.76, 394.75

Tricarbonyl chloro (aspartato) ruthenium(II) (CORM-Asp)

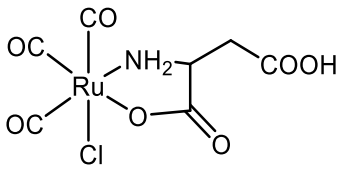

MF: $C_7H_6ClNO_7Ru$

MW: 352.65

Tricarbonyl chloro (aspartato) ruthenium(II) ([$Ru(CO)_3Cl$(aspartate)] or CORM-Asp) was synthesized starting from the commercially available CORM-2. Briefly, CORM-2 (1mol eq, 85mg, 0.166mmol), aspartic acid (2mol eq, 44.2mg, 0.332mmol) and MeONa (2mol eq, 17.94mg, 0.332mmol) were dissolved in dry MeOH (5mL) in a round-bottomed flask at r.t. under N_2 atmosphere maintained by a Schlenk line. The reaction was allowed to stir for 24h at r.t. with a N_2 balloon and protected from light. The solvent was then removed in vacuo and the yellow residue re-dissolved in dry THF (2mL) where solid started precipitating. The precipitation was enhanced with excess Et_2O and light PE. The yellowish supernatant was transferred to another flask and the off white solid was dried under N_2. Excess light PE was added to the supernatant until no more solid could be isolated. Both solids were dried under N_2 to yield the final CORM-Asp (115mg, 98.2% yield). CORM-Asp was stored in closed vials at -20°C and used freshly on the day of the experiments.

^{1}H NMR (500MHz, DMSO-d_6) δ ppm 8.34 (s broad, 2H, N$\underline{H}_2$) 4.08 – 4.06 (t, *J*= 5.5Hz, 1H, C$\underline{H}$) 2.85 – 2.83 (m, 2H, C$\underline{H}_2$)

^{13}C NMR (125MHz, DMSO-d_6) δ ppm 196.28, 191.02, 187.02 (3 CO) 171.40 (C=O ester) 170.48 (C=O acid) 51.67 ($\underline{C}$H) 35.08 (C$\underline{H}_2$)

MS (ESI) ES– *m/z* 323.91 [M-CO-H^+] *Expected:* 323.63

ESI+ *m/z* 317.95 [M-Cl^-+H^+] 340.29 [M-Cl^-+Na^+] *Expected:* 318.2, 340.18

Tricarbonyl chloro (cyclopentanato) ruthenium(II) (CORM-Cyclopent)

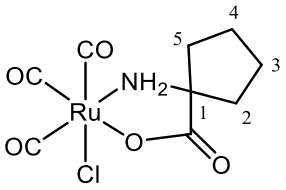

MF: $C_9H_{10}ClNO_5Ru$

MW: 348.70

Tricarbonyl chloro (cyclopentanato) ruthenium(II) ($[Ru(CO)_3Cl(cyclopentanate)]$ or CORM-Cyclopent) was synthesized starting from the commercially available CORM-2. Briefly, CORM-2 (1mol eq, 85mg, 0.166mmol), 1-aminocyclopentane-carboxylic acid (2mol eq, 42.9mg, 0.332mmol) and MeONa (2mol eq, 17.94mg, 0.332mmol) were dissolved in dry MeOH (6mL) in a round-bottomed flask at r.t. under N_2 atmosphere maintained by a Schlenk line. The reaction was allowed to stir for 24h at r.t. with a N_2 balloon and protected from light. The solvent was then removed in vacuo and the yellow residue re-dissolved in dry THF (2mL) where solid started precipitating. The precipitation was enhanced with excess Et_2O. The supernatant yellow liquid was continuously transferred to another flask using a glass pipette and the remaining powder was dried under N_2. In the transferred liquid, more Et_2O was added and fractions of solid isolated, until no solid could be further isolated. The different fractions of the solid were mixed together to yield the final CORM-Cyclopent (67mg, 57.8% yield). CORM-Cyclopent was stored in closed vials at -20°C and used freshly on the day of the experiments.

^{1}H NMR (500MHz, DMSO-d_6) δ ppm 8.5 (broad, 2H, $N\underline{H}_2$) 2.08 – 1.73 (m, 8H, $(C\underline{H}_2)_4$)

^{13}C NMR (125MHz, DMSO-d_6) δ ppm 201.30, 186.99, 185.11 (3 CO), 174.43 (C=O ester), 64.79 (C1), 36.58 (2C, $\underline{C}H_2$ (2, 5)), 25.55 (2C, $\underline{C}H_2$ (3, 4))

MS (ESI) ES+ *m/z* 335.97 [M-Cl^-+Na^+] *Expected:* 336.24

ES– *m/z* 347.94 [M-H^+] 319.95 [M-H^+-CO] 291.95 [M-H^+-2CO] *Expected:* 347.69, 319.68, 291.67

Tricarbonyl chloro (cyclohexanato) ruthenium(II) (CORM-Cyclohex)

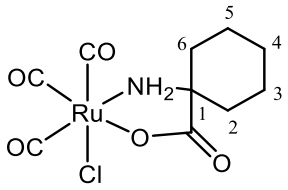

MF: $C_{10}H_{12}ClNO_5Ru$

MW: 362.73

Tricarbonyl chloro (cyclohexanato) ruthenium(II) ([$Ru(CO)_3Cl$(cyclohexanate)] or CORM-Cyclohex) was synthesized starting from the commercially available CORM-2. Briefly, CORM-2 (1mol eq, 85mg, 0.166mmol), 1-aminocyclohexane-carboxylic acid (2mol eq, 47.54mg, 0.332mmol) and MeONa (2mol eq, 17.94mg, 0.332mmol) were dissolved in dry MeOH (7mL) in a round-bottomed flask at r.t. under N_2 atmosphere maintained by a Schlenk line. The reaction was allowed to stir for 24h at r.t. with a N_2 balloon and protected from light. The solvent was then removed in vacuo and the yellow residue re-dissolved in dry THF (2mL) where solid started precipitating. The precipitation was enhanced with light PE. The supernatant yellow liquid was transferred to another flask using a glass pipette and the remaining powder was dried under N_2. In the transferred liquid, excess Et_2O was added and yellow solid was isolated. The different fractions of the solid were mixed together to yield the final CORM-Cyclohex (87mg, 72.3% yield). CORM-Cyclohex was stored in closed vials at -20°C and used freshly on the day of the experiments.

^{1}H NMR (500MHz, DMSO-d_6) δ ppm 8.5 (s broad, 2H, $N\underline{H}_2$) 1.93 – 1.34 (m, 10H, $(C\underline{H}_2)_5$)

^{13}C NMR (125MHz, DMSO-d_6) δ ppm 191.02 (CO), 65.37 (C1), 35.45 ($\underline{C}H_2$ (6)), 31.89 ($\underline{C}H_2$ (2)), 24.83 ($\underline{C}H_2$ (4)), 20.99 ($\underline{C}H_2$ (3)), 20.67 ($\underline{C}H_2$ (5))

MS (ESI) ES+ *m/z* 357.25 [M-CO+Na^+] *Expected:* 357.70

ES– *m/z* 361.95 [M-H^+] 333.96 [M-H^+-CO] *Expected:* 361.72, 333.71

Tricarbonyl chloro (3-nitrotyrosinato) ruthenium(II) (CORM-Nitro-Tyr)

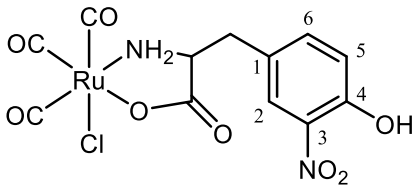

MF: $C_{12}H_9ClN_2O_8Ru$

MW: 445.73

Tricarbonyl chloro (3-nitro-tyrosinato) ruthenium(II) ([$Ru(CO)_3Cl$(3-nitrotyrosinate)] or CORM-Nitro-Tyr) was synthesized starting from the commercially available CORM-2. Briefly, CORM-2 (1mol eq, 85mg, 0.166mmol), 3-nitro-L-tyrosine (2mol eq, 75mg, 0.332mmol) and MeONa (2mol eq, 17.94mg, 0.332mmol) were dissolved in dry MeOH (5mL) in a round-bottomed flask at r.t. under N_2 atmosphere maintained by a Schlenk line. The reaction was allowed to stir for 24h at r.t. with a N_2 balloon and protected from light. The solvent was then removed in vacuo and the yellow residue re-dissolved in dry THF (1mL) and triturated with excess Et_2O until solid started precipitating. The supernatant yellow liquid was transferred to another flask using a glass pipette and the remaining powder was air dried to yield the final CORM-Nitro-Tyr (112mg, 75.6% yield). CORM-Nitro-Tyr was stored in closed vials at -20°C and used freshly on the day of the experiments.

^{1}H NMR (500MHz, MeOD) δ ppm 8.14 -8.04 (m, 1H, Ar-H2) 7.66 – 7.58 (m, 1H, Ar-H6) 7.19 – 7.12 (m, 1H, Ar-H5) 3.99 – 3.93 (m, 1H, C<u>H</u>) 3.40 – 3.35 (m, 1H, C<u>H$_2$</u>) 3.26 – 2.96 (m, 1H, C<u>H$_2$</u>)

^{13}C NMR (125MHz, MeOD) δ ppm 187.77, 186.01, 184.06 (3 CO) 181.77 (C=O ester) 153.26 (Ar-C4) 137.64 (Ar-C6) 129.01 (Ar-C3) 128.70 (Ar-C1) 125.42 (Ar-C2) 120.09 (Ar-C5) 56.60 (<u>C</u>H) 37.54 (<u>C</u>H$_2$)

MS (ESI) ES– *m/z* 444.93 [M-H$^+$] 416.93 [M-H$^+$-CO] 388.93 [M-H$^+$-2CO]

Expected: 444.72, 416.72, 388.70

Tricarbonyl chloro (3,5-dinitrotyrosinato) ruthenium(II) (CORM-Dinitro-Tyr)

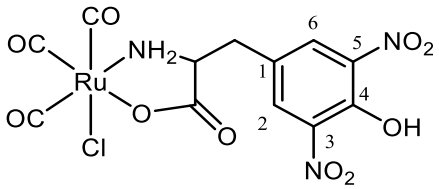

MF: $C_{12}H_8ClN_3O_{10}Ru$

MW: 490.73

Tricarbonyl chloro (3,5-dinitro-tyrosinato) ruthenium(II) ([$Ru(CO)_3Cl$(3,5-dinitrotyrosinate)] or CORM-Dinitro-Tyr) was synthesized starting from the commercially available CORM-2. Briefly, CORM-2 (1mol eq, 85mg, 0.166mmol), 3,5-dinitro-L-tyrosine (2mol eq, 90mg, 0.332mmol) and MeONa (2mol eq, 17.94mg, 0.332mmol) were dissolved in dry MeOH (5mL) in a round-bottomed flask at r.t. under N_2 atmosphere maintained by a Schlenk line. The reaction was allowed to stir for 24h at r.t. with a N_2 balloon and protected from light. The solvent was then removed in vacuo and the orange residue re-dissolved in dry THF (2mL) and triturated with excess Et_2O until solid started precipitating. The solid was dried in vacuo to yield the final CORM-Dinitro-Tyr (120mg, 73.7% yield). CORM-Dinitro-Tyr was stored in closed vials at -20°C and used freshly on the day of the experiments.

^{1}H NMR (500MHz, MeOD) δ ppm 8.20 (s, 2H, Ar-H2, H6) 3.92 – 3.82 (m, 1H, C<u>H</u>) 3.22 – 3.103 (m, 2H, C<u>H_2</u>)

^{13}C NMR (125MHz, MeOD) δ ppm 198.47, 196.50, 188.05 (3 CO) 186.26 (C=O ester) 148.82 (Ar-C4) 140.00, 139.80 (Ar-C3, C5) 139.47 (Ar-C1) 131.87, 131.53 (Ar-C2, C6) 56.71 (<u>C</u>H) 38.14 (<u>C</u>H_2)

MS (ESI) ES– *m/z* 489.93 [M-H^+] 461.94 [M-H^+-CO] *Expected:* 489.72, 461.71

Tricarbonyl chloro (4-nitrophenylalaninato) ruthenium(II) (CORM-Nitro-Phe)

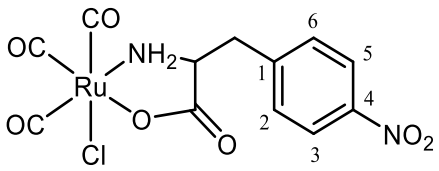

MF: $C_{12}H_9ClN_2O_7Ru$

MW: 429.73

Tricarbonyl chloro (4-nitro-phenylalaninato) ruthenium(II) ([$Ru(CO)_3Cl$(4-nitrophenylalaninate)] or CORM-Nitro-Phe) was synthesized starting from the commercially available CORM-2. Briefly, CORM-2 (1mol eq, 85mg, 0.166mmol), 4-nitro-L-phenylalanine (2mol eq, 69.8mg, 0.332mmol) and MeONa (2mol eq, 17.94mg, 0.332mmol) were dissolved in dry MeOH (5mL) in a round-bottomed flask at r.t. under N_2 atmosphere maintained by a Schlenk line. The reaction was allowed to stir for 24h at r.t. with a N_2 balloon and protected from light. The solvent was then removed in vacuo and the yellow residue was re-dissolved in dry THF (1mL) and triturated with excess Et_2O until solid started precipitating. Each fraction of solid isolated was washed with excess Et_2O and the different fractions were combined to yield the final CORM-Nitro-Phe (135mg, 94.7% yield). CORM-Nitro-Phe was stored in closed vials at -20°C and used freshly on the day of the experiments.

^{1}H NMR (500MHz, DMSO-d_6) δ ppm 8.51 (s broad, 2H, N$\underline{H_2}$) 8.22 – 8.08 (m, 2H, Ar-H3, H5) 7.71 – 7.46 (m, 2H, Ar-H2, H6) 4.18 – 4.17 (m, 1H, C$\underline{H}$) 3.09 – 2.97 (m, 1H, C$\underline{H_2}$, second hydrogen obscured by traces of H_2O in the NMR solvent)

^{13}C NMR (125MHz, DMSO-d_6) δ ppm 176.62 (CO) 170.45 (C=O ester) 147.22 (Ar-C4) 144.22 (Ar-C1) 131.45 (Ar-C2) 131.28 (Ar-C6) 123.96 (Ar-C3) 123.78 (Ar-C5) 53.43 ($\underline{C}$H) 35.91 ($\underline{C}H_2$)

MS (ESI) ES– *m/z* 428.94 [M-H^+] 400.95 [M-H^+-CO] 372.95 [M-H^+-CO]

Expected: 428.72, 400.71, 372.70

Tricarbonyl chloro (4-aminophenylalaninato) ruthenium(II) (CORM-Am-Phe)

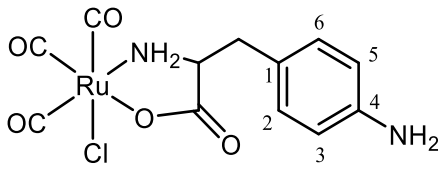

MF: $C_{12}H_{11}ClN_2O_5Ru$

MW: 399.75

Tricarbonyl chloro (4-amine-phenylalaninato) ruthenium(II) ($[Ru(CO)_3Cl$(4-aminophenylalaninate)] or CORM-Am-Phe) was synthesized starting from the commercially available CORM-2. Briefly, CORM-2 (1mol eq, 85mg, 0.166mmol), 4-amine-L-phenylalanine (2mol eq, 59.8mg, 0.332mmol) and MeONa (2mol eq, 17.94mg, 0.332mmol) were dissolved in dry MeOH (5mL) in a round-bottomed flask at r.t. under N_2 atmosphere maintained by a Schlenk line. The reaction was allowed to stir for 24h at r.t. with a N_2 balloon and protected from light. The solvent was then removed in vacuo and the yellow residue was re-dissolved in dry THF (1mL) and excess Et_2O was added. The solid was then dried in vacuo to yield the final CORM-Am-Phe (139mg, 97.9% yield). CORM-Am-Phe was stored in closed vials at -20°C and used freshly on the day of the experiments.

^{1}H NMR (500MHz, MeOD) δ ppm 7.4 – 7.03 (m, 4H, Ar-H2, H3, H5, H6) 4.87 (s, 2H, $N\underline{H_2}$, obscured by traces of H_2O in the NMR solvent) 4.13 – 3.93 (m, 1H, C<u>H</u>) 3.30 – 2.94 (m, 2H, $C\underline{H_2}$)

^{13}C NMR (125MHz, MeOD) δ ppm 187.74, 186.04, 184.61 (3 CO) 183.99 (C=O ester) 144.42 (Ar-C4) 130.85 (Ar-C6) 130.39 (Ar-C2) 120.90 (Ar-C5) 119.97 (Ar-C3) 56.70 (<u>C</u>H) 38.07 ($\underline{C}H_2$)

MS (ESI) ES– *m/z* 398.97 [M-H$^+$] 370.98 [M-H$^+$-CO] 342.97 [M-H$^+$-2CO]

Expected: 398.74, 370.73, 342.72

Tricarbonyl chloro (O-benzyloserinato) ruthenium(II) (CORM-Benz-Ser)

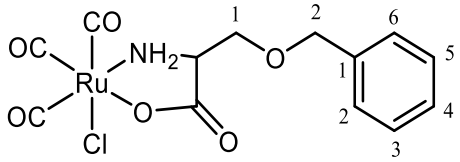

MF: $C_{13}H_{12}ClNO_6Ru$

MW: 414.76

Tricarbonyl chloro (O-benzyl-serinato) ruthenium(II) ([$Ru(CO)_3Cl$(O-benzyloserinate)] or CORM-Benz-Ser) was synthesized starting from the commercially available CORM-2. Briefly, CORM-2 (1mol eq, 85mg, 0.166mmol), O-benzyl-L-serine (2mol eq, 64.8mg, 0.332mmol) and MeONa (2mol eq, 17.94mg, 0.332mmol) were dissolved in dry MeOH (5mL) in a round-bottomed flask at r.t. under N_2 atmosphere maintained by a Schlenk line. The reaction was allowed to stir for 24h at r.t. with a N_2 balloon and protected from light. The solvent was then removed in vacuo and the yellow residue was re-dissolved in dry THF (1mL) and small excess of Et_2O was added. The solid was then dried in vacuo to yield the final CORM-Benz-Ser (120mg, 87.1% yield). CORM-Benz-Ser was stored in closed vials at -20°C and used freshly on the day of the experiments.

^{1}H NMR (500MHz, THF-d_8) δ ppm 7.36 – 7.22 (m, 5H, Ar-H) 4.62 – 4.47 (m, 2H, CH_2-2) 3.95 – 3.69 (m, 3H, CH_2-1, CH)

^{13}C NMR (125MHz, THF-d_8) δ ppm 187.4, 185.16, 182.98 (3 CO), 175.34 (C=O ester) 136.36 (Ar-C1), 126.12 (Ar-C5) 126.06 (Ar-C3) 125.75 (Ar-C6) 125.68 (Ar-C2) 125.44 (Ar-C4) 71.20 (CH_2-2) 69.57 (CH_2-1) 53.35 (CH)

MS (ESI) ES– *m/z* 413.97 [M-H^+] 385.97 [M-H^+-CO] 357.97 [M-H^+-2CO]

Expected: 413.75, 385.74, 357.73

Tricarbonyl chloro (O-(4-acetoxybenzoyl)serinato) ruthenium(II) (CORM-MK4a)

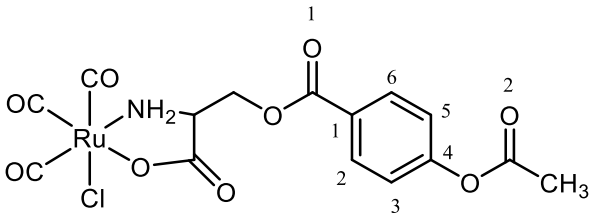

MF: $C_{15}H_{12}ClNO_9Ru$

MW: 486.78

Tricarbonyl chloro (O-(4-acetoxybenzoyl)serine) ruthenium(II) ($[Ru(CO)_3Cl(O\text{-}(4\text{-}acetoxybenzoyl)serinate)]$ or CORM-MK4a) was synthesized starting from the commercially available CORM-2 and the synthesized MK4a. Briefly, CORM-2 (1mol eq, 95mg, 0.185mmol), O-(4-acetoxybenzoyl)-serine (MK4a) (2mol eq, 88mg, 0.37mmol) and MeONa (2mol eq, 20mg, 0.37mmol) were dissolved in dry MeOH (5mL) in a round-bottomed flask at r.t. under N_2 atmosphere maintained by a Schlenk line. The reaction was allowed to stir for 24h at r.t. with a N_2 balloon and protected from light. The solvent was then removed in vacuo and the off-white residue was re-dissolved in dry THF (2mL) and excess Et_2O was added. The solid was then dried in vacuo to yield the final CORM-MK4a (156mg, 86.6% yield). CORM-MK4a was stored in closed vials at -20°C and used freshly on the day of the experiments.

^{1}H NMR (500MHz, THF-d_8) δ ppm 8.22 – 8.07 (m, 2H, Ar-H2, H6) 7.22 – 7.19 (m, 2H, Ar-H3, H5) 4.71 – 4.65 (m, 2H, C$\underline{H}_2$) 4.12 – 3.98 (m, 1H, C$\underline{H}$) 2.25 (s, 3H, C$\underline{H}_3$)

^{13}C NMR (125MHz, THF-d_8) δ ppm 184.21 (CO) 174.70 (C=O ester) 165.91 (C=O 2) 163.30 (C=O 1) 153.1 (Ar-C4) 129.32 (Ar-C2) 129.00 (Ar-C6) 125.2 (Ar-C1) 119.75 (Ar-C3) 119.62 (Ar-C5) peak of CH_2 within the solvent signal (expected around 64) 52.68 (C$\underline{H}$) 17.90 (C$\underline{H}_3$)

MS (ESI) ES– *m/z* 485.31 [M-H$^+$] *Expected:* 485.77

Synthesis of Ligands

Procedures and spectral data

Described below are the standard procedures followed in the synthesis of the ligands for the new CORM analogues and the spectral data for each compound. Everything was purchased from Alfa Aesar and used without further purification unless otherwise stated.

4-(2-((tert-butoxycarbonyl)amino)-3-methoxy-3-oxopropyl)phenyl 4-acetoxy-benzoate (MK1)

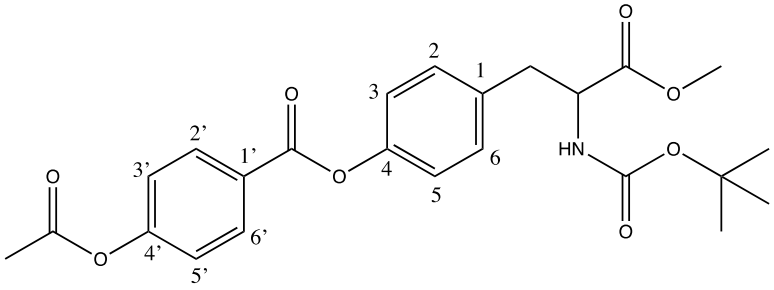

MF: $C_{24}H_{27}NO_8$

MW: 457.48

This compound was synthesized starting from the commercially available 4-acetoxybenzoic acid and N-Boc-L-Tyrosine methyl ester. N-Boc-L-Tyrosine methylester was activated by reacting with NaH dispersed in 60% mineral oil (Sigma-Alrich). Briefly NaH (1mol eq, 753.12mg, 2.55mmol) was dissolved in dry dichloromethane (CH_2Cl_2) (1mL) in a round-bottomed flask in ice and under N_2 atmosphere. N-Boc-L-Tyrosine methyl ester (1.2mol eq, 123mg, 3.06mmol) was dissolved in dry CH_2Cl_2 (2mL) and added dropwise in the NaH suspension, keeping everything in ice. After the addition, the reaction was left to stir for 30min at r.t. 4-Acetoxybenzoic acid (1mol eq, 306.26mg, 1.7mmol) was activated by reacting with hydroxybenzotriazole (HOBt) (1.2mol eq, 276mg, 2.04mmol) (Sigma-Aldrich) and 1-ethyl-3-(3-dimethylamino-propyl)carbodiimide (EDC) (1.2mol eq, 391mg, 2.04mmol) in dry CH_2Cl_2 (5mL) in a separate flask under N_2 and left to stir for 30min at r.t. The first reaction was then added to the second under N_2 and the reaction was allowed to stir for 3h at r.t. The crude was filtered and the organic layer washed twice with H_2O and once with Brine. It was left to dry over Na_2SO_4 for more than 2h and after the

filtration of the Na_2SO_4, the solvent was removed in vacuo. The white residue was further purified by column chromatography using $CHCl_3$:EtOAc 99-1% – 90-10% gradient system. The product was isolated as a white oil – solid (593mg, 76% yield).

^{1}H NMR (500MHz, $CDCl_3$) δ ppm 8.34 – 8.23 (m, 1H, Ar-H2'), 7.43 – 7.25 (m, 1H, Ar-H3'), 7.22 – 7.15 (m, 3H, Ar-H2, H3, H6), 7.05 – 7.03 (m, 1H, Ar-H5), 4.64 – 4.58 (m, 1H, C<u>H</u>), 3.75 – 3.73 (m, 3H, COOC<u>H$_3$</u>), 3.18 – 3.04 (m, 2H, C<u>H$_2$</u>), 2.38 – 2.29 (m, 3H, OCOC<u>H$_3$</u>), 1.48 – 1.44 (m, 9H, (C<u>H$_3$</u>)$_3$)

^{13}C NMR (125MHz, $CDCl_3$) δ ppm 172.22 (C=O, <u>C</u>OOCH$_3$), 169.41 (C=O, O<u>C</u>OCH$_3$), 168.79 (C=O, middle ester), 164.31 (Ar-C4'), 154.85 (C=O, Boc), 149.73 (Ar-C4), 132.01 (Ar-C1), 131.92 – 131.78 (2C-H, Ar-C2', C6'), 130.37 – 130.27 (2C-H, Ar-C2, C6), 127.05 (Ar-C1'), 122.16 – 121.62 (4C-H, Ar-C3, C5, C3', C5'), 80.02 (<u>C</u>(CH$_3$)$_3$), 54.37 (<u>C</u>H), 52.28 (COO<u>C</u>H$_3$), 37.71 (<u>C</u>H$_2$), 28.30 (C(<u>C</u>H$_3$)$_3$), 21.13 (OCO<u>C</u>H$_3$)

MS (ESI) ES+ *m/z* 480.17 [M+Na$^+$] *Expected:* 480.47

4-(2-((tert-butoxycarbonyl)amino)-3-methoxy-3-oxopropyl)phenyl 4-hydroxy-benzoate (MK1a)

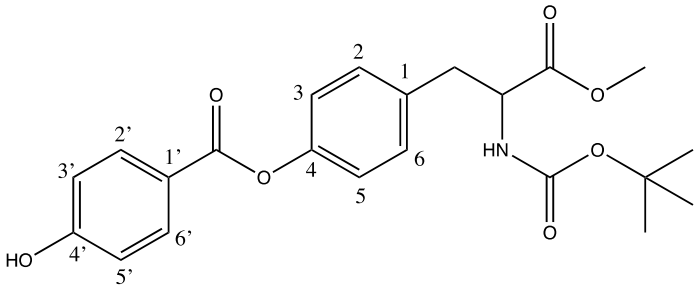

MF: $C_{22}H_{25}NO_7$

MW: 415.44

This compound was synthesized starting from the synthesized MK1 with the following two methods:

1. MK1 (1mol eq, 400mg, 0.874mmol) was dissolved in MeOH (5mL) in a round-bottomed flask and sodium bicarbonate ($NaHCO_3$) (6mol eq, 440.68mg, 5.25mmol) was added in the flask. After the addition, the reaction was left to stir for 24h at r.t. The solvent was then removed in vacuo and the crude was dissolved in water, where it was acidified with a few millilitres of 1M HCl. The aqueous layer was extracted twice with $CHCl_3$ and once with ethyl acetate (EtOAc). It was then left to dry over Na_2SO_4 for more than 2h and after the filtration of the Na_2SO_4, the solvent was removed in vacuo. The crude was further purified by column chromatography using $CHCl_3$:EtOAc 99-1% – 50-50% gradient system. The product was isolated as a white waxy oil (326mg, 90% yield).

2. MK1 (1mol eq, 593mg, 1.29mmol) was dissolved in MeOH (5mL) in a round-bottomed flask and potassium hydroxide (KOH) (1.5mol eq, 109.1mg, 1.94mmol) dissolved in 1mL H_2O and 3mL of CH_3OH was added in the flask. After the addition, the reaction was left to stir for 2h at r.t. The solvent was then removed in vacuo and the crude was dissolved in water, where it was acidified with a few millilitres of 1M HCl. The aqueous layer was extracted three times with CH_2Cl_2 and the organic layer was left to dry over Na_2SO_4 for more than 2h. After the filtration of the Na_2SO_4, the solvent was removed in vacuo and the crude was further purified by column chromatography using $CHCl_3$:EtOAc 99-1% – 80-20% gradient system. The product was isolated as a white waxy oil (446mg, 83% yield).

^{1}H NMR (500MHz, $CDCl_3$) δ ppm 8.12 – 8.09 (m, 1H, Ar-H3'), 7.20 – 7.18 (d, J= 10MHz, 1H, Ar-H3), 7.14 – 7.13 (d, J= 5MHz, 1H, Ar-H5), 7.00 – 6.99 (d, J= 5MHz, 1H, Ar-H2), 6.92 – 6.90 (d, J= 10MHz, 1H, Ar-H6), 6.77 – 6.76 (d, J= 5MHz, 1H, Ar-H2'), 4.64 – 4.54 (m, 1H, C<u>H</u>), 3.76 – 3.74 (m, 3H, COOC<u>H_3</u>), 3.18 – 2.98 (m, 2H, C<u>H_2</u>), 1.46 – 1.45 (d, J=5.5MHz, 9H, (C<u>H_3</u>)$_3$)

^{13}C NMR (125MHz, $CDCl_3$) δ ppm 172.39 (C=O, <u>C</u>OOCH_3), 165.13 (C=O, middle ester), 161.19 (Ar-C4'), 155.37 (C=O, Boc), 150.12 (Ar-C4), 133.44 (Ar-C1), 132.69 – 132.56 (2C-H, Ar-C2', C6'), 131.89 (Ar-C5), 130.40 – 130.27 (2C-H, Ar-C2, C6), 121.95 (Ar-C1'), 115.60 – 115.51 (2C-H, Ar-C3', C5'), 80.44 (<u>C</u>(CH_3)$_3$), 54.63 (<u>C</u>H), 52.30 (COO<u>C</u>H_3), 37.53 (<u>C</u>H_2), 28.32 (9C, C(<u>C</u>H_3)$_3$)

MS (ESI) ES+ *m/z* 438.15 [M+Na^+] *Expected:* 438.43

2-((tert-butoxycarbonyl)amino)-3-(4-((4-hydroxybenzoyl)oxy)phenyl)propanoic acid (MK1b)

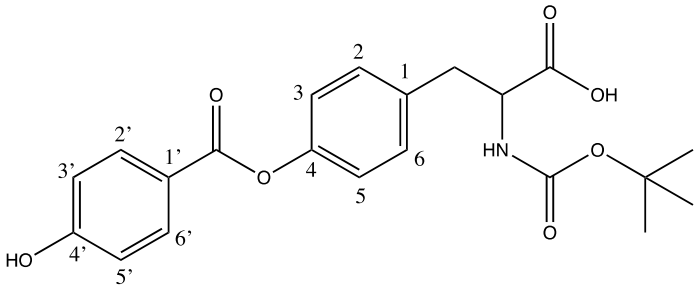

MF: $C_{21}H_{23}NO_7$

MW: 401.42

This compound was synthesized starting from the synthesized MK1a with the following method:

MK1a (1mol eq, 560mg, 1.35mmol) was dissolved in 1,4-dioxane (5mL) in a round-bottomed flask and lithium hydroxide (LiOH) (6mol eq, 193.7mg, 8.09mmol) dissolved in 1mL H_2O and 3mL of 1,4-dioxane was added in the flask. After the addition, the reaction was left to stir for 24h at 35^oC. The solvent was then removed in vacuo and the crude was redissolved in water, where it was neutralized with a few millilitres of 1M HCl (pH=6). The aqueous layer was extracted three times with EtOAc and dried in vacuo. The product MK1b was isolated as a white waxy solid from the aqueous phase (500mg, 92.4% yield).

^{1}H NMR (500MHz, MeOD) δ ppm 7.89 – 7.87 (m, 1H, Ar-H2'), 7.29 – 2.28 (m, 1H, Ar-H3), 7.06 – 7.05 (m, 2H, Ar-H2, H6), 6.69 – 6.68 (m, 2H, Ar-H5, H3'), 4.24 – 4.14 (m, 1H, C<u>H</u>), 3.21 – 2.82 (m, 2H, C<u>H$_2$</u>), 1.42 – 1.33 (m, 9H, (C<u>H$_3$</u>)$_3$)

^{13}C NMR (125MHz, MeOD) δ ppm 177.19 (C=O, <u>C</u>OOH), 166.58 (C=O, middle ester), 156.08 (Ar-C4'), 155.60 (C=O, Boc), 149.95 (Ar-C4), 135.45 (Ar-C1), 132.11 (2C-H, Ar-C2', C6'), 130.15 (2C-H, Ar-C2, C6), 128.82 (Ar-C1'), 121.14 (Ar-C5') 117.91 (2C-H, Ar-C3, C5), 114.71 (Ar-C3'), 78.81 (<u>C</u>(CH$_3$)$_3$), 56.92 (<u>C</u>H), 37.71 (<u>C</u>H$_2$), 27.40 (C(<u>C</u>H$_3$)$_3$)

MS (ESI) ES+ *m/z* 424.16 [M+Na$^+$] 408.19 [M-OH+Na$^+$] *Expected*: 424.40, 408.40

ES- *m/z* 400.15 [M-H$^+$] *Expected:* 400.41

2-amino-3-(4-((4-hydroxybenzoyl)oxy)phenyl)propanoic acid (MK1c)

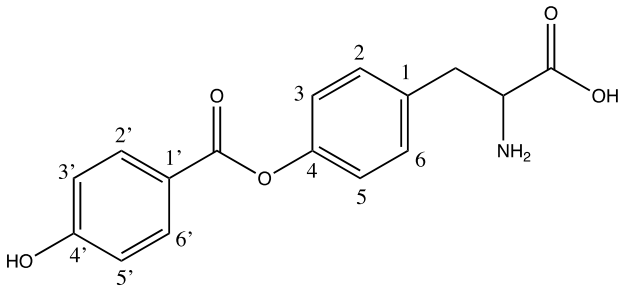

MF: $C_{16}H_{15}NO_5$

MW: 301.29

This compound was attempted to be synthesized starting from MK1b with the following method:

MK1b (1mol eq, 150mg, 0.373mmol) was suspended in dry CH_2Cl_2 (1mL) and dry MeOH (1mL) in a round-bottomed flask and 0.3mL trifluoroacetic acid (TFA) (10mol eq, 447mg, 3.8mmol) were added in the flask. After the addition, the reaction was left to stir for 2h at r.t. The solvent was then removed in vacuo. The product was attempted to be purified with flash chromatography and preparative TLC using 8:2:1 iPrOH:MeOH:NH_4OH as the eluent system. However, MK1c could not be purified completely, so only a mixed product was isolated as a white sticky solid (38mg, 34% yield). NMR and MS spectra of the isolated crude were taken and the final product was detected in them, even though impure (only MS spectra reported here).

MS (ESI) ES+ *m/z* 302.13 [$M+H^+$] *Expected*: 302.31

ES- *m/z* 300.10 [$M-H^+$] *Expected:* 300.29

3-(benzyloxy)-2-(((benzyloxy)carbonyl)amino)-3-oxopropyl 4-acetoxybenzoate (MK4)

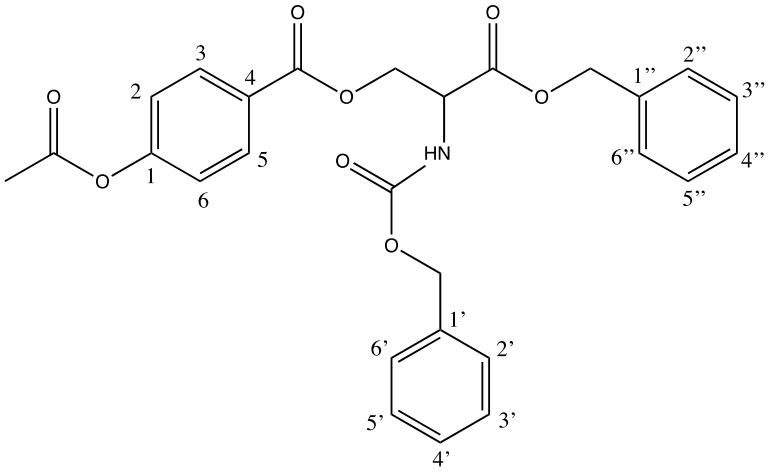

MF: $C_{27}H_{25}NO_8$

MW: 491.50

MK4 was synthesized starting from the commercially available N-benzyloxycarbonyl-L-serine benzyl ester and 4-acetoxybenzoic acid. The ester (1mol eq, 548.43mg, 1.665mmol) along with the acid (1mol eq, 300mg, 1.665mmol) and dimethylaminepyridine (DMAP) (0.3mol eq, 61.5mg, 0.5mmol) were dissolved in dry CH_2Cl_2 (2mL) in a round-bottomed flask under N_2 and kept in ice. N,N'-dicyclohexylcarbodiimide (DCC) (1mol eq, 343.58mg, 1.665mmol) was dissolved in 6mL of dry CH_2Cl_2 and added in the flask. After the addition, the reaction was left to stir for 5min in ice and for 4h at r.t. under N_2. The mixture was then filtrated to remove the formed dicyclohexylurea (DCU) and the filtrate was concentrated in vacuo. The crude was redissolved in dry CH_2Cl_2, and a new filtration was performed to remove any residual DCU. The filtrate was washed twice with 1M HCl and once with 0.1M NaOH and the organic layer was dried over Na_2SO_4 for more than 2h. After the filtration of the Na_2SO_4, the solvent was removed in vacuo and the crude was dissolved in i-PrOH with medium heating. The solution was left in the freezer for the final product to crystallize as a white waxy solid (600mg, 73.3% yield).

^{1}H NMR (500MHz, MeOD) δ ppm 7.93 – 7.92 (d, *J*= 7Hz, 2H, Ar-H3, H5), 7.34 – 7.23 (m, 11H, NH, Ar-H2', H3', H4', H5', H6', H2'', H3'', H4'', H5'', H6'') 7.16 – 7.15 (d, *J*= 7Hz, 2H, Ar-H2, H6), 5.26 – 5.11 (m, 4H, COOC$\underline{H_2}$Ph, NHCOOC$\underline{H_2}$Ph), 4.75 – 4.56 (m, 3H, C$\underline{H_2}$-C$\underline{H}$), 2.34 – 2.30 (m, 3H, C$\underline{H_3}$)

^{13}C NMR (125MHz, $CDCl_3$) δ ppm 169.33 (C=O, $CH_3\underline{C}OO$), 168.77 (C=O, $\underline{C}OOCH_2Ph$), 165.09 (C=O, Ar-$\underline{C}OO$-CH_2-CH), 155.70 (C=O, NH-$\underline{C}OO$-CH_2Ph), 154.59 (Ar-C1), 135.97 (Ar-C1''), 134.84 (Ar-C1'), 131.92 (2C, Ar-C3, C5), 131.39 (2C, Ar-C3', C5'), 131.30 (2C, Ar-C3'', C5''), 128.64 (2C, Ar-C4', C4''), 128.58 (Ar-C2'), 128.46 (Ar-C6'), 128.31 (Ar-C2''), 128.19 (Ar-C6''), 126.73 (Ar-C4), 122.01 (Ar-C2), 121.71 (Ar-C6), 67.86 (NH-COO-$\underline{C}H_2Ph$), 67.32 (CH-COO-$\underline{C}H_2Ph$), 64.86 (Ar-COO-$\underline{C}H_2$-CH), 53.59 ($\underline{C}H$), 21.17 ($\underline{C}H_3$)
MS (ESI) ES+ *m/z* 492.19 [$M+H^+$] 514.17 [$M+Na^+$] *Expected:* 492.50, 514.49

O-(4-acetoxybenzoyl)serine (MK4a)

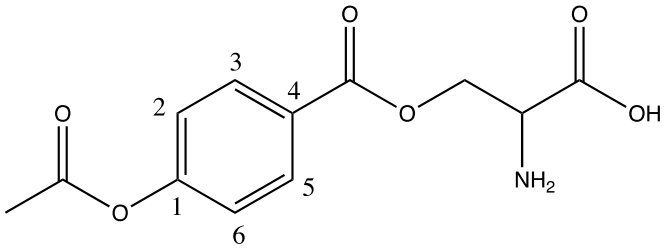

MF: $C_{12}H_{13}NO_6$

MW: 267.24

MK4a was synthesized starting from the synthesized MK4.

MK4 (1mol eq, 239mg, 0.486mmol) was dissolved in dry MeOH (5mL) and dry CH_2Cl_2 (1mL) in a round-bottomed flask. 28% of the starting material weight in 10% Pd/C were added and the mixture was stirred for a few minutes under N_2. The stirring stops and the N_2 balloon is replaced with a H_2 balloon and the reaction is left to stir at r.t. for 3h under H_2 (1 atmosphere). The mixture was then filtrated through a pad of cellite and washed many times with dry MeOH. The filtrate and the washings were combined and concentrated in vacuo to yield the final product MK4a as a white solid. (100mg, 77% yield).

^{1}H NMR (500MHz, MeOD) δ ppm 8.17 – 8.15 (d, *J* = 9Hz, 2H, Ar-H5, H3) 7.27 – 7.25 (d, *J* = 9Hz, 2H, Ar-H2, H6) 4.79 – 4.76 (dd, *J* = 3Hz, 12Hz, 1H, C$\underline{H}_2$) 4.69 – 4.66 (dd, *J* = 6.5Hz, 12.5Hz, 1H, C$\underline{H}_2$) 4.03 – 4.01 (m, 1H, C$\underline{H}$) 2.32 (s, 3H, C$\underline{H}_3$)

^{13}C NMR (125MHz, MeOD) δ ppm 169.38 (C=O acid) 169.07 (C=O Ac) 165.36 (C=O ester) 154.95 (Ar-C1) 131.07 (Ar-C3, C5) 126.83 (Ar-C4) 121.59 (Ar-C2, C6) 63.69 (C$\underline{H}_2$) 53.90 (C$\underline{H}$) 19.49 (C$\underline{H}_3$)

MS (ESI) ES+ *m/z* 268.0820 [M+H$^+$] *Expected:* 268.0816 (Accurate MS)

ES+ *m/z* 268.10 [M+H$^+$] 290.10 [M+Na$^+$] *Expected:* 268.24, 290.20

ES- *m/z* 266.08 [M-H$^+$] *Expected:* 266.24

3-(benzyloxy)-2-(((benzyloxy)carbonyl)amino)-3-oxopropyl 4-hydroxybenzoate (MK5)

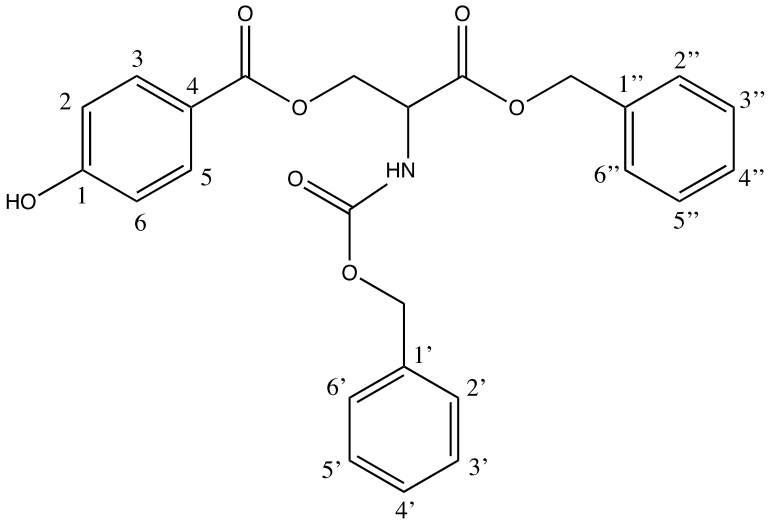

MF: $C_{25}H_{23}NO_7$

MW: 449.46

MK5 was attempted to be synthesized starting from the commercially available N-benzyloxycarbonyl-L-serine benzyl ester and 4-hydroxybenzoic acid. The ester (1mol eq, 272.9mg, 0.828mmol) along with the acid (1mol eq, 114.47mg, 0.828mmol) and DMAP (0.3mol eq, 30.37mg, 0.249mmol) were dissolved in dry CH_2Cl_2 (2mL) in a round-bottomed flask under N_2 and kept in ice. DCC (1mol eq, 170.98mg, 0.828mmol) was dissolved in 6mL of dry CH_2Cl_2 and added in the flask. After the addition, the reaction was left to stir for 5min in ice and for 6h at r.t. under N_2. The mixture was then filtered to remove the formed DCU and the filtrate was concentrated in vacuo. The crude was redissolved in dry CH_2Cl_2, and a new filtration was performed to remove any residual DCU. The filtrate was washed twice with 1M HCl and once with 0.1M NaOH and the organic layer was dried over Na_2SO_4 for more than 2h. After the filtration of the Na_2SO_4, the solvent was removed in vacuo and the crude was dissolved in i-PrOH for the final product to crystallize. The solution was left in the freezer for long time, but the final product was never recovered.

MS (ESI) ES+ *m/z* 472.15 [M+Na^+] *Expected:* 472.45

ES- *m/z* 448.15 [M-H^+] *Expected*: 448.49

4.3 Discussion

CORM synthesis

As discussed in detail in section 4.1, 15 new CORMs were synthesized starting from the commercially available CORM-2 and different amino acids, either purchased or synthesized. The protocol used for the synthesis has been reported in all the relevant publications, and all studies using synthesized CORM-3 agree on that (Clark et al. 2003). The mechanism of the reaction is a nucleophilic substitution, where the pairs of electrons of the nitrogen (amine group) and oxygen (hydroxyl group of the carboxylic acid) attack both ruthenium cores in subsequent steps and replace the middle chorines creating two monomers (**Figure 4.4**).

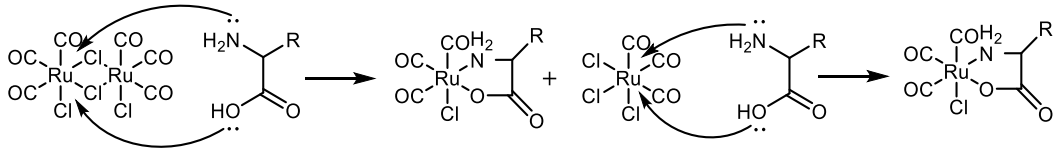

Figure 4.4: Mechanism of reaction for the synthesis of CORM-3 analogues

However, during the synthesis, some problems were encountered concerning the purification and characterization of the final products. In the corresponding protocol, there is no further purification step, apart from the crystallization of the final product inside the mixture. After the formation of the crystals, the solvent is removed in vacuo, which is quite uncommon, since all the impurities will eventually end up on the surface of the formed crystals. Therefore, several techniques were employed in order to remove the solvent and the dissolved by-products all together. Filtration under N_2 or normal atmosphere and through normal paper filter or glass filters with different pore sizes were employed, but none of the methods provided pure CORM-3 crystals. A different technique was also tried, to pipette out the supernatant and dry the solid under N_2 atmosphere or vacuum. The best product isolated was the one after removal of the supernatant in successive steps, following crystallization of CORM-3.

The synthesized product was subsequently compared to the commercially available one via ^{1}H and ^{13}C NMR spectra and the results are shown in **Figures 4.5** and **4.6**, respectively. The solvent used for the ^{1}H spectra was DMSO-d_6, which has some inherent limitations, such as the existence of water within the solvent, which

produces a quite broad ^{1}H NMR peak at δ 3.33 and the very strong and sharp signal of DMSO-d_6 itself at δ 2.50. THF-d_8 was preferred for the ^{13}C spectra because its peaks do not interfere with the expected signals of the molecule (THF-d_8 61.50, 126.28ppm).

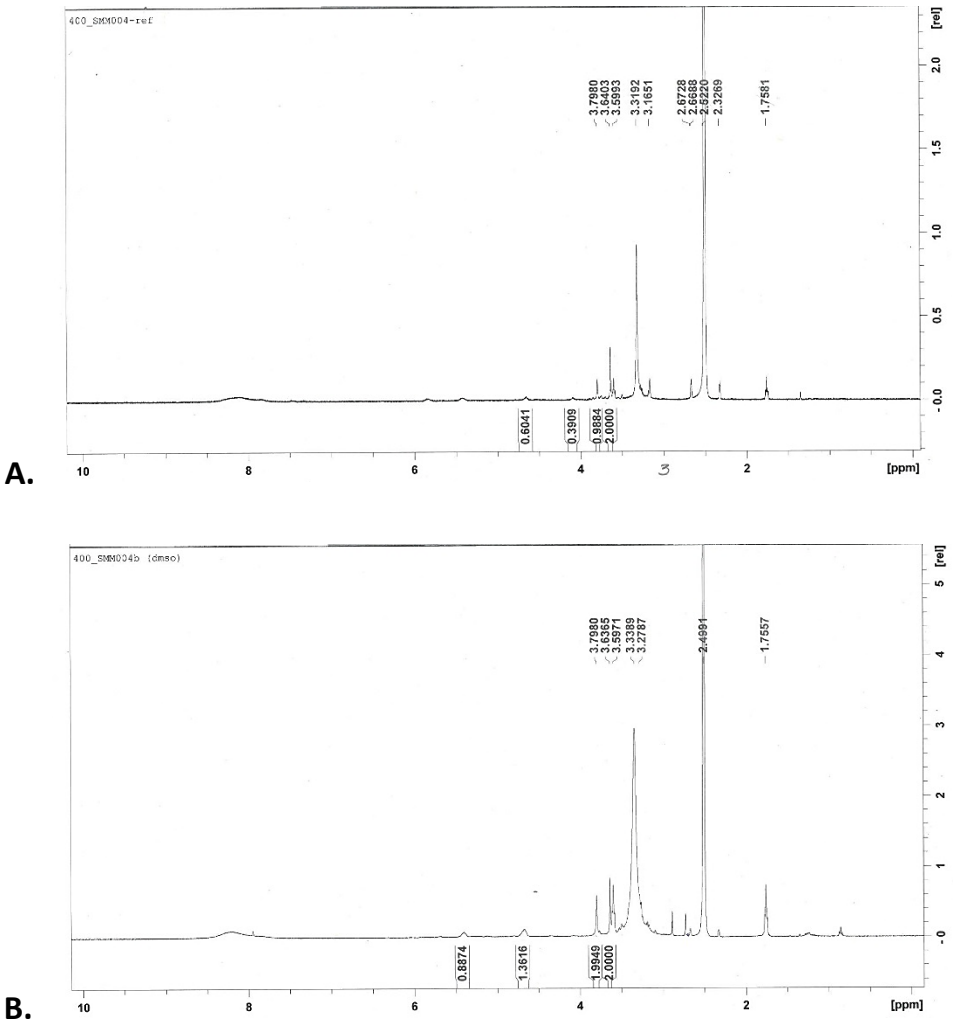

Figure 4.5: A. ^{1}H NMR spectra of reference and **B.** synthesized CORM-3 in DMSO-d_6.

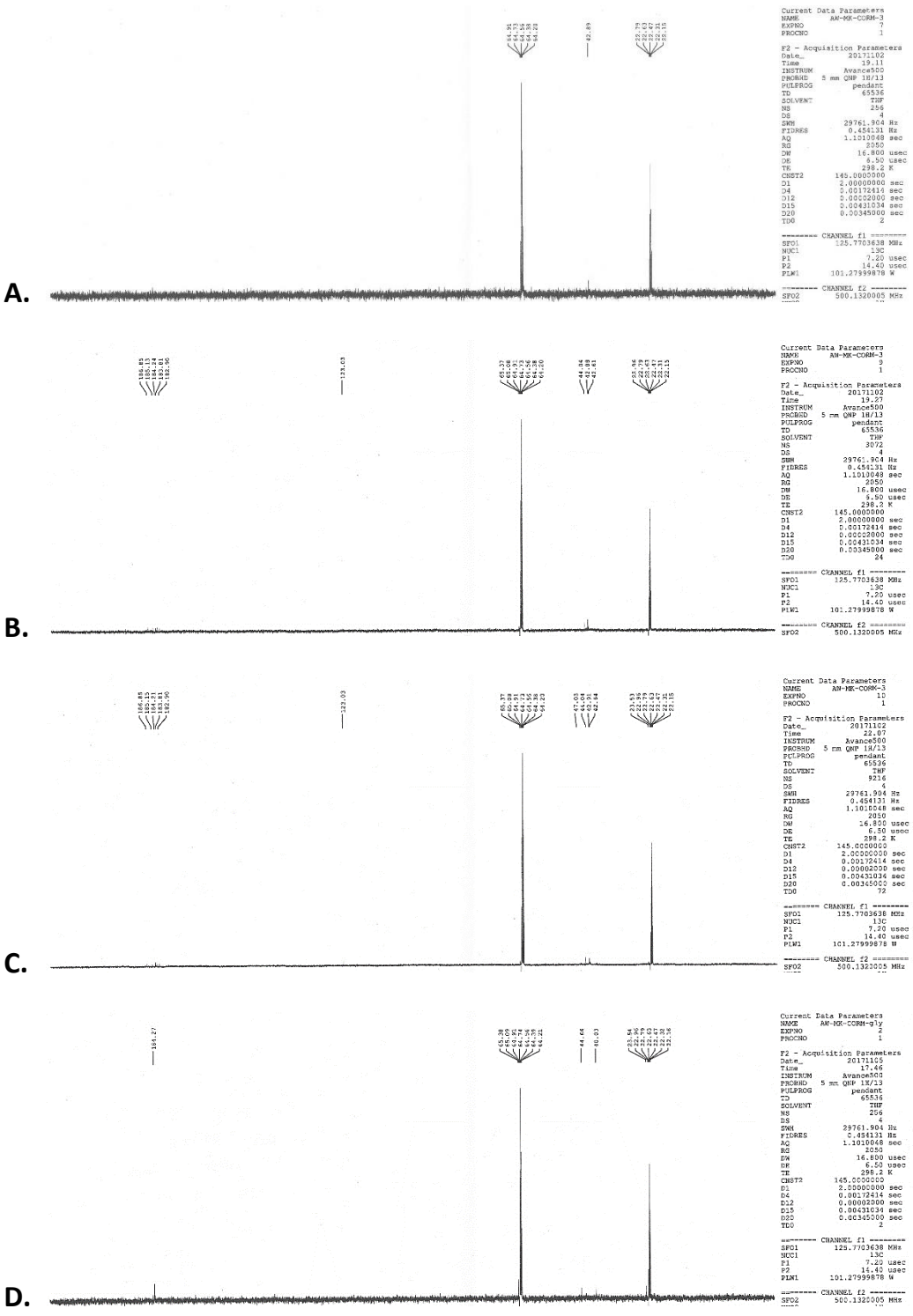

Figure 4.6: ^{13}C NMR spectra of purchased CORM-3 in THF-d_8 at **A.** 256 scans, **B.** 3072 scans and **C.** 9216 scans. **D.** ^{13}C NMR spectrum of synthesized CORM-3 in THF-d_8.

As observed in the figures, both products had very similar NMR spectra. In the ^{1}H NMR, both compounds showed a peak for two protons at around δ 3.60 and there were also the peaks of DMSO, H_2O and in both situations there were traces of THF solvent originating from the synthetic procedure. This means that the products cannot be completely dry, a phenomenon observed also in the other synthesized CORMs. Apart from that, there were some minor peaks further downfield that did not integrate into protons and a small broad peak resembling the ones produced by amine groups at around δ 8.00.

A few unexpected observations were reported for the ^{13}C NMR spectra, which were obtained using THF-d_8 as the solvent. The first spectrum was taken at 256 scans, but as expected the carboxyl group or the 3 carbonyl groups were not visible. When the number of scans was increased to 3072, more peaks started to come out, that do not originally belong to the molecule *per se*. More specifically, two extra peaks showed at 44.04 and 42.61ppm, and further downfield one peak showed at 123.03ppm and five peaks at around 185.00ppm. These peaks could not be assigned to specific carbons in the molecule, since there should be only one peak at around 42.00ppm for the CH_2 group and four peaks downfield of 180.00ppm for the one carboxyl and three carbonyl groups. This was quite unexpected, since the purchased product was confirmed to be more than 98% pure and even though the company was contacted, no extra information could be obtained. Taking a longer ^{13}C NMR spectrum at 9216 scans revealed one more peak at 47.03ppm, however the ratios between the pre-existing peaks was different than in the shorter spectrum.

For the synthesized CORM-3, at low number of scans two peaks were visible at 44.66 and 40.03ppm, very close to the commercially available ones, and one peak existed at 184.27ppm, probably belonging to the carboxyl group. The spectrum was very similar to the purchased CORM-3's and since the MS were also identical, no further characterization was carried out. Moreover, during the work up of the synthesized CORM-3 some well-structured crystals formed, that were subsequently characterized by Dr. B. Kariuki in the School of Chemistry and found to be a by-product of the synthesis containing Ru, with the structure $Ru(CO)_3Cl_3Na{\cdot}1.5(H_2O)$ (**Figure 4.7**).

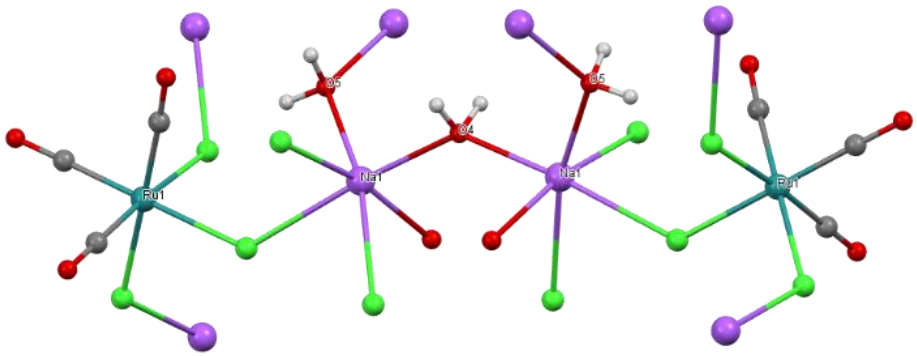

Figure 4.7: Crystal structure of by-product from synthesis of CORM-3

This unusual behaviour could suggest a potential change in the molecule while in the NMR tube, maybe as a consequence of its interaction with the solvent or other impurities. It could also imply a higher polymeric structure and not a monomeric one. This has also been proposed by other researchers (Johnson et al. 2007; Kunz et al. 2013; Seixas et al. 2015), where problematic spectra were again obtained for CORM-3 and derivatives, and isomers or a complex oligomeric structure were proposed, along with potential interactions with solvents and an extensive aqueous chemistry.

In the next step, other derivatives of CORM-3 were synthesized, using alternative amino acids. During these procedures all the different methods of crystallization and isolation of the final product were explored and the reported ones were the most effective for each individual derivative. Most of the times, a successive titration of the formed solid with PE or Et_2O and removal of the supernatant was used to obtain as pure products as possible. Most of them were dried under N_2 or vacuum, but certain times this drying step resulted in complete loss of the crystals, which had to be re-precipitated. In summary, each individual CORM had to be worked up in a different way in order to obtain the best possible result.

Three of the synthesized CORMs have been reported before in the literature. In the work of Kunz et al, CORM-Phe was synthesized for comparison purposes with its functionalized counterpart on the surface of maghemite nanoparticles. In the work of Wang et al, several CORM-3 derivatives were synthesized and evaluated, including CORM-Phe and CORM-Ala (Kunz et al. 2013; Wang et al. 2014). Finally, CORM-Ser has been briefly mentioned in a patent that was not readily available at the time of the production of this thesis. Neither the exact experimental procedure, nor the full

compound characterization was provided, therefore no comparison could be made for the CORM-3 derivatives.

The same problems that occurred during the characterization of CORM-3 were also experienced in the characterization of its derivatives. In short ^{13}C NMR scannings (low scan number), the peaks of the carboxyl or carbonyl groups were not visible most of the times, whereas when longer duration was used, more peaks arose for each carbon. This event resembled the observation for the purchased CORM-3, where longer spectra showed more peaks for the CH_2 or CO groups. For all CORM derivatives, several durations of ^{13}C NMR were employed and a study for each CORM was conducted, where the highest number of scans used were 10240 (10h) (a selection of spectra is attached in the Appendix). The same unusual observation was also reported in the ^{1}H NMR spectra, where apart from the peaks originating from the molecule itself, other little peaks were also visible and most of them had traces of THF. When the three reported CORMs were compared with the literature, similar peaks were found, but no publication referred to problems with the NMR spectra. However, in both these studies referenced here, NMR peaks were reported for the three complexes, but no spectrum was attached in the publication itself or the supporting material.

As a consequence of the unusual problems with the NMR spectra, certain purification methods were employed, in order to further purify the solids. Along with the exploration of different synthetic procedures and work up steps described previously, both high-performance liquid chromatography (HPLC)/UV and HPLC/MS were used to purify the final products in a variety of conditions and different ratios of the eluent system, but the products were never recovered.

Due to these unforeseen circumstances, and since all the MS confirmed the prevalent existence of the desired products in the isolated solids, the products were used as crudes and without further purification.

Ligand synthesis

Two ligands were aimed to be synthesized starting from the amino acid serine or tyrosine and the *p*-hydroxy-benzoic acid, in order to add an extra pro-oxidant moiety to the final complex.

As for the first ligand, 2-amino-3-(4-((4-hydroxybenzoyl)oxy)phenyl)propanoic acid (MK1c), the designed synthetic pathway is shown in **Figure 4.8**.

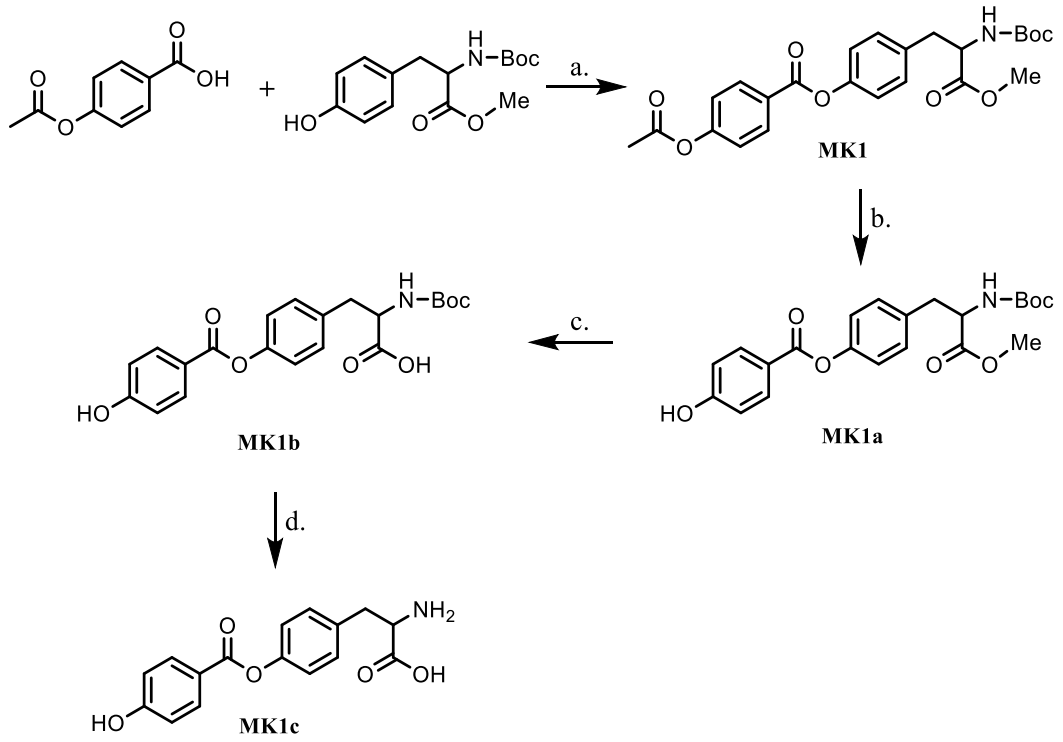

Figure 4.8: Synthetic pathway of MK1c. a) 1. NaH, CH_2Cl_2, N_2, 0°C-rt, 30min **2.** HOBt, EDC, CH_2Cl_2, N_2, rt, 30min **3.** N_2, rt, 3h, 76% **b)** 6eq $NaHCO_3$, MeOH, rt, 24h, 90% OR 1.5eq KOH, MeOH-H_2O, rt, 2h, 83% **c)** 6eq LiOH, 1,4-dioxane-H_2O, 35°C, 24h, 92.4% **d)** TFA, CH_2Cl_2-MeOH, rt, 2h, 34%

The first step includes the activation of both the carboxylic acid and the hydroxyl group of the protected tyrosine. The mechanisms of both activations are depicted in Figure **4.9 A** and **B**.

A.

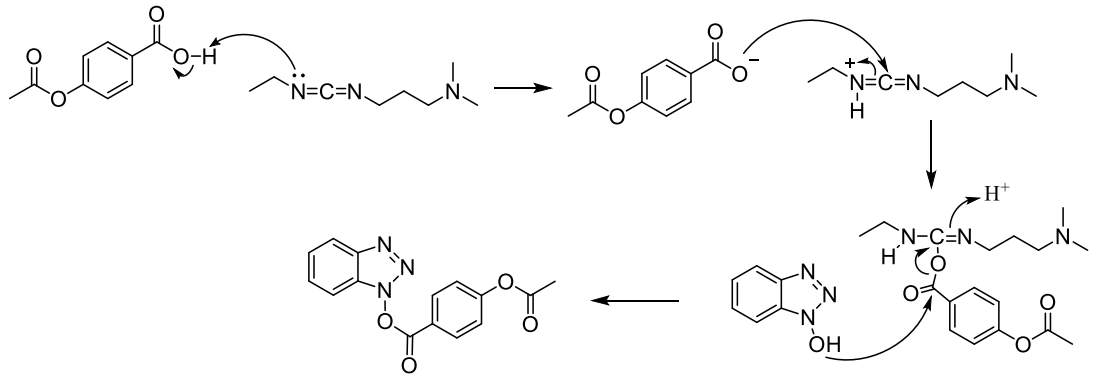

B.

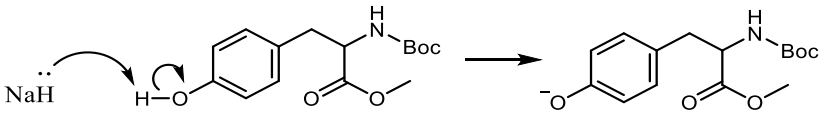

Figure 4.9: Activation of starting materials. A. Activation of *p*-hydroxy-benzoic acid with HOBt and EDC. **B.** Activation of tyrosine derivative with NaH.

After the activation, the two reactions are added together and the final product is yielded following the mechanism shown in **Figure 4.10**.

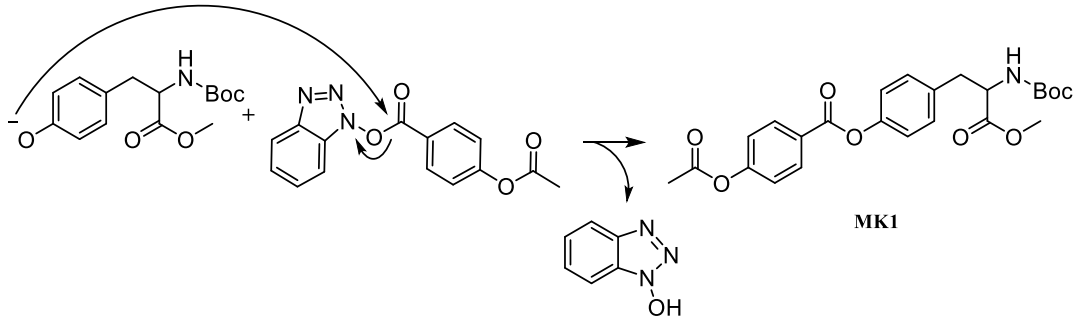

Figure 4.10: Mechanism of reaction for the synthesis of MK1

Product MK1 is then deprotected from the acetyl group in basic conditions and two different bases were explored, that is 6eq $NaHCO_3$, a relatively soft base, and 1.5eq KOH, a stronger base. Both methods formed the final product MK1a in good yields.

The next step is the deprotection of the carboxyl group from the methyl ester under basic conditions, using an even stronger base, LiOH, in excess. This step required moderate heating, and different conditions were explored. However, during the work up, the final product MK1b was unexpectedly isolated from the aqueous phase and was not possible to be completely dried from the remaining water. Nevertheless, the NMR and MS confirmed its formation, and it was subjected to the next step without further purification.

Finally, the final product MK1c was attempted to be synthesized from MK1b using an acidic hydrolysis of the Boc group (**Figure 4.11**). However, the final product yielded was not completely pure and the subsequent flash chromatography or preparative TLC employed to purify it were not successful. This product is very polar, which might be the reason why the chromatography did not succeed, even though a very polar eluent system was used for both, reported previously in literature for the purification of amino acids (Mota et al. 2003).

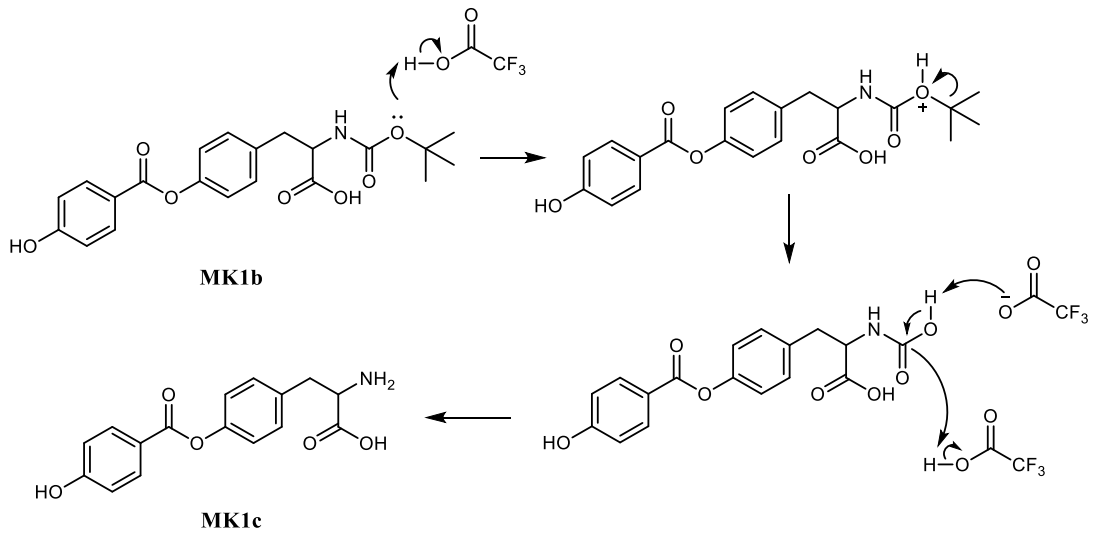

Figure 4.11: Mechanism of deprotection of the Boc group under acidic conditions for the synthesis of MK1c

The second ligand, O-(4-acetoxybenzoyl)serine (MK4a), was synthesized using the synthetic pathway shown in **Figure 4.12**.

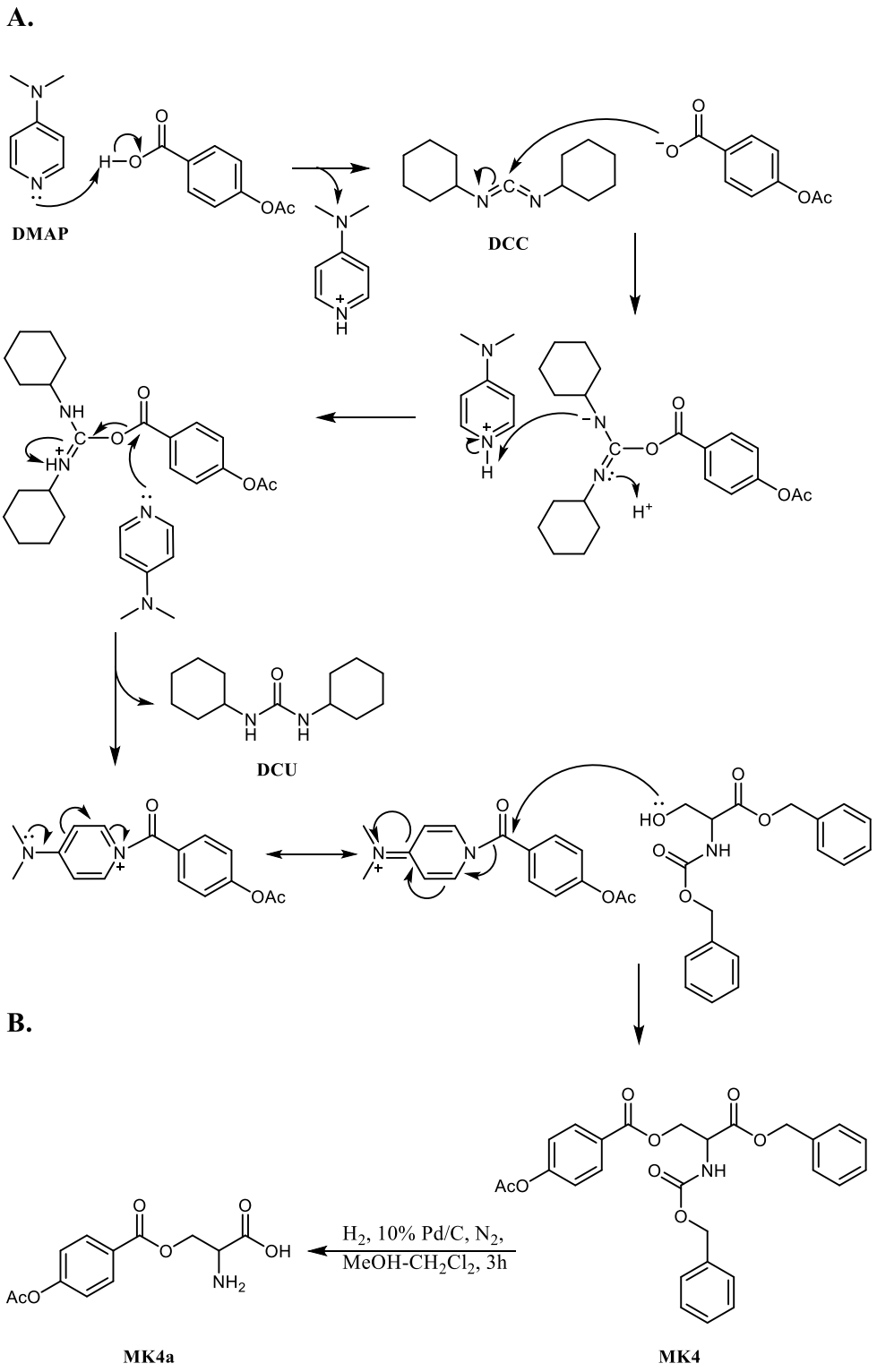

Figure 4.12: Synthetic pathway of MK4a. A. Steglich esterification for the synthesis of MK4. **B.** Hydrogenolysis for the synthesis of MK4a.

This ligand was successfully synthesized with very good yields of 73.3% for the first step and 77% for the second. The corresponding ^{1}H and ^{13}C NMR spectra for MK4a are attached in the Appendix (**Figures A.1** and **A.2**, respectively).

The same technique was employed also for the synthesis of the free hydroxyl derivative of MK4a (MK5a), however the first step did not yield the desired product, probably due to its high lipophilicity, or possibly a different purification method other than crystallization should have been explored. Nevertheless, the free hydroxyl derivative would have gone through an extensive metabolism within the cells or the organism, therefore a protecting group such as an ester could prove useful in delaying the rapid excretion and MK4a was used further.

Calculated lipophilicity data for all 15 new analogues of CORM-3 is shown in **Table 4.4** (as calculated in ChemDraw Professional 15.0).

CORM	CLogP	tPSA
CORM-3	-2.318	94.61
CORM-Ala	-1.799	94.61
CORM-Ser	-2.768	97.77
CORM-Phe	-0.381	94.61
CORM-Tyr	-1.048	114.84
CORM-His	-2.782	119.00
CORM-Trp	-0.391	106.64
CORM-Asp	-2.329	131.91
CORM-Cyclopen	-0.886	94.61
CORM-Cyclohex	-0.327	94.61
CORM-Nitro-Tyr	-1.305	166.65
CORM-Dinitro-Tyr	-1.562	218.46
CORM-Nitro-Phe	-0.638	146.42
CORM-Am-Phe	-1.71	120.63
CORM-Benz-Ser	-0.259	103.84
CORM-MK4a	-0.792	147.21

Table 4.4: Lipophilicity data of new CORM-3 analogues

As observed, all the complexes have polar characteristics and their CLogP values are negative, with CORM-His having the most hydrophilic and CORM-Benz-Ser the most lipophilic structure. However, CORM-Ala, CORM-Phe, CORM-Cyclopent and CORM-Cyclohex share the same tPSA with CORM-3. The other CORMs have more extended polar areas and the one with the highest tPSA is CORM-Dinitro-Tyr, due to its two nitro groups. These different characteristics also indicate different solubility in the various

solvents. As this was critical for further experiments, the new CORMs were tested for their solubility in different solvents, and the results are shown in **Table 4.5**:

CORM	H_2O	MeOH	DMSO	THF
CORM-3	+		+	+
CORM-Ala			+	+
CORM-Ser			+	
CORM-Phe			+	
CORM-Tyr			+	
CORM-His	+		+	
CORM-Trp			+	+
CORM-Asp			+	
CORM-Cyclopen			+	
CORM-Cyclohex			+	
CORM-Nitro-Tyr		+	+	
CORM-Dinitro-Tyr		+	+	
CORM-Nitro-Phe			+	
CORM-Am-Phe		+	+	
CORM-Benz-Ser			+	+
CORM-MK4a			+	+

Table 4.5: Solubility of new CORMs in different solvents

As observed, none of the new complexes is soluble in water apart from CORM-His, even though they are all very hydrophilic and with significant polar areas. This was quite unexpected, however since they are all very well soluble in DMSO, this was the solvent chosen for further experiments.

In summary, a set of 15 new analogues of CORM-3 were synthesized, 12 of them novel. These complexes were subsequently subjected to *in vitro* evaluation, in order to reveal any potential anti-angiogenic properties related to tumour angiogenesis in TNBC. The molecules were kept in tightly sealed vials at -20^{o}C and fresh stocks were prepared for each individual experiment. The stocks were kept in dark until tested and were diluted seconds before their addition on the cells.

Chapter V

Screening of new analogues

5.1 Cytotoxicity Assessment

5.1.1. Introduction

It has been extensively discussed that cell-based assays can be used for the assessment of cytotoxicity of anti-cancer compounds against diseased and normal cells (Ganot et al. 2013). The preclinical toxicity testing is a necessary step, as determined by the FDA, and it should include various biological systems (Berridge and Tan 1993; Parasuraman 2011). Any potential cytotoxicity of the novel compounds may be related to their capability to release CO, a lethal gas, as well as their metal core, that could also be responsible for toxicity (Egorova and Ananikov 2017).

Based on previous studies on the commercially available CORMs, it was considered useful to compare the novel compounds to the parent compound and look for any differences in the toxicological profile. Therefore, all the 15 newly synthesized candidates were screened against the aggressive MDA-MB-231 TNBC cell line and the most potent analogues were also screened against endothelial (HECV) and epithelial (MCF-10A) cells.

For the toxicological testing, the MTT assay was chosen, as a colorimetric assay for measuring the activity of NAD(P)H–dependent MTT–reducing enzymes to reduce MTT to its insoluble formazan, which has a purple colour. The quantity of formazan (presumably directly proportional to the number of viable cells) is measured by recording changes in absorbance at 540nm using a plate reading spectrophotometer.

5.1.2 Materials & Methods

Cell lines and treatments

MDA-MB-231 and HECV cell lines, maintained in DMEM media with 10% FBS and antibiotics, were used for the MTT assay. In addition, MCF-10A cells were used and maintained in MEBM media with the necessary MEGM supplements, cholera toxin and antibiotics. All cells were maintained at 37°C with 5% CO_2. The cells were treated with various concentrations of CORMs or DMSO for 72h. Then they were subjected to MTT assay.

MTT assay

$5x10^3$ cells were seeded in 120µL of normal medium per well in a 96-well plate. Three replicates were undertaken per treatment concentration and an identical plate was also prepared with no cells (blank). The cells were left to attach overnight and then were treated with various concentrations of CORMs as indicated or DMSO as the used vehicle. The concentration range used was a serial dilution between 100µM and 0.39µM, and the vehicle treated cells were used as controls. The blank plate received the same treatments. The cells were left in an incubator for 72h and then supplemented with MTT solution. The plates were incubated for further 4h and then the medium was removed and acidified isopropanol was used to dissolve the purple formazan crystals. The absorbance of both plates was read at 540nm and the blank plate was used to subtract any background absorbance from the test plate absorbance. The method is detailed in section 2.2.2.1.

IC_{50} calculation

The absorbance was normalized to the corresponding absorbance of the vehicle treated cells prior to plotting. Data was statistically analysed using non-linear regression (curve fit) to calculate the IC_{50} of each compound against each cell line in GraphPad Prism (www.graphpad.com).

5.1.3 Results

The effect of CORM treatments on the viability of different cell lines using the MTT assay

Consistent with previous experiments, the cytotoxicity of the novel compounds was assessed using an MTT colorimetric assay. MDA-MB-231 TNBC cells, MCF-10A epithelial cells and HECV ECs, following treatments with the new CORMs in different concentrations, were assessed for their viability.

No major cytotoxicity against the TNBC cells was observed for the new compounds compared to the vehicle. All calculated IC_{50} values exceeded 100µM, except for CORM-Cyclopent, which had an IC_{50} at 89µM. However, many values were very close to 100µM, that is for CORM-Ala, CORM-His, CORM-Nitro-Tyr, CORM-Dinitro-Tyr and

CORM-MK4a. Therefore, these compounds, along with CORM-Phe, CORM-Tyr, CORM-Cyclohex and CORM-Am-Phe, were chosen to be tested against the two other cell lines, as well.

First of all, the MCF-10A breast epithelial cells were assessed, representing the control cells in a normal breast environment. Almost all the newly synthesized CORMs tested had IC_{50} values of more than 200μM, although CORM-Cyclopent, CORM-Nitro-Tyr and CORM-Dinitro-Tyr appeared to be more cytotoxic than the others (IC_{50} of 71μM, 107μM and 156μM, respectively). For CORM-His an IC_{50} could not be calculated.

Following up, HECV cells were checked for cytotoxicity representing normal ECs, and all novel CORMs showed very low toxicity (**Figure 5.1** shows the calculated IC_{50} values for all the compounds and cell lines tested).

IC_{50} (μM)	*MDA-MB-231*	*HECV*	*MCF-10A*
CORM-3	312.5	996.3	Not converged
CORM-Ala	198.8	4866	787.4
CORM-Phe	325.3	1857	340.7
CORM-Trp	448.9	n.d.	n.d.
CORM-Ser	1429	n.d.	n.d.
CORM-Tyr	320.5	1681	373.3
CORM-Asp	353.4	n.d.	n.d.
CORM-His	162.1	1340	Not converged
CORM-Cyclopent	89.07	530.5	71.14
CORM-Cyclohex	460.9	n.d.	219.7
CORM-Benz-Ser	376.4	n.d.	n.d.
CORM-Nitro-Tyr	151.8	892.8	106.6
CORM-Dinitro-Tyr	171	1031	156
CORM-Nitro-Phe	273.4	n.d.	n.d.
CORM-Am-Phe	278.7	1642	339.5
CORM-MK4a	232.9	700.3	698.2

Figure 5.1: Cytotoxicity of novel CORMs. Mean IC_{50} values for all compounds and cell lines tested (calculated in GraphPad Prism) (n=3, N=3). The compounds which were significantly more cytotoxic against MDA-MB-231 compared to HECV and MCF-10A cells are highlighted in red boxes. (n.d.=not determined)

5.1.4 Discussion

Following previous experiments, the novel compounds were initially subjected to a cytotoxicity assessment. Since Ru has been the chosen metal for the new CORMs and heavy metals are generally believed to be more toxic compared to lighter ones, it was necessary to determine any potential toxicity of the new compounds against TNBC, epithelial and ECs.

The MTT assay was chosen for the cytotoxicity assessment, since previous results showed no difference between the three endpoint methods used. MDA-MB-231 cells were chosen to represent the target cancer subtype, that is TNBC, along with the control epithelial breast cells, MCF-10A and HECV as ECs. As shown in **Figure 5.1**, these compounds had a moderate cytotoxicity against the cell lines tested.

The most potent compound against MDA-MB-231 was CORM-Cyclopent, with an IC_{50} of 89μM. However, the IC_{50} against MCF-10A cells was also very low, namely 71μM, thus showing no selectivity between the cancer and normal cells. This agrees with previous literature, stating the cytotoxicity of ACPC, even though it has also been reported to be selectively taken up by tumour tissue (Connors et al. 1960). CORM-Cyclohex did not share the same cytotoxicity as CORM-Cyclopent, and this might be explained by the greater freedom in the conformation of its ring, making it less rigid and probably inducing less interaction with other cell components.

Other CORMs with elevated toxicity against MDA-MB-231 compared to the parent structure were CORM-Ala, CORM-His, CORM-Nitro-Tyr and CORM-Dinitro-Tyr, all with IC_{50} values between 100μM and 200μM. This toxicity was expected for CORM-Nitro-Tyr and CORM-Dinitro-Tyr, since as discussed earlier, the addition of nitro groups amplifies the ability of a compound to induce ROS production, and after a certain threshold, these levels might become toxic for the cells. Apart from that, nitro compounds are known toxicants that share toxicological effects with aromatic amines, since the nitro group can be readily reduced to amine group. These aromatic amines can yield reactive intermediates after metabolic activation that leads to toxicity (Lai and Woo 2015). However, CORM-Nitro-Tyr and CORM-Dinitro-Tyr were also toxic against MCF-10A cells, with lower IC_{50} values compared to the ones against

cancer cells. Therefore, no selectivity was observed for these CORMs, probably making them inappropriate candidates for further study. At this point, it should be also noted that the addition of an extra nitro group in the CORM-Dinitro-Tyr compared to CORM-Nitro-Tyr did not enhance the cytotoxicity of this compound, but on the contrary, its IC_{50} values were slightly lower than the corresponding ones for CORM-Nitro-Tyr. This might suggest an additional mechanism of toxicity for these two CORMs that does not rely solely on the existence of the nitro group.

The compounds that had a very favourable selectivity profile were CORM-MK4a, CORM-His and CORM-Ala, highlighted in red boxes (**Figure 5.1**). These three CORMs had a significantly higher cytotoxicity against MDA-MB-231 cells compared to ECs or MCF-10A. For CORM-Ala this result was unexpected, as there is nothing in its structure to correlate it with increased toxicity compared to other novel CORMs. Its relatively simple structure and small substituent (one methyl group) would make it less bulky and more versatile than others, but no specific characteristics are attributed to this one, apart from the major similarity with the parent compound, CORM-3. Nevertheless, CORM-Ala seemed to be more potent in killing TNBC cells than CORM-3 (198.8μM vs 312.5μM).

The same result was observed also for CORM-His that had a vast difference of almost 9-times between the toxicity against MDA-MB-231 and against HECV, whereas for MCF-10A the IC_{50} value was not converged. A big advantage of this complex is its solubility in water like CORM-3, while the imidazole ring may also confer a favourable interaction with any potential cellular target. The increased cytotoxicity compared to the parent complex may be related to the imidazole ring or the higher tPSA of this compound compared with CORM-3, although it is not the only one with a more extended polar surface. Nevertheless, CORM-His is the most potent of the three, having a relatively low IC_{50} value of 162.1μM against the MDA-MB-231.

As for CORM-MK4a, this result was expected to some extent, as from the design point of view, it was targeted to be more toxic due to the ability to enhance ROS production. The addition of the *p*-hydroxy-benzoic acid as an ester with serine could probably amplify the pro-oxidant activity of the whole complex compared to the simple CORM-Ser analogue. Thus, CORM-MK4a could potentially establish oxidative stress in cancer

cells over normal cells, since cancer cells are energetically challenged and their reduction defence mechanisms are more easily depleted due to their rapid division (Gorrini et al. 2013). This hypothesis was very well supported by the fact that CORM-MK4a was selectively cytotoxic against MDA-MB-231 cells and not against MCF-10A or HECV, where the IC_{50} values were as high as 700μM.

5.2 Protein expression quantification

5.2.1. Introduction

Tumour angiogenesis is linked to the expression of several proteins-enzymes that play various roles in the pro-angiogenic signalling and the formation of new capillaries. In line with the studies conducted for the commercially available CORMs, the new molecules were assessed for their ability to affect two main events implicated in angiogenesis. The first event was the ability of TNBC cells to express high concentrations of VEGF and the second one was the successful transduction of the pro-angiogenic signal starting from the EC surface receptor VEGFR2, in order to stimulate the angiogenic behaviour in ECs. Therefore, TNBC cells were treated with all novel CORMs and the expression levels of VEGF were quantified at three different time points. Two of them were chosen for further studies, based on the degree of VEGF reduction. HO-1 levels of TNBC cells were also quantified after treatment with the two chosen CORMs, in order to detect any potential decrease in the levels of this anti-oxidant and cyto-protective enzyme. Finally, ECs were subjected to treatments with the two CORMs and phosphorylation levels of Y1175 and other relevant downstream proteins were assessed upon VEGF stimulation.

5.2.2 Materials & Methods

Cell lines and treatments

MDA-MB-231 maintained in DMEM media with 10% FBS and antibiotics, were used for the quantification of VEGF expression after novel CORM treatments. All cells were maintained at 37°C with 5% CO_2. Cells were treated with 100μM CORMs or 0.1% DMSO or normal media 6h, 12h or 24h before collecting the supernatant.

MDA-MB-231 maintained in DMEM media with 10% FBS and antibiotics, were used for the quantification of HO-1 expression after CORM treatments. All cells were maintained at 37°C with 5% CO_2. Cells were treated with 100μM CORM-Phe or CORM-Tyr or 0.1% DMSO or normal media 12h before collecting the supernatant.

HUVEC maintained in EBM-2 media were treated with CORM-Phe or CORM-Tyr and then stimulated with 100ng/mL VEGF in order to be used for the quantification of pVEGFR2 and other downstream phosphorylated proteins. All cells were maintained at 37°C with 5% CO_2. Cells were treated with 100μM CORM-Phe or CORM-Tyr or 0.1% DMSO or serum free media for 15min and then stimulated with VEGF for 5min before the cell lysate was collected. An unstimulated sample was also obtained.

VEGF expression after treatment with CORMs

Upon reaching adequate confluence (~70%), the normal media of a T25 flask was removed and the cells were washed twice with PBS. Fresh media containing the corresponding concentration of CORMs or 0.1% DMSO or no treatment was added to each flask and the cells were left in the normal incubator for 6h, 12h or 24h. After the indicated incubation time, the supernatants of the cultures were collected, centrifuged and aliquoted in 1mL Eppendorf tubes that were kept at -80^{o}C until required. Protein was also extracted from the cells using 100μL lysis buffer, quantified using the Bio-Rad DC Protein Assay kit (Bio-Rad laboratories) and used for normalization of the results. Each aliquot was thawed and used only once and the VEGF content was quantified using the human VEGF ELISA kit (Life Technologies Ltd.) following the manufacturer's instructions. The assay is described in section 2.2.6.1.

HO-1 expression in MDA-MB-231 after treatment with novel CORMs

Upon reaching adequate confluence (~70%), the normal media of a T25 flask was removed and the cells were washed twice with PBS. Fresh media containing 100μM CORMs or 0.1% DMSO or no treatment was added to each flask and the cells were left in the normal incubator for 12h. After that, the supernatant of the culture was discarded and the total protein was extracted from the cells using 100μL lysis buffer, quantified and used for Western blot analysis.

Expression of phosphorylated proteins in VEGF stimulated HUVEC after treatment with novel CORMs

HUVEC cells were seeded in 6-well plates and upon reaching adequate confluence (~80%), the normal media was replaced with serum free media for 12h. Treatments of 100μM CORMs or 0.1% DMSO or no treatment were added to each well and the cells were left in the normal incubator for 15min. After that, 100ng/mL VEGF was added for further 5min. The supernatant of the cells was then discarded and the total protein was extracted from the cells using 100μL lysis buffer and quantified. The lysate was used either for ELISA (diluted 1:3 with Sample Diluent) or for Western blot analysis.

Statistical analysis

Statistical analysis was performed using GraphPad Prism. Unpaired Student's *t*-test with Welch's correction and nonparametric Mann-Whitney *t*-test were performed to check for statistical significance, with a p-value of <0.05 considered statistically significant. Asterisk notation (*) was used to identify significances: * $p<0.05$, ** $p<0.01$, *** $p<0.001$ and **** $p<0.0001$.

5.2.3 Results

VEGF expression in MDA-MB-231 cells after CORM treatments

In line with the screening of the four commercially available CORMs, the novel compounds were tested for any effects on the VEGF expression from TNBC cells. MDA-MB-231 cells were treated with 100μM CORMs for three different time periods and the concentration of VEGF excreted in the cell culture media was then quantified. As discussed in detail previously, MDA-MB-231 cells excrete a high concentration of VEGF, hence behave aggressively on angiogenesis and have a high metastatic capability. If this expression could be reduced, angiogenic signals towards tumour microenvironment could be potentially limited. Taking this into consideration, three different treatment periods were tested, that is 6h, 12h and 24h.

For matters of consistency, all the percentage values were calculated comparing the CORM treated cells with normal media treated ones. As explained for the four initial

CORMS, due to high variations throughout the experiments in the vehicle treated group the results were normalised to the media treated ones. Even though the concentration of the vehicle was now lower and very high variations were not observed in the vehicle groups, the decision to proceed this way was made in order to make the data comparable to the previous results and reach conclusions.

As depicted in **Figures 5.2 A**, **B** and **C**, all the novel CORMs could reduce the VEGF excreted from TNBC cells in the three time points tested. In each graph, the three CORMs that reduced VEGF by the highest percentage compared to the corresponding control group, were highlighted in red boxes. In the 6h treatment (**Figure 5.2 A**), CORM-Ala, CORM-Tyr and CORM-Nitro-Phe reduced VEGF expression by more than 50% each, reaching high statistical significance ($p=0.011$, $p=0.009$, $p=0.006$ respectively). Even though at a lower level, CORM-Asp, CORM-His and CORM-MK4a also managed to reduce VEGF with a higher statistical significance compared to the three above (p-values of 0.001, 0.0009 and 0.0008, respectively).

The reduction in the expression of VEGF in MDA-MB-231 cells was also observed in the longer time treatments. As depicted in **Figure 5.2 B**, in the 12h treatment, again all CORMs decreased the levels of VEGF expressed, although for most of the treatments this did not reach statistical significance. The three best CORMs in this subset were CORM-Phe, CORM-Benz-Ser and CORM-Nitro-Tyr, which reduced VEGF by almost 50% with statistical significance reached only for CORM-Benz-Ser ($p=0.0081$). However, other CORMs such as CORM-Ala and CORM-Asp showed similar reduction levels but more significant differences compared to the above mentioned ones, with p-values of 0.0072 and 0.0065, respectively.

Finally, in the 24h treatment (**Figure 5.2 C**), CORMs showed higher reduction rates, with the best ones, CORM-Phe, CORM-Tyr and CORM-His, reducing VEGF expression by 50%, 60% and 55%, respectively ($p=0.0309$, $p=0.0002$ and $p=0.00815$, respectively). Other CORMs did not induce such a reduction or reach any higher statistical significance than the ones highlighted.

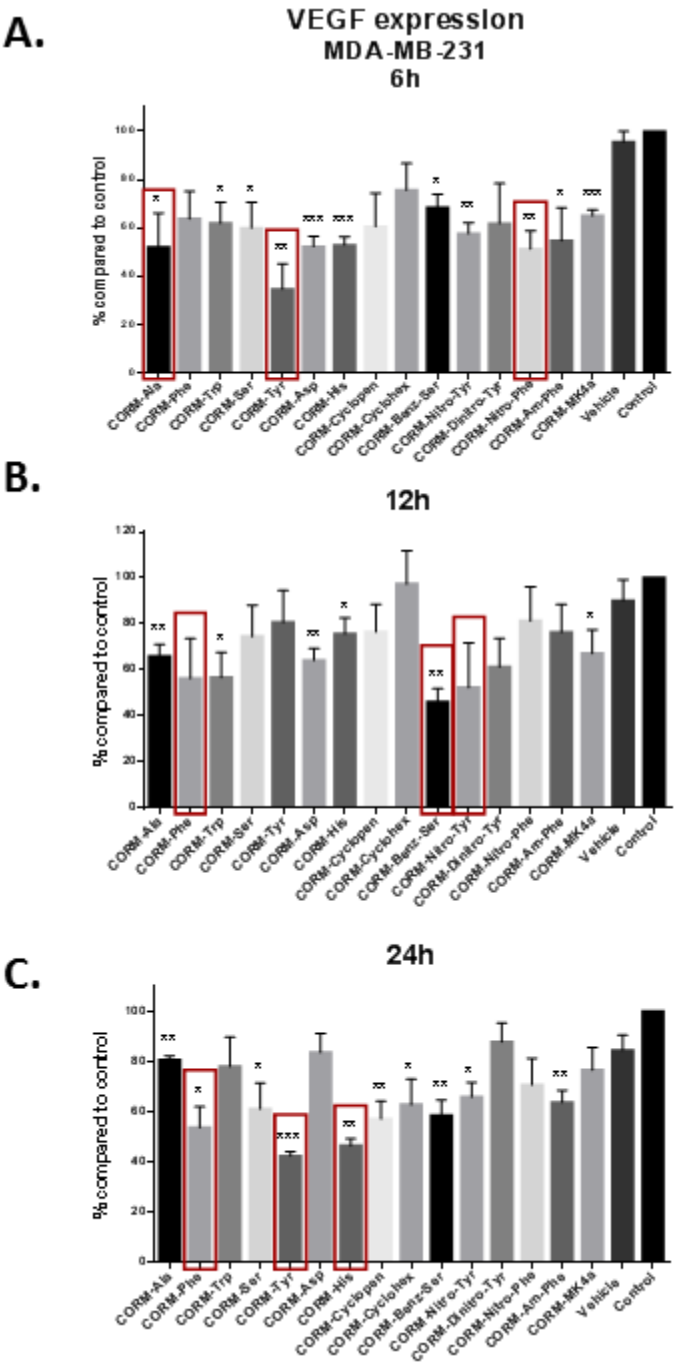

Figure 5.2: VEGF expression after novel CORM treatments. A. VEGF expression quantification in MDA-MB-231 cells 6h after treatment with 100µM CORMs, 0.1% DMSO or normal media, using a human VEGF ELISA kit. **B.** VEGF expression quantification in MDA-MB-231 cells 12h after treatment with 100µM CORMs, 0.1% DMSO or normal media, using a human VEGF ELISA kit. **C.** VEGF expression quantification in MDA-MB-231 cells 24h after treatment with 100µM CORMs, 0.1% DMSO or normal media, using a human VEGF ELISA kit. (All data is presented as % compared to control +SEM; n=3, N=3) (All data was statistically analysed against the corresponding duration normal media treated MDA-MB-231 cells (control) using un-paired *t*-test with Welch's correction: * $p<0.05$, ** $p<0.01$, *** $p<0.001$. In each time point, the three CORMs that reduce VEGF expression the most are highlighted in red boxes).

HO-1 expression in MDA-MB-231 cells after CORM treatments for 12h

Since HO-1 is a well-characterised cytoprotective enzyme in conditions of oxidative stress and excessive ROS production, any reduction in its expression would possibly sensitize cancer cells towards elevated production of ROS or other chemotherapeutic and anti-angiogenic agents. Thus, CORM-Phe and CORM-Tyr that were the most successful in reducing VEGF expression were also evaluated for their effects on HO-1 expression from TNBC cells after 12h of each CORM treatment at 100μM.

As observed in Figures **5.3 A** and **B**, CORM-Phe and CORM-Tyr could both reduce the expression of HO-1 ~20% after 12h of treatment, reaching statistical significance ($p=0.0268$ for both).

A.

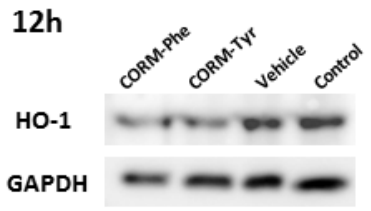

B.

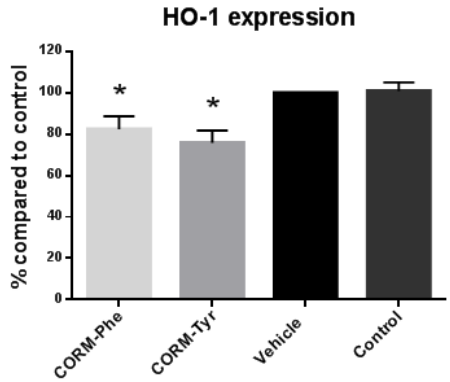

Figure 5.3: HO-1 expression after novel CORM treatments. A. Western blot of HO-1 expression following CORM or vehicle or media treatment for 12h in MDA-MB-231 cells. (Blot shows representative data; N=3). **B.** Assessment of HO-1 levels in MDA-MB-231 cells following 12h of treatment with CORM or vehicle or media (control) treatment. (Graph shows % compared to vehicle +SEM; N=3) (Data statistically analysed using nonparametric (Mann-Whitney) *t*-test with * $p<0.05$).

Expression of phosphorylated proteins in VEGF stimulated HUVEC after treatment with CORMs

For this experiment, 100μM CORMs or 0.1% DMSO or serum free media treatments were added to the cells for 15min prior to stimulation. After the 5min stimulation period, cell lysates were isolated and used either for ELISA against pY1175 of VEGFR2 or for Western blot analysis against pSrc (Y419), pERK1/2 (Y204), pFAK (Y397) and pAKT (S473) proteins.

As shown in **Figure 5.4 A**, CORM-Phe and CORM-Tyr reduced the phosphorylation of both pERK1 and pERK2 to baseline levels, reaching high statistical significance for both proteins (pERK1: p=0.0043 for CORM-Phe and p=0.0043 for CORM-Tyr, pERK2: p=0.0079 for CORM-Phe and p=0.0079 for CORM-Tyr). The levels of pSrc were both decreased to baseline, although they did not reach significance for the two new CORMs when compared to vehicle (**Figure 5.4 B**).

For pAKT levels, there was an obvious reduction induced by both CORMs, and the same trend was also observed for pFAK, even though more repeats would have generated a more robust result (**Figure 5.4 C**).

Finally, the phosphorylation levels of VEGFR2 at Y1175 were measured via ELISA and as shown in **Figure 5.5 A** both new CORMs managed to reduce phosphorylation at some level. However, this decrease reached statistical significance only for CORM-Tyr with p=0.0268. A similar outcome was also obtained by a Western blot analysis, where it was again shown that only CORM-Tyr moderately inhibited the activation of Y1175 of VEGFR2 (**Figure 5.5 B**).

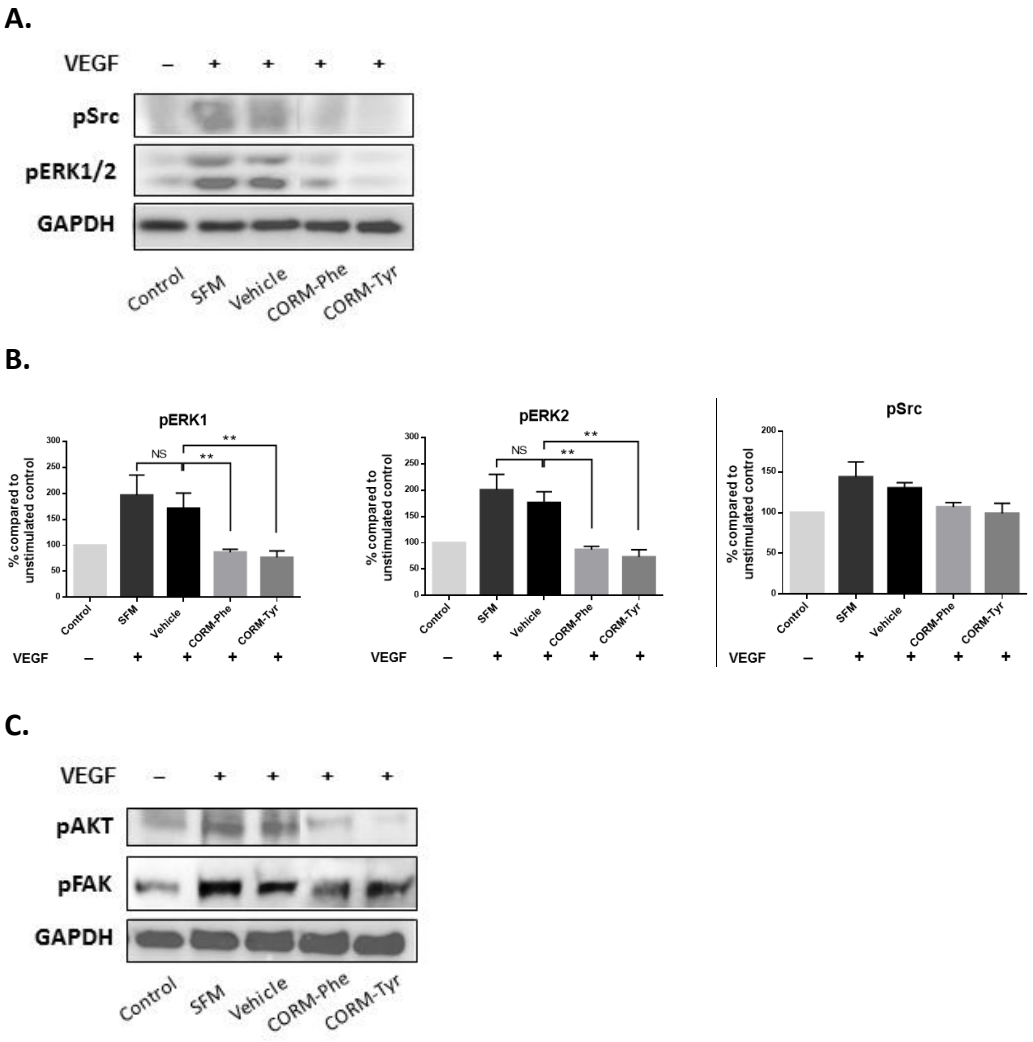

Figure 5.4: Expression of VEGFR2 pathway proteins in HUVEC after novel CORM pre-treatments and VEGF stimulation. A. Western blot of pSrc and pERK1/2 following 15min of CORM or vehicle pre-incubation and then stimulation with VEGF (100ng/ml) for 5 min. The first sample is the unstimulated control (Control) and the second is the stimulated control (SFM=serum free media). (Blot shows representative data; N≥4). **B.** Assessment of pERK1/2 and pSrc levels in HUVEC following the same protocol. (Graphs show % compared to Control +SEM; N≥4) (Data statistically analysed using nonparametric (Mann-Whitney) *t*-test with * p<0.05, ** p<0.01). **C.** Western blot of pAKT and pFAK following the same protocol. (Blot shows representative data; N=2).

A.

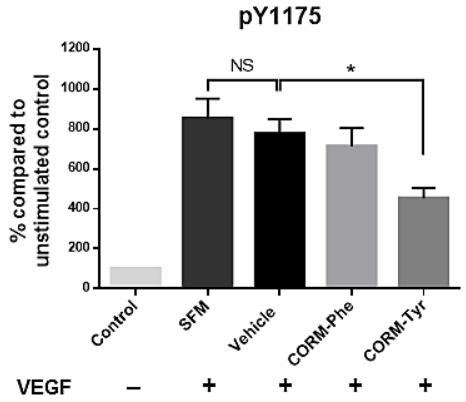

B.

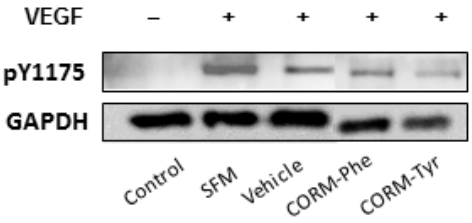

Figure 5.5: pY1175 levels for novel CORMs. A. Expression levels of pY1175 of VEGFR2 in HUVEC after 15min of CORM or vehicle pre-incubation and then stimulation with VEGF (100ng/ml) for 5 min, as measured with the human pY1175-VEGFR2 ELISA kit. The first sample is the unstimulated control (Control) and the second is the stimulated control (SFM=serum free media). (Graph shows % compared to Control +SEM; N=3) (Data statistically analysed using unpaired Student's *t*-test with Welch's correction * $p<0.05$). **B.** Western blot of pY1175 of VEGFR2 following the same protocol, which verifies the results of the ELISA. (Blot shows the obtained data; N=1).

5.2.4 Discussion

Angiogenesis depends on the expression of several proteins both by the cancer cells and the ECs that will line the new blood vessels. Based on previous experiments for the commercially available CORMs, all the synthesized analogues were screened for their ability to affect the expression of the main angiogenic signal from TNBC cells – VEGF – and the expression of downstream targets of the VEGF/VEGFR2 signalling pathway of ECs.

Previous literature suggested an increase in VEGF expression induced by CORMs in several *in vitro* models (Jözkowicz et al. 2003; Li Volti et al. 2005; Choi et al. 2010; Wilson et al. 2017), but other studies found an opposite effect for these complexes (Ahmad et al. 2015). Therefore, a study for any reduction in VEGF expression from TNBC cells was conducted, in line with the previous experiments for the commercially available CORMs (shown in Chapter 3).

When the aggressive MDA-MB-231 cell line was treated with the new CORMs for 6h, 12h and 24h, VEGF secretion was found reduced, and the three most successful CORMs for each time point were highlighted in red in **Figure 5.2**. The reduction was evident for all compounds, and for some of them managed to reach statistical significance. For the three most successful CORMs at each time point, the decrease reached a level of 45-65%, compared to the 47-57% for the parent complex, CORM-3. This suggests a potential anti-angiogenic profile for the new complexes, proving that the substitution of glycine with other amino acid moieties did not impair the ability to interfere with the VEGF expression from TNBC cells, possibly also decreasing the stimulation signals to the surrounding ECs.

Due to time restrictions limiting this study, only two CORMs were chosen for further exploration, based on their activity on lowering VEGF expression. CORM-Phe and CORM-Tyr were considered the most successful among the 15 new analogues and were therefore pursued further.

As limiting HO-1 expression in various cells may impair their proliferation and growth (Sass et al. 2008; Li et al. 2011; Szabo 2016), it would be useful to investigate how the two chosen CORMs affect HO-1 expression in MDA-MB-231 cells. In line with previous

experiments, a 12h incubation time was chosen and the concentration of 100μM, for comparison reasons with the commercial CORMs.

There was a downregulating activity observed for the two CORMs that was statistically significant. Both complexes reduced HO-1 expression by ~20%, almost at the same level as the parent compound which however failed to reach significance. A decrease in HO-1 expression might lead to more sensitive TNBC cells to chemo- or anti-angiogenic therapy and maybe also promote a less aggressive behaviour. Once again, the substitution of glycine did not impair this ability of the complex but did not significantly enhance it either.

Finally, the two chosen CORMs were subjected to experiments investigating any inhibitory activity on the VEGF/VEGFR2 pathway of ECs. As a successful pro-angiogenic signal transduction is linked to the effective new capillary formation, this pathway was explored as a potential target of the new molecules.

Some downstream proteins of VEGFR2 were investigated upon stimulation with VEGF that is pERK1/2, pSrc, pAKT and pFAK, in order to detect any inhibition induced by CORM-Phe and CORM-Tyr. It was found that both chosen CORMs had a decreasing activity on the activation of all studied proteins, even though specifically for ERK1/2, this inhibition was highly successful and statistically significant. The results for pSrc were not significant, although both CORMs managed to reduce the activation. It should be noted though that the activation achieved with VEGF was not very high, and the vehicle was less stimulated than the control, therefore this might have been the reason why they failed to reach significance.

As for pAKT and pFAK proteins, again both chosen CORMs seemed quite effective in reducing the activation induced by VEGF at such a high concentration, although this data needs to be confirmed via additional repeats in order to be statistically analysed and produce a trustworthy result.

In any case, the new CORMs showed better inhibitory activity than the parent compound CORM-3 that failed to reduce pSrc and pFAK levels at all. This suggests an enhanced anti-angiogenic activity for the new analogues, as well as a mechanism of action potentially involving ERK1/2, AKT and FAK proteins.

Finally, the activation of VEGFR2 upon stimulation with VEGF was explored, using the sensitive ELISA technique for the quantification of the results. Both chosen CORMs showed the same trend of reducing the activation of this receptor at Y1175, although the result was significant only for CORM-Tyr. The results were also verified by Western blot analysis. As CORM-3 failed to produce such an inhibition, the new analogues appeared to be more effective in this experiment altogether. This was a particularly interesting finding that needs further investigation, but definitely points toward an inhibition on the pro-angiogenic signal transduction after treatment especially with CORM-Tyr, even upon stimulation with a high dose of VEGF.

5.3 Angiogenic potential

5.3.1. Introduction

In line with previous experiments, the novel CORMs were tested for their potential to inhibit or reduce the ability of HECV cells to form tube-like structures. Since angiogenesis is involved in tumour growth, progression and metastasis, novel anti-angiogenic agents should be able to reduce tube formation induced in ECs, therefore less, or disrupted tube formations would be visible in the corresponding images.

The interaction between VEGF and its receptors promotes angiogenesis and tumour growth and data confirms this especially for TNBC, thus this study focuses on anti-angiogenic indications from the new molecules. Conditioned media from MDA-MB-231 cells which had been treated with the two chosen novel compounds or vehicle or media for three different durations, was used to stimulate tube formation in HECV cells. In addition, a separate experiment was conducted, where HECV cells were directly treated with the two chosen CORMs and their ability to form tube-like structures was measured.

5.3.2. Materials & Methods

Cell lines and treatments

HECV cells maintained in DMEM media with 10% FBS and antibiotics, were used for the tube formation assay. All cells were maintained at 37°C with 5% CO_2 prior to and during the experiments. Cells were treated with conditioned media from MDA-MB-

231 cells incubated with 100μM of CORMs or 0.1% DMSO or normal media for 6h, 12h or 24h. For the instant treatments, the same cells and conditions were used.

Tube formation assay using conditioned media

$3.5x10^4$ cells were seeded on top of a pre-set layer of Matrigel in each well of a 96-well plate. The plate was left in the normal incubator for cells to adhere and then the full media was replaced with serum free media containing conditioned media from treated MDA-MB-231 cells. After 6h, the wells were imaged using a Leica DM 1000 LED microscope capturing at least 3 images/well in random areas. Images were analysed using the ImageJ Software and the percentage of total tube length compared to the cells that received conditioned media from vehicle treated MDA-MB-231 cells was calculated.

Tube formation assay with instant treatment

$3.5x10^4$ cells were seeded on top of a pre-set layer of Matrigel in each well of a 96-well plate. The plate was left in the normal incubator for cells to adhere and then the full media was replaced with serum free media containing 100μM of CORMs or 0.1% DMSO or serum free media. After 6h, the wells were imaged using a Leica DM 1000 LED microscope capturing at least 3 images/well in random areas. Images were analysed using the ImageJ Software and the percentage of total tube length compared to the vehicle treated cells was calculated.

Statistical analysis

Statistical analysis was performed using GraphPad Prism. Unpaired Student's *t*-test with Welch's correction was performed to check for statistical significance, with a p-value of <0.05 considered statistically significant. Asterisk notation (*) was used to identify significances: * $p<0.05$, ** $p<0.01$, *** $p<0.001$ and **** $p<0.0001$.

5.3.3. Results

Tube formation after treatment with conditioned media from cancer cells

As the new CORMs were being screened for potential anti-angiogenic properties, a tube formation assay was deemed necessary for the characterization of their anti-

angiogenic capability. As a reduction of excreted VEGF from MDA-MB-231 cells was previously observed, any effects on the formation of tube-like structures from cancer conditioned media treated ECs were sought. As these compounds were not majorly cytotoxic against ECs, any effect observed should be a consequence of the lower concentration of VEGF expressed and excreted by the cancer cells.

After isolating media from CORM-Phe, CORM-Tyr, vehicle or media treated MDA-MB-231 cells, it was used to supplement ECs and check for angiogenic capability. As shown in **Figure 5.6 A**, both CORMs managed to reduce the formation of tubes. More specifically, conditioned media from CORM-Phe treated MDA-MB-231 cells for 6h, 12h or 24h, stimulated lower tube formation compared to conditioned media from vehicle and media treated cells. These differences reached statistical significance with p-values of 0.0197, 0.0302 and 0.005 for 6h, 12h and 24h, respectively (**Figure 5.6 B**).

Conditioned media from 6h and 24h CORM-Tyr treated cancer cells reduced the formation of tube-like structures by 40% and 30%, respectively, whereas the conditioned media from 12h treatment did not show a significant trend. For the 6h and 24h treatments, the differences were statistically significant with p-values of 0.0153 and 0.0019, respectively.

Tube formation after treatment with CORMs

Another tube formation experiment was carried out, where ECs were directly treated with the CORMs (100μM) or vehicle or serum free media and their tube formation activity was assessed by quantifying total tube length in images taken 6h after the treatments.

As shown in **Figure 5.6 C**, direct treatments did not affect the tubes and the images obtained were quite similar. The quantification of the total tube length did not reveal any statistically significant differences, with p-values calculated via *t*-test with Welch's correction exceeding p=0.05 (**Figure 5.6 D**).

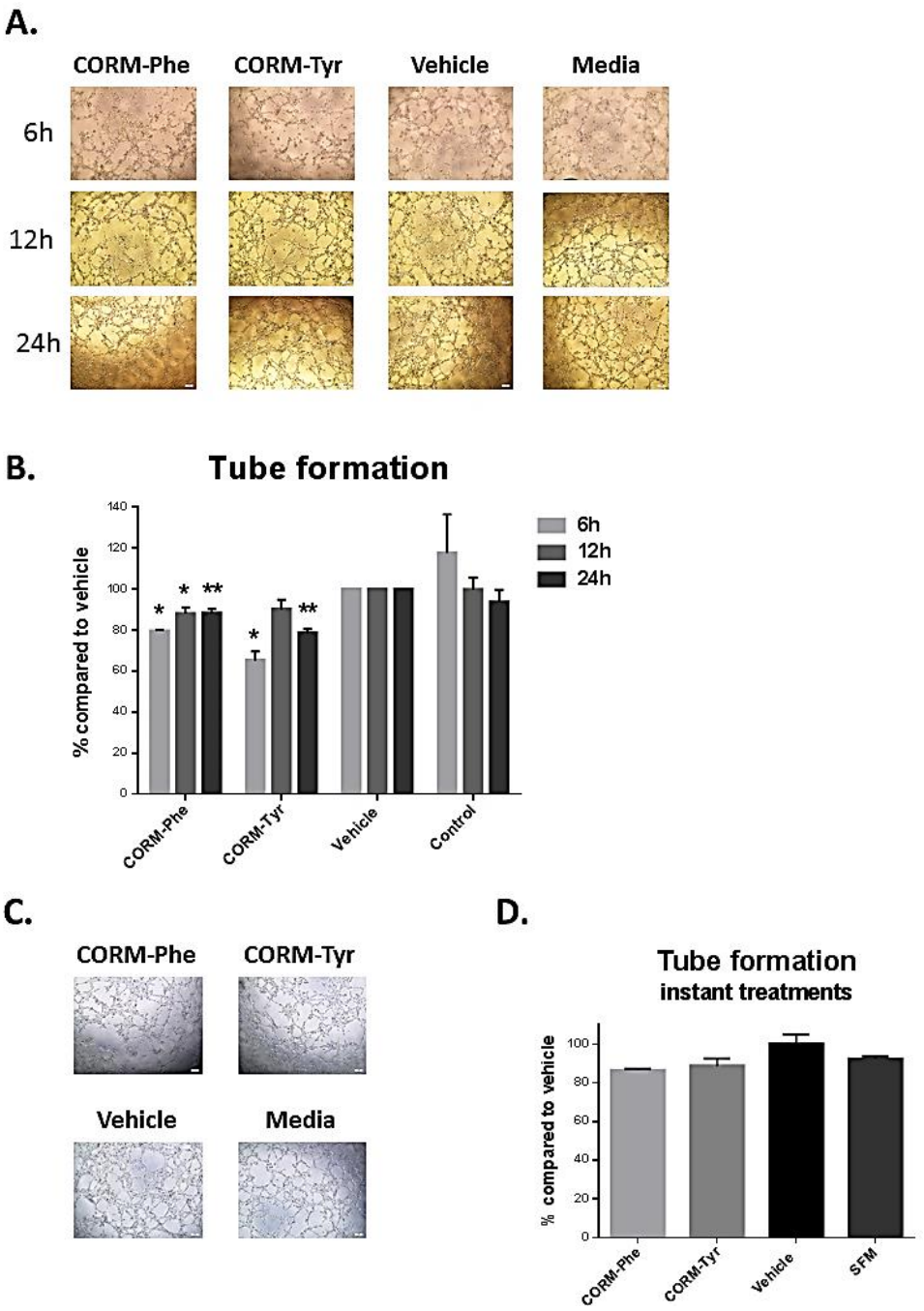

Figure 5.6: Tube formation ability of HECV after conditioned media or novel CORM treatments. **A.** Representative images from tube formation assay with HECV cells treated with conditioned media from variable duration incubation of MDA-MB-231 cells with 100µM CORMs or 0.1% DMSO or normal media. Objective 5x. **B.** Tube formation capacity of HECV cells after treatment with conditioned media from variable duration incubation of MDA-MB-231 cells with 100µM CORMs or 0.1% DMSO or normal media. (% total tube perimeter compared to vehicle +SEM; n=3, N=3) (All data was statistically analysed against the conditioned media from corresponding duration vehicle treated MDA-MB-231 cells using un-paired *t*-test with Welch's correction: * $p<0.05$, ** $p<0.01$). **C.** Representative images from tube formation assay with HECV cells treated with 100µM CORMs or 0.1% DMSO or serum free media. Objective 5x. **D.** Tube formation capacity of HECV cells after treatment with 100µM CORMs or 0.1% DMSO or serum free media. (% total tube perimeter compared to vehicle +SEM; n=3, N=2) (All data was statistically analysed against vehicle treated cells using un-paired *t*-test with Welch's correction: * $p<0.05$).

5.3.4. Discussion

Cancer cells are known to induce the expression of several growth factors, in order to support their rapid growth and potential to metastasize. One of these factors, VEGF, is mainly responsible for the induction of angiogenesis that will supply cancer cells with a functional network of blood vessels. VEGF excreted from TNBC cells reaches VEGFRs on the surface of ECs and stimulates pro-angiogenic pathways leading to increased angiogenic activity. ECs will eventually form tubules that will mature into fully functional blood vessels (Zhu and Zhou 2015). The *in vitro* formation of capillary-like structures by ECs seeded on basement matrix has been used as a reliable indication of the potential of different factors to affect angiogenesis (Menyhárt et al. 2016).

As shown also with previous CORMs, the newly synthesized CORMs seemed to induce a notable reduction in the levels of VEGF expressed by MDA-MB-231 cells. Following previous experiments, the effect of reduced growth factor expression caused by these compounds on the activation and angiogenic behaviour of ECs was studied, that is the ability of ECs to form tubes. Therefore, conditioned media from CORM treated MDA-MB-231 cells was used to stimulate angiogenesis on ECs and was compared to vehicle and normal media treatments.

Both CORMs managed to reduce the tube formation activity of ECs to some extent. Conditioned media from CORM-Phe treated cancer cells caused a small (15-20%) but significant decrease in the length and complexity of the formed tubes. The same was observed also with the conditioned media from CORM-Tyr treated TNBC cells, apart from the 12h treatment, which did not raise statistical significance. However, CORM-Tyr appeared to have a higher activity than CORM-Phe and the reduction after treatment with conditioned media from 6h pre-treated TNBC cells reached 35%.

These results correlated very well with the determined VEGF levels for each conditioned media. More specifically, CORM-Phe treated MDA-MB-231 cells appeared to have similar concentrations of VEGF after the three different treatment durations that resulted in a comparable reduction in the tube formation by ECs. CORM-Tyr on the other hand, showed a significant lowering effect at 6h and 24h, thus

these media were more efficient in reducing tube formation. Indeed, even though 6h and 24h pre-treated MDA-MB-231 cells expressed 60% less VEGF than vehicle treated cells, the 12h treatment resulted in only 20% decrease. This was reflected in the tube formation assay, where conditioned media from 6h and 24h inhibited tube formation by 35% and 25%, respectively, whereas the 12h media managed only a 10% reduction that did not reach significance. This anomaly might be a consequence of the differential expression of other pro-angiogenic factors that may have been more elevated at the 12h time point, resulting in a lower efficiency of the CORM treatment.

The same limitations discussed earlier for the four commercial CORMs also apply to these results. These are that the low level reduction in tube formation compared to the significant reduction in VEGF expression might be explained by the use of full normal media for the seeding of ECs on top of the Matrigel, the dilution of the conditioned media and the non-reduced concentration of growth factors of the Matrigel used. Thus, the mild inhibition of the tube formation activity of ECs did not reflect the big differences in the concentration of VEGF determined for these conditioned media. Another limiting factor might be other pro-angiogenic factors apart from VEGF that also regulate the formation of tube-like structures. In any case, the same trend was observed, that is TNBC cells expressed lower levels of VEGF because of CORM treatments and as a result there was a limited stimulation of ECs towards fewer and less complex tubes.

Finally, when instant CORM treatments were checked for inhibitory activity, the results were as expected. None of the CORMs managed to reduce tube formation in a significant manner, reflecting the lack of direct toxicity against HECV and the minimal interference with these cells.

In summary, the modest inhibition in the tube formation ability of ECs was a direct result of the reduced VEGF expression by TNBC cells because of CORM treatments. This observation suggests a potential of these CORMs to ablate the aggressiveness of MDA-MB-231 cells by limiting their growth factor expression and therefore their chemotactic ability.

Main findings and impact:

- Some novel CORMs more cytotoxic against TNBC cells and with more favourable cytotoxicity profiles compared to parent structure confirming the design strategy.
- VEGF expression of TNBC cells significantly reduced by most of the novel CORMs, especially CORMs -Phe and -Tyr – design did not affect parent compound's activity.
- HO-1 expression reduced after CORM-Phe and CORM-Tyr treatments – difference with previous literature about upregulation of HO-1 upon CORM treatment. Novel CORMs better than parent compound.
- Reduction of pY1175 of VEGFR2 upon CORM-Tyr treatment in VEGF stimulated HUVEC, similar reduction for pSrc and pFAK, much higher reduction in pERK1/2 and pAKT – novel analogue more efficient than parent compound.
- Reduction of ERK1/2, Src, AKT and FAK activation upon treatment with CORM-Phe in VEGF stimulated HUVEC – similar activity with CORM-Tyr, failure to inhibit VEGFR2 activation. New complex better than the parent complex CORM-3.
- Conditioned media from CORMs -Phe and -Tyr treated TNBC cells stimulated less tubule formation in ECs – studies on a more aggressive EC line than previous literature, with high tube formation activity.
- No inhibition in EC tube formation after direct treatment with novel CORMs – ECs not directly affected by novel CORMs.

Chapter VI

Final Discussion

6.1 First and second generation CORMs as anti-angiogenic agents

Carbon monoxide has been studied both as a toxic agent known to provoke death, and as a therapeutic agent used in low concentrations for its beneficial contribution to many pathological conditions (Maruyama et al. 2012). CORMs have been developed as alternative sources of CO for a safer and better controlled application (Motterlini et al. 2005a). Recent studies report contradicting results about the effects of CORMs on different pathologies and they conclude that CORMs act in a tissue and cell type-specific manner, as well as depend on different factors in order to exert their therapeutic activities (Ferrando et al. 2011).

First and second generation CORMs have been developed and studied against various diseases, but this study focuses on their potential as anti-angiogenic agents in TNBC. Being a highly aggressive and metastatic breast cancer subtype, TNBC has high recurrence rates and increased mortality, therefore new more targeted therapies are urgently needed (Marmé and Schneeweiss 2015). Angiogenesis is a necessary procedure that supplies tumour cells with oxygen and nutrients needed to sustain their rapid development (Carmeliet and Jain 2011). Therapies targeting angiogenesis, which appears elevated in TNBC, are not entirely successful, since they have several side effects and limited effectiveness, especially against TNBC. The insufficient efficacy can be attributed to the escape mechanisms via alternative growth factor signalling and the developing resistance. Thus, new therapies are under investigation and combination of different agents with complementary modes of action may prove a useful therapeutic intervention (Falcon et al. 2016; Missiaen et al. 2017).

The four CORMs that were commercially available at the time of initiating this study were investigated as potential anti-angiogenic agents in TNBC. These CORMs were CORM-1, CORM-2, CORM-3 and CORM-A1. Since heavy metal-based drugs present toxicological concerns to the living organisms (Egorova and Ananikov 2017), the cytotoxicity of the four analogues was first explored. CORM-1 is a Mn-based CORM, and Mn is known as an essential and biocompatible metal (Ali et al. 2017). Moreover, CORM-2 and CORM-3 are Ru-based, and have not been reported as highly toxic against any cell type tested (Winburn et al. 2012). Finally CORM-A1 does not have a

heavy metal core, instead boron serves as the metalloid centre (Motterlini et al. 2005b).

In this study, the four CORMs were shown moderately cytotoxic against the two TNBC cell lines, MDA-MB-231 and MDA-MB-436, with CORM-2 being the most effective one. However, this complex was also toxic against the control epithelial breast cells, MCF-10A and the ECs, HECV. A more favourable profile was found for CORM-1 and CORM-3 that were more toxic against TNBC cells than against the non-tumorigenic cell lines. These results fall in line with previous studies, where CORM-2 was shown to be toxic against various cell types (Lee et al. 2014; Vítek et al. 2014). Despite of the lack of high cytotoxicity, CORM-2 and CORM-3 were shown to be moderately cytostatic against MDA-MB-231 cells. Furthermore, caspase-3 and caspase-7 levels were not significantly affected by these compounds.

Following cancer cells' preference towards a glycolytic metabolism over an oxidative phosphorylation one (Alfarouk et al. 2014), these four CORMs were tested for any ability to alter or inhibit the glycolytic metabolism of MDA-MB-231 cells. CO has been shown to affect mitochondrial function and cell metabolism in a concentration-dependent manner (Szabo 2016), therefore four different concentrations of CORMs were tested. When the treatments were injected directly onto the cells at the beginning of the experiment, a reduction in the glycolytic metabolism of these cells was found at different concentrations for each compound, with CORM-2 being the most effective one at the highest concentrations used. When Avastin® was combined with CORMs no significant enhancement was observed, but rather a loss of activity for the CORMs. Thus, CORMs can potentially interfere with the glycolytic metabolism of TNBC cells, although higher concentrations than 100μM might be more effective.

Angiogenesis is a complex procedure that is vital for the survival and growth of the tumour. It is linked to the expression of several proteins that can either sustain the pro-angiogenic signal towards the surrounding tissues, or execute the angiogenic process itself (Abhinand et al. 2016). In line with that, CORMs were tested for their effects on the expression of proteins critical for angiogenesis. First of all, the two TNBC cell lines were quantified for their VEGF expression after CORM treatments, in order to reveal any reduction in the angiogenic signal originating from the tumour. Indeed,

all CORMs were shown to decrease the expressed and excreted VEGF from both MDA-MB-231 and MDA-MB-436, although more consistent results were reported for the first cell line. This result contradicted previous literature that suggested an increase in VEGF expression in different cell types upon treatment with CORMs and suggested the potential interference of other pro-angiogenic growth factors (Jözkowicz et al. 2003; Li Volti et al. 2005; Choi et al. 2010; Wilson et al. 2017).

The successful pro-angiogenic signal transduction within the ECs that are going to execute angiogenesis, involves the phosphorylation and activation of subsequent proteins, starting from the surface receptor VEGFR2 and following its complex downstream pathway. One important phosphorylation site on VEGFR2 is the tyrosine residue Y1175, but each site is linked to several functions (Lamalice et al. 2007). Taking this into consideration, the four CORMs were studied for their ability to interfere with the activation of the VEGFR2 signal pathway in a primary EC line, HUVEC, and upon VEGF stimulation. The obtained results suggested that CORM-2 inhibited the VEGF-induced phosphorylation on Y1175 of VEGFR2, whereas CORM-3 was more successful in reducing the activation of ERK1/2 proteins. In fact, CORM-2 was effective against all proteins tested, correlating well with previous literature (Ahmad et al. 2015), which pointed towards a different mechanism of action for CORM-2 and CORM-3. The inherent toxicity of CORM-2 against ECs might have also been a reason why this complex was more successful, whereas CORM-3 was shown to preferentially inhibit ERK proteins and maybe AKT, as well. In any case, both compounds seem to have anti-angiogenic potential and as suggested by other researchers, the combination of agents that can reduce the expression of angiogenic factors with ones that target these factors and their signalling pathways might provide future therapeutic regimens for TNBC (Wang et al. 2015).

Another important protein linked to CO and CORMs is HO-1. HO-1 is responsible for the endogenous production of CO and is also involved in the cytoprotective mechanisms against oxidative stress (Dulak et al. 2008). Since suppression of HO-1 could impair the proliferation of cancer cells (Li et al. 2011), CORMs were also studied for their effects on HO-1 expression in TNBC cells. It was shown that CORMs downregulated HO-1 expression in MDA-MB-231, with CORM-1 and CORM-2 being

the most effective ones, although CORM-A1 showed a completely opposite effect. This might have been a consequence of the non-transition metal core of CORM-A1 but the result pointed towards a reduced protection for TNBC cells after transition metal CORM treatments.

The angiogenic process depends highly on the ability of ECs to migrate to distant areas, and there are many therapeutic agents that block this function (Missiaen et al. 2017; Potente and Carmeliet 2017). The four available CORMs were tested for any inhibitory activity against the migration of HECV cells, and three of them were found to inhibit this process at a significant level. The only unsuccessful CORM was CORM-A1, again showing a different behaviour than the other complexes. When TNBC cells were tested in the same experimental set up, in the scope of the high metastatic nature of MDA-MB-231 cells, they were found not affected by CORMs, so probably there would be minor interference with the ability of these cells to induce metastasis.

The final angiogenesis-related investigation involved the ability of ECs to form tube-like structures upon treatment with conditioned media from CORM-treated TNBC cells (Menyhárt et al. 2016). As VEGF is the main angiogenic stimulant that initiates vessel formation, the VEGF reducing activity of CORMs in TNBC cells might be translated into a decreased stimulation for ECs. Indeed, both CORM-2 and CORM-3 limited the tube-formation activity of HECV cells, even though the reduction was not of the same level as the reduction in VEGF expression from cancer cells. This was an expected result, as VEGF is not the only pro-angiogenic stimulant and HECV cells are more aggressive than other similar EC lines expressing many growth factors (Puddu et al. 2016). In a similar experiment, the ability of direct treatments of CORMs to inhibit tube formation in ECs was assessed, and it was revealed that only CORM-2 interfered with these cells directly, reflecting the previous results about the inhibition in activation of the VEGFR2 pathway in ECs upon VEGF stimulation. This meant that CORM-2 affected the ECs *per se*, whereas CORM-3 probably interfered with the VEGF expression mechanism in TNBC cells and directly inhibited only the ERK phosphorylation and activation in ECs.

In summary, there are clear indications of anti-angiogenic activity for CORM-2 and CORM-3, which appear to have a different but similar mechanism of action.

6.2 Design and synthesis of new analogues

Based on the obtained data, CORM-3 was chosen as the lead compound for structural modifications. This decision was based on several favourable characteristics, such as water solubility and good inhibiting activity on the VEGF expression from TNBC cells, the activation of downstream proteins of VEGFR2 and the migration of ECs. It was also based on several limitations of the other complex with good results, CORM-2, such as being water insoluble, toxic against breast epithelial cells and a Ru-based dimer that could not be easily modified without affecting the general structure. Hence, a set of 15 new analogues based on CORM-3 were designed and synthesized, and most of them were novel structures not reported before in literature.

These complexes explored different strategies for the substitution of the glycine moiety of CORM-3, such as amino acids with various lipophilicity features, addition of nitro and amino groups and ligation with an additional pro-oxidant substituent. Even though the purification of the synthesized products proved challenging, the crudes used were very close to purity and higher polymeric structures might explain the abnormalities shown in the NMR spectra, instead of the existence of impurities.

All the new molecules were isolated as white to yellow powders, kept in tightly sealed vials in the dark at -20^{o}C and used fresh on the day of the experiments. Only CORM-Ser appeared to be heavily affected by light and humidity, as from yellow powder it transformed to a dark yellow waxy solid, probably owing to its free hydroxyl group that can be easily oxidized by the atmospheric oxygen.

6.3 Third generation CORMs as anti-angiogenic agents

The 15 new analogues were first subjected to cell viability tests, in order to determine their toxicity against the cell lines used in this study. The results showed a better cytotoxicity profile for the new CORMs, especially for CORM-Ala, CORM-His and CORM-MK4a, which pointed towards a favourable selectivity profile. The other analogues correlated well with the designing strategies, and molecules that were expected to be more toxic had indeed lower IC_{50} values.

In line with previous experiments, the new CORMs were tested for their ability to reduce VEGF expression in MDA-MB-231 cells. In fact, all new CORMs showed very promising results, and the decrease of the excreted VEGF reached a high point of 65%.

Based on the data, only two CORMs were chosen for further studies, that is CORM-Phe and CORM-Tyr. This was inevitable due to time restrictions for this study, and the choice of the two analogues derived from their ability to reduce VEGF expression in TNBC cells more effectively than the other analogues.

Another effect of the two chosen analogues on MDA-MB-231 cells was that they were both proven to lower the expression of the cytoprotective HO-1 enzyme in these TNBC cells, possibly interfering with their defence mechanisms against oxidative stress and excess ROS production.

Taking into consideration that angiogenesis involves the successful signal transduction from VEGFR2 on the surface of ECs towards the cell nucleus, the two chosen CORMs were investigated for their ability to interfere with the VEGFR2 pathway in HUVEC upon VEGF stimulation. The data showed that both CORMs inhibited the activation of ERK1/2, Src, AKT and FAK proteins at some level. In fact, CORM-Tyr was the most effective, especially against ERK1/2 and AKT phosphorylation. It was also the most successful of the two in reducing the activation of Y1175 of VEGFR2 upon stimulation with VEGF.

Finally, the new CORMs were tested for their ability to reduce the tube-formation activity of HECV cells, as an *in vitro* model imitating the process of angiogenesis *in vivo*. Conditioned media from CORM-treated TNBC cells was used to stimulate tube formation in ECs and both CORMs had a modest inhibitory effect, with CORM-Tyr showing a higher reduction when 6h and 24h conditioned media was used. Nevertheless, both CORMs showed similar results that pointed towards anti-angiogenic ability. None of them had a direct effect on the ECs *per se*, meaning that the reduction in VEGF from TNBC cells was probably the reason for the decreased tube formation observed in the treated ECs.

In summary, there are several features of the new analogues which are favourable for an anti-angiogenic behaviour, and the two chosen CORMs were shown to be effective in limiting certain events crucial for a successful angiogenic process.

6.4 Comparison between old and new analogues and selection of the final lead compound

Four commercially available CORMs were chosen to be investigated in this study, for their potential as anti-angiogenic agents. Based on the obtained data and other important characteristics, one of them was chosen for further modification; hence 15 new CORMs were successfully designed and synthesized. The new complexes were subjected to *in vitro* evaluation and a comparison made between the old and the new molecules.

Three of the newly synthesized CORMs showed a more favourable cytotoxicity profile than the parent compound, CORM-3, and the more toxic CORM-2. CORM-Ala, CORM-His and CORM-MK4a were all more effective in reducing the viability of TNBC cells than the other non-tumorigenic cell lines. This selectivity was not observed for the other more toxic analogues, such as CORM-Nitro-Tyr and CORM-Cyclopent, but CORM-Cyclopent was more cytotoxic than CORM-2 against MDA-MB-231 cells and less toxic against MCF-10A.

The new CORMs were similarly able to reduce the VEGF expression in TNBC cells when compared with CORM-2 and CORM-3. No major enhancement was observed, but all new analogues retained this activity, which means that the substitution of the glycine moiety of the parent CORM with other amino acids did not impair the ability of the new CORMs to interfere with the VEGF expression mechanism in MDA-MB-231 cells. This is an indication that the common characteristic between all these CORMs – the released CO – might be responsible for the reduction of this growth factor. Otherwise, the change in the conformation of the complex by substituting a specific ligand would have severe impact on the activity of the whole molecule.

In line with this observation, the two new CORMs, CORM-Phe and CORM-Tyr, had the same downregulating activity over HO-1 expression as the parent compound CORM-

3, CORM-2 and CORM-1. This might be an indication that this downregulation in both VEGF and HO-1 expression is a result of the CO released and not of the whole molecule. The Ru core, which is also a common characteristic between CORM-2, CORM-3, CORM-Phe and CORM-Tyr might also play a role in the observed effects, especially for the downregulation of VEGF, since the new analogues are slightly more active than CORM-1.

As for the ability to inhibit the activation of the VEGFR2 pathway, CORM-Phe and CORM-Tyr were far more successful than CORM-3 in halting the phosphorylation of VEGFR2 in Y1175 upon VEGF stimulation. However, none of them was better than CORM-2, which managed to return the phosphorylation levels to baseline. Similarly for the rest of the pathway proteins tested, the new CORMs were more effective than CORM-3 in all cases, and especially for ERK1/2 and Src, they managed to decrease the activation even more than CORM-2, reaching significance for the ERK1/2 data.

Finally, when conditioned media from CORM-treated TNBC cells was used to stimulate tube formation in ECs, CORM-Tyr managed to reduce the tubes by 40% at 6h treatment, whereas CORM-2 and CORM-3 reached 30% and 20% reduction, respectively. Even though CORM-Phe was less successful in decreasing the length of the tubes formed, both new analogues showed a consistent inhibition. Only CORM-2 was shown to affect ECs directly, whereas the activities of the other molecules were merely attributed to their ability to reduce VEGF expression from cancer cells.

All in all, it seems that CORM-2 is the best analogue of the original series, but its activities might also be related to its inherent toxicity against ECs and its higher toxicity against MDA-MB-231 cells compared to CORM-3. On the other hand, CORM-Phe and CORM-Tyr have lower toxicities that would be quite improbable to affect the observed abilities, pointing towards a mechanism of action targeting VEGF expression in TNBC cells and the activation of ERK1/2 proteins in ECs. As they are both better than CORM-3 in most of the experiments conducted, it seems that the new amino acid substituents are more suitable in reaching their cellular targets due to different lipophilicity or because they force the complex to a different conformation in space. In any case, CORM-Tyr showed an enhanced activity over the parent compound CORM-3, but they both share a similar mechanism of action slightly different to the

one of CORM-2. Therefore, the observed abilities cannot be solely attributed to the released CO, otherwise a very similar effect would have been reported for all tested CORMs. The Ru core might also play an important role in these results, as well as the possible higher polymeric formation of CORM-Tyr compared to the dimer CORM-2. Hence, CORM-2 can be suggested for a more holistic approach against angiogenesis, due to its interference with several steps of the process, whereas CORM-Tyr could be explored as a more targeted CORM against specific proteins.

6.5 Future work

In the present study commercially available and newly synthesized CORMs were assessed for their effects on different cell function and for their anti-angiogenic potential. Since it was shown that they interfere with the molecular mechanisms executing angiogenesis, it would be interesting to investigate their exact mechanism of action. CORM-2 seemed to have a slightly different behaviour than CORM-3 and its analogues, hence both cases would have to be explored and any different targets identified and characterized. The clear indication of interference of CORM-2 with ECs was not shared by CORM-3 or its analogues, so different targets could be expected for these cases.

Another important aspect of this study would be to examine the ability of newly synthesized CORMs to induce ROS production in TNBC cells and maybe correlate this activity with the mechanism of action for each complex. In any case, more pro-oxidant CORMs should be synthesized in order to get a clear indication of ROS participation in the observed effects.

Other EC lines could also be tested against these CORMs, since it was shown that even though HECV and HUVEC are both ECs, they respond diversely to CORM treatments, hence they have distinctive characteristics that are differently affected by CORMs. It would be useful to show these differences discussed earlier in this study and their impact on the *in vitro* and *in vivo* anti-angiogenic activities of these complexes.

Finally, another interesting exploration would involve the combination of the lead CORMs with other chemotherapeutic or anti-angiogenic agents, for example Avastin® as suggested by the title of this study. Depending on the accompanying agent, the

combination might present higher cytotoxic or anti-angiogenic efficiency against TNBC and help with the reduction of the recommended dose for the combined agent, as well. For example, it is known that Avastin® provokes serious side-effects which would be reduced or avoided if the necessary therapeutic dose could be lowered. A combination of drugs that leads to synergy is particularly welcome when it comes to anticancer therapies, since anticancer drugs have severe and frequent adverse effects that derive from the high doses recommended for the desired activity.

List of References

Abhinand, C. S. et al. 2016. VEGF-A/VEGFR2 signaling network in endothelial cells relevant to angiogenesis. *Journal of Cell Communication and Signaling* 10(4), pp. 347-354. doi: 10.1007/s12079-016-0352-8

Adeyinka, A. et al. 2002. Analysis of gene expression in ductal carcinoma in situ of the breast. *Clinical Cancer Research* 8(12), pp. 3788-3795.

Ahmad, S. and Ahmed, A. 2004. Elevated placental soluble vascular endothelial growth factor receptor-1 inhibits angiogenesis in preeclampsia. *Circulation Research* 95(9), pp. 884-891. doi: 10.1161/01.RES.0000147365.86159.f5

Ahmad, S. et al. 2015. Carbon monoxide inhibits sprouting angiogenesis and vascular endothelial growth factor receptor-2 phosphorylation. *Thrombosis and Haemostasis* 113(2), pp. 329-337. doi: 10.1160/TH14-01-0002

Ahmad, S. et al. 2006. Direct evidence for endothelial vascular endothelial growth factor receptor-1 function in nitric oxide-mediated angiogenesis. *Circulation Research* 99(7), pp. 715-722. doi: 10.1161/01.RES.0000243989.46006.b9

Akeson, A. et al. 2010. Endothelial cell activation in a VEGF-A gradient: Relevance to cell fate decisions. *Microvascular Research* 80(1), pp. 65-74. doi: 10.1016/j.mvr.2010.02.001

Al-Ani, B. et al. 2010. Activation of proteinase-activated receptor 2 stimulates soluble vascular endothelial growth factor receptor 1 release via epidermal growth factor receptor transactivation in endothelial cells. *Hypertension* 55(3), pp. 689-697. doi: 10.1161/HYPERTENSIONAHA.109.136333

Alessio, E. 2017. Thirty Years of the Drug Candidate NAMI-A and the Myths in the Field of Ruthenium Anticancer Compounds: A Personal Perspective. *European Journal of Inorganic Chemistry* 2017(12), pp. 1549-1560. doi: 10.1002/ejic.201600986

Alfarouk, K. O. 2016. Tumor metabolism, cancer cell transporters, and microenvironmental resistance. *Journal of Enzyme Inhibition and Medicinal Chemistry* 31(6), pp. 859-866. doi: 10.3109/14756366.2016.1140753

Alfarouk, K. O. et al. 2014. Glycolysis, tumor metabolism, cancer growth and dissemination. A new pH-based etiopathogenic perspective and therapeutic approach to an old cancer question. *Oncoscience* 1(12), pp. 777-802. doi: 10.18632/oncoscience.109

Ali, B. et al. 2017. Techniques in the synthesis of mononuclear manganese complexes: A review. *Reviews in Inorganic Chemistry* 37(3-4), pp. 105-130. doi: 10.1515/revic-2017-0004

Allardyce, C. S. and Dyson, P. J. 2016. Metal-based drugs that break the rules. *Dalton Transactions* 45(8), pp. 3201-3209. doi: 10.1039/c5dt03919c

Allred, D. C. et al. 2001. Histological and biological evolution of human premalignant breast disease. *Endocrine-Related Cancer* 8(1), pp. 47-61. doi: 10.1677/erc.0.0080047

Almeida, A. S. et al. 2012. Carbon monoxide modulates apoptosis by reinforcing oxidative metabolism in astrocytes: Role of Bcl-2. *Journal of Biological Chemistry* 287(14), pp. 10761-10770. doi: 10.1074/jbc.M111.306738

Almeida, A. S. et al. 2016. Carbon monoxide improves neuronal differentiation and yield by increasing the functioning and number of mitochondria. *Journal of Neurochemistry*, pp. 423-435. doi: 10.1111/jnc.13653

Alonso, J. R. et al. 2003. Carbon monoxide specifically inhibits cytochrome C oxidase of human mitochondrial respiratory chain. *Pharmacology and Toxicology* 93(3), pp. 142-146. doi: 10.1034/j.1600-0773.2003.930306.x

Anand, P. et al. 2008. Cancer is a preventable disease that requires major lifestyle changes. *Pharmaceutical Research* 25(9), pp. 2097-2116. doi: 10.1007/s11095-008-9661-9

Andreopoulou, E. et al. 2015. Therapies for triple negative breast cancer. *Expert Opinion on Pharmacotherapy* 16(7), pp. 983-998. doi: 10.1517/14656566.2015.1032246

André, L. et al. 2011. Carbon monoxide exposure enhances arrhythmia after cardiac stress: Involvement of oxidative stress. *Basic Research in Cardiology* 106(6), pp. 1235-1246. doi: 10.1007/s00395-011-0211-y

Anisimov, V. N. 2007. Biology of aging and cancer. *Cancer Control* 14(1), pp. 23-31. doi: 10.1177/107327480701400104

Arsenyan, P. et al. 2014. Selenium analogues of raloxifene as promising antiproliferative agents in treatment of breast cancer. *European Journal of Medicinal Chemistry* 87, pp. 471-483. doi: 10.1016/j.ejmech.2014.09.088

Aucott, B. J. et al. 2017. Redox-Tagged Carbon Monoxide-Releasing Molecules (CORMs): Ferrocene-Containing [Mn(C^N)(CO)4] Complexes as a Promising New CORM Class. *Inorganic Chemistry* 56(9), pp. 5431-5440. doi: 10.1021/acs.inorgchem.7b00509

Bannenberg, G. L. and Vieira, H. L. A. 2009. Therapeutic applications of the gaseous mediators carbon monoxide and hydrogen sulfide. *Expert Opinion on Therapeutic Patents* 19(5), pp. 663-682. doi: 10.1517/13543770902858824

Basu, B. et al. 2015. First-in-human pharmacokinetic and pharmacodynamic study of the dual m-TORC 1/2 inhibitor AZD2014. *Clinical Cancer Research* 21(15), pp. 3412-3419. doi: 10.1158/1078-0432.CCR-14-2422

Berberat, P. O. et al. 2005. Inhibition of heme oxygenase-1 increases responsiveness of pancreatic cancer cells to anticancer treatment. *Clinical Cancer Research* 11(10), pp. 3790-3798. doi: 10.1158/1078-0432.CCR-04-2159

Berlinguet, L. et al. 1962a. Autoradiographic studies of the distribution of 1-aminocyclopentane carboxylic acid in normal and cancerous mice. *Canadian journal of biochemistry and physiology* 40, pp. 1111-1114.

Berlinguet, L. et al. 1962b. Biochemical studies of an unnatural and antitumor amino acid: 1-aminocyclopentanecarboxylic acid. I. Toxicity and tissue distribution. *Canadian journal of biochemistry and physiology* 40, pp. 425-432.

Berridge, M. V. et al. 2005. Tetrazolium dyes as tools in cell biology: New insights into their cellular reduction. *Biotechnology Annual Review*.

Berridge, M. V. and Tan, A. S. 1993. Characterization of the Cellular Reduction of 3-(4,5-dimethylthiazol-2- yl)-2,5-diphenyltetrazolium bromide (MTT): Subcellular Localization, Substrate Dependence, and Involvement of Mitochondrial Electron Transport in MTT Reduction. *Archives of Biochemistry and Biophysics* 303(2), pp. 474-482. doi: 10.1006/abbi.1993.1311

Bertucci, F. et al. 2008. How basal are triple-negative breast cancers? *International Journal of Cancer* 123(1), pp. 236-240. doi: 10.1002/ijc.23518

Bilban, M. et al. 2008. Heme oxygenase and carbon monoxide initiate homeostatic signaling. *Journal of Molecular Medicine* 86(3), pp. 267-279. doi: 10.1007/s00109-007-0276-0

Bishayee, A. and Darvesh, A. S. 2012. Angiogenesis in hepatocellular carcinoma: A potential target for chemoprevention and therapy. *Current Cancer Drug Targets* 12(9), pp. 1095-1118.

Bodner-Adler, B. et al. 2016. The role of fibroblast growth factor 2 in patients with uterine smooth muscle tumors: an immunohistochemical study. *European Journal of*

Obstetrics Gynecology and Reproductive Biology 207, pp. 62-67. doi: 10.1016/j.ejogrb.2016.10.028

Bousquet, G. et al. 2017. Targeting autophagic cancer stem-cells to reverse chemoresistance in human triple negative breast cancer. *Oncotarget* 8(21), pp. 35205-35221. doi: 10.18632/oncotarget.16925

Bouïs, D. et al. 2001. Endothelium in vitro: A review of human vascular endothelial cell lines for blood vessel-related research. *Angiogenesis* 4(2), pp. 91-102. doi: 10.1023/A:1012259529167

Brouard, S. et al. 2000. Carbon monoxide generated by heme oxygenase 1 suppresses endothelial cell apoptosis. *Journal of Experimental Medicine* 192(7), pp. 1015-1025. doi: 10.1084/jem.192.7.1015

Browne, G. et al. 2016. MicroRNA-378-mediated suppression of Runx1 alleviates the aggressive phenotype of triple-negative MDA-MB-231 human breast cancer cells. *Tumor Biology* 37(7), pp. 8825-8839. doi: 10.1007/s13277-015-4710-6

Bruce, D. and Tan, P. H. 2011. Vascular endothelial growth factor receptors and the therapeutic targeting of angiogenesis in cancer: Where do we go from here? *Cell Communication and Adhesion* 18(5), pp. 85-103. doi: 10.3109/15419061.2011.619673

Bussolati, B. et al. 2001. Vascular endothelial growth factor receptor-1 modulates vascular endothelial growth factor-mediated angiogenesis via nitric oxide. *American Journal of Pathology* 159(3), pp. 993-1008. doi: 10.1016/S0002-9440(10)61775-0

Cai, J. et al. 2003. Activation of Vascular Endothelial Growth Factor Receptor-1 Sustains Angiogenesis and Bcl-2 Expression Via the Phosphatidylinositol 3-Kinase Pathway in Endothelial Cells. *Diabetes* 52(12), pp. 2959-2968. doi: 10.2337/diabetes.52.12.2959

Cai, Y. et al. 2016. Construction of a disulfide-stabilized diabody against fibroblast growth factor-2 and the inhibition activity in targeting breast cancer. *Cancer Science* 107(8), pp. 1141-1150. doi: 10.1111/cas.12981

Carmeliet, P. and Jain, R. K. 2011. Molecular mechanisms and clinical applications of angiogenesis. *Nature* 473(7347), pp. 298-307. doi: 10.1038/nature10144

Chakraborty, I. et al. 2015. Rapid Eradication of Human Breast Cancer Cells through Trackable Light-Triggered CO Delivery by Mesoporous Silica Nanoparticles Packed with a Designed photoCORM. *Chemistry of Materials* 27(24), pp. 8387-8397. doi: 10.1021/acs.chemmater.5b03859

Chakraborty, I. et al. 2014. Design strategies to improve the sensitivity of photoactive metal carbonyl complexes (photoCORMs) to visible light and their potential as CO-donors to biological targets. *Accounts of Chemical Research* 47(8), pp. 2603-2611. doi: 10.1021/ar500172f

Chatterjee, P. K. 2007. Physiological activities of carbon monoxide-releasing molecules: Ça ira. *British Journal of Pharmacology* 150(8), pp. 961-962. doi: 10.1038/sj.bjp.0707185

Chau, L. Y. 2015. Heme oxygenase-1: Emerging target of cancer therapy. *Journal of Biomedical Science* 22(1), doi: 10.1186/s12929-015-0128-0

Chaves-Ferreira, M. et al. 2015. Spontaneous CO release from RuII(CO)2-protein complexes in aqueous solution, cells, and mice. *Angewandte Chemie - International Edition* 54(4), pp. 1172-1175. doi: 10.1002/anie.201409344

Chigaev, A. et al. 2014. Carbon monoxide down-regulates α4β1 integrin-specific ligand binding and cell adhesion: A possible mechanism for cell mobilization. *BMC Immunology* 15(1), doi: 10.1186/s12865-014-0052-1

Chin, B. Y. et al. 2007. Hypoxia-inducible factor 1α stabilization by carbon monoxide results in cytoprotective preconditioning. *Proceedings of the National Academy of Sciences of the United States of America* 104(12), pp. 5109-5114. doi: 10.1073/pnas.0609611104

Choi, Y. K. et al. 2010. Carbon monoxide promotes VEGF expression by increasing HIF-1α protein level via two distinct mechanisms, translational activation and stabilization of HIF-1α protein. *Journal of Biological Chemistry* 285(42), pp. 32116-32125. doi: 10.1074/jbc.M110.131284

Clark, J. E. et al. 2003. Cardioprotective actions by a water-soluble carbon monoxide-releasing molecule. *Circulation research* 93(2), pp. e2-8.

Clarke, P. and Tyler, K. L. 2009. Apoptosis in animal models of virus-induced disease. *Nature Reviews Microbiology* 7(2), pp. 144-155. doi: 10.1038/nrmicro2071

Cloughesy, T. F. et al. 2008. Antitumor activity of rapamycin in a phase I trial for patients with recurrent PTEN-deficient glioblastoma. *PLoS Medicine* 5(1), pp. 0139-0151. doi: 10.1371/journal.pmed.0050008

Connors, T. A. et al. 1960. The pharmacology and tumour growth inhibitory activity of 1-aminocyclopentane-1-carboxylic acid and related compounds. *Biochemical Pharmacology* 5(1-2), pp. 108-129. doi: 10.1016/0006-2952(60)90014-9

Connors, T. A. and Ross, W. C. J. 1960. 428. Some derivatives of 1-aminocyclopentanecarboxylic acid and related compounds. *Journal of the Chemical Society (Resumed)*, pp. 2119-2132.

Creedon, H. et al. 2014. Exploring mechanisms of acquired resistance to HER2 (human epidermal growth factor receptor 2)-targeted therapies in breast cancer. *Biochemical Society Transactions* 42(4), pp. 822-830. doi: 10.1042/BST20140109

Cudmore, M. et al. 2007. Negative regulation of soluble Flt-1 and soluble endoglin release by heme oxygenase-1. *Circulation* 115(13), pp. 1789-1797. doi: 10.1161/CIRCULATIONAHA.106.660134

Cudmore, M. J. et al. 2012. The role of heterodimerization between VEGFR-1 and VEGFR-2 in the regulation of endothelial cell homeostasis. *Nature Communications* 3, doi: 10.1038/ncomms1977

D'Amico, G. et al. 2006. Inhibition of cellular respiration by endogenously produced carbon monoxide. *Journal of Cell Science* 119(11), pp. 2291-2298. doi: 10.1242/jcs.02914

Davidge, K. S. et al. 2009. Carbon monoxide-releasing antibacterial molecules target respiration and global transcriptional regulators. *Journal of Biological Chemistry* 284(7), pp. 4516-4524. doi: 10.1074/jbc.M808210200

Dent, R. et al. 2007. Triple-negative breast cancer: Clinical features and patterns of recurrence. *Clinical Cancer Research* 13(15), pp. 4429-4434. doi: 10.1158/1078-0432.CCR-06-3045

Desmard, M. et al. 2009. A carbon monoxide-releasing molecule (CORM-3) exerts bactericidal activity against Pseudomonas aeruginosa and improves survival in an animal model of bacteraemia. *FASEB Journal* 23(4), pp. 1023-1031. doi: 10.1096/fj.08-122804

Dulak, J. et al. 2008. Heme oxygenase-1 and carbon monoxide in vascular pathobiology: Focus on angiogenesis. *Circulation* 117(2), pp. 231-241. doi: 10.1161/CIRCULATIONAHA.107.698316

Dushyanthen, S. et al. 2017. Agonist immunotherapy restores T cell function following MEK inhibition improving efficacy in breast cancer. *Nature Communications* 8(1), doi: 10.1038/s41467-017-00728-9

Dördelmann, G. et al. 2012. CuAAC click functionalization of azide-modified nanodiamond with a photoactivatable CO-releasing molecule (PhotoCORM) based on [Mn(CO) 3(tpm)]+. *Chemical Communications* 48(94), pp. 11528-11530. doi: 10.1039/c2cc36491c

Ebos, J. M. L. et al. 2009a. Accelerated Metastasis after Short-Term Treatment with a Potent Inhibitor of Tumor Angiogenesis. *Cancer Cell* 15(3), pp. 232-239. doi: 10.1016/j.ccr.2009.01.021

Ebos, J. M. L. et al. 2009b. Tumor and host-mediated pathways of resistance and disease progression in response to antiangiogenic therapy. *Clinical Cancer Research* 15(16), pp. 5020-5025. doi: 10.1158/1078-0432.CCR-09-0095

Egorova, K. S. and Ananikov, V. P. 2017. Toxicity of Metal Compounds: Knowledge and Myths. *Organometallics* 36(21), pp. 4071-4090. doi: 10.1021/acs.organomet.7b00605

Falcon, B. L. et al. 2016. Antagonist antibodies to vascular endothelial growth factor receptor 2 (VEGFR-2) as anti-angiogenic agents. *Pharmacology and Therapeutics* 164, pp. 204-225. doi: 10.1016/j.pharmthera.2016.06.001

Fallahpour, S. et al. 2017. Breast cancer survival by molecular subtype: a population-based analysis of cancer registry data. *CMAJ open* 5(3), pp. E734-E739. doi: 10.9778/cmajo.20170030

Ferrando, M. et al. 2011. Heme oxygenase 1 (HO-1) challenges the angiogenic switch in prostate cancer. *Angiogenesis* 14(4), pp. 467-479. doi: 10.1007/s10456-011-9230-4

Ferrara, N. et al. 2003. The biology of VEGF and its receptors. *Nature Medicine* 9(6), pp. 669-676. doi: 10.1038/nm0603-669

Foresti, R. et al. 2008. Use of carbon monoxide as a therapeutic agent: Promises and challenges. *Intensive Care Medicine* 34(4), pp. 649-658. doi: 10.1007/s00134-008-1011-1

Foresti, R. et al. 2004. Vasoactive properties of CORM-3, a novel water-soluble carbon monoxide-releasing molecule. *British Journal of Pharmacology* 142(3), pp. 453-460. doi: 10.1038/sj.bjp.0705825

Fosu-Mensah, N. et al. 2015. Advances in small-molecule drug discovery for triple-negative breast cancer. *Future Medicinal Chemistry* 7(15), pp. 2019-2039. doi: 10.4155/fmc.15.129

Fouqué, A. et al. 2015. A Novel Covalent mTOR Inhibitor, DHM25, Shows in Vivo Antitumor Activity against Triple-Negative Breast Cancer Cells. *Journal of Medicinal Chemistry* 58(16), pp. 6559-6573. doi: 10.1021/acs.jmedchem.5b00991

Fouqué, A. et al. 2016. Review of PI3K/mTOR inhibitors entering clinical trials to treat triple negative breast cancers. *Recent Patents on Anti-Cancer Drug Discovery* 11(3), pp. 283-296. doi: 10.2174/1574892811666160519113731

Gacche, R. N. and Meshram, R. J. 2014. Angiogenic factors as potential drug target: Efficacy and limitations of anti-angiogenic therapy. *Biochimica et Biophysica Acta - Reviews on Cancer* 1846(1), pp. 161-179. doi: 10.1016/j.bbcan.2014.05.002

Ganot, N. et al. 2013. Anticancer metal complexes: synthesis and cytotoxicity evaluation by the MTT assay. *Journal of visualized experiments : JoVE* (81),

García-Gallego, S. and Bernardes, G. J. L. 2014. Carbon-monoxide-releasing molecules for the delivery of therapeutic co in vivo. *Angewandte Chemie - International Edition* 53(37), pp. 9712-9721. doi: 10.1002/anie.201311225

Gasser, G. et al. 2011. Organometallic anticancer compounds. *Journal of Medicinal Chemistry* 54(1), pp. 3-25. doi: 10.1021/jm100020w

Gatenby, R. A. and Gillies, R. J. 2004. Why do cancers have high aerobic glycolysis? *Nature Reviews Cancer* 4(11), pp. 891-899. doi: 10.1038/nrc1478

Gessner, G. et al. 2017. CO-independent modification of K+ channels by tricarbonyldichlororuthenium(II) dimer (CORM-2). *European Journal of Pharmacology* 815, pp. 33-41. doi: 10.1016/j.ejphar.2017.10.006

Goldberg, M. A. and Schneider, T. J. 1994. Similarities between the oxygen-sensing mechanisms regulating the expression of vascular endothelial growth factor and erythropoietin. *Journal of Biological Chemistry* 269(6), pp. 4355-4359.

Gorrini, C. et al. 2013. Modulation of oxidative stress as an anticancer strategy. *Nature Reviews Drug Discovery* 12(12), pp. 931-947. doi: 10.1038/nrd4002

Govender, P. et al. 2013. Next generation photoCORMs: Polynuclear tricarbonylmanganese(I)- functionalized polypyridyl metallodendrimers. *Inorganic Chemistry* 52(9), pp. 5470-5478. doi: 10.1021/ic400377k

Guarneri, V. et al. 2013. Relapsed triple-negative breast cancer: Challenges and treatment strategies. *Drugs* 73(12), pp. 1257-1265. doi: 10.1007/s40265-013-0091-6

Gucalp, A. et al. 2013. Phase II trial of bicalutamide in patients with androgen receptor-positive, estrogen receptor-negative metastatic breast cancer. *Clinical Cancer Research* 19(19), pp. 5505-5512. doi: 10.1158/1078-0432.CCR-12-3327

Gullotta, F. et al. 2012. Carbon monoxide: An unusual drug. *IUBMB Life* 64(5), pp. 378-386. doi: 10.1002/iub.1015

Guo, Y. et al. 2004. Administration of a CO-releasing molecule at the time of reperfusion reduces infarct size in vivo. *American Journal of Physiology - Heart and Circulatory Physiology* 286(5 55-5), pp. H1649-H1653. doi: 10.1152/ajpheart.00971.2003

Hall, A. G. and Tilby, M. J. 1992. Mechanisms of action of, and modes of resistance to, alkylating agents used in the treatment of haematological malignancies. *Blood Reviews* 6(3), pp. 163-173. doi: 10.1016/0268-960X(92)90028-O

Hanahan, D. and Weinberg, R. A. 2011. Hallmarks of cancer: The next generation. *Cell* 144(5), pp. 646-674. doi: 10.1016/j.cell.2011.02.013

Hayes, R. L. et al. 1976. Carboxyl labeled 11C 1 aminocyclopentanecarboxylic acid, a potential agent for cancer detection. *Journal of Nuclear Medicine* 17(8), pp. 748-751.

Hillen, F. and Griffioen, A. W. 2007. Tumour vascularization: Sprouting angiogenesis and beyond. *Cancer and Metastasis Reviews* 26(3-4), pp. 489-502. doi: 10.1007/s10555-007-9094-7

Hornig, C. et al. 2000. Release and complex formation of soluble VEGFR-1 from endothelial cells and biological fluids. *Laboratory Investigation* 80(4), pp. 443-454. doi: 10.1038/labinvest.3780050

Jang, M. et al. 2007. Caspase-7 mediated cleavage of proteasome subunits during apoptosis. *Biochemical and Biophysical Research Communications* 363(2), pp. 388-394. doi: 10.1016/j.bbrc.2007.08.183

Jansson, S. et al. 2014. The three receptor tyrosine kinases c-KIT, VEGFR2 and PDGFRα, closely spaced at 4q12, show increased protein expression in triple-negative breast cancer. *PLoS ONE* 9(7), doi: 10.1371/journal.pone.0102176

Jemal, A. et al. 2010. Cancer statistics, 2010. *CA Cancer Journal for Clinicians* 60(5), pp. 277-300. doi: 10.3322/caac.20073

Jitawatanarat, P. and Ma, W. W. 2013. Update on antiangiogenic therapy in colorectal cancer: Aflibercept and regorafenib. *Journal of Gastrointestinal Oncology* 4(2), pp. 231-238. doi: 10.3978/j.issn.2078-6891.2013.008

Johnson, T. R. et al. 2007. Metal carbonyls as pharmaceuticals? [Ru(CO)3Cl(glycinate)], a CO-releasing molecule with an extensive aqueous solution chemistry. *Dalton Transactions* (15), pp. 1500-1508. doi: 10.1039/b613629j

Johnston, S. R. D. 2010. New strategies in estrogen receptor-positive breast cancer. *Clinical Cancer Research* 16(7), pp. 1979-1987. doi: 10.1158/1078-0432.CCR-09-1823

Jözkowicz, A. et al. 2003. Heme oxygenase and angiogenic activity of endothelial cells: Stimulation by carbon monoxide and inhibition by tin protoporphyrin-IX. *Antioxidants and Redox Signaling* 5(2), pp. 155-162.

Kaczara, P. et al. 2015. Carbon monoxide released by CORM-401 uncouples mitochondrial respiration and inhibits glycolysis in endothelial cells: A role for mitoBK<inf>Ca</inf> channels. *Biochimica et Biophysica Acta - Bioenergetics* 1847(10), pp. 1297-1309. doi: 10.1016/j.bbabio.2015.07.004

Kalimutho, M. et al. 2015. Targeted Therapies for Triple-Negative Breast Cancer: Combating a Stubborn Disease. *Trends in Pharmacological Sciences* 36(12), pp. 822-846. doi: 10.1016/j.tips.2015.08.009

Kaufmann, M. et al. 2013. Breakthroughs in research and treatment of early breast cancer: An overview of the last three decades. *Archives of Gynecology and Obstetrics* 288(6), pp. 1203-1212. doi: 10.1007/s00404-013-3069-4

Keller, E. T. 2002. Overview of metastasis and metastases. *Journal of Musculoskeletal Neuronal Interactions* 2(6), pp. 567-569.

Kendall, R. L. and Thomas, K. A. 1993. Inhibition of vascular endothelial cell growth factor activity by an endogenously encoded soluble receptor. *Proceedings of the National Academy of Sciences of the United States of America* 90(22), pp. 10705-10709. doi: 10.1073/pnas.90.22.10705

Kendall, R. L. et al. 1996. Identification of a natural soluble form of the vascular endothelial growth factor receptor, FLT-1, and its heterodimerization with KDR. *Biochemical and Biophysical Research Communications* 226(2), pp. 324-328. doi: 10.1006/bbrc.1996.1355

Kim, J. W. and Dang, C. V. 2006. Cancer's molecular sweet tooth and the warburg effect. *Cancer Research* 66(18), pp. 8927-8930. doi: 10.1158/0008-5472.CAN-06-1501

Kim, Y. W. and Byzova, T. V. 2014. Oxidative stress in angiogenesis and vascular disease. *Blood* 123(5), pp. 625-631. doi: 10.1182/blood-2013-09-512749

Koch, S. et al. 2011. Signal transduction by vascular endothelial growth factor receptors. *Biochemical Journal* 437(2), pp. 169-183. doi: 10.1042/BJ20110301

Kourti, M. et al. 2017. Aspects of Carbon Monoxide in Form of CO-Releasing Molecules Used in Cancer Treatment: More Light on the Way. *Oxidative Medicine and Cellular Longevity* 2017, p. 12. doi: 10.1155/2017/9326454

Kruk, J. and Aboul-Enein, H. Y. 2017. Reactive oxygen and nitrogen species in carcinogenesis: Implications of oxidative stress on the progression and development of several cancer types. *Mini-Reviews in Medicinal Chemistry* 17(11), pp. 904-919. doi: 10.2174/1389557517666170228115324

Kunz, P. C. et al. 2013. Metal carbonyls supported on iron oxide nanoparticles to trigger the CO-gasotransmitter release by magnetic heating. *Chemical Communications* 49(43), pp. 4896-4898. doi: 10.1039/c3cc41411f

Lai, D. Y. and Woo, Y. T. 2015. Amino and Nitro Compounds.*Hamilton and Hardy's Industrial Toxicology: Sixth Edition*. pp. 615-642.

Lamalice, L. et al. 2007. Endothelial cell migration during angiogenesis. *Circulation Research* 100(6), pp. 782-794. doi: 10.1161/01.RES.0000259593.07661.1e

Lamkanfi, M. and Kanneganti, T. D. 2010. Caspase-7: A protease involved in apoptosis and inflammation. *International Journal of Biochemistry and Cell Biology* 42(1), pp. 21-24. doi: 10.1016/j.biocel.2009.09.013

Lee, W. Y. et al. 2014. The induction of heme oxygenase-1 suppresses heat shock protein 90 and the proliferation of human breast cancer cells through its byproduct carbon monoxide. *Toxicology and Applied Pharmacology* 274(1), pp. 55-62. doi: 10.1016/j.taap.2013.10.027

Leeson, P. D. and Springthorpe, B. 2007. The influence of drug-like concepts on decision-making in medicinal chemistry. *Nature Reviews Drug Discovery* 6(11), pp. 881-890. doi: 10.1038/nrd2445

Lehmann, B. D. et al. 2011. Identification of human triple-negative breast cancer subtypes and preclinical models for selection of targeted therapies. *Journal of Clinical Investigation* 121(7), pp. 2750-2767. doi: 10.1172/JCI45014

Leppänen, V. M. et al. 2010. Structural determinants of growth factor binding and specificity by VEGF receptor 2. *Proceedings of the National Academy of Sciences of the United States of America* 107(6), pp. 2425-2430. doi: 10.1073/pnas.0914318107

Li Volti, G. et al. 2005. Carbon monoxide signaling in promoting angiogenesis in human microvessel endothelial cells. *Antioxidants and Redox Signaling* 7(5-6), pp. 704-710. doi: 10.1089/ars.2005.7.704

Li, X. et al. 2013. Targeting mitochondrial reactive oxygen species as novel therapy for inflammatory diseases and cancers. *Journal of Hematology and Oncology* 6(1), doi: 10.1186/1756-8722-6-19

Li, X. et al. 2004. A contemporary understanding of progesterone receptor function. *Mechanisms of Ageing and Development* 125(10-11 SPEC. ISS.), pp. 669-678. doi: 10.1016/j.mad.2004.04.007

Li, Y. et al. 2011. PTEN deletion and heme oxygenase-1 overexpression cooperate in prostate cancer progression and are associated with adverse clinical outcome. *Journal of Pathology* 224(1), pp. 90-100. doi: 10.1002/path.2855

Li, Z. et al. 2016. Quinazoline derivative compound (11d) as a novel angiogenesis inhibitor inhibiting VEGFR2 and blocking VEGFR2-mediated Akt/mTOR /p70s6k signaling pathway. *Iranian Journal of Basic Medical Sciences* 19(4), pp. 411-416.

Lin, C. Y. et al. 2004. Discovery of estrogen receptor alpha target genes and response elements in breast tumor cells. *Genome biology* 5(9),

Liou, G. Y. and Storz, P. 2010. Reactive oxygen species in cancer. *Free Radical Research* 44(5), pp. 479-496. doi: 10.3109/10715761003667554

Lo Iacono, L. et al. 2011. A carbon monoxide-releasing molecule (CORM-3) uncouples mitochondrial respiration and modulates the production of reactive oxygen species. *Free Radical Biology and Medicine* 50(11), pp. 1556-1564. doi: 10.1016/j.freeradbiomed.2011.02.033

Loboda, A. et al. 2015a. Carbon monoxide: Pro- or anti-angiogenic agent? Comment on Ahmad et al. (Thromb Haemost 2015; 113: 329-337). *Thrombosis and Haemostasis* 114(2), pp. 432-433. doi: 10.1160/TH15-01-0082

Loboda, A. et al. 2015b. HO-1/CO system in tumor growth, angiogenesis and metabolism - Targeting HO-1 as an anti-tumor therapy. *Vascular Pharmacology* 74, pp. 11-22. doi: 10.1016/j.vph.2015.09.004

Long, R. et al. 2014. CORM-3, a water soluble CO-releasing molecule, uncouples mitochondrial respiration via interaction with the phosphate carrier. *Biochimica et Biophysica Acta - Bioenergetics* 1837(1), pp. 201-209. doi: 10.1016/j.bbabio.2013.10.002

López-Lázaro, M. 2008. The Warburg effect: Why and how do cancer cells activate glycolysis in the presence of oxygen? *Anti-Cancer Agents in Medicinal Chemistry* 8(3), pp. 305-312. doi: 10.2174/187152008783961932

Mahamodhossen, Y. A. et al. 2013. Triple-negative breast cancer: New perspectives for novel therapies. *Medical Oncology* 30(3), doi: 10.1007/s12032-013-0653-1

Mahan, V. L. 2012. Neuroprotective, neurotherapeutic, and neurometabolic effects of carbon monoxide. *Medical Gas Research* 2, pp. 32-32. doi: 10.1186/2045-9912-2-32

Malhotra, G. K. et al. 2010. Histological, molecular and functional subtypes of breast cancers. *Cancer Biology and Therapy* 10(10), pp. 955-960. doi: 10.4161/cbt.10.10.13879

Marmé, F. and Schneeweiss, A. 2015. Targeted Therapies in Triple-Negative Breast Cancer. *Breast Care* 10(3), pp. 159-166. doi: 10.1159/000433622

Marshall, M. and Hess, H. 1981. Acute effects of low carbon monoxide concentrations on blood rheology, platelet function, and the arterial wall in the minipig. *Research in Experimental Medicine* 178(3), pp. 201-210. doi: 10.1007/BF01851008

Maruyama, K. et al. 2012. Carbon monoxide (CO)-releasing molecule-derived CO regulates tissue factor and plasminogen activator inhibitor type 1 in human endothelial cells. *Thrombosis Research* 130(3), pp. e188-e193. doi: 10.1016/j.thromres.2012.07.002

Matulonis, U. A. et al. 2017. Phase I dose escalation study of the PI3kinase pathway inhibitor BKM120 and the oral poly (ADP ribose) polymerase (PARP) inhibitor olaparib for the treatment of high-grade serous ovarian and breast cancer. *Annals of Oncology* 28(3), pp. 512-518. doi: 10.1093/annonc/mdw672

Maughan, K. L. et al. 2010. Treatment of breast cancer. *American Family Physician* 81(11), pp. 1339-1346.

Mayer, I. A. et al. 2014. New strategies for triple-negative breast cancer-deciphering the heterogeneity. *Clinical Cancer Research* 20(4), pp. 782-790. doi: 10.1158/1078-0432.CCR-13-0583

McGrogan, B. T. et al. 2008. Taxanes, microtubules and chemoresistant breast cancer. *Biochimica et Biophysica Acta - Reviews on Cancer* 1785(2), pp. 96-132. doi: 10.1016/j.bbcan.2007.10.004

McIlwain, D. R. et al. 2013. Caspase functions in cell death and disease. *Cold Spring Harbor perspectives in biology* 5(4), doi: 10.1101/cshperspect.a008656

McLean, S. et al. 2013. Analysis of the bacterial response to Ru(CO)3Cl(Glycinate) (CORM-3) and the inactivated compound identifies the role played by the ruthenium compound and reveals sulfur-containing species as a major target of CORM-3 Action. *Antioxidants and Redox Signaling* 19(17), pp. 1999-2012. doi: 10.1089/ars.2012.5103

Mede, R. et al. 2016. CORM-EDE1: A Highly Water-Soluble and Nontoxic Manganese-Based photoCORM with a Biogenic Ligand Sphere. *Inorganic Chemistry* 55(1), pp. 104-113. doi: 10.1021/acs.inorgchem.5b01904

Megías, J. et al. 2007. The carbon monoxide-releasing molecule CORM-2 inhibits the inflammatory response induced by cytokines in Caco-2 cells. *British Journal of Pharmacology* 150(8), pp. 977-986. doi: 10.1038/sj.bjp.0707184

Menyhárt, O. et al. 2016. Guidelines for the selection of functional assays to evaluate the hallmarks of cancer. *Biochimica et Biophysica Acta - Reviews on Cancer* 1866(2), pp. 300-319. doi: 10.1016/j.bbcan.2016.10.002

Missiaen, R. et al. 2017. Targeting endothelial metabolism for anti-angiogenesis therapy: A pharmacological perspective. *Vascular Pharmacology* 90, pp. 8-18. doi: 10.1016/j.vph.2017.01.001

Mizuguchi, S. et al. 2009. CORM-3-derived CO modulates polymorphonuclear leukocyte migration across the vascular endothelium by reducing levels of cell surface-bound elastase. *American Journal of Physiology - Heart and Circulatory Physiology* 297(3), pp. H920-H929. doi: 10.1152/ajpheart.00305.2009

Mohr, F. et al. 2012. Synthesis, structures, and CO releasing properties of two tricarbonyl manganese(I) complexes. *Zeitschrift fur Anorganische und Allgemeine Chemie* 638(3-4), pp. 543-546. doi: 10.1002/zaac.201100422

Mosmann, T. 1983. Rapid colorimetric assay for cellular growth and survival: Application to proliferation and cytotoxicity assays. *Journal of Immunological Methods* 65(1-2), pp. 55-63. doi: 10.1016/0022-1759(83)90303-4

Mota, A. J. et al. 2003. Simple methodology for the purification of amino acids. *Organic Preparations and Procedures International* 35(4), pp. 414-417. doi: 10.1080/00304940309355851

Motterlini, R. et al. 2002. Carbon monoxide-releasing molecules: characterization of biochemical and vascular activities. *Circulation research* 90(2), pp. E17-24.

Motterlini, R. et al. 2005a. Therapeutic applications of carbon monoxide-releasing molecules. *Expert Opinion on Investigational Drugs* 14(11), pp. 1305-1318. doi: 10.1517/13543784.14.11.1305

Motterlini, R. and Otterbein, L. E. 2010. The therapeutic potential of carbon monoxide. *Nature Reviews Drug Discovery* 9(9), pp. 728-743. doi: 10.1038/nrd3228

Motterlini, R. et al. 2005b. CORM-A1: A new pharmacologically active carbon monoxide-releasing molecule. *FASEB Journal* 19(2), pp. 284-286. doi: 10.1096/fj.04-2169fje

Murray, T. S. et al. 2012. The carbon monoxide releasing molecule CORM-2 attenuates Pseudomonas aeruginosa biofilm formation. *PLoS ONE* 7(4), doi: 10.1371/journal.pone.0035499

Mykhailiuk, P. K. et al. 2013. 1-Amino-4,4-difluorocyclohexanecarboxylic acid as a promising building block for drug discovery: Design, synthesis and characterization. *Tetrahedron* 69(20), pp. 4066-4075. doi: 10.1016/j.tet.2013.03.072

Ndagi, U. et al. 2017. Metal complexes in cancer therapy – An update from drug design perspective. *Drug Design, Development and Therapy* 11, pp. 599-616. doi: 10.2147/DDDT.S119488

Ng, C. T. et al. 2015. Comparison of invasion by human microvascular endothelial cell lines in response to vascular endothelial growth factor (VEGF) and basic fibroblast growth factor (bFGF) in a three-dimensional (3D) cell culture system. *Malaysian Journal of Pathology* 37(3), pp. 219-225.

Niesel, J. et al. 2008. Photoinduced CO release, cellular uptake and cytotoxicity of a tris(pyrazolyl)methane (tpm) manganese tricarbonyl complex. *Chemical Communications* (15), pp. 1798-1800. doi: 10.1039/b719075a

Nobre, L. S. et al. 2007. Antimicrobial action of carbon monoxide-releasing compounds. *Antimicrobial Agents and Chemotherapy* 51(12), pp. 4303-4307. doi: 10.1128/AAC.00802-07

O'Donovan, N. et al. 2003. Caspase 3 in breast cancer. *Clinical Cancer Research* 9(2), pp. 738-742.

Olas, B. 2014. Carbon monoxide is not always a poison gas for human organism: Physiological and pharmacological features of CO. *Chemico-Biological Interactions* 222, pp. 37-43. doi: 10.1016/j.cbi.2014.08.005

Otterbein, L. E. et al. 2000. Carbon monoxide has anti-inflammatory effects involving the mitogen- activated protein kinase pathway. *Nature Medicine* 6(4), pp. 422-428. doi: 10.1038/74680

Page, S. 2012. Ruthenium compounds as anticancer agents. *Education in Chemistry* 49(1), pp. 26-29.

Pang, B. et al. 2013. Drug-induced histone eviction from open chromatin contributes to the chemotherapeutic effects of doxorubicin. *Nature Communications* 4, doi: 10.1038/ncomms2921

Papa, A. et al. 2015. Triple-negative breast cancer: Investigating potential molecular therapeutic target. *Expert Opinion on Therapeutic Targets* 19(1), pp. 55-75. doi: 10.1517/14728222.2014.970176

Parasuraman, S. 2011. Toxicological screening. *Journal of Pharmacology and Pharmacotherapeutics* 2(2), pp. 74-79. doi: 10.4103/0976-500X.81895

Patterson, E. K. et al. 2014. Carbon monoxide-releasing molecule 3 inhibits myeloperoxidase (MPO) and protects against MPO-induced vascular endothelial cell activation/dysfunction. *Free Radical Biology and Medicine* 70, pp. 167-173. doi: 10.1016/j.freeradbiomed.2014.02.020

Pena, A. C. et al. 2012. A novel carbon monoxide-releasing molecule fully protects mice from severe malaria. *Antimicrobial Agents and Chemotherapy* 56(3), pp. 1281-1290. doi: 10.1128/AAC.05571-11

Pfeiffer, H. et al. 2009. Sonogashira and "click" reactions for the N-terminal and side-chain functionalization of peptides with [Mn(CO)3(tpm)] +-based CO releasing molecules (tpm = tris(pyrazolyl)methane). *Dalton Transactions* (22), pp. 4292-4298. doi: 10.1039/b819091g

Pfister, N. T. et al. 2015. Mutant p53 cooperates with the SWI/SNF chromatin remodeling complex to regulate VEGFR2 in breast cancer cells. *Genes and Development* 29(12), pp. 1298-1315. doi: 10.1101/gad.263202.115

Piantadosi, C. A. 2008. Carbon monoxide, reactive oxygen signaling, and oxidative stress. *Free Radical Biology and Medicine* 45(5), pp. 562-569. doi: 10.1016/j.freeradbiomed.2008.05.013

Piantadosi, C. A. et al. 2006. Carbon monoxide, oxidative stress, and mitochondrial permeability pore transition. *Free Radical Biology and Medicine* 40(8), pp. 1332-1339. doi: 10.1016/j.freeradbiomed.2005.11.020

Piantadosi, C. A. et al. 1997. Apoptosis and delayed neuronal damage after carbon monoxide poisoning in the rat. *Experimental Neurology* 147(1), pp. 103-114. doi: 10.1006/exnr.1997.6584

Pinto, M. N. et al. 2017. Eradication of HT-29 colorectal adenocarcinoma cells by controlled photorelease of CO from a CO-releasing polymer (photoCORP-1) triggered by visible light through an optical fiber-based device. *Journal of Controlled Release* 264, pp. 192-202. doi: 10.1016/j.jconrel.2017.08.039

Pliška, V. et al. 2008. *Lipophilicity in Drug Action and Toxicology*.

Porter, A. G. and Jänicke, R. U. 1999. Emerging roles of caspase-3 in apoptosis. *Cell Death and Differentiation* 6(2), pp. 99-104.

Potente, M. and Carmeliet, P. 2017. The Link between Angiogenesis and Endothelial Metabolism. *Annual Review of Physiology*.

Poulos, T. L. 2006. Soluble guanylate cyclase. *Current Opinion in Structural Biology* 16(6), pp. 736-743. doi: 10.1016/j.sbi.2006.09.006

Prütz, W. A. 1986. Nitro-tyrosine as promoter of free radical damage in a DNA model system. *Free Radical Research* 2(1-2), pp. 77-83. doi: 10.3109/10715768609088057

Puddu, A. et al. 2016. Response to anti-VEGF-A treatment of endothelial cells in vitro. *Experimental Eye Research* 146, pp. 128-136. doi: 10.1016/j.exer.2015.12.014

Qian, X. L. et al. 2017. Dasatinib inhibits c-src phosphorylation and prevents the proliferation of triple-negative breast cancer (TNBC) cells which overexpress syndecan-binding protein (SDCBP). *PLoS ONE* 12(1), doi: 10.1371/journal.pone.0171169

Queiroga, C. S. F. et al. 2010. Glutathionylation of adenine nucleotide translocase induced by carbon monoxide prevents mitochondrial membrane permeabilization and apoptosis. *Journal of Biological Chemistry* 285(22), pp. 17077-17088. doi: 10.1074/jbc.M109.065052

R. Oliveira, S. et al. 2016. Mitochondria and carbon monoxide: cytoprotection and control of cell metabolism – a role for Ca2+? *Journal of Physiology* 594(15), pp. 4131-4138. doi: 10.1113/JP270955

Radomska-Leśniewska, D. M. et al. 2016. Reactive oxygen species and synthetic antioxidants as angiogenesis modulators: Clinical implications. *Pharmacological Reports* 68(2), pp. 462-471. doi: 10.1016/j.pharep.2015.10.002

Reddy, S. et al. 2012. Targeting angiogenesis in metastatic breast cancer. *Oncologist* 17(8), pp. 1014-1026. doi: 10.1634/theoncologist.2012-0043

Riedl, S. J. and Shi, Y. 2004. Molecular mechanisms of caspase regulation during apoptosis. *Nature Reviews Molecular Cell Biology* 5(11), pp. 897-907. doi: 10.1038/nrm1496

Rini, B. I. 2007. Vascular endothelial growth factor-targeted therapy in renal cell carcinoma: Current status and future directions. *Clinical Cancer Research* 13(4), pp. 1098-1106. doi: 10.1158/1078-0432.CCR-06-1989

Rodon, J. et al. 2014. Phase I dose-escalation and -expansion study of buparlisib (BKM120), an oral pan-Class I PI3K inhibitor, in patients with advanced solid tumors. *Investigational New Drugs* 32(4), pp. 670-681. doi: 10.1007/s10637-014-0082-9

Rodríguez-Ropero, F. et al. 2008. Application of 1-aminocyclohexane carboxylic acid to protein nanostructure computer design. *Journal of Chemical Information and Modeling* 48(2), pp. 333-343. doi: 10.1021/ci700291x

Romanski, S. et al. 2011. Acyloxybutadiene iron tricarbonyl complexes as enzyme-triggered CO-releasing molecules (ET-CORMs). *Angewandte Chemie - International Edition* 50(10), pp. 2392-2396. doi: 10.1002/anie.201006598

Romão, C. C. and Vieira, H. L. A. 2015. Metal Carbonyl Prodrugs: CO Delivery and Beyond.*Bioorganometallic Chemistry: Applications in Drug Discovery, Biocatalysis, and Imaging*. pp. 165-202.

Rydén, L. et al. 2010a. Evidence for tissue factor phosphorylation and its correlation with protease-activated receptor expression and the prognosis of primary breast cancer. *International Journal of Cancer* 126(10), pp. 2330-2340. doi: 10.1002/ijc.24921

Rydén, L. et al. 2010b. Epidermal growth factor receptor and vascular endothelial growth factor receptor 2 are specific biomarkers in triple-negative breast cancer. Results from a controlled randomized trial with long-term follow-up. *Breast Cancer Research and Treatment* 120(2), pp. 491-498. doi: 10.1007/s10549-010-0758-6

Ryter, S. W. et al. 2006. Heme oxygenase-1/carbon monoxide: From basic science to therapeutic applications. *Physiological Reviews* 86(2), pp. 583-650. doi: 10.1152/physrev.00011.2005

Sagara, A. et al. 2017. Endocan as a prognostic biomarker of triple-negative breast cancer. *Breast Cancer Research and Treatment* 161(2), pp. 269-278. doi: 10.1007/s10549-016-4057-8

Sahlberg Bang, C. et al. 2016. Carbon monoxide releasing molecule-2 (CORM-2) inhibits growth of multidrug-resistant uropathogenic Escherichia coli in biofilm and following host cell colonization. *BMC Microbiology* 16(1), doi: 10.1186/s12866-016-0678-7

Santos-Silva, T. et al. 2011. Towards improved therapeutic CORMs: Understanding the reactivity of CORM-3 with proteins. *Current Medicinal Chemistry* 18(22), pp. 3361-3366. doi: 10.2174/092986711796504583

Sass, G. et al. 2008. Inhibition of heme oxygenase 1 expression by small interfering RNA decreases orthotopic tumor growth in livers of mice. *International Journal of Cancer* 123(6), pp. 1269-1277. doi: 10.1002/ijc.23695

Sato, K. et al. 2001. Carbon monoxide generated by heme oxygenase-1 suppresses the rejection of mouse-to-rat cardiac transplants. *Journal of Immunology* 166(6), pp. 4185-4194.

Sawle, P. et al. 2005. Carbon monoxide-releasing molecules (CO-RMs) attenuate the inflammatory response elicited by lipopolysaccharide in RAW264.7 murine macrophages. *British Journal of Pharmacology* 145(6), pp. 800-810. doi: 10.1038/sj.bjp.0706241

Schatzschneider, U. 2011. PhotoCORMs: Light-triggered release of carbon monoxide from the coordination sphere of transition metal complexes for biological applications. *Inorganica Chimica Acta* 374(1), pp. 19-23. doi: 10.1016/j.ica.2011.02.068

Schatzschneider, U. 2015. Novel lead structures and activation mechanisms for CO-releasing molecules (CORMs). *British Journal of Pharmacology* 172(6), pp. 1638-1650. doi: 10.1111/bph.12688

Seixas, J. D. et al. 2015. An N-Acetyl Cysteine Ruthenium Tricarbonyl Conjugate Enables Simultaneous Release of CO and Ablation of Reactive Oxygen Species. *Chemistry - A European Journal* 21(42), pp. 14708-14712. doi: 10.1002/chem.201502474

Shalini, S. et al. 2015. Old, new and emerging functions of caspases. *Cell Death and Differentiation* 22(4), pp. 526-539. doi: 10.1038/cdd.2014.216

Shan, Y. L. et al. 2014. The new therapeutic strategy for inhibition of cancer metastasis: Targeting extravasation of cancer cells. *Tumor* 34(8), pp. 754-757. doi: 10.3781/j.issn.1000-7431.2014.08.013

Sharma, G. N. et al. 2010. Various types and management of breast cancer: An overview. *Journal of Advanced Pharmaceutical Technology and Research* 1(2), pp. 109-126.

Shibuya, M. 2004. Vascular endothelial growth factor receptor-2: Its unique signaling and specific ligand, VEGF-E. *Gann Monographs on Cancer Research*.

Shibuya, M. 2013. VEGFR and type-V RTK activation and signaling. *Cold Spring Harbor Perspectives in Biology* 5(10), doi: 10.1101/cshperspect.a009092

Shyh-Chang, N. et al. 2013. Stem cell metabolism in tissue development and aging. *Development (Cambridge)* 140(12), pp. 2535-2547. doi: 10.1242/dev.091777

Simić, A. et al. 2007. Electrochemical behavior and antioxidant and prooxidant activity of natural phenolics. *Molecules* 12(10), pp. 2327-2340. doi: 10.3390/12102327

Simpson, P. V. and Schatzschneider, U. 2014. Release of Bioactive Molecules Using Metal Complexes.*Inorganic Chemical Biology: Principles, Techniques and Applications*. pp. 309-339.

Sjöstrand, T. 1949a. Endogenous formation of carbon monoxide in man under normal and pathological conditions. *Scandinavian Journal of Clinical and Laboratory Investigation* 1(3), pp. 201-214. doi: 10.3109/00365514909069943

Sjöstrand, T. 1949b. Endogenous formation of carbon monoxide in man [14]. *Nature* 164(4170), pp. 580-581.

SjöStrand, T. 1951. Endogenous Formation of Carbon Monoxide. The Co Concentration in the Inspired and Expired Air of Hospital Patients. *Acta Physiologica Scandinavica* 22(2-3), pp. 137-141. doi: 10.1111/j.1748-1716.1951.tb00762.x

Smith, H. et al. 2011. The carbon monoxide-releasing molecule, corm-3 (ru(co) 3cl(glycinate)), targets respiration and oxidases in campylobacter jejuni, generating hydrogen peroxide. *IUBMB Life* 63(5), pp. 363-371. doi: 10.1002/iub.476

Somanath, P. R. et al. 2006. Akt1 in endothelial cell and angiogenesis. *Cell Cycle* 5(5), pp. 512-518. doi: 10.4161/cc.5.5.2538

Song, H. et al. 2011. Carbon monoxide releasing molecule-3 inhibits concurrent tumor necrosis factor-α- and interleukin-1β-induced expression of adhesion molecules on human gingival fibroblasts. *Journal of Periodontal Research* 46(1), pp. 48-57. doi: 10.1111/j.1600-0765.2010.01307.x

Song, R. et al. 2003. Carbon monoxide induces cytoprotection in rat orthotopic lung transplantation via anti-inflammatory and anti-apoptotic effects. *American Journal of Pathology* 163(1), pp. 231-242.

Staykova, S. T. et al. 2015. Synthesis and in vitro antitumor activity of new octapeptide analogs of somatostatin containing unnatural amino acids. *Amino Acids* 47(5), pp. 1007-1013. doi: 10.1007/s00726-015-1929-x

Steiger, C. et al. 2016. Localized delivery of carbon monoxide. *European Journal of Pharmaceutics and Biopharmaceutics*, doi: 10.1016/j.ejpb.2016.11.002

Szabo, C. 2016. Gasotransmitters in cancer: From pathophysiology to experimental therapy. *Nature Reviews Drug Discovery* 15(3), pp. 185-203. doi: 10.1038/nrd.2015.1

Taillé, C. et al. 2005. Mitochondrial respiratory chain and NAD(P)H oxidase are targets for the antiproliferative effect of carbon monoxide in human airway smooth muscle. *Journal of Biological Chemistry* 280(27), pp. 25350-25360. doi: 10.1074/jbc.M503512200

Takeda, S. et al. 2017. Cannabidiolic acid-mediated selective down-regulation of c-fos in highly aggressive breast cancer MDA-MB-231 cells: possible involvement of its down-regulation in the abrogation of aggressiveness. *Journal of Natural Medicines* 71(1), pp. 286-291. doi: 10.1007/s11418-016-1030-0

Tamemasa, O. et al. 1968. Inhibition and Simulation of the Biosynthesis of Protein and Nucleic Acid. II.1) Inhibition Sites of 4-Fluoro- and 4-Nitro-phenylalanines on the Incorporation of Phenylalanine into Proteins of Ehrlich Mouse Ascites Tumor Cells in vitro. *Chemical and Pharmaceutical Bulletin* 16(4), pp. 672-678. doi: 10.1248/cpb.16.672

Tan, Q. et al. 2015. Src/STAT3-dependent heme oxygenase-1 induction mediates chemoresistance of breast cancer cells to doxorubicin by promoting autophagy. *Cancer Science* 106(8), pp. 1023-1032. doi: 10.1111/cas.12712

Tao, J. J. et al. 2014. Antagonism of EGFR and HER3 enhances the response to inhibitors of the PI3K-Akt pathway in triple-negative breast cancer. *Science Signaling* 7(318), doi: 10.1126/scisignal.2005125

Tavares, A. F. et al. 2013. The bactericidal activity of carbon monoxide-releasing molecules against helicobacter pylori. *PLoS ONE* 8(12), doi: 10.1371/journal.pone.0083157

Tavares, A. F. N. et al. 2011. Reactive oxygen species mediate bactericidal killing elicited by carbon monoxide-releasing molecules. *Journal of Biological Chemistry* 286(30), pp. 26708-26717. doi: 10.1074/jbc.M111.255752

Tertil, M. et al. 2010. Oxidative stress in tumor angiogenesis - therapeutic targets. *Current Pharmaceutical Design* 16(35), pp. 3877-3894. doi: 10.2174/138161210794454969

Thomssen, C. et al. 2012. First-line bevacizumab-containing therapy for triple-negative breast cancer: Analysis of 585 patients treated in the ATHENA study. *Oncology* 82(4), pp. 218-227. doi: 10.1159/000336892

Turner, N. et al. 2010. Integrative molecular profiling of triple negative breast cancers identifies amplicon drivers and potential therapeutic targets. *Oncogene* 29(14), pp. 2013-2023. doi: 10.1038/onc.2009.489

Ulyatt, C. et al. 2011. Hypoxia differentially regulates VEGFR1 and VEGFR2 levels and alters intracellular signaling and cell migration in endothelial cells. *Biochemical and Biophysical Research Communications* 404(3), pp. 774-779. doi: 10.1016/j.bbrc.2010.12.057

Upadhyay, M. et al. 2013. The Warburg effect: Insights from the past decade. *Pharmacology and Therapeutics* 137(3), pp. 318-330. doi: 10.1016/j.pharmthera.2012.11.003

Ushio-Fukai, M. 2006. Redox signaling in angiogenesis: Role of NADPH oxidase. *Cardiovascular Research* 71(2), pp. 226-235. doi: 10.1016/j.cardiores.2006.04.015

Ushio-Fukai, M. and Nakamura, Y. 2008. Reactive oxygen species and angiogenesis: NADPH oxidase as target for cancer therapy. *Cancer Letters* 266(1), pp. 37-52. doi: 10.1016/j.canlet.2008.02.044

Vadori, M. et al. 2009. In vitro and in vivo effects of the carbon monoxide-releasing molecule, CORM-3, in the xenogeneic pig-to-primate context. *Xenotransplantation* 16(2), pp. 99-114. doi: 10.1111/j.1399-3089.2009.00521.x

Veber, D. F. et al. 2002. Molecular properties that influence the oral bioavailability of drug candidates. *Journal of Medicinal Chemistry* 45(12), pp. 2615-2623. doi: 10.1021/jm020017n

Verma, A. et al. 1993. Carbon monoxide: A putative neural messenger. *Science* 259(5093), pp. 381-384.

Vivanco, I. and Sawyers, C. L. 2002. The phosphatidylinositol 3-kinase-AKT pathway in humancancer. *Nature Reviews Cancer* 2(7), pp. 489-501. doi: 10.1038/nrc839

Vítek, L. et al. 2014. Antiproliferative effects of carbon monoxide on pancreatic cancer. *Digestive and Liver Disease* 46(4), pp. 369-375. doi: 10.1016/j.dld.2013.12.007

Wang, D. and Lippard, S. J. 2005. Cellular processing of platinum anticancer drugs. *Nature Reviews Drug Discovery* 4(4), pp. 307-320. doi: 10.1038/nrd1691

Wang, P. et al. 2014. Syntheses and evaluation of drug-like properties of CO-releasing molecules containing ruthenium and group 6 metal. *European Journal of Medicinal Chemistry* 74, pp. 199-215. doi: 10.1016/j.ejmech.2013.12.041

Wang, Z. et al. 2015. Broad targeting of angiogenesis for cancer prevention and therapy. *Seminars in Cancer Biology* 35, pp. S224-S243. doi: 10.1016/j.semcancer.2015.01.001

Ward, J. S. et al. 2016. Photoactivated Functionizable Tetracarbonyl(phenylpyridine)manganese(I) Complexes as CO-Releasing Molecules: A Direct Suzuki–Miyaura Cross-Coupling on a Thermally Stable CO-RM. *European Journal of Inorganic Chemistry* 2016(31), pp. 5044-5051. doi: 10.1002/ejic.201600775

Ward, J. S. et al. 2017. Toxicity of tryptophan manganese(i) carbonyl (Trypto-CORM), against Neisseria gonorrhoeae. *MedChemComm* 8(2), pp. 346-352. doi: 10.1039/c6md00603e

Wareham, L. K. et al. 2015. CO-releasing metal carbonyl compounds as antimicrobial agents in the post-antibiotic era. *Journal of Biological Chemistry* 290(31), pp. 18999-19007. doi: 10.1074/jbc.R115.642926

Watson, C. A. et al. 1995. Variability among human umbilical vein endothelial cultures. *Science* 268(5209), pp. 447-448. doi: 10.1126/science.7716553

Wegiel, B. et al. 2013. Carbon monoxide expedites metabolic exhaustion to inhibit tumor growth. *Cancer Research* 73(23), pp. 7009-7021. doi: 10.1158/0008-5472.CAN-13-1075

Wehland, M. et al. 2012. Target-based anti-angiogenic therapy in breast cancer. *Current Pharmaceutical Design* 18(27), pp. 4244-4257. doi: 10.2174/138161212802430468

Westbrook, K. and Stearns, V. 2013. Pharmacogenomics of breast cancer therapy: An update. *Pharmacology and Therapeutics* 139(1), pp. 1-11. doi: 10.1016/j.pharmthera.2013.03.001

Wilson, J. L. et al. 2017. Carbon monoxide reverses the metabolic adaptation of microglia cells to an inflammatory stimulus. *Free Radical Biology and Medicine* 104, pp. 311-323. doi: 10.1016/j.freeradbiomed.2017.01.022

Winburn, I. C. et al. 2012. Cell Damage Following Carbon Monoxide Releasing Molecule Exposure: Implications for Therapeutic Applications. *Basic and Clinical Pharmacology and Toxicology* 111(1), pp. 31-41. doi: 10.1111/j.1742-7843.2012.00856.x

Wolff, A. C. et al. 2013. Randomized phase III placebo-controlled trial of letrozole plus oral temsirolimus as first-line endocrine therapy in postmenopausal women with locally advanced or metastatic breast cancer. *Journal of Clinical Oncology* 31(2), pp. 196-202. doi: 10.1200/JCO.2011.38.3331

Wu, L. and Wang, R. 2005. Carbon monoxide: Endogenous production, physiological functions, and pharmacological applications. *Pharmacological Reviews* 57(4), pp. 585-630. doi: 10.1124/pr.57.4.3

Wu, L. W. et al. 2000. Utilization of distinct signaling pathways by receptors for vascular endothelial cell growth factor and other mitogens in the induction of endothelial cell proliferation. *Journal of Biological Chemistry* 275(7), pp. 5096-5103. doi: 10.1074/jbc.275.7.5096

Yadav, B. S. et al. 2014. Systemic treatment strategies for triple-negative breast cancer. *World Journal of Clinical Oncology* 5(2), pp. 125-133. doi: 10.5306/wjco.v5.i2.125

Yamamoto, Y. and Iwase, H. 2010. Clinicopathological features and treatment strategy for triple-negative breast cancer. *International Journal of Clinical Oncology* 15(4), pp. 341-351. doi: 10.1007/s10147-010-0106-1

Yang, J. et al. 2014. Potent anti-angiogenesis and anti-tumor activity of a novel human anti-VEGF antibody, MIL60. *Cellular and Molecular Immunology* 11(3), pp. 285-293. doi: 10.1038/cmi.2014.6

Yin, H. et al. 2014. Upregulation of heme oxygenase-1 in colorectal cancer patients with increased circulation carbon monoxide levels, potentially affects chemotherapeutic sensitivity. *BMC Cancer* 14(1), doi: 10.1186/1471-2407-14-436

Zhang, C. H. et al. 2015. Design, synthesis, and structure-Activity relationship studies of 3-(Phenylethynyl)-1H-pyrazolo[3,4-d]pyrimidin-4-amine derivatives as a new class of Src inhibitors with potent activities in models of triple negative breast cancer. *Journal of Medicinal Chemistry* 58(9), pp. 3957-3974. doi: 10.1021/acs.jmedchem.5b00270

Zhao, Q. et al. 2015. Synthesis of six phenylalanine derivatives and their cell toxicity effect on human colon cancer cell line HT-29. *Letters in Drug Design and Discovery* 12(6), pp. 466-470. doi: 10.2174/1570180812666141206001604

Zhu, X. and Zhou, W. 2015. The emerging regulation of VEGFR-2 in triple-negative breast cancer. *Frontiers in Endocrinology* 6(OCT), doi: 10.3389/fendo.2015.00159

Zobi, F. 2013. CO and CO-releasing molecules in medicinal chemistry. *Future Medicinal Chemistry* 5(2), pp. 175-188. doi: 10.4155/fmc.12.196

Zobi, F. et al. 2012. 17 e - rhenium dicarbonyl CO-releasing molecules on a cobalamin scaffold for biological application. *Dalton Transactions* 41(2), pp. 370-378. doi: 10.1039/c1dt10649j

Zou, C. et al. 2011. Heme oxygenase-1: A molecular brake on hepatocellular carcinoma cell migration. *Carcinogenesis* 32(12), pp. 1840-1848. doi: 10.1093/carcin/bgr225

Zuckerbraun, B. S. et al. 2007. Carbon monoxide signals via inhibition of cytochrome c oxidase and generation of mitochondrial reactive oxygen species. *FASEB Journal* 21(4), pp. 1099-1106. doi: 10.1096/fj.06-6644com

Üstün, E. et al. 2016. CO-releasing properties and anticancer activities of manganese complexes with imidazole/benzimidazole ligands. *Journal of Coordination Chemistry* 69(22), pp. 3384-3394. doi: 10.1080/00958972.2016.1231921

Appendix

Antibacterial activity assessment and Selected NMR spectra

Antibacterial activity assessment

Introduction

In the early 2000's, the newly characterized group of CORMs started receiving major scientific interest. One of the first studies to investigate potential applications of these compounds revealed a potent anti-microbial profile, which was originally attributed to the released CO. In the study of Nobre et al. (Nobre et al. 2007), cell growth experiments showed an interesting bactericidal effect of CORM-2 and CORM-3 against Escherichia coli (E. coli) and Staphylococcus aureus (S. aureus) at 250μM for CORM-2 and 400μM for CORM-3. The effectiveness of CORMs appeared to be much greater in near-anaerobic environments, resembling the anaerobic nature of the microorganisms themselves and the most common pathogen colonization environments. The researchers ascribed the results to the preferential binding of the released CO to the ferrous haem proteins and the impairment of the respiratory chain due to the inhibition of cytochrome oxidase, even though the latter might also conveniently explain the bactericidal activity of CORMs under aerobic conditions too.

In the following years, many groups studied the anti-microbial activity of CORMs, for example CORM-3 was shown to inhibit Pseudomonas aeruginosa (P. aeruginosa) at 0.1-100μM, probably through inhibition of cysteine moieties on respiratory proteins and independently of the overproduction of ROS caused by the inhibition of the respiratory chain (Desmard et al. 2009). CORM-3 was also investigated against E. coli under aerobic conditions in a separate study by Davidge et al. (Davidge et al. 2009) and inhibition of electron transfer to cytochrome c oxidase, generation of ROS and redox modulation of cysteine residues were identified as potential targets of the strong anti-microbial activity of CORM-3, even at low concentrations. Moreover, this study revealed a gene expression profile extensively modified by CORM-3, correlated with metal metabolism, homeostasis and transporting proteins, as well as respiratory complexes.

Other investigations include the work against Campylobacter jejuni (C. jejuni), which was not inhibited with up to 100μM of CORM-3. However this insensitivity was not due to failure of CORM-3 to inhibit membrane-associated respiratory oxidases, and

even at almost 200µM oxygen, CORM-3 could inhibit formate-dependent respiration and lead to generation of hydrogen peroxide (H_2O_2) (Smith et al. 2011).

CORM-2 was also shown to have antibacterial activity, for example against uropathogenic E. coli and other strains, at 500µM (Sahlberg Bang et al. 2016). Interestingly, CORM-2 was also combined with other antibiotics, such as metronidazole, amoxicillin and clarithromycin and found to enhance their effect against Helicobacter pylori (H. pylori) and with tobramycin against P. aeruginosa (Murray et al. 2012; Tavares et al. 2013).

Most of these studies suggest the ROS hypothesis, that is CORMs based on Ru such as CORM-2 and CORM-3, induce the generation of ROS due to the inhibition of respiratory oxidases and thioredoxin reductase. The produced ROS contribute to the killing properties of CORMs and CORMs should not be solely seen as CO delivery systems, but rather that the whole molecule contributes to the observed properties (Tavares et al. 2011; Tavares et al. 2013). In fact, transcriptomics revealed that both CORM-3 and the CO-depleted molecule affected several systems linked to energy metabolism, membrane transport, motility and metabolism of sulphur species (McLean et al. 2013). All in all, it seems that ROS play an important role not only in the bactericidal activity of CORMs but also in their general properties, hence ROS formation should be considered when using this class of organometallic compounds (Wareham et al. 2015).

Following this, CORMs -2, -3 and -A1 were subjected to an anti-microbial testing using a broth microdilution method. The strains tested were NCTC/ATCC control strains both sensitive and resistant, as well as strains that belong to the strain collection of the laboratory. An anti-microbial activity of CORMs may be unrelated to TNBC, however the involvement of ROS production and the opportunity to check the CORMs against a wide collection of microorganisms were considered interesting, therefore these experiments were chosen to be included in this study.

Dilution procedures were used to determine the minimum inhibitory concentrations (MICs) of antimicrobial agents as they are the reference method for antimicrobial susceptibility testing. MIC methods are used in several cases, such as resistance

surveillance or comparative testing of new agents. In dilution tests, microorganisms are tested for their ability to produce visible growth in broth-containing serial dilutions of the antimicrobial agent. The lowest concentration of an antimicrobial agent (mg/L) that under defined *in vitro* conditions prevents the appearance of visible growth of a microorganism within a defined period of time is known as the MIC.

In the broth microdilution technique, containers filled with identical volumes of broth and antimicrobial agent solution in incrementally (two-fold) increasing concentrations are inoculated with a known number of microorganisms.

Materials & Methods

ISO broth microdilution method

Working solutions of the compounds to be tested were dispensed into microdilution trays with double the desired final concentrations of antimicrobial agent. The trays were inoculated within 30min of standardizing the bacterial suspension, in order to maintain viable cell number concentration. To each well with diluted antimicrobial agent in broth, the same volume of bacterial suspension was added.

After the addition of the bacterial suspension, microdilution trays were sealed in polyethylene bags before incubation, in order to prevent desiccation. The trays were incubated at 37^{o}C in ambient air for (18 ± 2)h. The amount of growth in each well was compared with that in the positive growth control, and the MIC recorded was the lowest concentration of the agent that completely inhibited visible growth.

Results

Several bacterial strains were used in this study, both sensitive and resistant to specific antibiotics. The well-known antibiotic ampicillin was used as a control antibiotic to ensure reliable results.

In contrast with many other reports (as will be discussed further), in these experiments only CORM-2 managed to kill most of the strains tested, with MIC values from 64 to 128mg/L (**Table 1, Table 2**). In more detail, Klebsiella pneumoniae and S. aureus resistant strains appeared to be affected by CORM-2 with MIC of 128mg/L, whereas C. coli and jejuni were not affected by this compound. Enterococcus faecalis

resistant to vancomycin was inhibited by CORM-2 with MIC= 64mg/L and also other sensitive bacteria, such as Salmonella enteritidis and Burkholderia cepacia were killed by it with MIC values of 128mg/L. CORM-3 and CORM-A1 were not effective against these microorganisms.

It must be stressed here that the highest concentration used for these experiments (128mg/L) corresponds to different molar concentrations of CORMs. More specifically, 128mg/L are equivalent to 250μM CORM-2, 434μM CORM-3 and 1.233mM CORM-A1.

Organism ID	Resistances	CORM-A1 MIC (mg/L)	CORM-2 MIC (mg/L)	CORM-3 MIC (mg/L)	Amp MIC (mg/L)
Escherichia coli	Sensitive strain	>128	128	>128	8
Klebsiella pneumoniae	Sensitive strain	>128	>128	>128	>128
Proteus mirabilis	Sensitive strain	>128	128	>128	>128
Pseudomonas aeruginosa	Sensitive strain	>128	128	>128	>128
Salmonella enteritidis	Sensitive strain	>128	128	>128	4
Acinetobacter baumannii	Sensitive strain	>128	128	>128	128
Burkholderia cepacia	Sensitive strain	>128	128	>128	>128
Staphylococcus aureus	Sensitive strain	>128	128	>128	4
Enterococcus faecalis	Sensitive strain	>128	128	>128	2
Escherichia coli	Ampicillin	>128	>128	>128	>128
Klebsiella pneumoniae	Carbapenems	>128	128	>128	>128
Escherichia coli	3rd gen Cephalosporins	>128	128	>128	>128
Escherichia coli	Nitro / Trim	>128	>128	>128	>128

Table 1: Anti-bacterial assessment expressed as MIC of each CORM against different bacterial strains. Results from antibacterial assessment of CORM-A1, CORM-2 and CORM-3. Organism identity, known resistances and MIC in mg/L for each compound are given at the table. Ampicillin (Amp) was used as the control antimicrobial. MIC values ≤128mg/L are highlighted in blue.

Organism ID	Resistances	CORM-A1 MIC (mg/L)	CORM-2 MIC (mg/L)	CORM-3 MIC (mg/L)	Amp MIC (mg/L)
Klebsiella pneumoniae	4th gen Cephalosporins	>128	128	>128	>128
Klebsiella pneumoniae	Carbapenems	>128	128	>128	>128
Staphylococcus aureus	Flucloxacillin	>128	128	>128	>128
Staphylococcus aureus	ERY/CLIND	>128	128	>128	64
Staphylococcus aureus	Vancomycin	>128	>128	>128	>128
Staphylococcus aureus	Tetracycline	>128	>128	>128	>128
Enterococcus faecalis	Vancomycin	>128	64	>128	4
Enterococcus faecalis	Vancomycin	>128	64	>128	8
Campylobacter coli	Sensitive strain	>128	>128	>128	-
Campylobacter coli	Sensitive strain	>128	>128	>128	-
Campylobacter jejuni	Sensitive strain	>128	>128	>128	-
Campylobacter jejuni	Sensitive strain	>128	>128	>128	-
Campylobacter jejuni	Sensitive strain	>128	>128	>128	-

Table 2: Anti-bacterial assessment expressed as MIC of each CORM against different bacterial strains. Results from antibacterial assessment of CORM-A1, CORM-2 and CORM-3. Organism identity, known resistances and MIC in mg/L for each compound are given at the table. Ampicillin (Amp) was used as the control antimicrobial. MIC values ≤128mg/L are highlighted in blue.

Discussion

The findings of this experiment were quite unexpected. Based on previous literature, it was expected to find lower MIC values for both CORM-2 and CORM-3 against some of the tested bacteria, but instead only CORM-2 showed some anti-microbial activity in this experiment. These observations may have various explanations.

First of all, as discussed extensively in the work by Smith et al. (Smith et al. 2011), complex media such as broth may have abolished the effects of CORM-3 due to components acting as scavengers of CO or inhibiting CO release. Sulphur-containing species such as cysteine and glutathione may have also abrogated the effects of CORM-3, as shown in other studies (Sawle et al. 2005; Desmard et al. 2009). The potential existence of certain reductases that can metabolize CO in these bacteria could be another explanation of the atypical results observed in this study. Finally, some of the tested bacteria may have had a CO-insensitive respiratory pathway that can induce micro-aerobic proliferation and growth.

In any case, these results might need further optimization before conclusions can be drawn, however the bactericidal activity of CORM-2 was indeed confirmed and for CORM-3 a different method might have been better and more effective. These results do not contradict previous literature though, that has decisively shown a good anti-microbial activity for both CORM-2 and CORM-3 against a variety of microorganisms. The ROS hypothesis is still involved in studies about CORMs and might also prove useful in the fight against TNBC.

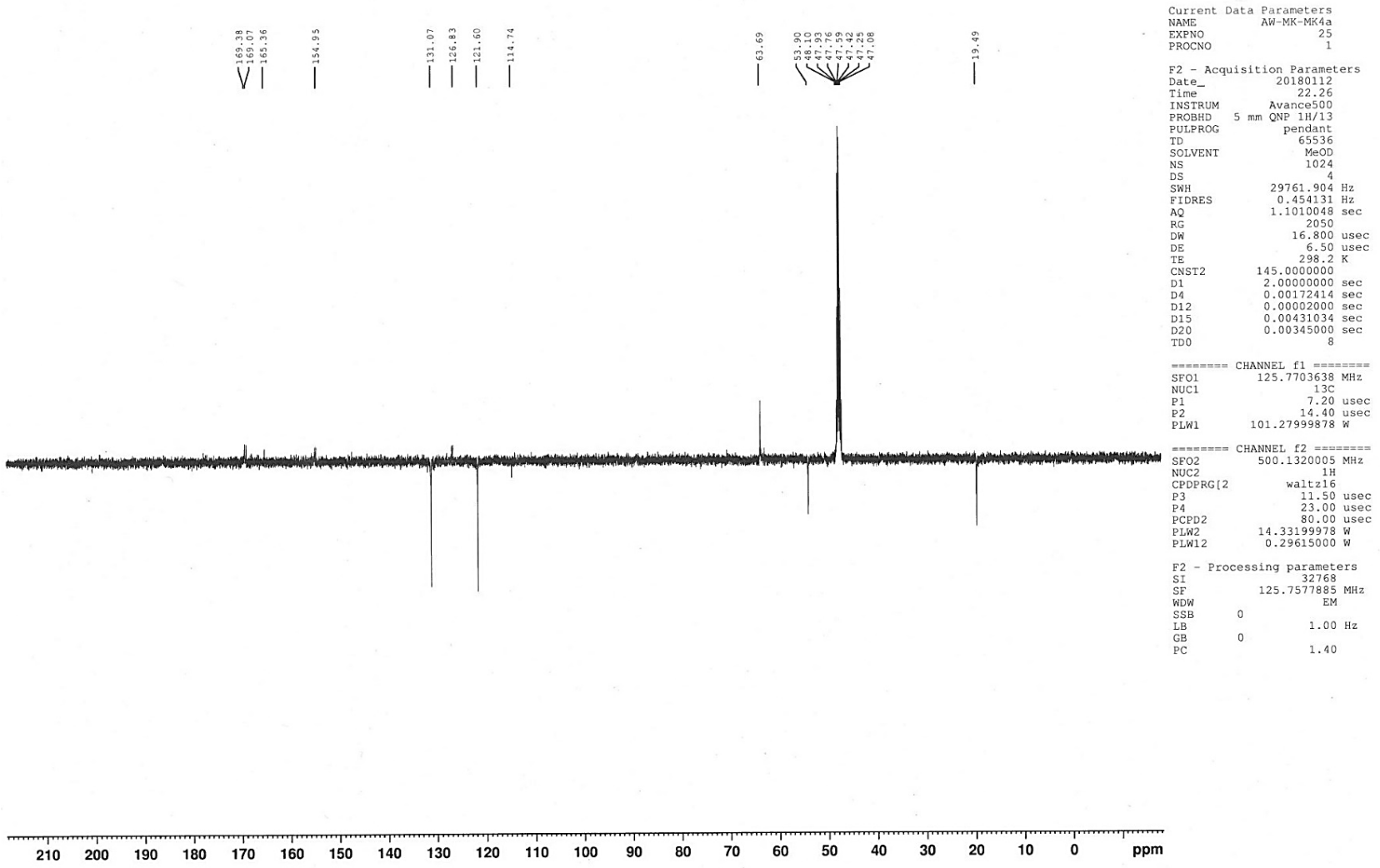

Figure A.1: ^{13}C NMR spectrum of MK4a

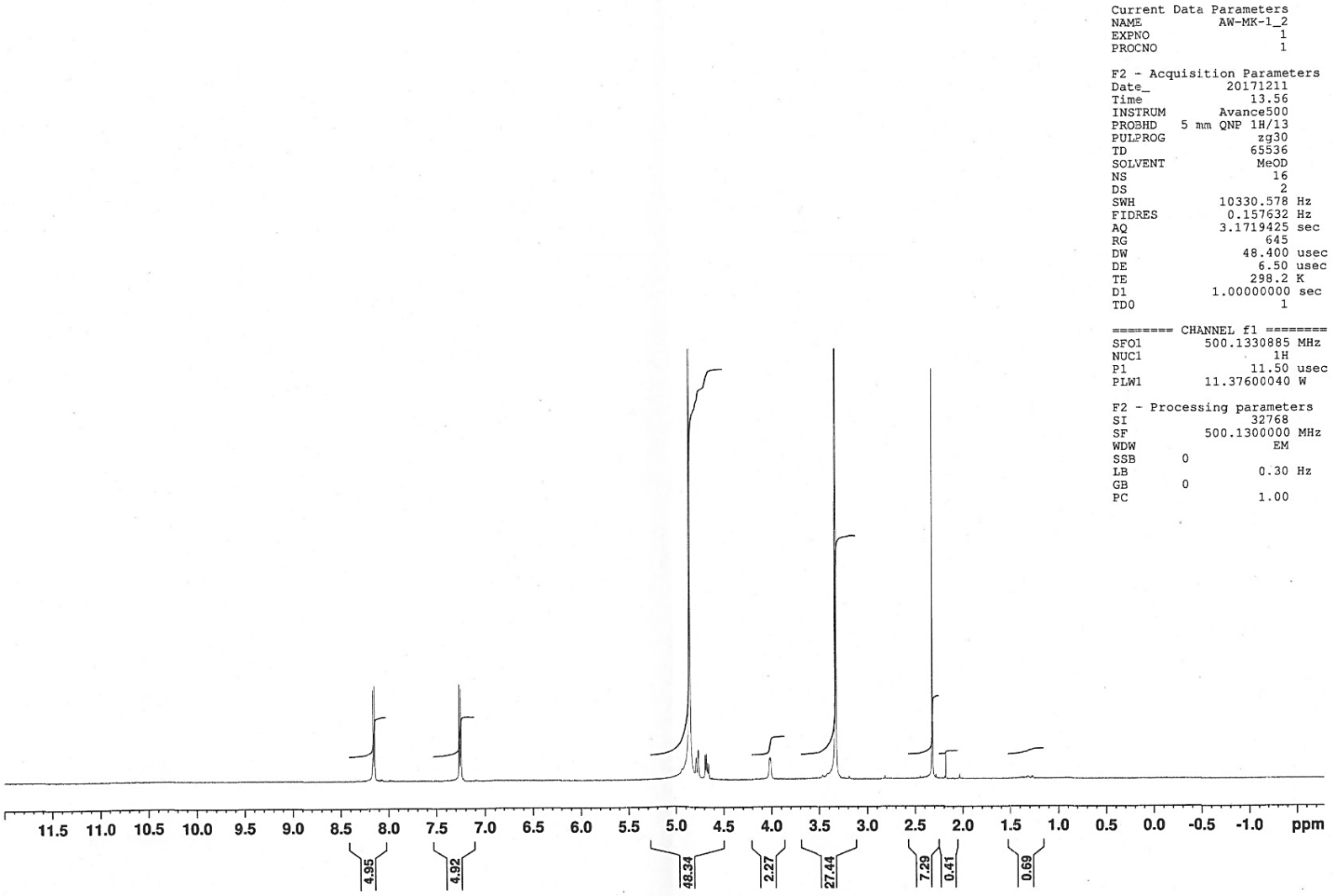

Figure A.2: ^{1}H NMR spectrum of MK4a

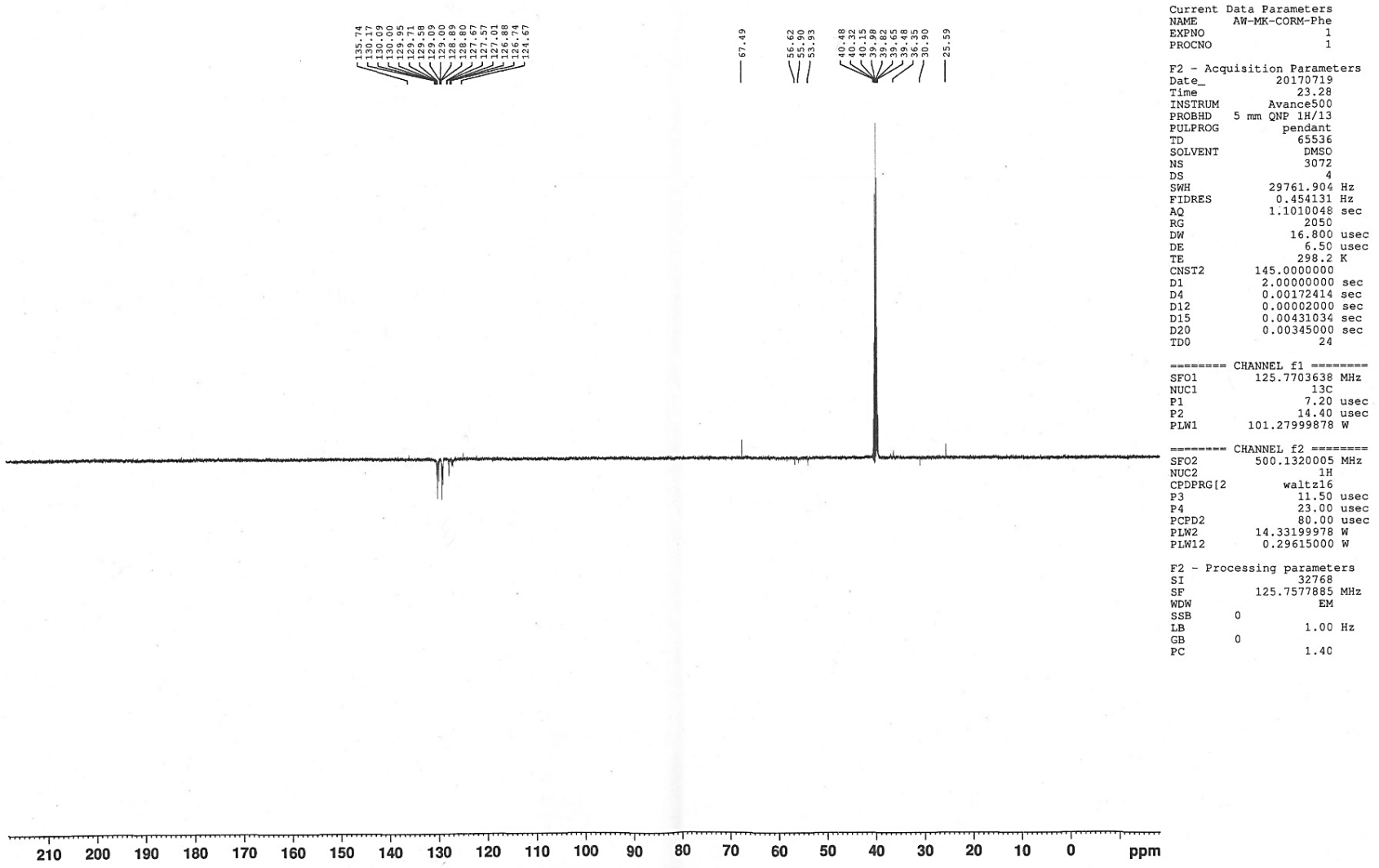

Figure A.3: ^{13}C NMR spectrum of CORM-Phe

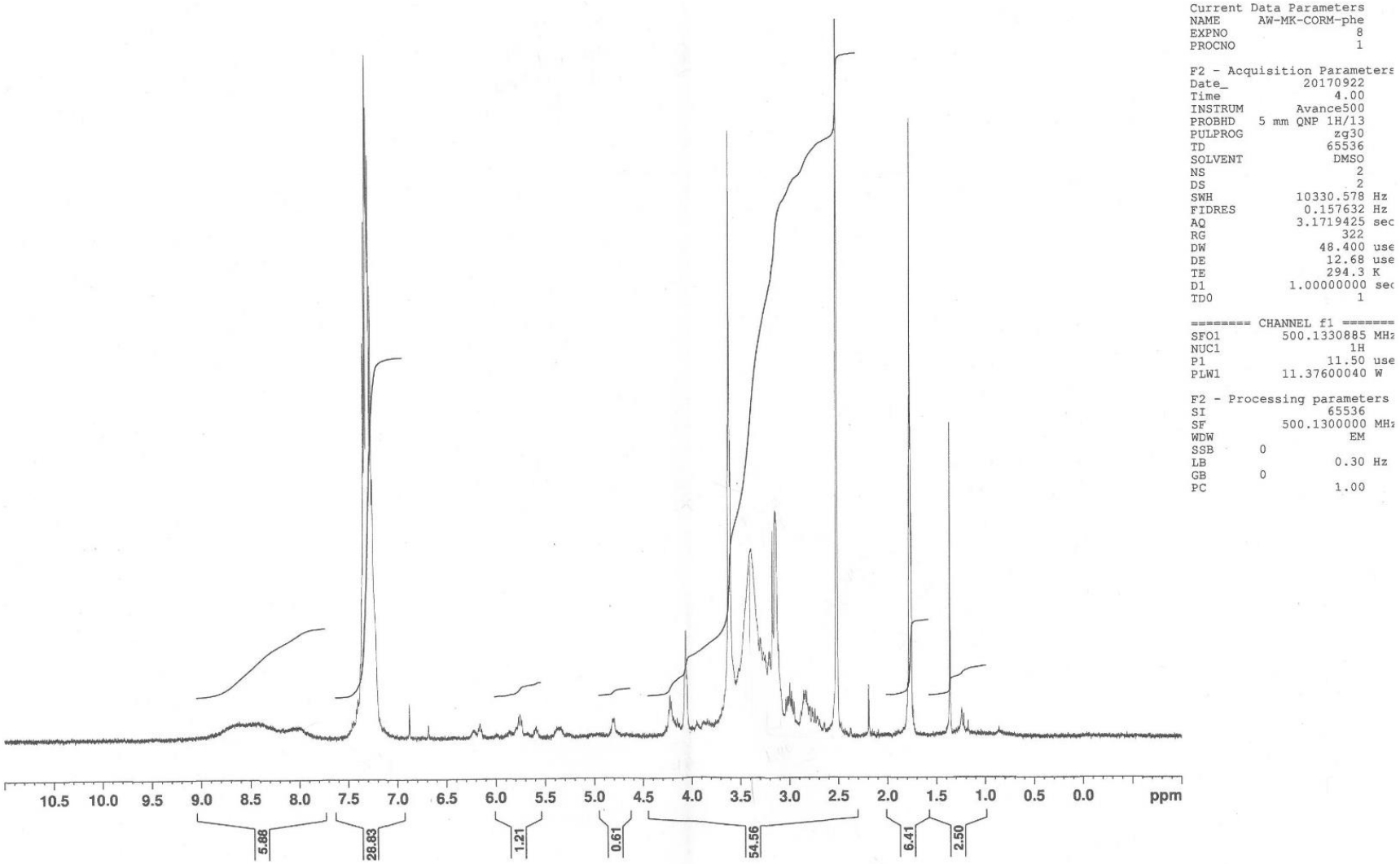

Figure A.4: ^{1}H NMR spectrum of CORM-Phe

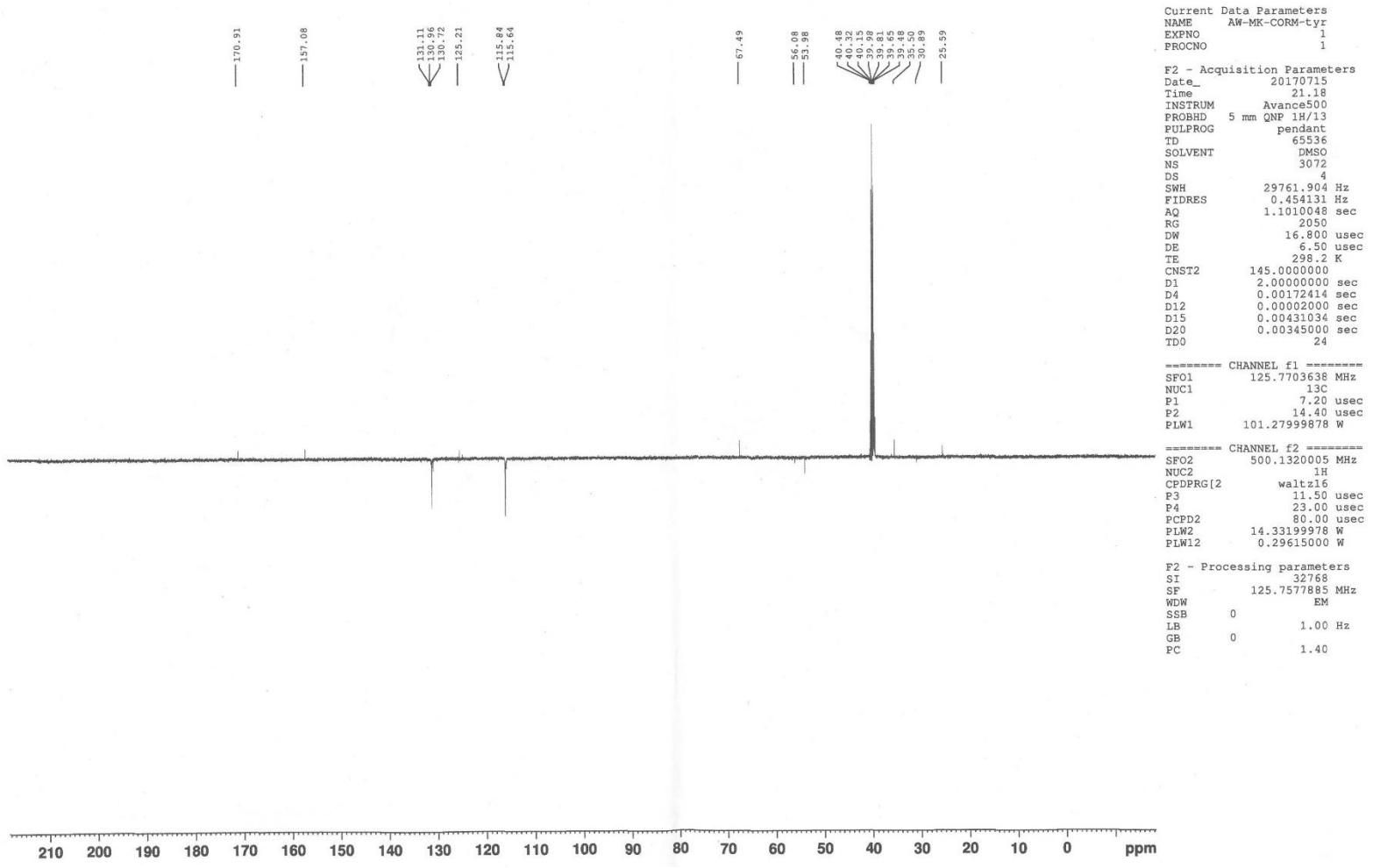

Figure A.5: ^{13}C NMR spectrum of CORM-Tyr

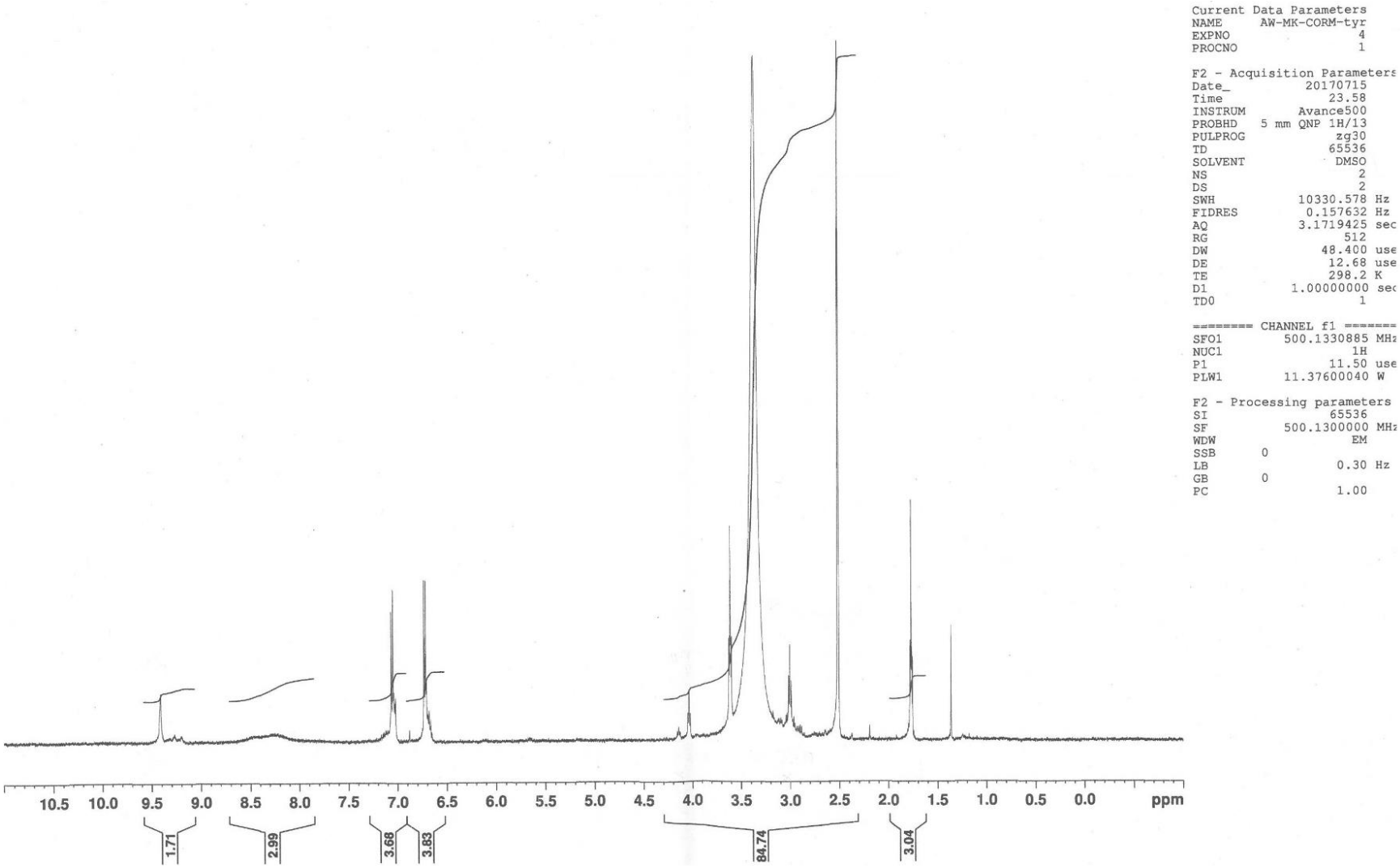

Figure A.6: ^{1}H NMR spectrum of CORM-Tyr

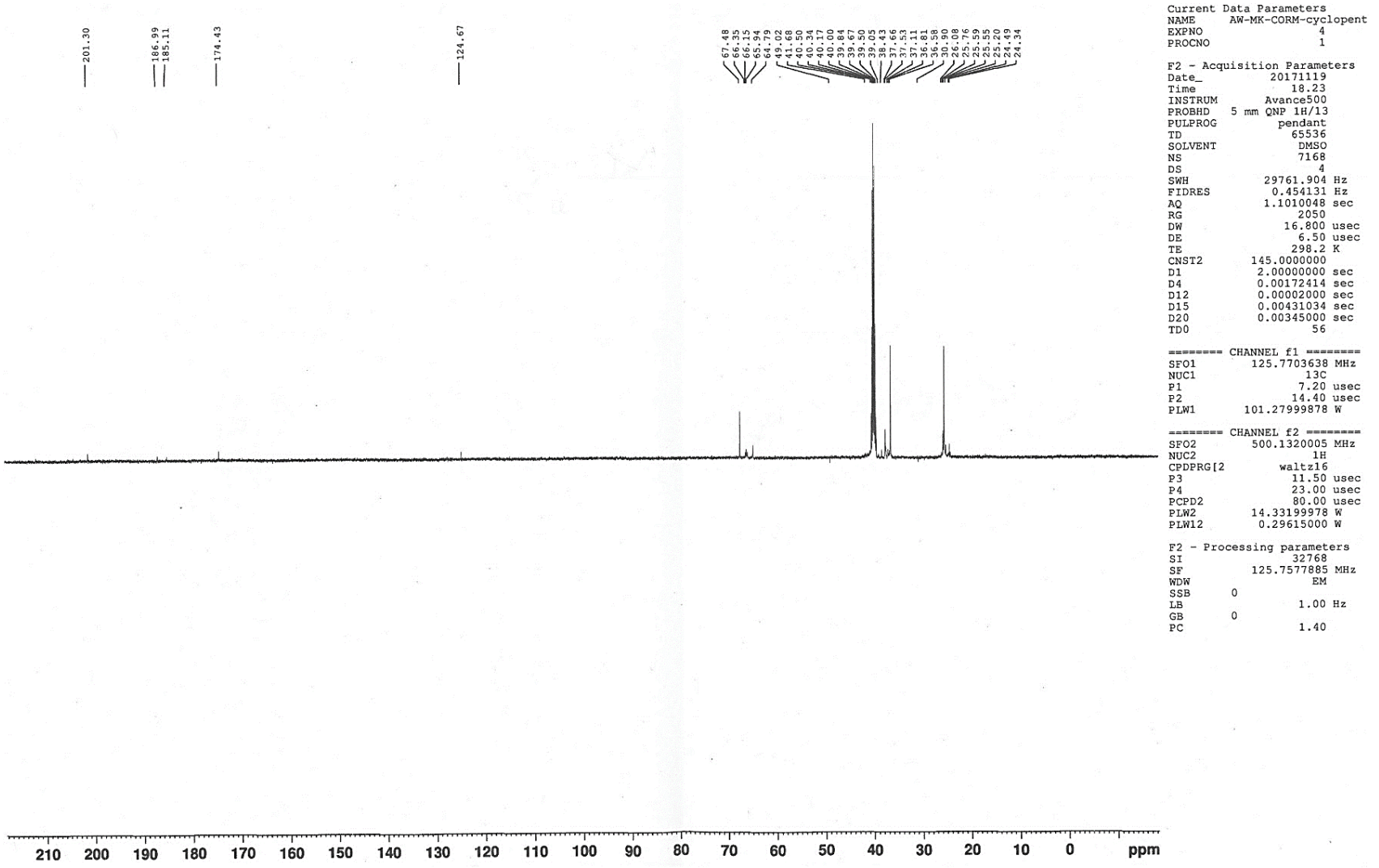

Figure A.7: ^{13}C NMR spectrum of CORM-Cyclopent

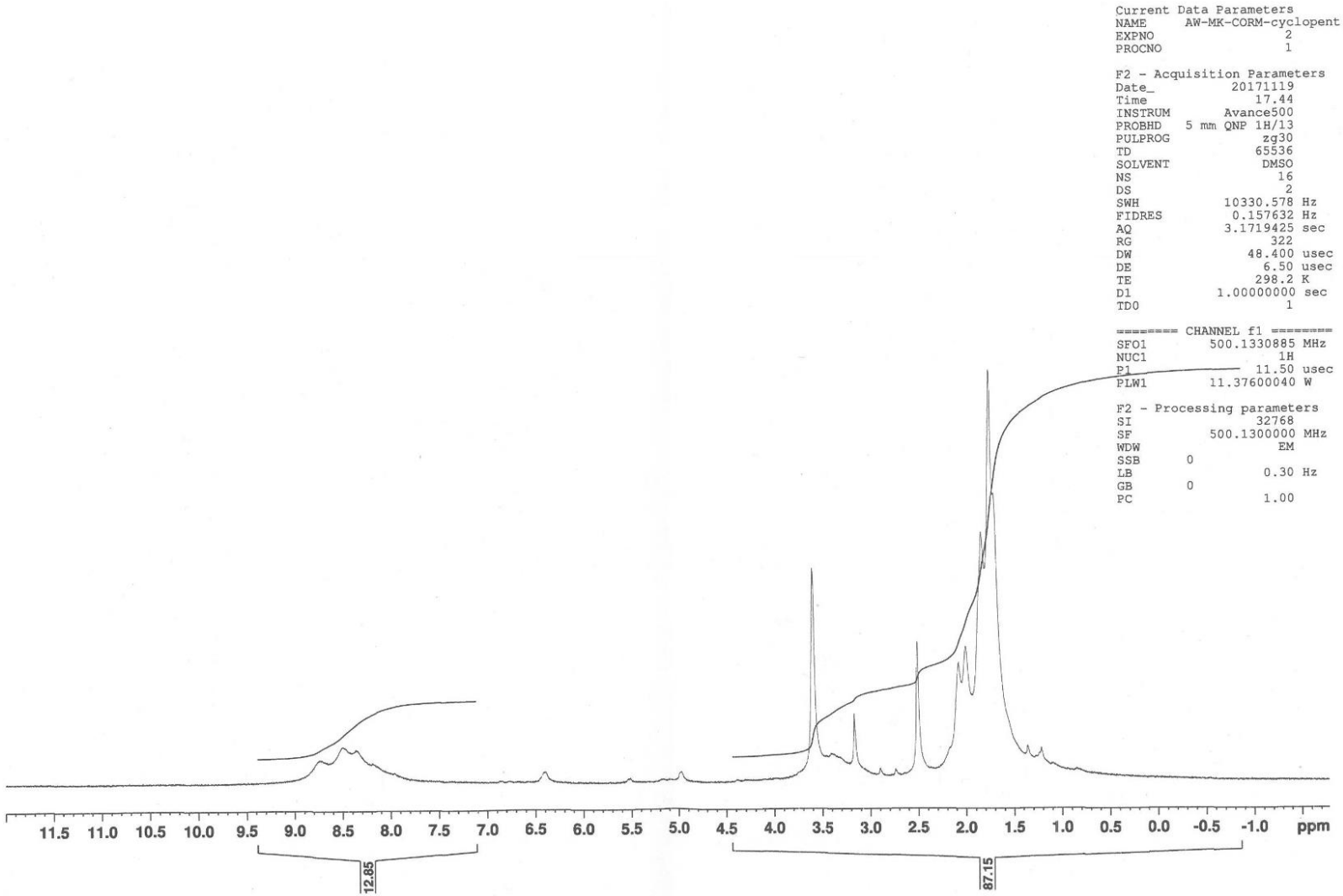

Figure A.8: ^{1}H NMR spectrum of CORM-Cyclopent

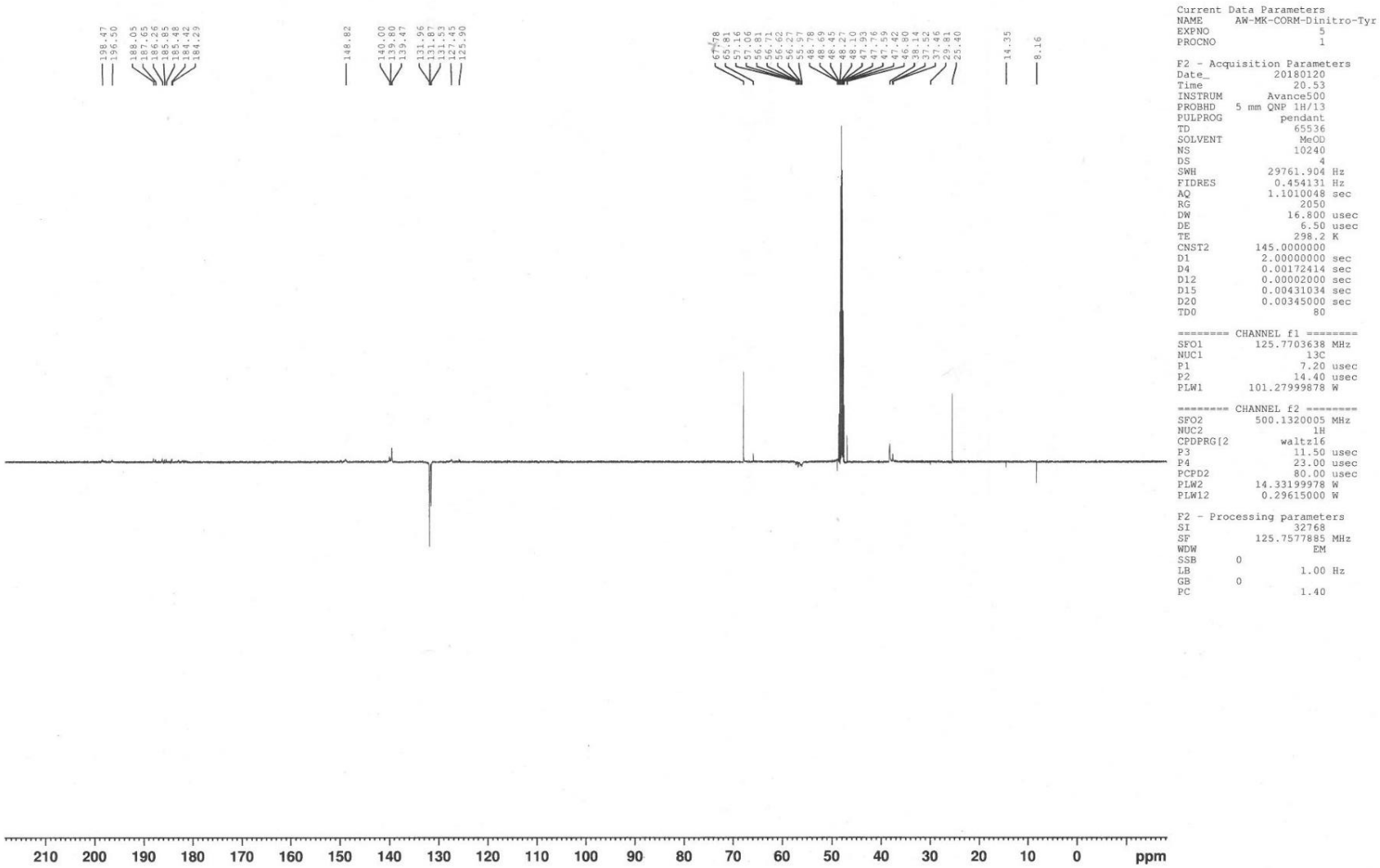

Figure A.9: ^{13}C NMR spectrum of CORM-Dinitro-Tyr

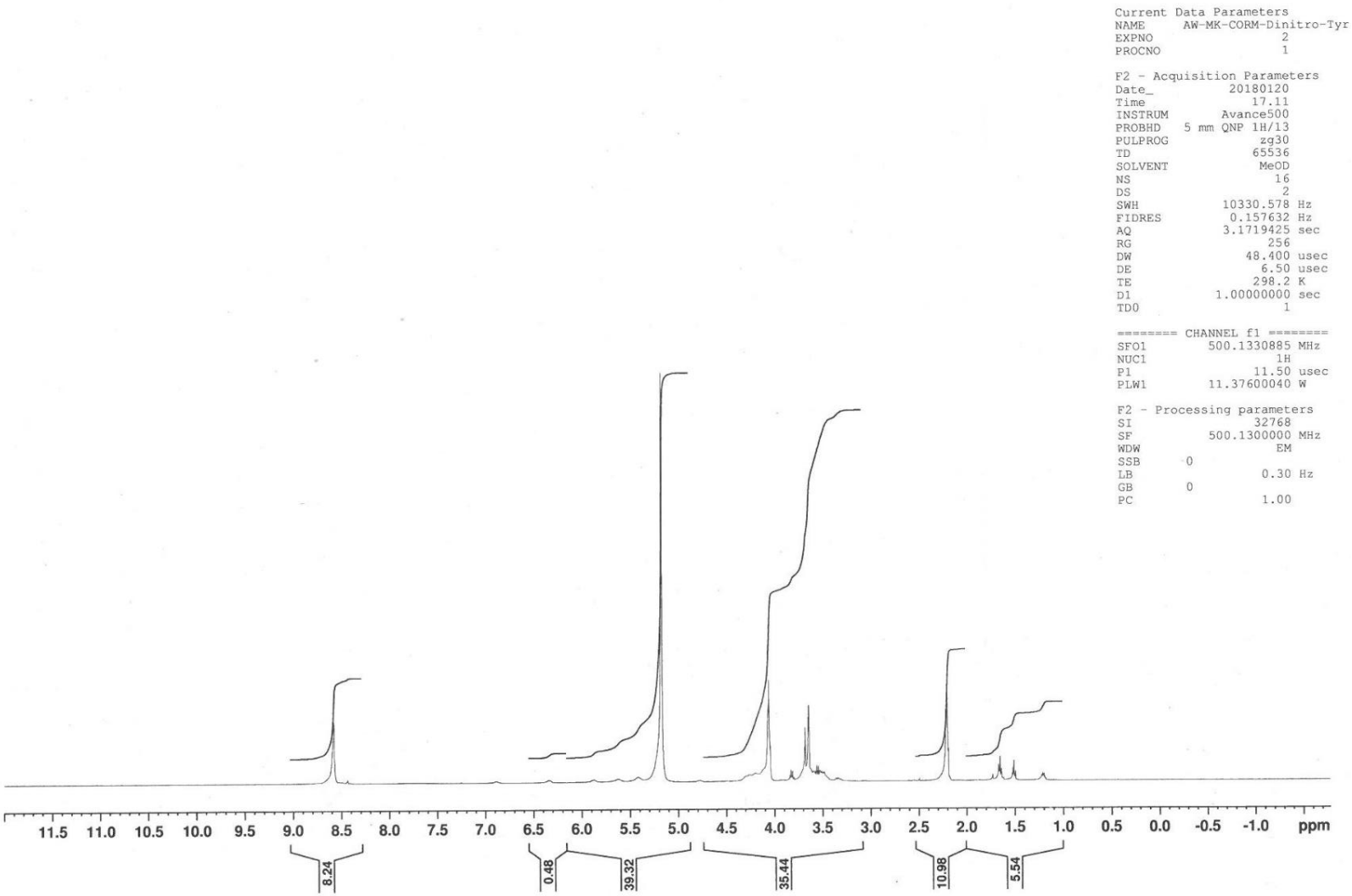

Figure A.10: ^{1}H NMR spectrum of CORM-Dinitro-Tyr